КРИСТАЛЛОГРАФИЯ

SOVIET PHYSICS

Crystallography

VOLUME 2 NUMBER 4

A Translation
of the journal
Crystallography
of the
Academy of Sciences of the USSR

(RUSSIAN ORIGINAL VOL. 2, NO. 4)

Published by the
AMERICAN INSTITUTE OF PHYSICS
INCORPORATED

SOVIET PHYSICS

Crystallography

A translation of the journal "Crystallography" of the Academy of Sciences of the USSR

A publication of the
AMERICAN INSTITUTE OF PHYSICS

Governing Board

FREDERICK SEITZ, *Chairman*

Members

WALTER S. BAIRD
JESSE W. BEAMS
RAYMOND T. BIRGE
R. H. BOLT
J. W. BUCHTA
J. H. DILLON
VERNET E. EATON
HERBERT A. ERF
IRVINE C. GARDNER
S. A. GOUDSMIT
C. KITTEL
WINSTON E. KOCK
R. BRUCE LINDSAY
WALTER C. MICHELS
G. E. PAKE
R. RONALD PALMER
JOSEPH B. PLATT
RALPH A. SAWYER
H. D. SMYTH
JOHN STRONG
GEORGE E. UHLENBECK

Officers and Staff

ELMER HUTCHISSON
Director
HENRY A. BARTON
Associate Director
WALLACE WATERFALL
Secretary and Treasurer
EDWARD P. TOBER
Mgr., Production and Distribution
THEODORE VORBURGER
Advertising Manager
RUTH F. BRYANS
Publication Manager
KATHRYN SETZE
Assistant Treasurer
ALICE MASTROPIETRO
Circulation Manager
EUGENE H. KONE
Director of Public Relations
WILLIAM C. KELLY
Director of Education Projects

American Institute of Physics Advisory Board on Russian Translations

ROBERT T. BEYER, *Chairman*

FREEMAN DYSON, DWIGHT GRAY, MORTON HAMERMESH, DAVID HARKER, VLADIMIR ROJANSKY, HARROLD F. WEAVER

Advisory Editor, Soviet Physics – Crystallography: DAVID HARKER, Protein Structure Project, Polytechnic Institute of Brooklyn, Brooklyn 2, New York.

"Soviet Physics – Crystallography" is published by the American Institute of Physics, with the cooperation of the American Crystallographic Association, for the purpose of making available in English reports of current Soviet research in crystallography as contained in the journal "Crystallography" of the Academy of Sciences of the USSR. The translation begins with the 1957 issues.

Transliteration of the names of Russian authors follows the system employed by the Library of Congress.

This translating and publishing project was undertaken by the Institute in the conviction that dissemination of the results of research everywhere in the world is invaluable to the advancement of science. The National Science Foundation of the United States encouraged the project initially and is supporting it in large part by a grant. Translation and printing are being handled by Consultants Bureau, Inc.

The American Institute of Physics and its translators propose to translate faithfully all of the scientific material in the "Crystallographic Journal of the Academy of Sciences of the USSR" appearing after January 1, 1957. The views expressed in the translated material, therefore, are intended to be those expressed by the original authors, and not those of the translators nor of the American Institute of Physics.

One volume is published annually. The volume numbering coincides with that of the original Russian journal.

Subscription Prices:

Per year (6 issues), starting with Vol. 2, No. 1

General: United States and Canada	*$25.00*
Elsewhere	*27.00*
Libraries of non-profit academic institutions:	
United States and Canada	*10.00*
Elsewhere	*12.00*
Back numbers, all issues	5.00

Subscriptions should be addressed to the American Institute of Physics, 335 East 45th Street, New York 17, New York.

Copyright American Institute of Physics Incorporated, 1959

SOVIET PHYSICS

Crystallography

VOLUME 2, NUMBER 4 JULY-AUGUST 1957

ON THE REPRESENTATION OF CRYSTAL ATOMS AS SYMMETRICAL BODIES

S. T. Konobeevskii

This article attempts the further development of a previously published [1, 2] method of calculating atomic x-ray scattering factors for atoms showing anisotropic electron density distributions. The symmetry of the atom must conform to the position that it occupies in the lattice and the configuration of the group of nearest neighbors. Calculation of the anisotropy of the atom "shape" leads to corrections of the intensities of various interferences. It is shown that in certain cases extinctions are removed and so-called forbidden interferences appear. A method of calculating the anisotropy coefficients from the intensities of the forbidden x-ray interferences is given. The "shapes" of the atoms show graphically the peculiarities of the chemical bonds in crystals.

I

There are two basic problems involved in x-ray crystal structure analysis: 1) determining the exact positions of the atoms in the crystal lattice,and 2) finding the distribution of the electrons in those atoms. Only the solution of both problems may be considered as a complete crystallochemical study, clarifying the chemical nature of any solid body. X-ray structural analysis provides the means of accomplishing this because x-rays are diffracted by crystals. It is well known that x-rays are scattered by electrons and therefore the direct result to be deduced from the experimental data is the distribution of electrons or, as it is called, the electron density throughout the entire crystal space. It would seem that both problems mentioned above would be thus immediately solved. Local condensations of the electron cloud establish the positions of the atoms, and the path of the lines of equal density show the contours of the atoms, their forms and their boundaries. It is true that the isolation of individual atoms from a continuous electron cloud is not always unique; however,there is often a sufficient number of qualitative peculiarities of the electron density distribution to allow conclusions to be drawn as to the nature of the chemical bonds between individual atoms.

At the present time the majority of studies in the field of x-ray crystallography are directed toward the development and refinement of a method of constructing a periodic electron density distribution by means of the diffracted x-ray intensities (Fourier synthesis). Studies of this type have recently taken a great stride forward due to new means of finding the phases (by a scheme of inequalities) and also to the use of calculating machines.

However, in spite of the "objectivity" of the Fourier synthesis method and its complete effectiveness for a precise determination of atomic coordinates, the use of this method to construct an electron density field has not been completely successful, because the results obtained were not sufficiently complete or reliable. The difficulties encountered here are due to incomplete summing (cutting off the series) and also to an insufficient "sensitivity" of the interference function to changes in electron distribution [3]. It must be remembered also that a two-dimensional projection is not sufficient for this problem, and one must have three-dimensional series, the calculation of which still presents considerable practical difficulties. It is therefore expedient to seek other methods of using the x-ray data to discover the distributions of electrons in atoms in crystals. One of these possible methods is given in an earlier paper by the author and Mamedov [1] and also in the latter's dissertation [2]. That study established a connection between the anisotropy of the electron density in the atoms of an elementary (single atom) crystal and the intensities of the maxima of the diffraction spectrum of that crystal. It was shown that the anisotropy effect is by no means small, reaching 10% of the measured intensity in the case of aluminum.

In the present paper an attempt has been made to develop this method further so that it can be used in more complex cases of crystal structure analysis.

In the process of structural analysis the atomic coordinates are first found by means of an electron density projection or by means of a trial and error method, supplemented by considerations based on structural analogies and crystallochemical laws; then the chosen atomic distribution is checked by substitution of the coordinates found into the structure factor. In this case, the possible anisotropy of the atomic scattering factor is not usually taken into consideration. It is well known that even with the best choice of atomic coordinates it is impossible to reach complete correspondence between measured and calculated intensities. The most carefully calculated structure factors will deviate from the measured ones by more than 10-20% and these deviations (and this is important) are irregular. Most researchers are reconciled to the situation, considering such discrepancies as due to inevitable mistakes in the intensity measurements. It must be noted, however, that in spite of greatly improved measurement technique, the irregular deviations do not tend to disappear, but rather are stabilized at a certain level. This apparently contradicts the assumption that the lack of correlation between calculated and measured intensities in a structural analysis is always of random nature. It might be added at this point that, if the indicated discrepancies are due to errors in measurement, it is hard to substantiate the validity of constructing electron density projections by a Fourier synthesis method which used equally poorly measured intensities.

We believe that the deviation between the measured and the calculated amplitudes is not always due so much to errors in measurement as to defects in the calculation of the atomic factor itself because, in the process of the calculation the anisotropy of the electron distribution in the atoms is not taken into account; in other words, the "shape" of the atom was not taken into consideration.

It seems self-evident that the atom, entering as a component unit into the crystal lattice, cannot keep the same symmetry which it possessed in a free state. In a crystal the shape of an atom is considerably changed, being determined to a great extent, if not entirely, by the coordination and distribution of its neighbors. A good example of this is the carbon atom in diamond, the tetrahedral symmetry of which has been experimentally established; it produces perceptible x-ray effects — the appearance of "forbidden" maxima with a sum of indices equal to

$$4n + 2\,(h_1, h_2, h_3 \neq 0).$$

Quantum-mechanical calculations carried out by Ewald [4] also substantiate theoretically the tetrahedral symmetry of the carbon atom in diamond.

In cases similar to that of diamond, where covalent bonds between atoms are particularly significant, the electron distribution of the atoms concentrates along the connecting lines between nearest neighbors. On the contrary, in cases where the electrostatic repulsion of electron shells is predominant, the atoms tend to penetrate each other as little as possible. In the directions of nearest neighbors a certain thinning of electron density is observed, and the shape of the atom approaches the polyhedral.

ion. However, if such a change did take place it would give rise to a smooth variation [illegible] tion and would not substantially affect the angle function ψ.

The functions S_i each have a definite symmetry. Some of these functions are shown in Table 1. The determination of the symmetry of any function S_i is easy to carry out if it is expressed in terms of coordinates (column 3, Table 1) and if one applies to the x, y, and z coordinates the corresponding symmetric transformations by means of matrices representing symmetry elements.* If one takes, as an example, function $S_7 = \cos\alpha \cdot \cos\beta \cdot \cos\gamma = xyz/r^3$, it is easy to show that it remains invariant when the following transformations are applied to it:

$$\left|\begin{array}{c} \bar{1}00 \\ 0\bar{1}0 \\ 001 \end{array}\right| = \left\{\begin{array}{l} \text{Symmetry} \\ \text{axis of the} \\ \text{second} \\ \text{order} \end{array}\right. \qquad \left|\begin{array}{c} 010 \\ 001 \\ 100 \end{array}\right| = \left\{\begin{array}{l} \text{Symmetry} \\ \text{axis of the} \\ \text{third} \\ \text{order} \end{array}\right. \qquad \left|\begin{array}{c} 0\bar{1}0 \\ 100 \\ 001 \end{array}\right| = \left\{\begin{array}{l} \text{Rotation-inver-} \\ \text{sion symmetry} \\ \text{axis of the} \\ \text{fourth order} \end{array}\right.$$

but not

$$\left|\begin{array}{c} 0\bar{1}0 \\ 100 \\ 001 \end{array}\right| = \left\{\begin{array}{l} \text{Symmetry} \\ \text{axis of the} \\ \text{fourth} \\ \text{order} \end{array}\right. \qquad \text{and} \qquad \left|\begin{array}{c} 100 \\ 010 \\ 00\bar{1} \end{array}\right| = \left\{\begin{array}{l} \text{Plane of} \\ \text{symmetry} \end{array}\right.$$

and shows, therefore, tetrahedral symmetry T_d.

TABLE 1

The Form-Functions S_i for Different Symmetries

	Function S_i		Symmetry
S_i	in angular terms	in coordinate terms	
S_1	$\cos\gamma$	z/r	$\bar{1}$
S_2	$\cos^2\gamma$	z^2/r^2	$1m$
S_3	$\cos\alpha\cos\beta$	xy/r^2	$2/m$
S_4	$\cos\alpha\cos\beta + \cos\alpha\cos\gamma + \cos\beta\cos\gamma$	$(xy + xz + yz)/r^2$	$\bar{2}(i)$
S_5	$\cos^2\alpha\cos^2\beta$	x^2y^2/r^4	$4/mmm$
S_6	$\cos^2\alpha\cos\beta - {}^1/_3\cos^3\beta$	$(x^2y - {}^1/_3y^3)\,r^3$	$\bar{3}/m$
S_7	$\cos\alpha\cos\beta\cos\gamma$	xyz/r^3	$\bar{4}3m\ (T_d)$
S_8	$\cos^2\alpha\cos^2\beta + \cos^2\alpha\cos^2\gamma + \cos^2\beta\cos^2\gamma$	$(x^2y^2 + x^2z^2 + y^2z^2)/r^4$	$m3m(O_h)$
S_9	$\cos^2\alpha\cos^2\beta\cos^2\gamma$	$x^2y^2z^2/r^6$	» »

A number of other functions may be added to those enumerated in Table 1; these are the higher terms of the expansion of the angle portion of the distribution density $\rho(r, \theta, \varphi)$. For example, functions $\cos^3\alpha\cos^3\beta$, $\cos^5\alpha\cos^5\beta$, etc., having the same symmetry may be added to the function $S_3 = \cos\alpha\cos\beta$ with $2/m$ symmetry.

Coefficients k_0, k_1, k_2, which we shall call anisotropy coefficients enter into the expression for ψ. The first of these, the constant term k_0, is determined by all the others, because of the normalizing conditions (4). The others must be determined from the experimental data. They must be chosen in such a way as to agree best with the accurately measured x-ray diffraction intensities. In order to describe the shape of the atom accurately, the number of terms in Formula (3) and therefore the number of k_i coefficients must be large. However, in order to describe the most essential properties of this "shape" which would make possible reliable conclusions as to the type of chemical bond between the atoms, the number of S_i terms may be considerably reduced, and apparently 2 or 3 determinable anisotropy coefficients k_i are sufficient.

Introducing the function ψ into the atom factor, which in turn enters into the structure factor which determines the x-ray diffraction intensity, we shall write the atom factor as

$$f(H) = \int_0^\infty R(r)\,4\pi r^2 dr \int_0^\pi e^{2\pi iHr\cos\theta} \sin\theta\, d\theta\, \frac{1}{4\pi} \int_0^{2\pi} (k_0 + k_1S_1 + k_2S_2 + \ldots)\,d\varphi. \tag{5}$$

---

* As far as the author knows this method of expressing symmetry elements was first introduced into Soviet literature by Shubnikov [5].

Here H is the modulus of the reciprocal lattice vector, which corresponds to the plane of the Bragg reflection with indices h_1, h_2, h_3 and which is taken as a polar axis.

In order to integrate Expression (5) the form-functions, referred, as has been said, to the axes associated with the atomic configuration, should be expressed in polar coordinates related to the vector $\bar{H}$.

This may be done in two steps, first by transforming expressions S_i to rectangular coordinates associated with the reflecting plane (h_1, h_2, h_3) and then transforming to polar coordinates θ and φ. We carry out the first operation by choosing as a new axis Z' the direction of the vector $\bar{H}$ and placing the other two axes arbitrarily in the plane (H). If, for example, one is interested in finding the atomic scattering factor for the reflection 311 of a crystal in the cubic system one may choose for the other two axes

$$\begin{array}{ccccc} \text{a} & & \text{b} & & \text{c} \\ \left\{\begin{matrix} 0\bar{1}1 \\ \bar{2}33 \end{matrix}\right\} & \text{or} & \left\{\begin{matrix} \bar{1}21 \\ 14\bar{7} \end{matrix}\right\} & \text{or} & \left\{\begin{matrix} 10\bar{3} \\ 3\bar{1}\bar{0}1 \end{matrix}\right\} \text{ etc.} \end{array}$$

Obviously the choice of any one of these pairs of X'Y' axes will eventually lead to the same result.

Rotation of the axes from X, Y, Z to X', Y', Z' may be brought about in the usual way, by means of the rotation matrices (D = 1)

$$\begin{array}{c|ccc} & x' & y' & z' \\ \hline x & a_{11} & a_{12} & a_{13} \\ y & a_{21} & a_{22} & a_{23} \\ z & a_{31} & a_{32} & a_{33} \end{array} \tag{6}$$

the elements of which are equal to the cosines of the angles formed by the new axes X', Y', Z' and the original X, Y, Z axes.

After this it is easy to find new expressions for the form-functions S_i', now referred to the new rectangular coordinate system.

As an example let us show the calculation for the function

$$xyz/r^3.$$

After appropriate manipulations using Matrix (6) and having performed the cross multiplications, we obtain a polynomial of the 3rd degree

$$S_7' = a_1x'^3 + a_2y'^3 + a_3z'^3 + a_4x'^2y' + a_5x'^2z' + a_6x'y'^2 + a_7x'z'^2 + a_8y'^2z' + \\ + a_9y'z'^2 + a_{10}x'y'z', \tag{7}$$

where the coefficients a_i are expressed through combinations of the elements of the conversion matrix (rotation). The somewhat clumsy expression for S_7' is simplified as soon as we change over to polar coordinates, having chosen the Z' axis as a polar axis. It is easy to see that with the integration of (5) all terms with odd powers of cos φ (corresponding to sin φ) must disappear, as a result of which only those terms in (7) remain which contain $\underline{x}$ and $\underline{y}$ in even powers. Thus in the formula for S_7' only three terms remain:

$$S_7' = a_3z'^3 + a_5x'^2z' + a_8y'^2z' = a_3\cos^3\theta + a_5\cos\theta\sin^2\theta\cos^2\varphi + \\ + a_8\cos\theta\sin^2\theta\sin^2\varphi. \tag{8}$$

The expanded expressions for a_3, a_5 and a_8 are

$$\begin{aligned} a_3 &= a_{13}a_{23}a_{33}, \\ a_5 &= a_{11}a_{21}a_{33} + a_{11}a_{31}a_{33} + a_{13}a_{21}a_{31}, \\ a_8 &= a_{12}a_{22}a_{33} + a_{12}a_{23}a_{32} + a_{13}a_{22}a_{32}. \end{aligned} \tag{9}$$

They are easily determined if the conversion matrices from the XYZ axes to the X'Y'Z' axes are known.

The form-functions S_i (chosen according to the position symmetry of the atom) with k_i coefficients, which up to now have remained indeterminate, form the angle function ψ, which enters into Expression (5) for the atom factor $f(H)$.

(5) is now integrated over φ and θ, which is not difficult as the dependence on φ is contained only in the expression for S_i' and the integrals over θ of the type

$$\int_0^{\pi} e^{2\pi i H r \cos\theta} f(\cos\theta)\sin\theta\, d\theta = \int_{-a}^{+a} e^{ia\mu} f(\mu)\, d\mu, \tag{10}$$

are easily evaluated when

$$a = 2\pi H r, \quad \mu = \cos\theta,$$

As a result, the atom factor $f(H)$ seems to be dependent not only on the modulus of the vector $\overline{\mathbf{H}}$ but also on its direction in relation to the symmetry elements of the atom. The general expression for $f(H)$ has the form

$$f(H) = \sum A_n I_n, \tag{11}$$

where the I_n represent integrals of the radial function*

$$I_n = \int_0^{\infty} R(r) \frac{\left.\begin{matrix}\cos\\ \sin\end{matrix}\right\} 2\pi H r}{r^{n-2}}\, dr\,, \tag{12}$$

and the A_n depend on the anisotropy coefficients $k_1, k_2, \ldots$ and on the elements a_{ij} of the conversion matrices from the XYZ axes to the polar coordinates associated with the vector of the reflecting plane $\overline{\mathbf{H}}$.

III

What then are the results of this calculation and what new light do they shed on the diffraction pattern of a crystal ?

First of all, the calculation of atomic anisotropy may introduce appreciable corrections to the intensity distribution of individual diffraction lines. Secondly, in certain cases, when the atom does not lie at a center of symmetry of the lattice, the introduction of the angle factor may remove certain "extinctions" and bring about the appearance of additional "forbidden" reflections.

This can be easily demonstrated by a simple example which will show best how the above described calculation scheme may be most practically used. Let us take the case of an atom with tetrahedral symmetry. Form-function S_7 is a function having this symmetry. Therefore, let us write the expression

$$\psi = k_0 + k_1 S_7 = k_0 + k_1 \cos\alpha\cos\beta\cos\gamma. \tag{13}$$

Let us transform S_7 to coordinates associated with the 111 Bragg reflection plane and the 001 plane of a cubic crystal. In order to do this we shall apply the conversion matrices to the new coordinates $(1\bar{1}0,\ 11\bar{2},\ 111)$ and $(1\bar{1}0,\ 110,\ 001)$:

$$\begin{array}{c|ccc} & x' & y' & z' \\ \hline x & 1/\sqrt{2} & 1/\sqrt{6} & 1/\sqrt{3} \\ y & \bar{1}/\sqrt{2} & 1/\sqrt{6} & 1/\sqrt{3} \\ z & 0 & \bar{2}/\sqrt{6} & 1/\sqrt{3} \end{array} \qquad \begin{array}{c|ccc} & x' & y' & z' \\ \hline x & 1/\sqrt{2} & 1/\sqrt{2} & 0 \\ y & \bar{1}/\sqrt{2} & 1/\sqrt{2} & 0 \\ z & 0 & 0 & 1 \end{array}$$

---

* See [1, 2].

As a result we obtain for the a_i (9)

a_i	for $H(111)$	for H (001)
a_3	${}^{1}{}_{3}/\sqrt{3}$	0
a_5	$-{}^{1}/{}_{2}\sqrt{3}$	$-{}^{1}/{}_{2}$
a_8	$-{}^{1}/{}_{2}\sqrt{3}$	${}^{1}/{}_{2}$

From this

$$S_7'(111) = 1/\sqrt{3}\,({}^{1}/{}_{3}\cos^3\theta - {}^{1}/{}_{2}\cos\theta\sin^2\theta),$$
$$S_7'(001) = {}^{1}/{}_{2}\cos\theta\sin^2\theta\,(\sin^2\varphi - \cos^2\varphi).$$

In the first case function S_7' does not depend on φ, and therefore integrating it over φ simply gives 2π. In the second case S_7', as is easily seen, when integrated over φ, disappears. From this we conclude that the value 1 must be assigned to k_0. After the integration of S_7' (111) over θ, we obtain

$$1/\sqrt{3}\int_0^{\pi}({}^{1}/{}_{3}\cos^3\theta - {}^{1}/{}_{2}\cos\theta\sin^2\theta)\,e^{2\pi iHr\cos\theta}\sin\theta d\theta =$$
$$= 1/\sqrt{3}\int_{-a}^{+a} e^{ia\mu}({}^{5}/{}_{6}\mu^3 - {}^{1}/{}_{2}\mu)\,d\mu = \frac{2i}{\sqrt{3}}({}^{5}/{}_{6}A - {}^{1}/{}_{2}B),$$

where

$$A = \frac{\sin a\,(3a^2 - 6) - a\cos a\,(a^2 - 6)}{a^4},$$

$$B = \frac{\sin a - a\cos a}{a^2},$$

and

$$a = 2\pi Hr.$$

Thus in the case of a tetrahedral (13) atom shape for reflections from face (111) the following expression serves as the atom factor:

$$f(H) = \int_0^{\infty} 4\pi R(r)\,r^2\left[\frac{\sin a}{a} + \frac{ik}{\sqrt{3}}({}^{5}/{}_{6}A - {}^{1}/{}_{2}B)\,dr,\right. \tag{14}$$

which differs from the "isotropic" atom factor

$$f_0(H) = \int_0^{\infty} 4\pi R(r)\,r^2\,\frac{\sin a}{a}\,dr$$

by the term

$$i\beta = \frac{ik}{\sqrt{3}}\int_0^{\infty} 4\pi R(r)\,r^2({}^{5}/{}_{6}A - {}^{1}/{}_{2}B)\,dr. \tag{15}$$

In order to integrate this last expression over r one does not have to know the exact value of R(r) but one can use an approximate value replacing R(r) by the most easily approximated analytic function. Then the integrals*

$$\int_0^\infty R(r)\, r^2 A dr\,, \quad \int_0^\infty R(r)\, r^2 B dr$$

may be easily evaluated.

Thus the introduction of an angle function into the expression for the electron density of the atom changes the intensity of individual diffraction lines. The overall amount of scattering should not change as the normalization adopted keeps the overall electron charge of the atom unchanged.

The tetrahedral form-function of the atom which we used as an example does not have a center of symmetry. The inversion of this function at the center of the tetrahedron brings about a change in the sign both of the function itself and also of the imaginary portion of the complex atom factor. By itself this change in orientation, as can be easily seen, does not change the intensity distribution of the scattering by an individual atom, but, in the case of the simultaneous presence in the crystal of both inverse orientations of the atoms, it may bring about the removal of degeneration and a change in the law of diffraction extinction. This is just what happens in the case of the diamond.

As is well known, the atomic-structure factor for diamond is

$$\sum = A_1 + A_2 e^{\frac{i\pi}{2}\Sigma h_i},$$

which when A_1 and A_2 are equal, leads to extinction of reflections of the type

$$\sum h_i = 4n + 2.$$

If, according to the above, the complex atom factor is written as

$$A_{1,2} = A_0 \pm i\beta,$$

then the structure factor will appear as

$$\sum = A_0(1 + e^{\frac{\pi i}{2}\Sigma h_i}) + i\beta(1 - e^{\frac{\pi i}{2}\Sigma h_i},$$

and the intensity, proportional to the square of the structure factor,

$$I \sim \left|\sum\right|^2 = 2A_0^2(1 + \cos{}^1/_2\pi \sum h_i) + 2\beta^2(1 - \cos{}^1/_2\pi \sum h_i)$$

for reflections of the $\Sigma h_i = 4n + 2$ type does not disappear, but is proportional to $4\beta^2$.

Actually it is well known that in diamond not only normal maxima are observed but also weak "forbidden" reflections of the 4n + 2 type. The appearance of such forbidden reflections is a direct result of the tetrahedral form of the carbon atoms and the presence in the diamond lattice of a center of symmetry half-way between two neighboring atoms. Experiment shows that of the reflections with a sum of indices equal to 4n + 2 only those appear having no index h_1, h_2, h_3 equal to zero. Thus reflections of the 200, 420, etc. types are twice "forbidden."

---

* When integration is carried out in the region of small r (consequently a) it is more convenient to separate the A and B functions into series in terms of the parameter a.

This result is also the result of the foregoing and may be checked most simply by direct calculation, if the method indicated above is applied to any one of such reflections, such as 420.

The diamond illustrates the method by which, from experimental data, one can determine the value of the anisotropy coefficients k_i, as the intensity of the reflection 222, as follows from (15), must be proportional to k_1^2. If Formula (13) is supplemented by other terms with tetrahedral symmetry, the corresponding anisotropic coefficients k_2, k_3, . . . may be found by a comparison of the relative intensity of other "forbidden" reflections.

In a more general case, when, as a result of the introduction of the form-function of the atom, there is no restoration of extinctions, parameters k_1, k_2, . . . may be found from a comparison of the lines of various indices. For the simple Al crystal, studied by Mamedov [2], this was easily done by comparing the crystal reflections 511 and 333, which have an equal modulus of the vector of the reciprocal lattice. In other cases the choice of these values k_i must be made in such a way that it best fits in with the whole system of accurately measured reflections. Of course, to what extent and when this may be carried out practically depends on the complexity of the crystal and also on the perfection of the technique of calculation. However, it is quite clear that in principle this problem is soluble.

After the symmetry of all the atoms has been found and the coefficients of anisotropy k_i have been determined, it is not difficult to build up the whole crystal from these atoms and to obtain any section of it as a network of lines of equal density. In this way the same result will be obtained as was expected with the first use of the Fourier synthesis method. Here it is obtained not directly from experimental data, but as a result of a certain assumption concerning the symmetry of the shapes of the atoms. However, these assumptions have such a general character that the degree of reliability of the results obtained is adequate. It has been noted above that the construction of a field of electron density by the Fourier synthesis method is rather difficult. This prompts the author to suggest in this paper a new alternate method for the solution of the same problem: the elucidation of the chemical nature of the bonds in crystals.

The practical application of the method given will simplify in the future the method of calculation and will make it useful in x-ray structural analysis of crystals.

LITERATURE CITED

[1] S. T. Konobeesvskii and K. P. Mamedov, "The anisotropy of the atom scattering factor for x-rays in aluminum and diamond crystal," J. Exptl.-Theoret. Phys. (USSR) 21, 9, 953 (1951).

[2] K. P. Mamedov, Anisotropy of the Atom Factor in Cubic Crystals (Author's Dissertation) [in Russian] (MGU, Moscow, 1950).

[3] S. T. Konobeevskii, "Study of atomic structure in crystals by the trial and error method," Uspekhi Fiz. Nauk 14, 1, 21 (1951).

[4] P. P. Ewald and H. Hõhl, "Die Rõntgeninterferenzen an Diamant als wellen mechanisches Problem," Ann. Physik (5), 25, 4, 281 (1936).

[5] A. V. Shubnikov, "On the symmetry of vectors and tensors," Izv. AN SSSR, Ser. Fiz. 13, 3, 347 (1949).

Received November 12, 1956

CONCEPTS OF ORGANIC CRYSTALLOCHEMISTRY

A. I. Kitaigorodskii

The thermodynamic aspect of the theory of close packing of molecules in crystals is discussed. New applications of the theory in deriving the possible structures of paraffin crystals are considered, as well as the conditions involved in the formation of solid solutions.

1. The Principle of Close Packing

The basic type of organic crystal is a crystal constructed of molecules.

The group of atoms forming a molecule is distinguished in a crystal by the interatomic distances (they are substantially smaller than the intermolecular), by the practical absence of electron exchange between adjacent molecules (which is indicated by the drop to zero of the electron density), and by the low energy of the intermolecular bonds.

In the world of organic substances the ideal molecular crystal is the rule; in inorganic chemistry molecular crystals are rare exceptions.

It may be said that organic crystallochemistry is the science of the structure of molecular crystals. With such an understanding of organic crystallochemistry, we must of course eliminate the salts of organic bases and crystals with a three-dimensional or two-dimensional network of hydrogen bonds, which are intermediate.

The question of the structure of an organic substance breaks up naturally into: the problem of the structure of a free molecule (which is not directly related to crystallochemistry), the question of the deformation of a molecule upon entering into the crystal, and the mutual distribution of molecules in the crystal.

We have very little data on the effect of the crystal field on a molecule. In any case this effect is not great, and in an analysis of the general rules of the structure of crystals it need not be taken into consideration.

Thus the task of organic crystallography consists in an investigation of the mutual distribution of molecules in the crystal.

In 1944 the author had shown* that the form of a molecule constructed with standard intermolecular radii has a distinct physical meaning: an organic crystal is always constructed in such a way that the projecting parts of one molecule penetrate the "hollows" of the adjacent one. An organic crystal can be viewed as a packing of bodies of a definite form.

The question of the character of this packing arises. What kind of packing leads to a minimum of free energy? At first glance it seems that a general answer to this question cannot be given. It may be thought that the chemical nature of the atoms which enter into the molecule, the dipole moments of the bonds, the polarizabilities and so on must in a substantial manner influence the character of the intermolecular interaction and determine the packing of molecules in the crystal. However, such is not the case: only the form of the molecule (the form of the electron cloud) plays the principal role in intermolecular interaction. The remaining properties of the molecule play a secondary and for the most part inconspicuous one. The packing of molecules in the crystal is determined by the geometric form of the molecule — moreover, minimum of energy is attained when the arrangement of molecules is the most compact.

---

* For references to preceding studies see the author's monograph "Organic Crystallochemistry," Akademizdat, 1955.

The existing theories of intermolecular interaction are correct only for distances much greater than the size of the molecule and are quite useless for predicting the character of powerful interactions of molecules in crystals. Our basic position on the character of the interaction of molecules consists, obviously, in assertions on the absence of directionality of the interaction and on the "local" character of the field of the molecule (i. e., the field of force of the molecule in the vicinity of a given atom does not depend on which molecule this atom enters). Consideration of the packing of rigid bodies is equivalent to the introduction of a square interaction potential (solid molecules, which are drawn into contact). Assumptions of such a nature concerning the character of the interaction must lead to the closest arrangement of adjacent molecules.

As a rule, not one but several close packings can be selected, differing little in density. In the choice of one of these packings secondary factors can enter – such as the dipole interaction of the atomic groups established.

In fact, the basic parameter which influences the free energy is the closeness of packing, which is attained by the disposition of an atom of one molecule between the atoms of the adjacent molecule (the principle of "projection into the hollow").

2. Closeness of Packing and Symmetry

Analysis of organic crystallochemical data leads to the conclusion that together with an increase in density of packing, an increase in the symmetry of the position of a molecule in the crystal, as well as an increase in the symmetry of the crystal, contribute to a decrease in free energy.

With rare exceptions, one symmetrically independent molecule is contained in the cell of a crystal. There is no doubt that an increase in the number of independent molecules is connected with an increase in free energy.

The indicated tendencies can be in conflict both among themselves and with a tendency toward close packing. In a number of cases the gain in symmetry compensates for the loss in density of packing. It is understood that opposite cases are to be met with. We do not have measurements of the decrease in free energy with an increase in symmetry and density, although experiment leads us to certain empirical rules.

As we have shown earlier, the preservation of an inversion center in a crystal does not in itself involve sacrifices of the density of packing. Therefore, a molecule possessing among its own elements of symmetry a center of inversion always retains it in a crystal.

The preservation in a crystal of the elements of symmetry 2 or m is connected with a small loss in density of packing. It appears that in the majority of cases the gain in symmetry reduces the free energy enough to compensate for the increase due to the loss in density. The preservation by a molecule in the crystal of a higher symmetry is connected with a very substantial loss in density and energetically is not profitable.

The considerations indicated make it possible to predict the symmetry of the crystal and the number of molecules in the cell. They explain the distribution of organic elements with respect to the space group. We shall not dwell on these questions here, since they are detailed in earlier papers and in the author's monograph.

We shall take up the question of phases of different crystalline forms for one substance. Two modifications frequently exist under the very same conditions. One of these is unstable. We hold that the unstable modification has either a less compact packing or a lower symmetry or both.

Up till now we have spoken of the effect of density of packing and symmetry on the free energy as a whole. Now we go further and make the following assertion: the internal energy of a crystal constructed from molecules depends basically on the packing density of the molecules, the symmetry of arrangement of the molecules being expressed only by entropy.

This hypothesis follows, it seems to us, from the concept of the "local" character of the molecular interactions. The internal energy is the sum of the elementary interactions of the "surface" sections of the molecules.* It is understood that in such a concept the symmetry of the arrangement of the molecules does not affect the magnitude of the internal energy.

---

* Such a viewpoint can be greatly reinforced by data on the heat of sublimation. It is found that the surface area of a molecule and the molar heat of sublimation change together.

According to the position taken, the entropy increases with an increase in symmetry. This happens because with an increase in symmetry the "volume" of the vibration of the molecule increases — the area of Gibbs' space occupied by the molecule is increased.

A phase transition on an increase in temperature is accompanied by an increase in the internal energy and entropy. From the viewpoint stated it must then follow: in a phase transition on an increase in temperature the volume of the cell must increase. This rule is usually fulfilled. In the case of rare exceptions one parameter (the volume of the cell) is obviously insufficient for characterizing the density of packing.

As for the entropy, however, it must be borne in mind here that the symmetry is only one of the factors which determines the "volume" of the vibration of the molecule. Therefore, an increase in entropy need not be accompanied by an increase in symmetry. A reduction in symmetry in the transition to a high-temperature phase also does not contradict our viewpoint, although such cases should be less frequently encountered.

3. Solid Solutions

Thus the properties of symmetry and close packing are quite sufficient for understanding the structure of an organic crystal. We find nothing of the kind in metallic and inorganic crystals, where the interatomic electron bonds can completely overwhelm the symmetry and close packing factors. An attempt can be made therefore expressly for organic substances (not applicable to other classes of compounds) to formulate a rule for the formation of solid solutions.

In organic crystals, substitution solid solutions are of chief interest. A foreign molecule is free to replace a molecule of the basic crystal if the molecules of these types are close in form and dimensions. The closeness of the atomic dimensions in inorganic and metallic crystals is a necessary condition for the formation of substitution solid solutions. In organic crystals the condition of closeness in form and dimensions of the molecules is necessary and sufficient.

However, it is considerably more difficult to characterize the isomorphism of molecules quantitatively.

Analysis of existing experimental data shows that substance A is dissolved in substance B under the following conditions. Imagine that one molecule of substance B is removed from the crystal. Into the freed space in the ideal structure of crystal B we insert molecule A. If the substitution can be accomplished with about the same number of contacts and with the preservation of the intermolecular radii within the permissible limits, then solid solutions are formed by combination.

The allowable limits of the intermolecular radii of H, C, N and O atoms are the respective values 1.05-1.35; 1.65-1.85; 1.45-1.65 and 1.30-1.50, all in A.

Substitution solid solutions of organic substances are also possible with unlimited solubility. However, for the formation of such solutions, isomorphism of the molecules is a necessary but not sufficient condition.

If molecules A and B are close in dimensions and form, then molecules A can replace molecules B in the crystal. During substitution the symmetry of arrangement of the molecules in crystal B can either stay the same or change all at once with the entry into B of the first molecules A.

The symmetry of arrangement of the molecules in crystal B can stay the same in the following cases: a) if molecule B occupies an asymmetrical* position in the crystal, then for any symmetry of molecules A; b) if molecule B occupies a nonasymmetrical position in the crystal, then for nonasymmetrical molecules A or with the presence of an equal number of left- and right-handed forms of molecules A.

The symmetry of arrangement of the molecules in a crystal changes all at once with the entry into solution of the first molecules A, if molecule B occupies a nonasymmetrical position in the crystal, and molecules A are asymmetric (one of the enantiomorphous forms).

Let A be soluble in B and B in A. With closely similar forms of molecules a continuous series of solid solutions is possible in the following cases: a) if the symmetry of arrangement of the molecules in crystals A and B is the same; b) if the symmetry of arrangement of the molecules in crystals A and B is different, but the symmetry of arrangement of the molecules in crystal B changes at once with the entry into crystal B of molecules A (this will be so in particular with a solution of asymmetrical molecules in a racemate).

---

* An asymmetrical position or body contains neither a center of inversion nor mirror planes of symmetry.

A continuous series of solid solutions is impossible if the symmetry of arrangement of the molecules in crystals A and B is different and, in addition, molecules A enter into B, not changing the symmetry of arrangement of the molecules in crystal B, and molecules B enter into A, not changing the symmetry of arrangement of the molecules in crystal A. In this case there are two solid phases and consequently there is also interruption of solubility.

If the asymmetrical molecules are ignored, then it may be said that the necessary condition for the formation of solid solutions in all proportions (this refers to all three types of continuous solid solutions) is identical symmetry of the mutual arrangement of the molecules of miscible substances, i. e., the same space groups and number of molecules in the cell.

Examples of organic substances are known where not only are the molecules very much alike in form and dimensions, but the packing of the molecules is also very similar. If with this similarity there is nevertheless a difference in the symmetry of the mutual arrangement of the molecules, then a continuous series of solid solutions becomes impossible. At some range of concentrations there must be a discontinuity in solubility or, to put it differently, continuous change of concentration in the solid state is possible only through a phase transition (as a rule, a transition of the first order).

Thus, up to a certain percentage molecules B are distributed in the crystal structure A; at the other end of the composition diagram crystals of solid solutions are formed where molecules A are distributed in the crystal structure B.

The closer the molecules of such crystals are in form and the more related their packing, the narrower the discontinuity of solubility should be. It is therefore no wonder that investigators did not notice this interruption and found a continuous series of solid solutions of types I and III where as a matter of fact there were respectively solutions of types IV and V (according to Roozeboom).

An exceedingly large number of systems are described erroneously in the literature as continuous solid solutions.

Thus, for example, the following systems are incorrectly attributed to a solid solution of type I (data taken from Landolt):

anthracene—carbazole,
anthracene—phenanthrene,
benzene—thiophene,
heptadecane—hexadecane,
heptadecane—octadecane,
diphenyl—3-fluorodiphenyl,
dibenzyl—stilbene,
dibenzyl—tolane,
naphthalene—β-naphthol.

Erroneously attributed to type III:

acridine—anthracene,
acridine—phenanthrene,
azobenzene—dibenzyl,
naphthalene—β-chloronaphthalene,
1,5-dinitronaphthalene-1,8-dinitronaphthalene,
1,5-dinitronaphthalene—1,8-trinitronaphthalene,
diphenyl—2-fluorodiphenyl,
diphenyl—3-fluorodiphenyl.

In a number of cases the rules of organic crystallochemistry permit the prediction of the possibility or impossibility of complete miscibility in the absence of data on the symmetry of the crystal cells. Actually, in centrosymmetrical molecules a center of inversion in the crystal is retained. The type of structure formed by centrosymmetrical molecules never coincides with a structure created by molecules without a center of inversion. Such molecules cannot give a continuous series of solid solutions (naphthalene—β-chloronaphthalene, diphenyl—2-fluorodiphenyl, etc.).

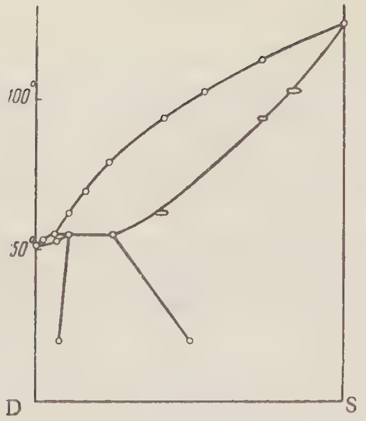

Fig. 1. Composition diagram of the dibenzyl—stilbene system (N. Ia. Kolosov).

These concepts have been verified by a study of the structure of monocrystals of the anthracene—phenanthrene, stilbene—dibenzyl and anthracene—acridine systems. All these systems have been described before as a series of continuous solid solutions. In accordance with expectations from the stated theory, these data have proved to be erroneous. The limits of solubility of the first component were found at 5% for the anthracene—phenanthrene system, at 8% for the anthracene—acridine system and at 25% for the dibenzyl—stilbene system. The composition diagram of the latter is shown in Fig. 1.

The study of the structure of these solid solutions shows that the substitution of molecules is random, quite in the same way as in metallic crystals.

The entry of a foreign molecule into the crystal is subject only to the requirement of the best packing. This means that a foreign molecule is placed so that the deviation of the intermolecular distances from the normal should be a minimum. From this point of view the rapid change in the form of the cell at the point of insolubility is also explained. A specific analysis for the three systems referred to will be published in other papers.

4. Geometric Derivation of the Possible Structure of a Crystal

Geometric analysis of the structure of an organic crystal as a means of determining the packing of the molecules was widespread at the time of our first work in this field (1946). A great many examples of its use are given in the author's monograph.

Geometric analysis is usually thought of as a means of finding the packing of the molecules in a crystal from data on the dimensions of the cell and the framework of the molecule. While examining all the possible mutual orientations, we come to an arrangement of molecules such that the structure represents a molecular close packing.

In the monograph referred to there may be found a great number of examples which show that geometric analysis gives results in excellent agreement with the results of a quantitative structure analysis based on x-ray intensities.

In the case where a molecule is found in a general position in the cell of a crystal, geometric analysis is for the most part not well-defined. If, however, the molecule is deprived of successive degrees of freedom, then, as a rule, geometric analysis permits rapid determination of the molecular packing.

The success of geometric analysis in organic crystallochemistry is explained by the peculiarities of the interaction forces between molecules stressed above, leading to the fact that the minimum of energy is determined in the first instance by the closeness of the packing and by the possibility of realizing a maximum number of contacts between adjacent molecules.

This does not of course mean that other factors do not affect the structure of a crystal. Geometric analysis explains the orientation of the molecules in a given cell; the selection of the form of the cell is obviously determined by features of the interaction potential of the molecules which do not yield to calculation.

However, in the case of symmetrical molecules of simple form, the general concepts of the theory of close packing of the molecules prove to be sufficient not only for predicting the arrangement of the molecules in the cell, but also for predicting a very limited number of possible forms of the unit cell. In other words, in the simplest cases the form of the molecule roughly determines two or three possible crystal structures.

The derivation of possible crystal structures proceeding from the form of the molecules is interesting. Among the packings derived by geometric analysis we find those which are achieved by nature. It is possible that under other thermodynamic conditions other geometrically permissible structures are also realized. Such a derivation "explains" the structures of the different phases which exist (i. e., demonstrates their energy advantage), predicts the possible existence of other modifications and, finally, encourages establishment of empirical rules connecting a change in the character of the molecular packing with an increase or decrease in energy and entropy.

It must be emphasized once more that a similar broadening of the field of application for geometric analysis is possible only for simple and symmetrical molecules.

5. The Packing of Infinite Aliphatic Chains

a) Statement of the problem. This section serves only to illustrate the possibilities of a geometric basis and derivation of structure; at the same time, however, the considerations given below are a part of the author's work on the packing of chain molecules.

Examination of the crystal structures of chain molecules is aided greatly by the following, which we shall use as a starting point: crystals of chain molecules consist of layers composed of parallel molecules. Analogously, the crystalline regions of polymers consist of parallel molecules.

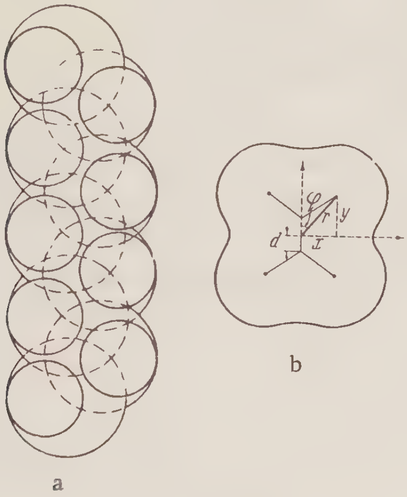

Fig. 2. Model of aliphatic chain. a) View perpendicular to axis of chain; b) view along axis of chain.

The problem of the packing of molecules breaks down into two questions: concerning the packing of molecules in a layer and the packing of the layers. For high polymers the second question is superseded by the problem of the linking of the crystalline regions. We shall dwell here only on the question of the packing of aliphatic molecules in layers without taking into account the effect of the end groups.

The form and dimensions of a normal aliphatic zigzag are shown in Fig. 2. As the diagram shows, the cross section of the molecule is fairly round; the intermolecular domains of the hydrogen atoms form small projections, two for each "storey." The structure of the chain is repeated at a distance of $2\Delta = 2.53$ A through a "storey," while, looking along the normal to the plane of the zigzag, the hydrogen "projections" alternate right and left.

For our reasoning, which aspires only to the derivation of the rough structure, the precise values of the interatomic distances and the intermolecular radii are not essential. We shall use for the intermolecular radii the values $R_H = 1.30$ A and $R_C = 1.85$ A, and for the parameters of the molecules the values: $r = 1.37$ A, $\varphi = 40°$ ($x = 0.88$ A, $y = 1.05$ A) and $d = 0.425$ A.

Three types of packing of chain molecules are possible. If the chains are arranged randomly along the azimuth (revolving near their own axes), then the cross section of the chain on the average is circular and circular (hexagonal) packing arises. In the case of a molecule of arbitrary cross section two types of most compact layers are possible: with an oblique-angled and with a right-angled cell. If the cross section of the chain is represented by an outline, then Fig. 3 gives all three types of packings. The hexagonal packing of chains ("rotating chains") is found in a series of paraffins at temperatures close to the melting point.

b) Arrangement of two adjacent chains. In order to examine the packing of nonrotating chains, we proceed as follows. We find the mutual arrangement of two translation-identical (parallel) molecules, separated by the maximum interatomic and intermolecular distances.

It is obvious that the length of a translation is a function of the angle α, formed by a translation (or its orthogonal projection) with the plane of the zigzag, and also of the mutual displacement of the molecules along the chain. Examining this function closely with the help of the diagram and models, we find only four such translations: translations t, t_1 and t_2, perpendicular to the axis of the chain, and translation t_k, operating at an angle to the chain. In the latter case the molecules are displaced with respect to one another by a "storey" of the chain. Corresponding arrangements of molecules are shown in Fig. 4.

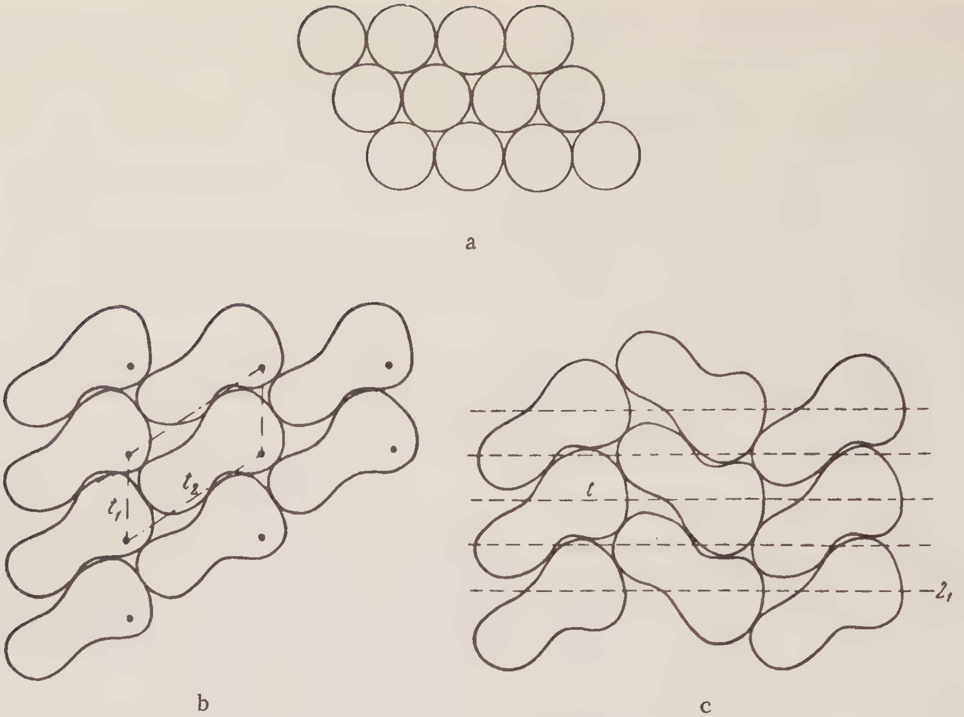

Fig. 3. Three possible types of close packing of chain molecule cross sections. a) Hexagonal cell; b) oblique-angled cell; c) right-angled cell.

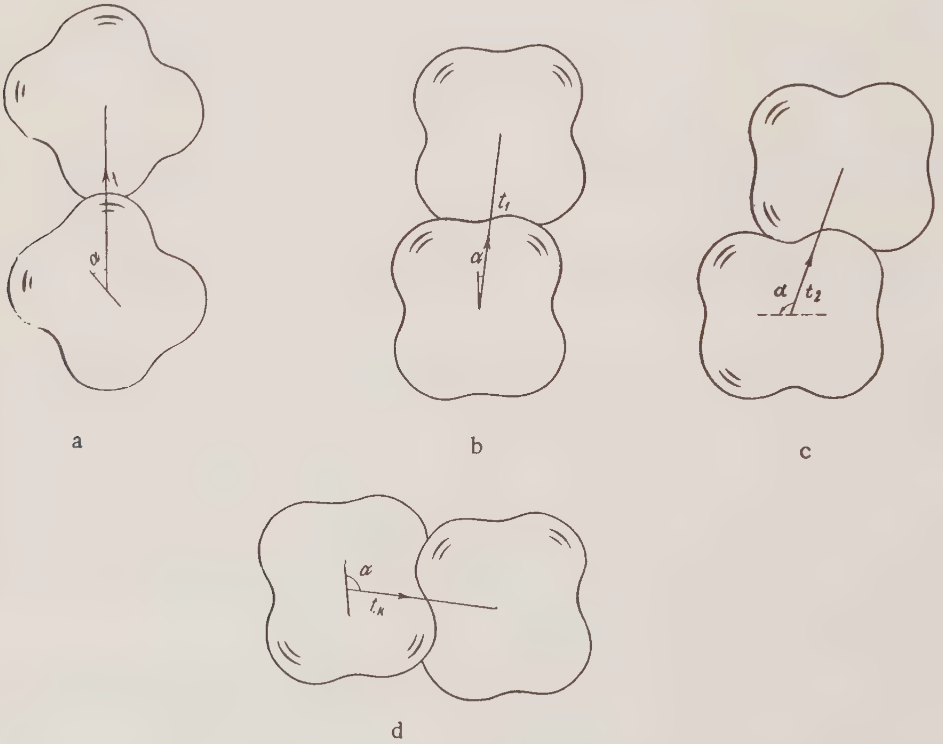

Fig. 4. Possible mutual arrangements of chain pairs. a) Translation t = 5.00 A, $\alpha = 40°$; b) translation $t_1 = 4.32$ A, $\alpha = 7°$ (with a small change in values of intermolecular radii the extremum arises with $\alpha = 0°$); c) translation $t_2 = 4.19$ A, $\alpha = 110°$; d) translation t_k; $(t_k)_{pr} = 3.98$ A, $\alpha = 100°$.

Translation t. In this the arrangements $\alpha = \varphi$ and $t = 2r + \sqrt{(2R_H)^2 - \Delta^2}$ are determined by the contacts of the hydrogen atoms. For standard dimensions this yields $\alpha = 40°$ and t = 5.00 A.

Translation t_1. The length of t_1 and angle α are determined from the conditions of equality of C . . . H and H. . .H distances by the equations

$$t_x^2 + (t_y - 2y)^2 + \Delta^2 = (2R_{\mathrm{H}})^2$$

$$(x - t_x)^2 + (t_y - y - d)^2 + \Delta^2 = (R_{\mathrm{C}} + R_{\mathrm{H}})^2.$$

For standard dimensions this yields α, close to zero; in particular, $\alpha = 7°$, t = 4.32 A.

Translation t_2. In this case the arrangement is determined completely by the H. . .H contacts – a hydrogen atom of one molecule (across a storey!) touches simultaneously three hydrogen atoms (one in the same storey, one in the storey above and one in the storey below) of another molecule. The translation vector is determined from the conditions

$$t_y = \frac{(2y^2) + \Delta^2}{4y}, \quad t_x = 2x + \sqrt{(2R_{\mathrm{H}})^2 - t_y^2}\,.$$

For standard dimensions this yields angle $\alpha = 110°$ and $t_2 = 4.19$ A.

Translation t_k. As in the preceding case, a hydrogen atom of one molecule touches hydrogen atoms of the adjacent molecule. However, unlike the previous case, hydrogen atoms of each storey are found in similar close contact. Translation t_k stands out from the others by the closeness of the contact. The condition t_k is determined by equations of the contacts:

$$t_y = \frac{(2y)^2 - \Delta^2}{4y}, \quad t_x = 2x + \sqrt{(2R_{\mathrm{H}})^2 - \Delta^2 - t_y^2}\,.$$

For standard dimensions $\alpha = 100°$ and the orthogonal projection of t_k equals 3.98 A. Hence the length of t_k equals $\sqrt{(3.98)^2 + (1.26)^2} = 4.17$ A.

c) Packings. With the help of the indicated translations we can construct layers with oblique-angled and right-angled cells. Proceeding in this way we assume that the advantage of the arrangement of two separate chains is also maintained collectively. The form of the molecule is such that the possible translation vectors are readily combined. The possible combinations result in two layers; layer t_1t_2 differs little from tt_2, and both of these layers are close to t_1t_2.*

As regards the right-angled layers, then, as follows from the considerations given in the author's monograph, a layer of symmetry 2_1t can be constructed with the help of any translation. The possible layers therefore are 2_1t, 2_1t_1 and 2_1t_2; layer 2_1t_k is impossible, since it leads to a lack of parallelism between the molecules.

Axis 2_1 can, generally speaking, be directed either perpendicular or parallel to the principal translation. Such a pair of layers will have identical projections. Their difference results only in the necessity of changing here and there the adjacent CH_2 groups of a molecule, translated by axis 2_1, which face to the right and to the left. If in any diagram representing layers 2_1t we wish to turn axis 2_1 by 90°, then it is only necessary to cross-hatch another pair of hydrogen atoms of a molecule translated by axis 2_1. Of the two possible arrangements of axis 2_1, one can always be chosen which will lead to a more compact structure. In this way there emerge three possible right-angled layers (5 layers altogether), shown in Fig. 5.

The areas of the cells, more accurately the areas of the orthogonal cross sections, which fit into one chain, are almost equal. However, the oblique-angled layers are noticeably more compact – in both layers there must be 16.2 A^2 per molecule. Three ideal right-angled layers with angles $\alpha = 7°$, 40° and 110° have areas per molecule of 17.5, 18, and 19 A^2, respectively.

What does experiment show? The packing of infinite aliphatic chains occurs for polythene. This packing is the type shown in Fig. 5, b. The structure is always close to the theoretical: the same direction of axis 2_1,

---

* As in original – Publisher's note.

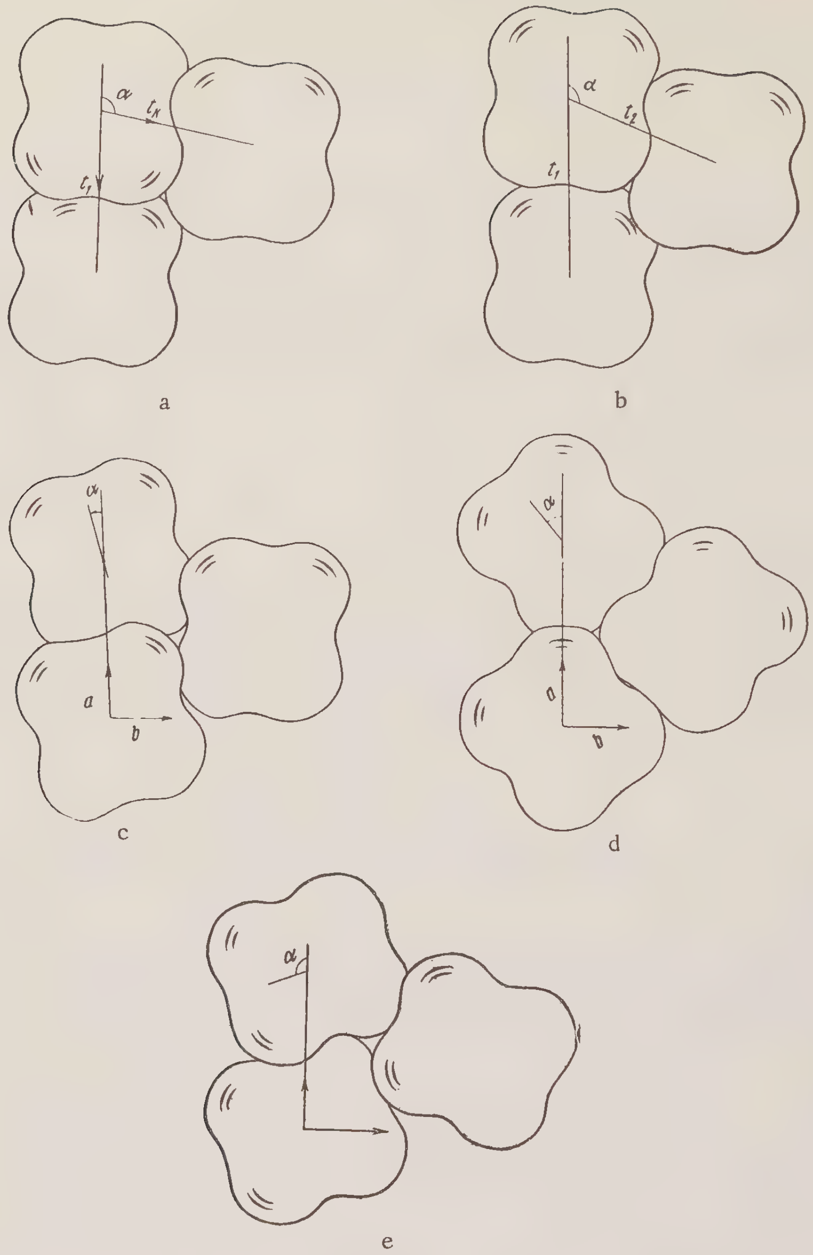

Fig. 5. Possible packings of cross sections of aliphatic chains. a) Oblique-angled cell t_1t_k; t_1 = 4.32 A, t_k = 4.17 A, α = 107° (or less down to 100°); b) oblique-angled cell t_1t_2; t_1 = = 4.32 A, t_2 = 4.19 A, α = 117°; c) right-angled cell, a = 4.35 A, b = 8.04 A, α = 7°, axis $2_1 \parallel$ a; d) right-angled cell, a = 5.00 A, b = 7.16 A, α = 40°, axis $2_1 \parallel$ b; e) right-angled cell, a = 4.20 A, b = 9.04 A, α = 110°, axis $2_1 \parallel$ b.

the same angle α, the same length of the short axis. The difference is in the long axis, which is longer by 0.2 A than the theoretical magnitude. It is understood that better agreement is not to be expected when using the assumption of a standard intermolecular sphere.

It is quite possible that under other thermodynamic conditions other forms of polythene result. The existence of a more compact polythene with an oblique-angled cell is especially probable.

Received February 22, 1957

Institute of Heteroorganic Compounds

X-RAY DIFFRACTION DETERMINATIVE TABLE OF MINERALS

V. I. Mikheev*

The development of exact and objective methods for mineral identification is one of the essential needs of mineralogy. Any such method is based on measuring one or several physical quantities. Factors that affect the practical value of a method are the quantity of the material needed for analysis, the complexity of the apparatus and of the manipulations connected with determining the mineral's properties, the cost of the material analyzed, and the independence of the method from the state of aggregation of the material (dispersion, intergrowth, face development of crystals, etc.).

There are three crystallographic methods for identifying substances, particularly minerals: the optical method, which was developed quite early; the geometric method, applicable only to crystals with well-developed faces; and the x-ray diffraction method. All three methods are based on the most important properties of minerals, connected with their compositions and structures. Each of these methods is independent of the others, and the most generally applicable of them all is that of x-ray diffraction, which is equally suitable for either transparent or opaque minerals and does not depend on the face development and degree of dispersion.

The eminent crystallographer and mineralogist A. K. Boldyrev has stated the principle of the x-ray diffraction method of mineral identification: any two different substances or minerals differ in the geometric peculiarities of their inner structure, as well as in their chemical constitution.

According to A. K. Boldyrev the x-ray method of mineral identification was based on the analysis of powder patterns, and not on structure determination. The arrangement and intensities of the lines of its powder pattern are a function of the inner structure and chemical composition of the mineral.

Under A. K. Boldyrev's direction a group of authors has been developing since 1934-1937 the method of photographing, measuring and evaluating powder patterns, in order to provide greater accuracy in determining interplanar distances. In addition, a form of "key" was worked out — the basic determinative table — according to which a mineral could be identified when the unknown substance was specified by x-ray diffraction data.

As a result of these researches, a rational scheme was found for identifying minerals by x-ray diffraction. It consisted of three parts. The first was a basic determinative table — a key, which contained the five strongest lines of each mineral, together with its name, chemical formula and a number under which the powder pattern of the mineral was described in detail in the second part.

All the minerals in the key are arranged in order of decreasing interplanar spacing of the most intense line. In addition, interplanar spacings and relative intensities for four other intense lines of the powder pattern of each mineral are given in each line of the key. In the second part, along with detailed descriptions of the power patterns of minerals, are given the most important physical and chemical properties, the symmetry types and space groups, the sizes of the unit cells and literature references. The third part is an alphabetical index of the minerals contained in the determinative table.

The first issue of the x-ray diffraction determinative tables came out in 1938, and included data for 142 minerals.

In 1939, V. I. Mikheev and V. N. Dubinina brought out a second issue of the tables in the same form, which included data for 146 minerals. These two issues represented the first practical method for identifying substances by x-ray diffraction.

---

* Deceased.

Soon afterwards such tables also began to appear abroad. In 1938 Hanawalt, Rinn and Frevel of the U. S. issued a powder pattern handbook for 1000 substances, in which were included 53 minerals and 75 substances corresponding in chemical composition to minerals. No key was given to this work; therefore, it cannot be considered as a determinative table.

In 1942 Harcourt issued a determinative table for 163 ore minerals.

The first issue of the American x-ray diffraction index appeared in 1943, based on the data in Hanawalt, Rinn and Frevel's work. It consisted of 4000 cards, but in number of minerals was inferior to the Soviet issues of 1938 and 1939.

The second issue of the American index came out in 1944 based on the material which had appeared in the literature. The Soviet powder patterns issued in the x-ray diffraction determinative tables were included. This first supplementary card index included 1400 substances of which 600 were minerals.

In 1953 the Portuguese determinative tables appeared, based on the material of the one which appeared in 1938, and supplemented with new data. It embraced 257 minerals. Its new features were the tables for the needle-shaped and flaky minerals, constructed on the basis of identity period along the fiber axis or perpendicular to the tablet plane.

At present we have two new issues ready. One of them, embracing 905 minerals, is in press, and the other, covering 300 minerals, is ready for press. The new issues are supplemented with a "mineral index," in which interplanar distances for the three most intense lines are given for each mineral. Unlike the determinative table of the "key" which makes possible the identification of a mineral systemically, the new "index" allows for the rapid checking of a sample of such minerals, the presence of which can be assumed on the basis of chemical composition, conditions of formation, or for other reasons.

This determinative table of minerals is the basis for the x-ray diffraction identification of substances.

This method has some advantages over others. They are as follows:

1. The simplicity of the method.

2. The quantity essential for the identification of a substance is 1000 times smaller than that required for chemical analysis.

3. The substance is not destroyed as a result of its identification.

4. As a result of the identification, a powder pattern remains which is an objective record of the accuracy of the analysis.

Its limited applicability for noncrystalline substances and the incompleteness of the determinative table can be regarded as disadvantages of this method.

The x-ray diffraction method can be applied successfully not only to mineral identification, but also to the analysis of complex mineral mixtures.

It can also be applied in the following areas of research:

1. Distinguishing and identifying minerals and the components of mineral mixtures.

2. Polymorphic transformations.

3. Phase transformations in all their varied manifestations in the processes of the mechanical and technological treatment of minerals and ores, and in general, of any crystalline materials.

4. Investigation of equilibrium diagrams.

5. Solid solutions and isomorphous substances.

6. Finely dispersed clay minerals.

7. Cement minerals and the manufacture of concrete.

8. Ocherous iron ores, aluminum, manganese, vanadium, wolfram, molybdenum, lead, antimony, arsenic, bismuth, uranium.

9. Gossan minerals of sulfide origin.
10. Secondary changes in minerals and ores; in particular, the mechanisms of such changes.
11. Rare earths and radioactive ores.
12. Metals and alloys.
13. Coal and the processes of metamorphism of coals.
14. Glasses, ceramics and stone casting.
15. Products of chemical manufacture and control over technological processes.
16. Correlation of the outline strata of clay and of sandstone with the mineral content of thin sections.
17. Composition of meteorites.

The correlation of the numerous data incorporated in the new issue of the determinative table made possible the finding of mathematical relations between the chemical compositions and the sizes of the unit cells for isomorphous groups of minerals. The size of the cell is a function of the average cation radius for many isomorphous series. At present, the formulas of the following groups of minerals have been found:

1. Nickeliferous iron (kamacite) $(Fe_{1-x}Ni_x)$, $a = 2.86124 + 0.00041\,x$.

2. Pyrrhotite $(Fe''_{1-x}Fe'''_{2/3x})S$, c = 9.655 + 2.50 r, where r is the average radius of iron.

3. Oxides of divalent metals with the sodium chloride structure, a = 2.632 + 2.095 r".

4. Spinels with the general formula $(A''_{1-x}B'''_{\frac{2x}{3}})B'''_2O_4$, which takes into account the possible excess of trivalent oxides, a = 5.778 + 0.95 r" + 2.79 r"', where r" is the average radius of the tetrahedral cations, and r"' is the average radius of the octahedral cations.

5. Carbonates $(Ca_{1-x}Mg_x)CO_3$, $d_{10\bar{1}4} = 1.989 + 1.12\,r''$.

6. Olivine $(Mg_{1-x}Fe''_x)_2SiO_4$, $c = 5.972 + 0.100\,x$.

7. Garnet $A''_3B'''_2Si_3O_{12}$, $a = 9.125 + 1.560\,r'' + 2.000\,r'''$.

8. Mica $d_{060} = 1.396 + 0{,}1821 \cdot r_{oct}$, where r_{oct} is the average radius of an octahedral ion.

9. Chlorites $Mg_{6-x-y-z}Fe''_z(Al, Fe''')_{x+2y}\{Al_xSi_{4-x}O_{10}\}[OH]_8$, $b = kr$, , where r is the radius of the octahedral cations of the talc layer; c is some function of x.

10. Ilmenite $Fe''_{1-x}Fe'''_{2x}Ti_{1-x}O_3$, $a = 4.356 + r_{oct}$.

The establishment of the analytical dependence between the composition and the parameters of the cell broadens greatly the possibilities of the x-ray diffraction method in mineralogy, because the objects of study are almost always substances of variable composition. It is applicable even to the most difficult cases of isomorphous series.

The x-ray diffraction method of identifying substances originated in crystallography and in mineralogy where its first practical application was discovered, but its scope is much broader than the problems of either. It can be successfully applied in such wide fields as geological exploration, metallurgy and metallography, chemical manufacturing, the cement and ceramics industry, physical and organic chemistry and the production of plastics, the textile and synthetic fiber industries, the food industry and medicine.

Further expansion of the method should proceed along the following lines:

a) greater accuracy in determining interplanar distances and simplifying the technique of preparing and evaluating the diffraction patterns;

b) increase in the number of standard patterns of minerals and of substances in general, with a view to amplifying the determinative table of minerals and substances; the development of principles for setting up a determinative table for metals and alloys;

c) the creation of objective and simple methods of measuring intensities, so that the x-ray diffraction method may be used for quantitative evaluation of the compositions of the components in mixtures.

Received February 22, 1957

Leningrad Institute of Metals

CONCERNING THE PECULIARITIES OF THE COLLAGEN STRUCTURE

N. S. Andreeva, N. G. Esipova, and M. I. Millionova

Experimental evidence was obtained for the existence of heteropolymers, containing mainly iminoacid residues and glycine in some parts of the collagen molecule and determining the specific folds of the chains. The water molecules in these parts are at a distance of about 3 A from the chain axis and appear to stabilize the structure. Hydrogen bonds of OH groups of hydroxyproline with carbonyl oxygen are the intramolecular bonds. Detailed description of these studies will be published in the journal Biofizika Vol.2, No. 3, 4, 5 (1957).

One of the important divisions of protein research is that of the laws of the geometry of polypeptide chains. In this area, structural studies of proteins of the collagen group, to which much attention has been devoted in recent years, are of considerable interest. These proteins are distinguished by the fact that their molecular chains in isolated regions have a highly specific configuration, differing sharply from that of all other proteins.

At present, a wealth of experimental material has been accumulated concerning the different structural characteristics of collagens [1-3]. On the basis of these data hypothetical atomic models of the polypeptide chains of these proteins have been worked out [1-7]. Recently a model was constructed which agrees most successfully with certain x-ray diffraction and physicochemical data [3, 6, 7].

Although this model is without doubt the most successful of all those offered recently, the premises which were accepted as the basis of its construction are as yet of a hypothetical nature. Therefore, experimental studies that would establish these premises directly are essential.

It is natural to assume that the special structural form of the collagen chains is conditioned by their chemical composition; nevertheless there are reasons to think that water takes part in the stabilization of their special configuration [8].

In order to determine the conditions necessary for the existence of the special structural form of collagen chains, we undertook studies of the dependence on various factors of the quantitative content of this special form.*

X-ray patterns of proteins of the collagen type are characterized by a group of interferences, among which the strong meridional reflection with d = 2.9 A and the equatorial with d = 11.5 A stand out. These interferences bring to mind somewhat diffuse Debye rings. Apparently, their integrated intensity and height above background in different samples must, to a certain degree, be a measure of the concentration in them of the special structural form, or, in other words, be a measure of the concentration of the "ordered phase."

To determine the peculiarities of the chemical composition of the molecular regions with the special chain configuration, the dependence of the quantity of the "ordered phase" in different collagens on their amino acid composition was studied.

In order to elucidate the role of water in a specific configuration of collagen chains, the dependence on moisture content of the quantity of the "ordered phase" of collagens was studied. At the same time the character of the intensity redistribution of the interferences of x-ray patterns was studied, as well as the change in the infrared absorption spectra.

---

* These questions are discussed in more detail in our studies published in the journal Biofizika Nos. 3 and 4, (1957).

In all cases the photographing of the x-ray patterns was made using monochromatic CuK$_\alpha$-radiation, obtained by reflection from a pentaerythrite monocrystal. The intensity of the reflections were measured photographically. In each case, a series of patterns was taken to minimize the incidence of error and the average values of the magnitudes measured were determined.

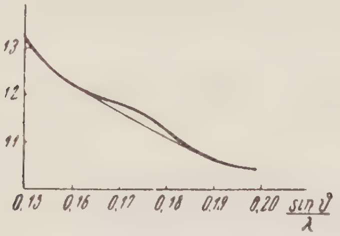

Fig. 1. Intensity distribution in the maximum with d ≈ 2.9 A for spongin.

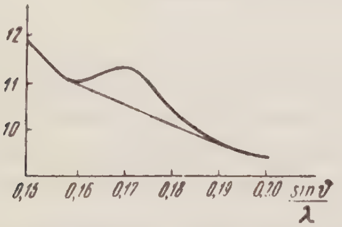

Fig. 2. Intensity distribution in the maximum with d ≈ 2.9 A for the collagen of cod skin.

In analyzing the dependence of the quantity of the "ordered phase" of collagen on the chemical structure of their polypeptide chains, samples were used, the amino acid composition of which varied within relatively wide limits. The following proteins were studied: collagen RTT, procollagen prepared by the Orekhovich [9] method, collagen from the skin of pike, cod and spongin. The data on the amino acid composition of these samples were taken from references in the literature [2, 9-11]. The samples were photographed in a disoriented condition, 10 microphotopatterns for each, and were then reduced to absolute units of scattering, for which purpose the elementary composition of the samples was expressly determined.

The structural changes during the moistening of the preparations were studied on two objects: oriented samples of RTT collagen and on unoriented films of procollagen. When photographed, the moist preparations were placed in special boxes with windows of thin monocrystal mica in which a definite tension of saturated vapor was preserved. The photographing was done with an intensity standard. The study of infrared absorption spectra was done using procollagen films.

Measurements of the integrated intensities and of the heights of the maxima of the interferences for various collagens led to the following results:

The intensity distribution in the maxima with d = 2.9 A and d = 11.5 A is different in different proteins (see Figs. 1 and 2). It was shown further that there is a definite dependence of the quantity of "ordered phase" on the content of definite groups in the protein, namely, on the general content of imino acids and glycine. A certain dependence on alanine was also observed.

Figures 3 and 4 show graphs of the dependence of the measured magnitudes on the general content of imino acids, expressed in weight percentages. Figure 5 shows a graph of the dependence of the height of the maxima with d = 11.5 A on the content of imino acid and glycine, expressed in moles of residue in 10^5 g of protein.

In studying the influence of moisture on the structure of collagen the following results were obtained:

A general decrease in the intensity of the reflections of the "ordered phase" as moisture was removed from the protein. The emergence of a diffuse ring in the $\frac{\sin \vartheta}{\lambda} \approx 0.11$ region was observed simultaneously. These effects were observed particularly clearly on procollagen. At the same time, a weakening was observed of the absorption band of the NH group at 3330 cm^{-1}, characteristic of the fold of the collagen chain, and a strengthening of the absorption band at 3200 cm^{-1}, characteristic of the amorphous part of the protein.

Simultaneously, with the general decrease in diffraction intensities from the "ordered phase" their redistribution was observed. This applies mainly to the equatorial reflections with d ≈ 11.5 and d ≈ 5.8 A. As moisture was removed from the protein the intensity of the reflection with d ≈ 5.8 A increased in relation to that with d ≈ 11.5 A. A sharp weakening of the intensity of the reflection at d ≈ 4 A was also observed.

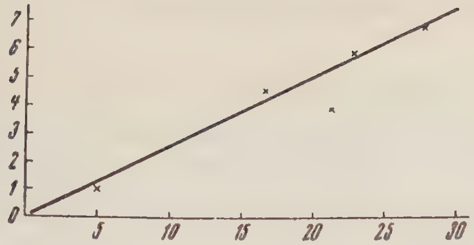

Fig. 3. Dependence of the integrated intensity of the interference with d ≈ 2.9 A (on the meridian) on the general concentration of imino acids in g per 100 g of protein.

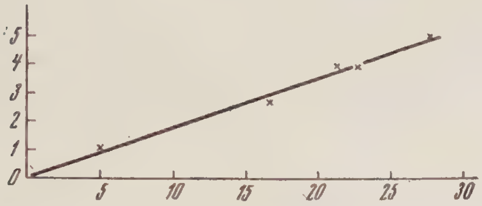

Fig. 4. Dependence of the height of the maxima at d ≈ 10 A on the general concentration of imino acids in g per 100 g of protein.

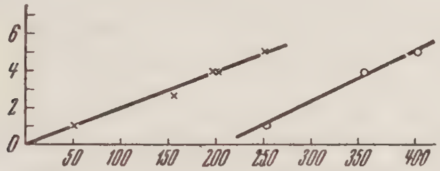

Fig. 5. Dependence of the quantity of "ordered phase" on the general concentration of imino acids (on the left) and glycine (on the right) expressed in moles of residue per 10^5 g of protein.

The data obtained can be interpreted as follows:

1) The imino acid residues are the essential elements of the special configuration of collagen chains. This is substantiated by the regular decrease down to zero of the quantity of the "ordered phase" in collagens as the general concentration in them of imino acid residue decreases. Insofar as there is no hydroxyproline in spongin, according to the data [11] available, the specific configuration of collagen chains must be determined in the main by the stereochemistry of the pyrrolidine rings. The hydrogen bonds of the OH groups of the hydroxyprolines with carbonyl oxygens evidently give only an additional stability to the configuration already assigned. The results of Gustavson's studies can be explained in those terms. According to our and Shpikiter's data,* these bonds are intermolecular, since for molecular solutions of collagen there is a temperature dependence of denaturation on the hydroxyproline concentration, analogous to that obtained by Gustavson for whole samples [10].

With a decrease in the quantity of imino acids in the samples studied, there was a parallel decrease in glycine. It was discovered that the glycine decrease is rectilinear in character, and that the slopes of the graphs showing the dependence of the quantity of "ordered phase" on the concentration of imino acids and glycine, expressed in moles of residue per 10^5 g of protein, are alike. If one were to consider the chemical data which point to the frequent correlation of imino acid and glycine residues in peptides isolated from collagen, then such a dependence is not accidental. If the amino acid composition be taken as a basis, then the growth of the quantity of the "ordered phase" in collagens is always connected with a similar growth in the quantity of glycine and imino acid residues. This agrees with a 1 : 1 ratio of glycine to imino acid residues in the regions with the ordered structure. However, for an exact determination of this ratio, samples in which the content of glycine varies while that of the imino acids remains constant are essential.

According to the analysis of the data obtained, there can be a considerable quantity of the "ordered phase" in some collagens when the content of alanine is zero or very small. Therefore, alanine cannot be a determining structural element of the special configuration of collagen chains. Apparently, the same can be said of other amino acids, inasmuch as no definite dependence was obtained for them.

The results allow us to conclude that a polymer containing imino acid and glycine residues determines the special configuration of collagen chains in separate regions of the molecules. These molecular regions can, apparently, contain a small amount of the residues of other amino acids, which do not play any determining structural role, but can successfully combine with them, or on the contrary, distort them. An analogous phenomenon was observed in the silk fibroins of Bombyx mori and Tussah, the chain configuration of which is determined by the glycyl-*l*-alanine polymer [12] in the first case, and *l*-alanine in the second [13].

The data obtained are a direct experimental proof of the correctness of some basic premises which were used in constructing the most recent and successful model of the collagen structure. However, there is no proof yet that every third residue in such regions is either glycine or alanine, which is the basic condition for the existence of the suggested configuration [3, 6].

---

* The work will be published in the journal Biofizika No. 4 (1957).

Recently, the results of the present work were confirmed by Grassman's [14] chemical researches.

The results of the x-ray studies of the process of moisture removal from collagen demonstrate the simultaneous partial amorphization of the protein. Consequently, water must contribute somehow to the stabilization of the "ordered phase" of the collagen. In regions containing imino acids and glycine, it must be so distributed as to scatter in phase with the planes separated by 11.5 A, and in antiphase with planes separated by 5.8 A. This is possible if water molecules are distributed at a distance of about 3 A from the chain axis. Such a short distance of water molecules from the framework of the polypeptide chain corresponds to the distance characteristic of hydrogen bonds. There are indications in the literature [8, 15] that it is possible for molecules of water absorbed by the protein to form hydrogen bonds with the protein itself. The results obtained also agree with a series of physicochemical studies on the hydration of collagen which point to the special role of the random hydrogen bonds of the carbonyl groups of the imino acid residues in the sorption process of water with this protein [2, 16-18].

We assume that further analyses of the structure of collagen must be along the line of studying the structures of polymers containing imino acid and glycine residues and including water molecules as a structural element.

The authors take this opportunity to express their gratitude to Professor V. I. Iveronova and V. N. Orekhovich for their valuable advice and comments.

SUMMARY

1. The dependence of the quantity of the "ordered phase" in various collagens due to different factors is analyzed in order to clarify the causes which condition the presence of the specific chain configuration in isolated molecular regions in proteins of the collagen group.

2. The studies made show that the special chain configuration in collagen is conditioned by accumulations of imino acids and glycine in isolated regions of the chain molecule. The other amino acid residues do not determine the presence of this special configuration, although they can occur in these regions in small amounts.

3. The studies of the influence of water on the structure of collagen indicate that water takes part in the stabilization of the special configuration of collagen chains, distributing itself in ordered regions in direct proximity to the frameworks of the chains (at a distance of about 3 A) and forming hydrogen bonds with them.

LITERATURE CITED

[1] R. S. Bear, "The structure of collagen fibrils," Advances in Protein Chemistry 7, 69 (1952).

[2] Nature and Structure of Collagen (edited by J. T. Randall) (Butterworths Scientific Publications, London, 1953).

[3] G. N. Ramachandran and G. Kartha, "Studies on collagen," Proc. Ind. Acad. Sci. 42, 215 (1955).

[4] L. Pauling and R. V. Corey, "Structure of collagen," Proc. Nat. Acad. Sci. 37, 276 (1951).

[5] F. H. C. Crick, "A structure for collagen," J. Chem. Phys. 22, 347 (1954).

[6] A. Rich and F. H. C. Crick, "The structure of collagen," Nature 176, 915 (1955).

[7] P. M. Cowan, S. McGavin, and A. C. T. North, "The polypeptide chain configuration of collagen," Nature 176, 1062 (1955).

[8] F. Gaurovitts, The Chemistry and Biology of Proteins [in Russian] (1953).

[9] V. N. Orekhovich, Procollagens, Their Chemical Composition, Properties and Biological Roles [in Russian] (1952).

[10] K. H. Gustavson, "Hydroxyproline and stability of collagens," Acta Chemica Scandinavica 16, 1298 (1954).

[11] R. J. Block and D. Bolling, "The amino acid composition of keratins," J. Biol. Chem. 127, 685 (1939).

[12] J. M. Nogucho, A. Asai, and S. Najakawa, "The structure of polyglycyl- *l*-alanine," J. Polymer Sci. 21, 147 (1956).

[13] R. Marsh, R. B. Corey, and L. Pauling, "The structure of Tussah silk (with comments about structure of poly-*l*-alanine)," Acta Cryst. 8, 710 (1955).

[14] W. Grassmann, "Aminosäurequenzen des Kollagens. 1. Mittel H—S," Z. physiol. Chem. 306, 123 (1956).

[15] A. N. Mikhailov, Physicochemical Bases of the Technology of Leather [in Russian] (1949).

[16] A. L. Zaides, "Changes in the fine structure of collagen during swelling in water vapor," Colloid. J. (USSR) 16, 267 (1954).

[17] L.Pauling, "The adsorption of water by proteins," J. Am. Chem. Soc. 67, 555 (1945).

[18] H. B. Bull, J. Am. Chem. Soc. 66, 1499 (1944).

Received March 1, 1957

M. V. Lomonosov Moscow State University

ELECTRON DIFFRACTION ANALYSIS OF THE MOLECULAR STRUCTURES OF HALIDES OF GROUP II ELEMENTS

P. A. Akishin and V. P. Spiridonov

The molecular structures of 30 halides of certain 2nd group elements have been studied in the gas phase by the electron diffraction method. As a result, new values of interatomic distances in 23 molecules were obtained for the first time, and the geometric parameters of 7 molecules which had been studied before were defined more precisely. The linear structure of all the molecules under examination was established. The data obtained allowed the calculation of the covalent radii of the 2nd group elements by the Schomaker-Stevenson rule.

The collection of experimental data on the geometric parameters and configurations of molecules of inorganic compounds is of great practical and theoretical interest. These data can be used in calculating thermodynamic functions of the gases and the equilibrium constants of gas reactions important in practice; they are indispensable for: establishing the relationships between the various physicochemical properties, and between the molecular structures of inorganic compounds; elucidating the specific laws and peculiarities of the molecular structures, so as to develop a general theory of the structures of organic and inorganic compounds.

The electron diffraction method, through its many advantages over other physical ones, is one of the most widely used and effective methods of studying polyatomic molecular structure in the gas phase. This method can be also used for the study of molecules of difficultly volatile inorganic compounds. However, there is very little experimental data in the literature [1] concerning the molecular geometry of inorganic compounds obtained by the electron diffraction method.

The problem of the present study was the determination of the molecular configurations and of the geometric parameters of the vapors of the halides of the 2nd group elements. The majority of them are difficultly-volatile with boiling points above 1000°C. The data in the literature on the geometry of these molecules are very limited [2-6]. This is due to the great experimental difficulties which arise in studying compounds with boiling points above 1000°C.

The present work was done by the electron diffraction method in the laboratory for molecular structure analysis of the MGU Chemistry Department. Figure 1 shows a diagram of the apparatus. It consists of a diffraction camera with a vaporizer that has its own feeding system, a camera, an electron gun and a vacuum system.

Two vaporizers were prepared for difficultly-volatile substances: in one the ampule is heated by radiation and in the other by electron bombardment. The radiation vaporizer could be used only at low temperatures, and with the heater turned off during exposure, because of the distortions in the diffraction pattern introduced by the alternating field of the heating element.

The electron bombardment vaporizer was mainly used in analyzing difficultly volatile compounds. The molybdenum, wolfram or graphite ampules have cylindrical bodies with ground-in inserts and a head with both a vertical channel for removing the vapor of the substance under study to the condensation surface, and a horizontal channel for the passage of the electron beam. The vaporizer is enclosed in a copper casing, cooled by running water.

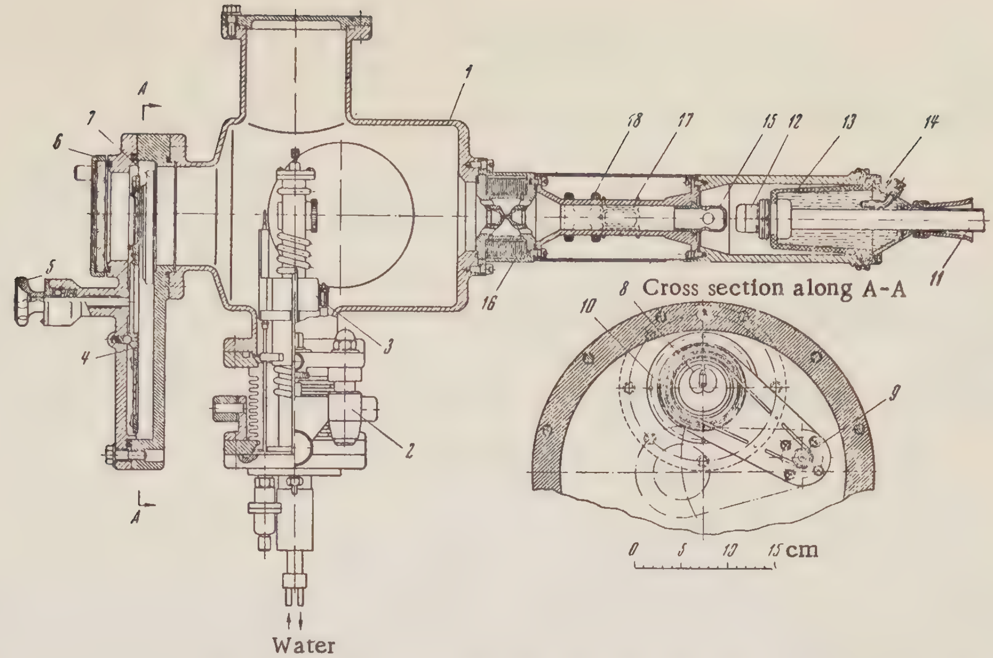

Fig. 1. Diagram of the apparatus for the study of difficultly-volatile compounds: 1) diffraction camera; 2) adjusting mechanism of the vaporizer; 3) vaporizer; 4) camera disk which carries photographic films; 5) vacuum lead of the drum which turns the camera disk; 6) view window; 7) sector arrangement; 8) blades of the sector; 9) pulley of the electric motor for the rotating sector; 10) ball bearing; 11) high voltage cable lead; 12) cathode; 13) steatite insulator; 14) compensator; 15) anode; 16) electromagnetic lens; 17) repelling spools; 18) magnetic lock.

The sector block is placed in the camera, thus making it possible to obtain patterns suitable for photometry by means of the rotating sector.

The electron diffraction apparatus is fitted with a metal-clad electron gun. The high voltage lead, to which is fastened the cathode complex, is mounted on a steatite insulator,the inner layer of which is filled with castor oil. The compact construction of the electron gun assures its safety and dependability. The electron gun is energized by a somewhat altered high voltage rectifier of the UEM-100 electron microscope.

NIKFI type MK (ionooptic) photographic films with a weakened sensitivity to light were used for the study of compounds with boiling points up to 1500°C. The construction of the vaporizer made it possible to reduce to a minimum the radiation surface of the ampule, as viewed from the direction of the photographic film. At higher temperatures (> 2000°C) diapositive films were used, and the following special methods protecting them from the light of the vaporizer were applied: 1) a thin layer (mirror) of calcium metal was sputtered immediately onto the emulsion in the diffraction camera prior to photographing, 2) aluminum foil, 5-7 μ thick was made to adhere closely to the photographic emulsion, and 3) the emulsion was sprayed with a thin layer of blackening. The last method gave the best results.

Because of the considerable deliquescence of the series of compounds ($MgCl_2$, $MgBr_2$, $BeCl_2$, $BeBr_2$, BeI_2, CaI_2) the loading of these substances into the vaporizer ampule was done in a dry box. After it was removed from this dry box, the ampule was inserted into the vaporizer, which was immediately joined to the diffraction camera. If the contact time of the substance with the air through the 0.3 mm diameter nozzle of the ampule did not exceed 2-3 min, the hydrolysis of the substance could not be considerable, and the small quantity of much less volatile basic salt formed could not influence the diffraction pattern.

From each substance 8-10 series of electron diffraction patterns were obtained (2-3 in a series) with different exposures (5-30 sec) at different accelerating voltages (40, 60, 80 kv). The electron wavelength was determined from patterns of crystalline zinc oxide, obtained before and after the vapor patterns. The measurement of the diffraction rings on the patterns was carried out along several (6-8) diameters in different directions. The intensity of the rings was evaluated visually. The interpretation of every diffraction pattern was done in two ways — by radial distribution [7] and by systematic approximations (trial and error) [8].

The radial distribution curves were constructed according to the Walter-Beach equation:

$$r^2 D(r) = \frac{r^2 a_k \cos a_k r}{\pi^2 - 4a_k^2 r^2} \sum_k I(s_k)\, s_k^2 \frac{\sin s_k r}{s_k r}; \qquad (1)$$

s_k is the measured location of the maximum, $I(s_k)$ is its estimated intensity, a_k is the half width of the maximum or minimum.

The theoretical molecular intensity curves were constructed according to a simplified equation:

$$I_{\text{mol.}}(s) = \sum_i \sum_j Z_i Z_j \frac{\sin s r_{ij}}{s r_{ij}} \quad \text{or} \qquad (2)$$

$$I_{\text{mol.}}(s) = \sum_i \sum_j Z_i Z_j \frac{\sin s r_{ij}}{s r_{ij}} e^{-a_{ij} s^2}; \qquad (2a)$$

here Z_i, Z_j are the nuclear charges of the i-th and j-th atoms of the molecule, r_{ij} is the distance between the i-th and j-th atoms, a_{ij} is a constant proportional to the root mean square amplitude of the vibration of the i-th and j-th atoms,

$$s = \frac{4\pi}{\lambda} \sin \vartheta/2,$$

ϑ is the scattering angle, λ is the wavelength of the impinging electrons.

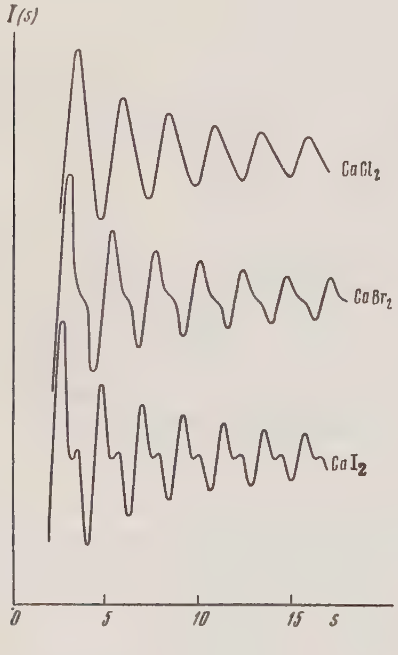

Fig. 2. Theoretical intensity curves for $CaCl_2$, $CaBr_2$ and CaI_2 molecules. The valence angle is 180°.

The diffraction patterns of halide vapors of group 2 elements have, as a rule, a regular decrease in the intensity of the diffraction rings from the center to the periphery. The ring asymmetry, almost absent in fluorides, increases on changing to chlorides, bromides and iodides, developing in special cases into intensity steps on the outward side of the ring. As an example, Fig. 2 shows the theoretical intensity curves for molecules of calcium halides, constructed on the assumption of a linear model. The theoretical intensities were computed from Eq. (2a) where the constant a_{ij} was calculated from the oscillatory part ω_e in the spectrum of the corresponding diatomic molecule. Theoretical curves with and without the temperature factor and an experimental curve are given as an example for the CaF_2 molecule in Fig. 3. It shows that the use of the temperature factor leads to better agreement between the theoretical and experimental curves.

Figure 4 shows radial distribution curves for CaF_2, $CaCl_2$, $CaBr_2$ and CaI_2 molecules, typical of 2nd group halides. They have two sharp peaks with values r and 2r, which corresponds to a molecular model with a valence angle of 180°. In all cases the data obtained from the radial distribution curves agree with the results obtained by systematic assumptions (trial and error).

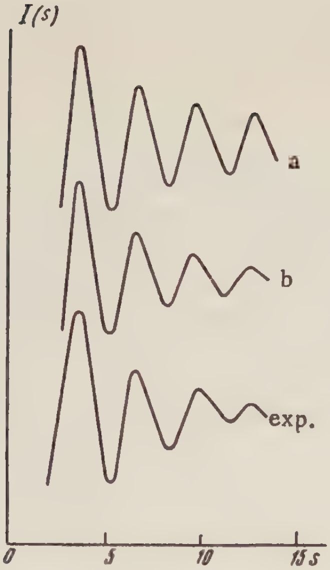

Fig. 3. The experimental and theoretical intensity curves for the linear molecule CaF_2: a) without the temperature factor, b) with the temperature factor.

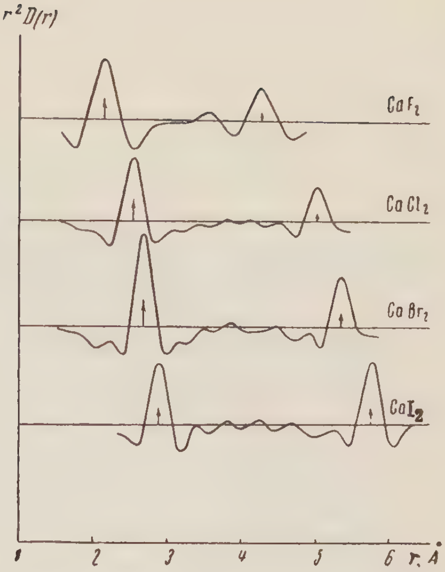

Fig. 4. Radial distribution curves constructed according to Eq. (1) for calcium halide molecules.

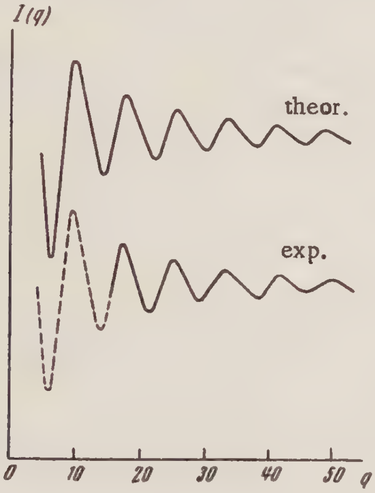

Fig. 5. Theoretical intensity curve for the linear HgI_2 molecules, and the experimental curve obtained photometrically.

The error in the valence angle X–Me–X was determined by trial and error. In iodided it is ± 10°, in bromides and chlorides ± 20-30°. The determination of the valence angle is difficult for the majority of fluorides because of the small charge on the fluoride atom, and the insensitivity of the theoretical curves I(s) to variation in the F–Me–F angle; the size of the angle F–Me–F is solved unequivocally by the help of the radial distribution curves, which give a second peak in all cases corresponding to the 180° valence angle. All patterns of the vapors of 2nd group element halides are well explained by the triatomic linear model for the MeX_2 molecules. However, inasmuch as the literature hints [9] that there is association of molecules in vapors of beryllium halides, we experimented with a series of assumed structures for the dimeric molecule Be_2X_4, but not one of these models proved satisfactory because of the lack of agreement between the theoretical and experimental curves. Therefore it was concluded that there is no association whatever in beryllium halides on the basis of electron diffraction experiments, or else that it exists to a degree beyond the limits of sensitivity of the diffraction method.

Due to the rotating sector in the apparatus, it is possible to obtain patterns suitable for photometering and to interpret them objectively. However, because of the simplicity of the geometric configuration of the MeX_2 molecules, and of the sufficient dependability of the data obtained visually, and also because of the considerable inefficiency of the objective method [10-13], it seemed expedient to carry out a microphotometric analysis of only one object – the mercury iodide molecule. The patterns obtained using the rotating sector at different exposures and different accelerating voltages were read with a photometer in different directions on the MF-4 recorder; the recorded data were averaged. The scattered electron intensity $I_{mol.}$, indispensable for the calculations, was obtained by subtracting the background from the over-all blackening by means of the equation

$$I_{mol.} = k\left(\frac{P_{sum}}{P_{bg}} - 1\right). \qquad (3)$$

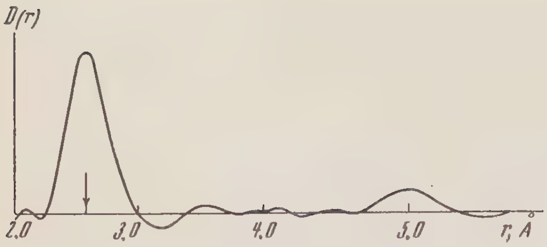

Fig. 6. The radial distribution curve for the HgI_2 molecule, constructed according to Eq. (4).

The experimental curve for HgI_2 calculated according to Eq. (3) was compared with the theoretical curve constructed for the linear model according to Eq. (2a). Figure 5 shows that these curves are quite similar; the asymmetry of the maxima characteristic of patterns of the vapors of the halide 2nd group elements is distinctly shown on the experimental curve. Using the microphotometric experimental I_{mol} intensity curve (the linear model for the initial region, including the first maximum, was extrapolated by the theoretical curve) a radial distribution curve was constructed (see Fig. 6) according to the equation

$$D(r) = \sum_{q=0}^{q_{\max}} q I_{mol}(q)\, e^{-aq^2} \sin \frac{\pi}{10} qr\, \Delta q, \tag{4}$$

where

$$q = \frac{40}{\lambda} \sin v/2, \quad e^{-aq^2_{\max}} = 0.1.$$

The interval $\Delta q = 1$ was taken in calculating. The curve has two maxima which correspond to the HgI_2 linear model; the ratios of the areas of the maxima are: theoretical, 6.04; experimental, 6.07.

It follows then that the sector-microphotometric analysis confirms in full the results obtained by the visual method.

TABLE 1

Interatomic Distances in 2nd Group Halide Molecules (in Å)

Element	F	Cl	Br	I
Be	1,40±0.03	1.75±0.02	1.91±0.02	2,18±0,02
Mg	1,77±0.02	2.18±0,02	2.34±0,03	(2,54)*
Ca	2,10±0,03	2.51±0,03	2.67±0.03	2.88±0.03
Sr	2.20±0.03	2.67±0.03	2,82±0,03	3,03±0,03
Ba	2,32±0.03	2.82±0.03	2,99±0.03	3,20±0,03
Zn	1.81±0.02	2.05±0.01	2.21±0.01	2.38±0.02 2.42±0.02[3]
Cd	1.97±0.02	2,21±0.02 2.23+0.03[2]	2.37±0,02 2.39+0.03[2]	2,55±0,02 2.56+0.02[2] 2.60±0.03[3]
Hg	—	2,29±0.02 2.28±0.05[4] 2.34±0.01[5] 2.27±0.03[6]	2,41±0.02 2.38±0,05[4] 2,44±0,01[5]	2.59±0.05 2,55±0.05[4] 2.61±0.01[5]

---

* Obtained from the values of covalent radii according to Eq. (5).

The electron diffraction analysis of 30 halide molecules of the 2nd group elements showed that all of them have a linear structure; this agrees with the valence condition of the central metal atom and with the quantum-mechanical description of valence directions. In addition, the values of the interatomic distances in 23 molecules have been obtained for the first time, and the geometric parameters of 7 molecules, previously studied by other authors, have been determined more accurately. Table 1 gives the geometric molecular parameters. Attempts to obtain MgI_2 and HgF_2 vapor patterns have failed because of the decomposition of these substances during heating.

The evaluation of the error in determining r(Me−X) was derived from the maximum error of the method, equal to ±1.0-1.5%. The data obtained here agree with those in the literature within the limits of experimental error.

A few laws of the variations of r(Me−X) in molecules of the compounds already studied should be noticed. If the atomic number of the halide atom X is laid off along the abscissa axis of the graph, and interatomic distances r(Me−X) in MeX_2 molecules (Fig. 7) along the ordinate axis, then an approximately linear dependence is obtained for the chlorides, bromides and iodides with a break in all straight lines (each corresponds to a definite metal) at the chlorides; a sharp decrease takes place in the Me−F distance in comparison with the value obtained from linear extrapolation. If the atomic numbers of the metals are laid off along the abscissa axis, then an analogous law is observed with the break in the straight lines corresponding to the halides of calcium (Fig. 8). The breaks in the straight lines on the two graphs can be explained by the sharp change in the effective nuclear charge on shifting from F^- to Br^-, or from Mg^{+2} to Sr^{+2}. Actually, Cl^- and Ca^{+2} are isoelectronic, having one two-electron and two eight-electron shells. The shift from F^- and Mg^{+2}, which each have one two-electron and one eight-electron shell, to Br^- and I^-, Sr^{+2} and Ba^{+2}, which have kernels containing one or eight electron shells, is accompanied by a sharp increase of nuclear screening by the electron shells, and consequently, by a decrease in the effective charge of the atomic nucleus. The changes indicated in the effective charge on the atom nuclei are apparently reflected in the interatomic distances, as is manifested in the breaks of the corresponding straight lines in Figs. 7 and 8. Similar breaks of the straight lines are also observed in the graphs relating the covalent or ionic radii of elements to their atomic numbers.

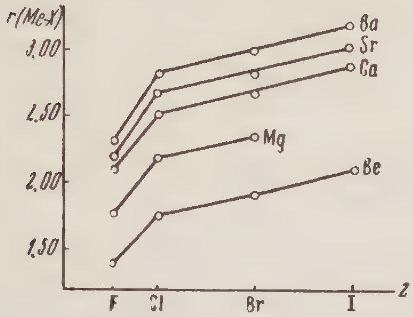

Fig. 7. The variation of interatomic distance r(Me−X) with atomic number of the halogen.

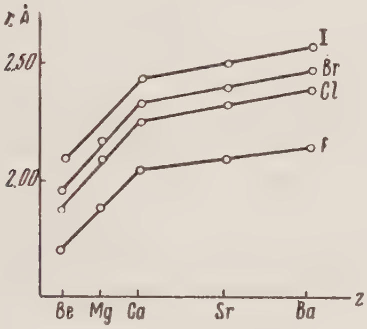

Fig. 8. The variation of interatomic distance r(Me−X) with atomic number of the metal.

It is of interest that on Figs. 7 and 8 there are families of straight lines, nearly parallel to each other, which proves the stability of the radii of the atoms which form Me−X bonds. Schomaker and Stevenson's [14] equation was used to find these radii:

$$R = r_A + r_B - \beta |x_A - x_B|. \qquad (5)$$

Here r_A and r_B are the covalent radii of the elements which form the bond A−B, x_A and x_B are the electronegativities of the elements A and B, β is an empirical constant, R is the interatomic distance sought. Schomaker and Stevenson proposed the value 0.09 for the constant β. Gordy [15], after studying a considerable amount of experimental material, discovered that if the coefficient β were assumed to equal 0.06 then there would be better agreement between the experimental values and those calculated by Formula (5). He estimated the covalent Zn, Cd and Hg radii given in Table 2, on the basis of data given in the literature and on β being equal to 0.06. On the basis of the experimental values of interatomic distances, the covalent radii of the 2nd group elements were calculated according to Eq. (5) where β = 0.06.

In addition, the covalent halide radii given in Gordy, Smith and Trambarulo's monograph [15] were used. The values of the electronegative elements Be, Mg, Ca, Sr, Ba, Zn, Cd, F, Cl, Br and I were taken from Gordy and Thomas' [16] work, the value of Hg-electronegativity from Pritchard and Skinner's [17] work. The covalent radii of the 2nd group elements are given in Table 2. It shows that the values of the covalent Zn, Cd and Hg radii coincide with those in the literature, but there is a considerable discrepancy for Be, apparently due to the fact that the value of the covalent Be radius, quoted by Gordy, was obtained by graphic extrapolation.

The interatomic Me–F distances do not comply with Schomaker and Stevenson's equation; therefore they were not used in calculating the covalent radii.

Obviously, the accuracy of the calculated covalent radii depend first on how much the application of Schomaker and Stevenson's relationship to the halides of the 2nd group elements was justified, and secondly on the choice of the empirical constant β.

TABLE 2

The Covalent Radii of the 2nd Group Elements

Element	Covalent radius		Element	Covalent radius	
	Our data	Gordy's data [15]		Our data	Gordy's data [15]
Be	0,85	(0.98)	Ba	1.96	—
Mg	1,29	—	Zn	1.14	1.16
Ca	1,64	—	Cd	1.30	1.34
Sr	1,79	—	Hg	1.33	1.34

It is possible that the calculated radii are not the radii in Pauling's sense; however,they make possible a rather exact evaluation of interatomic distances in molecules for which there are no data (viz. MgI_2). Therefore, it would be desirable to compare the calculated values of the covalent radii with those obtained by independent methods and from compounds of different structures, among them metallo-organic substances.

LITERATURE CITED

[1] P. Allen and L. Sutton, "Tables of interatomic distances and molecular configurations obtained by electron diffraction in the gas phase," Acta Cryst. 3, 46 (1950).

[2] M. W. Lister and L. E. Sutton, "The investigation by electron diffraction of some dihalides of cadmium, tin and lead," Trans. Farad. Soc. 37, 406 (1941).

[3] O. Hassel and L. C. Strömme, "Bestimmung der dampfförmigen Verbindungen ZnI_2 und CdI_2 mittels Elektronenstrahlen," Z. physik Chem. 38, 466 (1938).

[4] H. Braun and S. Knoke, "Die Kernabstände der Quecksilberhalogeniden (HgI_2, $HgBr_2$, $HgCl_2$)," Z. physik Chem. 23, 163 (1933).

[5] A. Gregg, G. Hampson, G. Jenkins, P. Jones, and L. Sutton, "The electron diffraction investigation of some inorganic halides," Trans. Farad. Soc. 33, 852 (1937).

[6] L. R. Maxwell and V. M. Mosley, "Internuclear distances in Se_2, Te_2 and HgCl by electron diffraction," Phys. Rev. 57, 21 (1940).

[7] J. Walter and J. Beach, "The radial distribution method in electron diffraction," J. Chem. Phys. 8, 601 (1940).

[8] L. Pauling and L. O. Brockway, "A study of the methods of interpretation of electron-diffraction photographs of gas molecules with results of benzene and carbon tetrachloride," J. Chem. Phys. 2, 1, 867 (1934).

[9] O. Rahlfs and W. Fischer, "Uber thermische Eigenschaften von Halogeniden. 6. Dampfdrucke und Dampfdichten von Berillium- und Zirkonium-Halogeniden," Z. anorg. u. allgem. Chem. 211, 349 (1933).

[10] H. Viervoll, "Electron diffraction investigation of molecular structures, I. Application of Fourier analysis to the rotating sector method," Acta Chem. Scand. 1, 120 (1947).

[11] I. L. Karle and J. Karle, "Internal motion and molecular structure studies by electron diffraction," J. Chem. Phys. 17, 1052 (1949).

[12] J. Karle and I. L. Karle, "Internal motion and molecular structures studies by electron diffraction. 2. Interpretation and method," J. Chem. Phys. 18, 957 (1950).

[13] I. L. Karle and J. Karle, "Internal motion and molecular structure studies by electron diffraction. 3. Structure of CH_2CF_2 and CF_2CF_2," J. Chem. Phys. 18, 963 (1950).

[14] V. Schomaker and D. P. Stevenson, "Some revisions of the covalent radii and the additivity rule for the lengths of partially ionic single covalent bonds," J. Am. Chem. Soc. 63, 37 (1941).

[15] W. Gordy, V. Smith, and P. Trambarulo, Radiospectroscopy [Russian translation] (GITTL, Moscow, 1955).

[16] W. Gordy and W. Thomas, "Electronegativities of the elements," J. Chem. Phys. 24, 439 (1956).

[17] H. O. Pritchard and H. A. Skinner, "The concept of electronegativity," Chem. Revs. 55, 745 (1955).

Received February 22, 1957

M. V. Lomonosov Moscow State University

ELECTRON DIFFRACTION INVESTIGATION OF PHASE TRANSITIONS IN THIN FILMS OF METALS AND OXIDES

D. V. Ignatov

By means of the electron diffraction method phase transitions in the thin films of metals (Al and Fe–Al) and oxides ($NiO-Cr_2O_3$ and $NiO-Al_2O_3$) by heating in the air have been investigated.

The investigation of phase transitions in thin films is of great value for elucidation of the mechanism of the interaction between the various contiguous phases as a function of temperature and time of heating. Such contiguous phases can be metal with metal, oxide with oxide, metal with oxide and other chemical combinations.

Interactions of this nature occur in the processes of sintering and oxidation and also between a base (metallic or other type) and a material applied to it in the form of a thin layer, different from the base in composition.

The present work gives the results of an electron diffraction study of the phase transitions occurring as a function of temperature and time of heating in oxide films on aluminum in the Fe–Al system and in the $NiO-Cr_2O_3$ and $NiO-Al_2O_3$ systems.

EXPERIMENTAL

Thin films of metals (400-500 A thicknesses) to be used as samples were obtained by means of vaporization and condensation in a vacuum ($\sim 2 \cdot 10^{-6}$ mm Hg) in the apparatus shown in Fig. 1. The thickness of the films was determined by weighing. Thin films of Fe–Al alloys were obtained either by means of the simultaneous vaporization of Fe and Al or by means of successive vaporization of these metals from two sources. By regulating the rate of the simultaneous vaporization from two centers, it is possible to obtain metallic systems in the form of films of any composition conforming to the phase diagram [1].

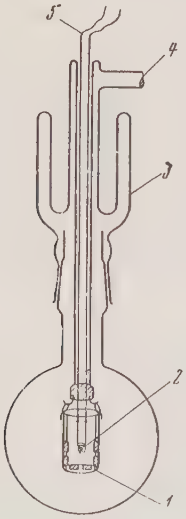

Fig. 1. Apparatus for obtaining thin films of metals in a vacuum. 1) Protective cylinder and sample holder (backings); 2) vaporizer in form of tungsten wire basket; 3) trap for oil vapors (filled with liquid air); 4) outlet for connection to the vacuum apparatus; 5) lead for supplying current to the vaporizer.

Thin films were prepared from oxides in the following manner. Firstly, films were obtained of aluminum and chromium, with mica leaves used as backings. The films of the metals were peeled from the mica by submersion in distilled water. The films were recovered from the surface of the water on platinum grids – flakes 10 mm long, 5 mm wide and 0.3 mm thick. The grids had 2-4 meshes of 0.6-0.8 mm diameter which were closed by the fragments of the thin film of the metal recovered from the surface of the water.

The samples obtained in this way were oxidized by means of heating in air for 20-30 min at 600° in the case of aluminum and 400° in the case of chromium. Then nickel vapors were condensed on them and two-layer films consisting of a layer of the oxide γ-Al_2O_3 or Cr_2O_3 and a layer of nickel were obtained. Upon heating these samples in air for 30 min at 400°C, two-layer films were obtained from the oxides NiO and γ-Al_2O_3 in the one case, and from NiO and α-Cr_2O_3 in the other. The thickness of the films of the Ni–Al and Ni–Cr alloys was selected in this way so that the oxides evolved would correspond to the stoichiometric composition of the $NiAl_2O_4$ and $NiCr_2O_4$ compounds.

In addition the samples were heated in air in the temperature range:

a) aluminum from 300 to 1300°;
b) Fe–Al from 100 to 900°;
c) NiO–Cr_2O_3 from 400 to 800°;
d) NiO–Al_2O_3 from 600 to 1300°.

The electron diffraction method (by transmission) was used as the basic method for determining the phases which arise as a function of time and temperature of heating.

In Fig. 2 is shown a photograph of the electron microscope (constructed by the author) with the help of which the electron diffraction patterns were obtained. The instrument was calibrated for the lines of the metals or the oxides.

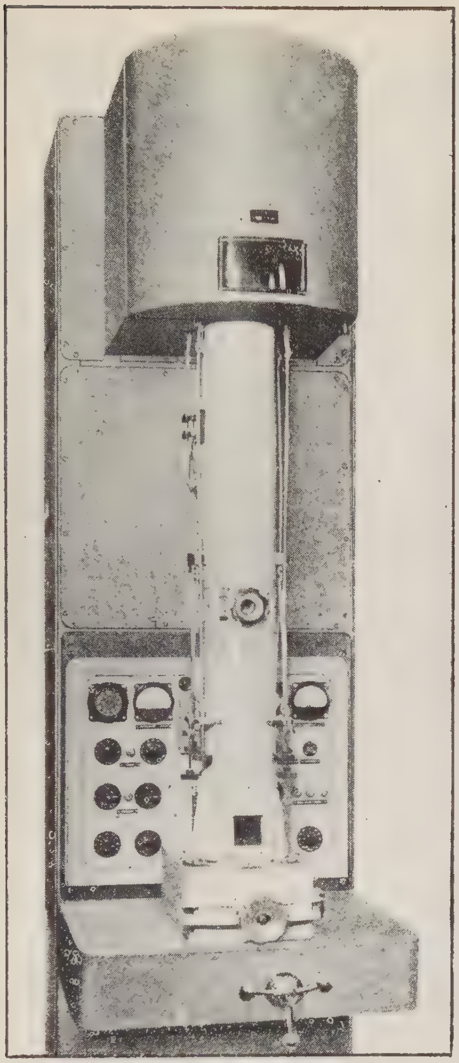

Fig. 2. Electron microscope (the low-voltage and high-voltage blocks are assembled in one unit with the column of the electron microscope).

Discussion of Results

In Fig. 3 are presented electron diffraction patterns from a thin film of aluminum heated in air at 300°C for 5 hrs and at 400, 450, 500, 600, 700°C for 10 min.

From these electron diffraction patterns it is observed that even at 300° an oxide phase γ'-Al_2O_3 begins to form, which exists up to 600° together with the metal. At 600° this phase is converted into γ-Al_2O_3. The phase γ-Al_2O_3 is stable up to 1300°. After 5 hrs of heating at 1300° γ-Al_2O_3 is converted α-Al_2O_3 (see Fig. 3).

Thus our results do not confirm those of Kubashevskii and Hopkins [2], who assert that oxide films on aluminum are amorphous upon heating in the 300-500°C temperature range. An amorphous oxide film, formed at room temperature on polycrystalline aluminum, exists only up to 300°C.

In Fig. 4 are presented electron diffraction patterns from a film of the Fe–Al alloy (both metals were vaporized simultaneously from two centers) obtained from the same sample heated in air in the temperature range from 20° to 900°C. The sample was heated in steps of 100° for 10 min.

Evaluation of the electron diffraction pattern 4,a showed that the given film consists of a mixture of Fe and Al crystals. The considerable increase in the intensity of the second diffraction ring on the electron diffraction pattern 4, a is caused by the exact coincidence of the reflection from Al with the first strongest ring from the iron.

As seen from the electron diffraction patterns 4,b and 4,c, the diffraction pictures from the sample heated at 100° and 200° do not differ, since under these conditions there still exists the mixture of Fe and Al. In the electron diffraction pattern 4,d, besides the lines from Fe and Al, there are included the strongest lines from Fe_3O_4, their low intensity arguing for the small quantity of this phase. Heating the sample at 400° leads to a

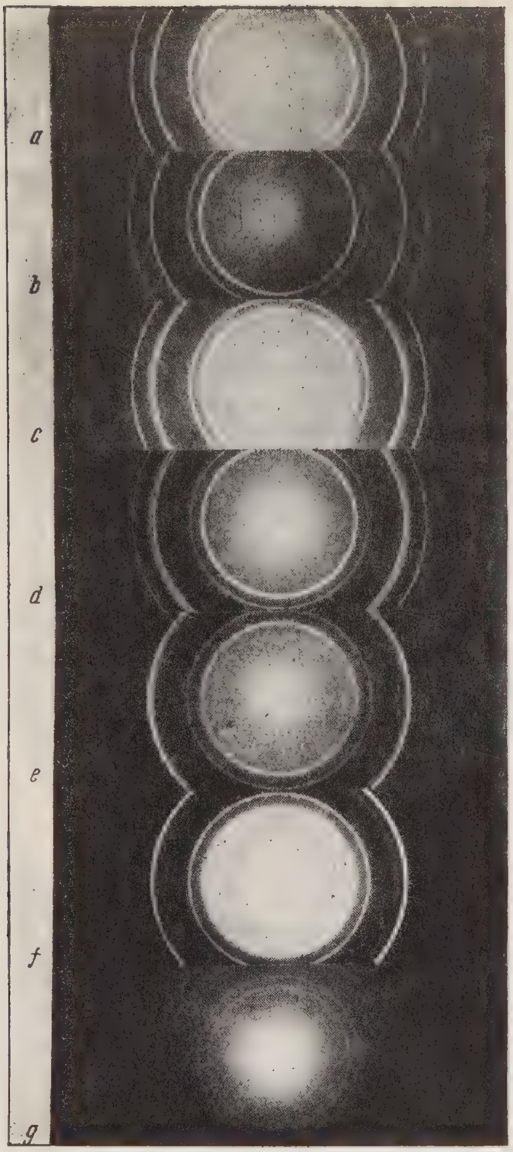

Fig. 3. Electron diffraction patterns from a thin film of aluminum heated at temperatures from 300 up to 1300°C: a) 300°; b) 400°; c) 450°; d) 500°; e) 600°; f) 700°; g) 1300° (5 hrs).

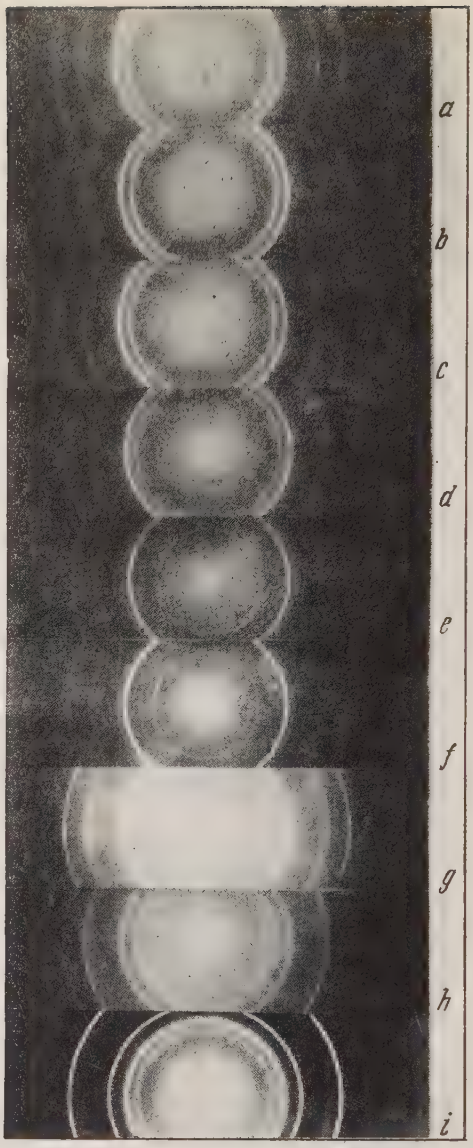

Fig. 4. Electron diffraction patterns from Fe–Al sample heated in air at temperatures from 20 up to 900°C: a) 20°; b) 100°; c) 200°; d) 300°; e) 400°; f) 500° and 600°; g) 700°; h) 800°; i) 900°.

sudden change in the diffraction picture, which is clearly visible on the electron diffraction pattern 4,f. Evaluation of this electron diffraction pattern showed that here the reflections pertain chiefly to the chemical compound Fe_2Al_5.

Besides the lines from Fe_2Al_5, on this electron diffraction pattern there are also lines from Fe_3O_4, but, as in the preceding case, their intensity is very low. Further heating of the film at 500 and 600° did not lead to a change in the diffraction picture.

Analysis of the electron diffraction patterns 4,g, h and i, obtained from samples heated at 700, 800 and 900°C, indicated the presence in the sample of the following phases: Fe_2Al_5, FeAl and γ-Al_2O_3 at 700; FeAl and $FeAl_2O_4$ at 800; $FeAl_2O_4$ at 900°C. Thus the compound Fe_2Al_5, beginning with 700°, gradually decomposes and the phase $FeAl_2O_4$ is formed in place of it.

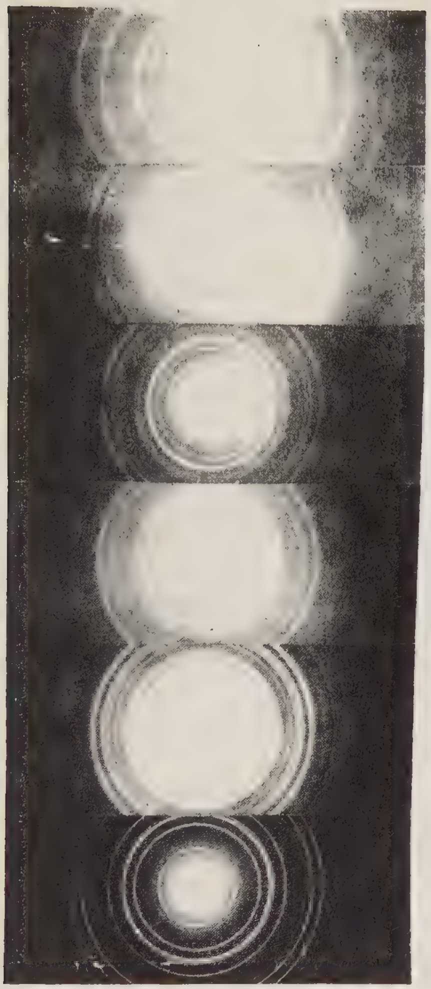

Fig. 5. Electron diffraction patterns from NiO$-$Cr$_2$O$_3$ sample heated in air at temperatures from 400 up to 800°C: a) 400°, 5 hrs; b) 600°, 5 hrs; c) 600°, 10 hrs; d) 600°, 15 hrs; e) 700°, 15 hrs; f) 800°, 15 hrs.

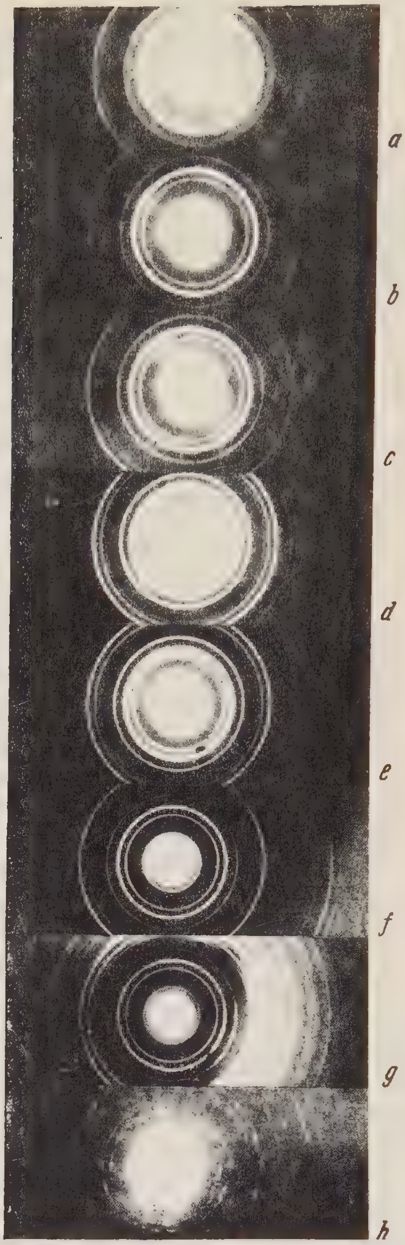

Fig. 6. Electron diffraction patterns from NiO$-$Al$_2$O$_3$ sample heated at temperatures from 600 up to 1300°C: a) 600°, 5 hrs; b) 800°, 5 hrs; c) 800°, 10 hrs; d) 800°, 15 hrs; e) 900°, 10 hrs; f) 1000-1200°, 15 hrs; g) 1300°, 1 hr; h) 1300°, 5 hrs.

In connection with these results it should be noted that the phase Fe$_2$Al$_5$ is more resistant to oxidation than iron and aluminum taken separately. Films of Fe and Al of the same thickness are completely oxidized after 10 min at 400 and 700°C, respectively. A film of Fe$_2$Al$_5$, however, is completely oxidized only at 900°C. Thus the protective properties of thin coatings of aluminum on steels (without the addition of chromium) apparently can be explained by the formation in the surface layer of the phase Fe$_2$Al$_5$ and by the subsequent formation upon heating of an oxide film consisting chiefly of FeAl$_2$O$_4$, as well as the phases Fe$_2$Al$_5$ and FeAl in the surface layer.

It should also be noted that in the simultaneous vaporization of the metals Fe and Al, Ni and Al from two very closely located centers (beads ~ 1 mm diameter) on cold blocks (up to 100°C) the products of the condensate always consisted of a mixture of the vaporized metals. In the case, however, of the vaporization of these metals on blocks (glass, mica, etc.) heated up to 400°C, there always occurred the formation of chemical compounds (for example, Fe_3Al, Fe_2Al_5, NiAl, etc.). Such compounds were also obtained on cold blocks if these compounds were taken as the vaporized material.

In Figs. 5 and 6 are given electron diffraction patterns from samples prepared in the form of two-layer films consisting of $NiO-Cr_2O_3$ (Fig. 5) and $NiO-Al_2O_3$ (Fig. 6). The results of an evaluation of these electron diffraction patterns are presented in Table 1. From Table 1 it follows that in the system $NiO-Cr_2O_3$ beginning with 700°C there occurs the formation of the chemical compound $NiCr_2O_4$ with spinel structure. The process of its formation is finished at 800°, and at 900° the samples disintegrated (probably owing to recrystallization), and it was therefore not possible to determine the dissociation products of the spinel $NiCr_2O_4$. Then heating of the $NiCr_2O_4$ samples in a vacuum (~ 10^{-6} mm Hg) was resorted to. For this purpose samples were obtained from a fine powder of $NiCr_2O_4$ by means of extrusion and sintering in the form of cylinders 10 mm in length and 3 mm in diameter with wall thickness 0.8-1 mm. As a heater, a spiral 4 mm in diameter made of 0.2 mm gauge tungsten wire was used. The temperature was measured by a platinum-rhodium thermocouple, the tip of which is placed inside the cylinder. The temperature both in the given case and in all succeeding cases was determined correct to ± 10°.

TABLE 1

Change of Phase Composition as a Function of Temperature in $NiO-Cr_2O_3$ and $NiO-Al_2O_3$ Systems (Heating time 15 hrs)

Temperature, °C	$NiO-Cr_2O_3$ phases	$NiO-Al_2O_3$ phases
	Mixture:	Mixture:
400	α-Cr_2O_3 + NiO	γ-Al_2O_3 + NiO
500	The same	The same
600	Chiefly the same mixture and traces of $NiCr_2O_4$	The same
700	α-Cr_2O_3 + NiO and appreciable quantity of $NiCr_2O_4$	The same
800	Chiefly $NiCr_2O_4$ and traces of oxides NiO and Cr_2O_3	γ-Al_2O_3 + NiO and appreciable quantity of $NiAl_2O_4$
900	Disintegration of samples	Chiefly $NiAl_2O_4$; traces of oxides NiO and Al_2O_3
1000		$NiAl_2O_4$
1200		$NiAl_2O_4$
1300		α-Al_2O_3 and traces of $NiAl_2O_4$

The dissociation products of the spinel $NiCr_2O_4$, i. e., the products of its vaporization, were condensed in the form of films on thin mica leaves. Then, as in the case of the metals, they were peeled from the mica by means of submersion in water and were recovered by the platinum grids.

Analysis of the electron diffraction patterns obtained from similar films showed that the vaporization products contain Ni, NiO and α-Cr_2O_3 in approximately the proportion that corresponds to the spinel $NiCr_2O_4$. This conclusion is based on the fact that upon heating of such films in air at 800° the spinel $NiCr_2O_4$ was again observed in them.

A noticeable vaporization of the above samples in a vacuum occurred at 1100° after a few hours (2-3 hrs). Upon heating of these same samples in air a noticeable vaporization was observed at 1100 and 1200° (heating for 50 and 20 hrs, respectively). The phase α-Cr_2O_3 was one of the products of vaporization in the latter case.

As follows from Table 1, the system $NiO-\gamma-Al_2O_3$ exists in the form of a mixture of $NiO + \gamma-Al_2O_3$ upon heating in air in the temperature range from 400 to 800°C. At 800° the formation of the phase $NiAl_2O_4$ occurs. An almost complete conversion of the film into $NiAl_2O_4$ (in the case of films of 800-900 A thickness) is accomplished after 15 hrs of heating in air at 900°. This phase is stable up to 1300°, no new chemical compounds being observed upon heating in the temperature range from 900 to 1300°C.

After an hour's heating in air at 1300°C the decomposition of the indicated spinel into $NiAl_2O_4$ and $\alpha-Al_2O_3$ is clearly marked and the phase $\alpha-Al_2O_3$ is highly recrystallized, as seen in the electron diffraction pattern Fig. 6 (6, g). Heating at 1300° for 5 hrs leads to almost complete decomposition of the spinel $NiAl_2O_4$, while in the electron diffraction pattern from this sample there were chiefly observed reflections from $\alpha-Al_2O_3$, which was also in this case highly recrystallized, as judged by the breaking up of the diffraction rings in the sharpened reflections (Fig. 6, h). In the electron diffraction pattern from this sample the phase NiO is not observed. From this fact it may be concluded that the spinel $NiAl_2O_4$ is decomposed at 1300° on account of the NiO phase. Such a conclusion was confirmed by heating samples of $NiAl_2O_4$ in a vacuum, which was carried out in the same way as in the case of the samples of $NiCr_2O_4$.

Upon heating the samples of $NiAl_2O_4$ in a vacuum (at 1100°) for 20-30 min the blue color of the spinel changed to white, characteristic of baked samples from pure aluminum oxide. Electron diffraction analysis of the vaporization and condensation products showed that they consist of Ni and NiO. In a vacuum of $\sim 10^{-6}$ mm Hg, the NiO phase partially dissociates into nickel and oxygen, whereupon the oxygen is pumped out. In this way, the spinel $NiAl_2O_4$ decomposes upon heating into NiO and $\alpha-Al_2O_3$ (at 1300°C), whereupon the oxide NiO is vaporized and the phase $\alpha-Al_2O_3$ is highly recrystallized. It is interesting to note that the $\gamma-Al_2O_3$ is converted at 1300° (after 5 hrs) into $\alpha-Al_2O_3$, which is also highly recrystallized, as seen in the electron diffraction pattern in Fig. 3,g. On the basis of these results it is possible to form certain ideas on the mechanism of formation of spinels differing from those expressed by Hauffe and Pschera [3]. These authors investigated the mechanism of formation of the spinels $NiCr_2O_4$, $ZnCr_2O_4$, $NiAl_2O_4$ and $ZnAl_2O_4$ during the interactions of specimens of the original oxides in the form of baked tablets pressed together and heated in air at 1100 and 1200°. As a result they came to the conclusion that the vapor phase of the more volatile component (oxide) contributes in a considerable degree to the formation of spinels, for example, ZnO in the $ZnO-Cr_2O_3$ and $ZnO-Al_2O_3$ systems or $\alpha-Cr_2O_3$ in the $NiO-Cr_2O_3$ system.

According to Wagner's theory [4], a spinel, for example $MgAl_2O_4$, is formed by contact of specimens of the oxides MgO and Al_2O_3 on account of the diffusion both of an ion of the divalent metal (Mg^{+2}) and of the trivalent (Al^{+3}).

Taking into account our experimental data on the decomposition of spinels and taking into consideration the heat of formation of the oxides NiO, Cr_2O_3 and Al_2O_3, it is possible to assume that the spinel $NiCr_2O_4$ is formed by means of the diffusion both of the Ni^{+2} ions and of the Cr^{+3} ions. The spinel $NiAl_2O_4$, in our opinion, is formed chiefly on account of the diffusion of the nickel ions Ni^{+2}. The vaporization factor in our case cannot play an effective part, since the formation of spinels occurred in the temperature range of 700-900°. On the contrary, here the vaporization factor played a negative part, since at 1100-1200°C the spinels decomposed on account of the vaporization of the oxides $\alpha-Cr_2O_3$ or NiO.

These data on the thermal stability of the spinels $NiCr_2O_4$ and $NiAl_2O_4$ have an important practical value since the sinter in alloys of the Ni–Cr and Ni–Cr–Al type with various additions consists for the most part of these compounds. Besides this, the composition Ni–Cr–Al is often used for coating steels and some heat-resistant alloys based on molybdenum. The oxides $\alpha-Cr_2O_3$ and $\alpha-Al_2O_3$ themselves are often used as basic components of oxide or enamel coatings.

The examples of the use of the electron diffraction method considered here, along with all the evidence, show that the method can be used successfully for the investigation of phase transitions in free thin films of complex composition, in surface films on metals and alloys and on interphase faces in the same way as the x-ray method is used for the investigation of phase transitions which occur in the volume of a solid.

LITERATURE CITED

[1] S. A. Vekshinskii, A New Method of Metallographic Investigation of Alloys [in Russian] (1944).

[2] O. Kubaschewski and B. Hopkins, Oxidation of Metals and Alloys [Russian translation] (IL, 1955).

[3] K. Hauffe and K. Pschera, "Uber den Mechanismus der Spinellbildung bei höheren Temperaturen," Z. anorg. Chem. 262, 147 (1950).

[4] C. Wagner, "Uber den Mechanismus der Bildung von Ionenverbindungen höherer Ordnung," Z. phys. Chem. 34, 304 (1936).

Received February 20, 1957

Institute of Metallurgy, Academy of Sciences, USSR

ATOMIC CHAINS AND FINE STRUCTURE OF GLASS

V. V. Tarasov

The structures of simple glasses and a number of glass-forming substances are considered on the basis of the theory of the low-temperature specific heat of chain and lamellar structures proposed earlier by the author.

A great number of facts leads us to assume that, by their atomic nature, many glass-forming substances are branched-chain inorganic macromolecules. On the other hand, most glasses are branched-chain, high-polymer anions containing "dissolved" monomer cations of modifiers.

We regard glasses as heterodynamic structures, i. e., as structures with two or more kinds of bonds differing in their energies and especially in their force constants. The framework of the glass-former (such as the Si—O framework) is formed by the more rigid bonds; metal cations are bound to the framework by weaker bonds. The "constitutional individuality" of the framework was demonstrated in our studies of the heat capacity of glasses at low temperatures [1].

In silicate and other glasses, the glass-former frameworks are oxygen acceptors, while modifiers such as $M_2^{1+}O$, $M_1^{2+}O$, etc. are oxygen donors (they give oxygen to the framework).

With increase of the O/Si ratio from 2 to 3 the branching of the framework continuously diminishes, down to a purely chain structure.

Results obtained by infrared spectroscopy show that ordinary vitreous silica always gives an absorption band in the 2.72 μ region; however, as it was shown by Foex and by Garino-Ganina [2, 3], this absorption band may be absent in the spectrum of specially prepared fused quartz. Foex fused perfect crystals of native quartz ("rock crystal") in the focus of a solar furnace in a laboratory situated in a mountainous region of Pyrennes Orientales. The conditions for the fusion of quartz in these experiments were such that the presence of water vapor was excluded. The quartz glass so formed did not give an absorption band due to hydroxyl groups. From the results of these investigations it may be assumed with confidence that the absorption band in the 2.72 μ region is due to hydroxyl groups present in the structure of quartz glass.

These experiments justify the view that the interaction of fused quartz with water at high temperatures and pressures is to some extent similar to modification by metal oxides. Water acts as a modifier in the SiO_2-H_2O system. The water molecules dissociate into H^{1+} and $(OH)^{1-}$ and enter the structure of the framework in quartz glass and other silicate glasses, forming tetrahedrons not linked by oxygen bridges. The vertices of these tetrahedrons contain hydroxyl groups. Modification of quartz glass by means of protons may be of great practical significance, as it should lower the viscosity of the fused silica and thus facilitate the removal of bubbles, i. e., the fining process.

In his interesting papers, Stevels [4, 5] has developed the concept of glasses considered as inorganic high polymers. In our opinion, this concept needs only a little modification; it is quite legitimate to identify glass frameworks, formed by firmly bonded atoms, with high polymers. However, it is more correct to regard the modifier cations as monomeric ions dissolved in the framework. Glasses differ from true organic polymers in that their polymeric portion (the framework) is of the nature of a high-polymeric anionic radical. Silicate and other glasses are substances of peculiar constitution; their anions are polymerized and the cations are monomeric. It is very important to stress that the degree of branching of the structure formed by the silicon—oxygen framework does not depend solely on the composition, i. e., on the ratio of oxygen to silicon atoms. It is also necessary to take into consideration the role of the cooling (i. e., chilling) rate as a factor which may influence considerably the degree of branching of the glass framework.

To clarify this idea, let us consider the structure of sodium metasilicate. In the limiting case, $(Na_2SiO_3)_\infty$ is an infinite sinuous chain. We can imagine that, between the bends in the chain, oxygen bridges are formed; i. e., the SiO_4 tetrahedra are additionally joined by their vertices, with simultaneous appearance of terminal atoms; thus, each such tetrahedron is linked to others through one vertex only. This transformation without change in the (Na_2SiO_3) composition is understandable if it is taken into account that an Na_2O group is excluded in the formation of each bridge between the chain bends. If it is remembered, however, that for each such elementary process (bridge formation) there is a break in the chain at one point, i. e., formation of two ends (with Si and O atoms at the ends), it becomes clear that the excluded Na_2O group is used for "sealing" these ends.

The meaning of all this becomes clear on consideration of a melt of Na_2SiO_3 or other glass composition. The melt contains many small chain fragments, joined by an equivalent number of oxygen bridges. On rapid cooling of the melt we obtain a glass containing oxygen end atoms or, more accurately, end O—M groups. If the melt is cooled more slowly, a structure with a higher degree of polymerization is formed.

This occurs with disappearance of end atoms, i. e., of tetrahedra linked to the framework through single vertices only.

In this case, in full harmony with Stevels' views [4], the framework contains only tetrahedra linked to each other through two, three, or four vertices. There is reason to believe that the formation of "end" tetrahedra in rapid chilling should influence a number of properties, including the activity of glass catalysts used in petroleum cracking, and many other properties, including the mechanical properties of chilled glasses.

Richter, Breitling, and Herre [6, 7] concluded that there is a considerably higher degree of order in SiO_2, B_2O_3, and amorphous Sb than the Zachariasen theory suggests.

The results of heat-capacity determinations of glass formers and certain simple glasses at low temperatures, and analysis of these data on the basis of our heat-capacity functions for chain structures [1], lead to the conclusion that annealed metasilicates, and metaphosphate and metaborate glasses, often have a framework with a chain structure. Deviations from compositions corresponding to metasilicate (or metaphosphate and metaborate, etc.) glasses result in the formation of branched-chain frameworks; the degree of branching increases with decreasing ratio of oxygen to silicon (or phosphorus or boron) atoms.

Thus, investigations of heat capacities at low temperatures lead to the concept of glasses and many "pure" glass-formers as branched chain structures.

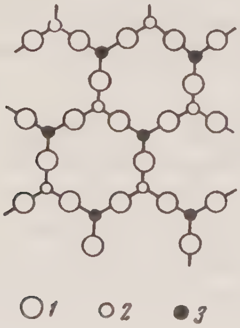

Fig. 1. Schematic representation of the structure of B_2O_3, after Richter, Breitling, and Herre [6]. 1) Oxygen atoms in the plane of the diagram; 2) boron atoms below the plane of the diagram; 3) boron atoms above the plane of the diagram.

In the Zachariasen structure of glassy B_2O_3 only two-dimensional polymerization is really possible. The new structure proposed by Richter, Breitling, and Herre [6] (see Fig. 1) does not eliminate this difficulty.

If boric anhydride has a Zachariasen two-dimensional structure, the formation of a three-dimensional space framework is evidently impossible, and this has apparently been noted by many workers, especially in recent years. In this connection we refer once again to the work of Richter, Breitling, and Herre [7] on the structure of vitreous B_2O_3, to the paper by K. Fajans and S. Barber [8], and also to the paper by Grjotheim and Krogh-Moe on the anomaly of glasses containing B_2O_3 [9].

This last paper contains an explanation of the anomalous properties of glasses formed by B_2O_3 with oxides of alkali metals, and it is noted that the coordination number of boron with respect to oxygen decreases from four to three on addition of Na_2O.

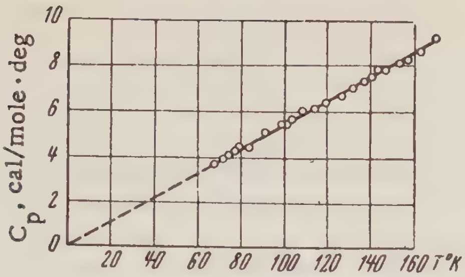

Fig. 2. Heat capacity of glassy B_2O_3 as a function of temperature [10].

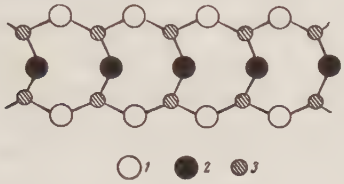

Fig. 3. Schematic representation of the chain of orthorhombic Sb_2O_3 (valentinite). 1) Oxygen atoms below the plane of the diagram; 2) oxygen atoms above the plane of the diagram; 3) Sb atoms.

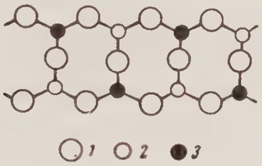

Fig. 4. Possible structure of B_2O_3 chains. 1) Oxygen atoms in the plane of the diagram; 2) boron atoms above the plane of the diagram; 3) boron atoms below the plane of the diagram.

The measurements of the low-temperature heat capacity of crystalline B_2O_3, carried out by Kerr, Hersh, and Johnston [11], and our determinations of the heat capacity of vitreous B_2O_3, show that the heat capacity is directly proportional to the temperature, as is shown in Fig. 2.

It follows from the theory of the heat capacity of chain structures that vitreous B_2O_3 [10] has a chain or a branched-chain structure, similar to the structure of the orthorhombic modification of Sb_2O_3 (Fig. 3).

These considerations were put forward in our earlier papers [10, 17, 18] which contain all the numerical results and their theoretical analysis on the basis of our formulas (see below).

In the transition from the structure shown in Fig. 4 (unbranched chain) to the structure in Fig. 5, no end atoms are ejected or added, as both structures – the simple chain and the branched chain (Fig. 5) – conform to the same stoichiometric composition: A_2X_3.

It must be also emphasized that in the case of a glassy substance the chains are bent in space, and branching results in a three-dimensionally polymerized framework, characteristic of a glassy substance.

Figure 6 shows the possible structure of a chain with the composition A_2X_3 in the form of a close-packing of oxygen atoms (large spheres), the "triangular" interstices of which are filled alternately (in front of and behind the diagram) with small cations. Clearly, this packing is quite equivalent to that shown in Fig. 4.

In the case of B_2O_3 the ratio of the radii of the oxygen and boron atoms is such that the centers of the smaller spheres (boron) are 0.45 A above the plane of the diagram; i. e., we have a structure consisting of

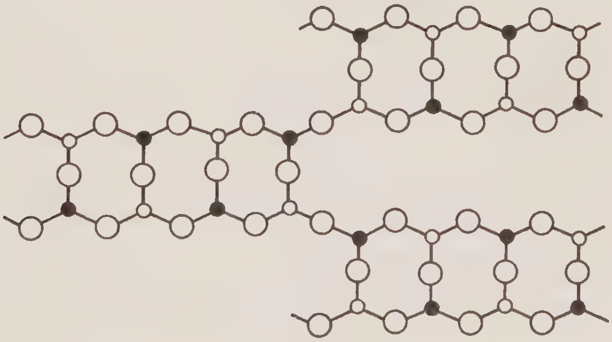

Fig. 5. Possible branched-chain structure of B_2O_3 or of A_2X_3 in general.

triangular flattened pyramids (if we fix our attention on the centers of the boron and oxygen atoms only), with vertices alternately toward us and away from us. The chain structure (Fig. 5) has the advantage that it accounts for the linear course of the low-temperature heat capacity of glassy B_2O_3, shown in Fig. 2.

On examination of the proposed structure of B_2O_3 it becomes clear why it is considerably more compressible than SiO_2, as shown by the high-pressure investigations of Weir and Shartsis [12].

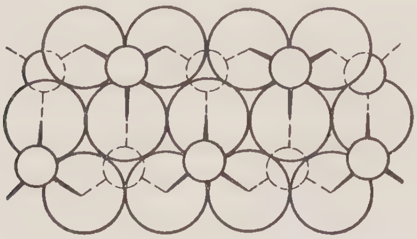

Fig. 6. Schematic representation of the atomic "packing" in the A_2X_3 chain.

Evidence in favor of the proposed chain structure is also provided by the difference in the rates of diffusion of He and A through B_2O_3 and SiO_2 [13]. According to the results of our investigations, a branched structure is postulated in glassy As_2O_3, Sb_2O_3, Bi_2O_3 [18], P_2O_5, Nb_2O_5.

Kordes, Vogel, and Feterowsky [14] consider the structure of pure vitreous P_2O_5 to be analogous to that of SiO_2. The structure of vitreous P_2O_5 is shown schematically in Fig. 7, which is taken from their paper. In this diagram the oxygen atoms linked by single bonds to the PO_4^{3-} tetrahedra are shown as white circles, while the oxygen atoms linked to pentavalent phosphorus atoms by double bonds are shown as circles containing two parallel lines; phosphorus atoms are shown as small circles.

It must be pointed out, however, that the structure of glassy P_2O_4 can easily be represented in the form of branched chains, i. e., in a form differing considerably from that shown in Fig. 7. The structure of glassy P_2O_5 can be represented in the form of the chains shown in Fig. 6 with the addition, "above" and "below," of oxygen atoms linked by double bonds to P^{5+}. The structure of such a chain of the composition A_2X_5 is shown schematically in Fig. 8.

In reality, the chains in glassy P_2O_5 may be branched. This does not involve any disturbance of the stoichiometric composition of P_2O_5 in the transition from unbranched to branched chains (see Fig. 5).

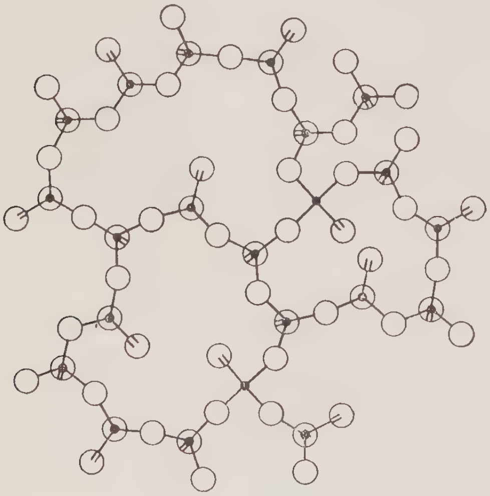

Fig. 7. Structure of glassy P_2O_5, after Kordes et al. [14].

An important argument in favor of the new hypothesis of the chain structure of glassy pentoxides is provided by analysis based on the quantum theory of heat capacity.

The heat capacity of a chain structure without lateral interaction of the chains is represented by the function*

$$C_1 = 3R\left(\frac{T}{\Theta_1}\right)^1 \int\limits_0^{\Theta/T} \frac{x^2 e^x dx}{(e^x - 1)^2} = $$

$$= 3R\left(\frac{T}{\Theta_1}\right)^1 \int\limits_0^{\Theta/T} \frac{\left(\frac{x}{2}\right)^2 dx}{sh^2\left(\frac{x}{2}\right)},$$

where $$x = \frac{h\nu}{kT}, \ \theta_1 = \frac{h\nu_{\max}}{k} \qquad (1)$$

The heat capacity of a chain structure with lateral interaction of the chains is represented, in accordance with [1a] or [1e], by the following expression, which is a combination of the unidimensional Function (1) and the Debye three-dimensional function:

$$C_3 = 9R\left(\frac{T}{\Theta}\right)^3 \int\limits_0^{\Theta_3/T} \frac{x^4 e^x dx}{(e^x - 1)^2};$$

---

* 'sh' ≡ 'sinh' — Publisher.

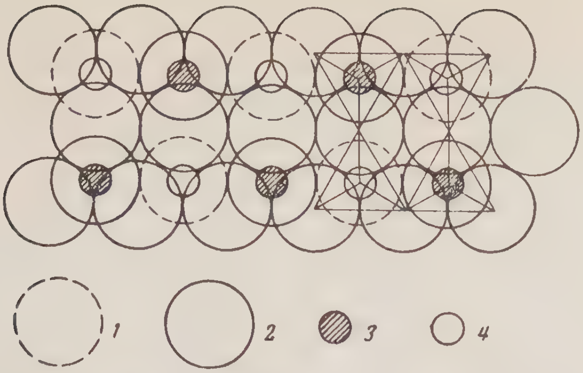

Fig. 8. Schematic representation of a chain of the composition $A_2^{5+}X_5^{2-}$. 1) X^{2-} ions below the plane of the diagram; 2) X^{2-} anions in or above the plane of the diagram; 3) A^{5+} cations above the plane of the diagram; 4) A^{5+} cations below the plane of the diagram.

$$C_{1(3)} = 3R\frac{T}{\Theta_1}\int_0^{\Theta_1/T}\frac{x^2e^x dx}{(e^x-1)^2} - \frac{\Theta_3}{\Theta_1}\left[3R\frac{T}{\Theta_3}\int_0^{\Theta_3/T}\frac{x^2e^x dx}{(e^x-1)^2} - 9R\left(\frac{T}{\Theta_3}\right)^3\int_0^{\Theta_3/T}\frac{x^4e^x dx}{(e^x-1)^2}\right. . \qquad (2)$$

After simple rearrangements, Eq. (2) may be written in more elegant and compact form as the sum of two integrals:

$$C_{1(3)} = 3R\,\frac{T}{\Theta_1}\int_{\Theta_3/T}^{\Theta_1/T}\frac{\left(\frac{x}{2}\right)^2}{sh^2\left(\frac{x}{2}\right)}dx + 36\cdot R\cdot\frac{T}{\theta_1^1\,\theta_3^2}\int_0^{\Theta_3/T}\frac{\left(\frac{x}{2}\right)^4}{sh^2\left(\frac{x}{2}\right)}dx . \qquad (2a)$$

Here Θ_1 is the maximum characteristic temperature, and Θ_3 is the characteristic temperature corresponding to lateral interaction between the chains.

At high temperatures Θ_3 plays no part, and instead of the more complex function (2) we have the simple one-parameter function (1).

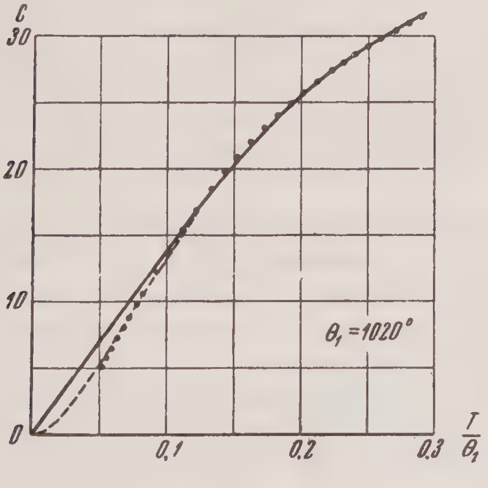

Fig. 9. Heat capacity of Nb_2O_5 from 53.24°K to 296.64°K after King [15]. The points represent experimental values of C_p in cal · mole^{-1} · deg^{-1}; the continuous curve represents the unidimensional Debye chain function (1) for $\Theta_1 = 1020°$; the dash curve represents our two-parameter function (2a) for interacting chains, from tabulated data [16] for $\Theta_1 = 1020$; $\Theta_3/\Theta_1 = 0.2$.

Analysis of data on the heat capacity of Nb_2O_5 with the aid of tables for the unidimensional function (1) [16] confirms the hypothesis of the chain structure of niobium pentoxide. Figure 9 shows a theoretical curve corresponding to the one-parameter function (1) for "noninteracting" chains. In conformity to the chemical composition of Nb_2O_5, the ordinates of the theoretical curve in this diagram are given for seven g-atoms, i. e., they correspond to the heat capacities of Nb_2O_5 in cal per mole · deg. The theoretical curve in Fig. 9 also shows the experimental values of the heat capacity of Nb_2O_5, taken from King's paper [15] (see Table 1). Below 100°K the experimental points lie below the theoretical one-parameter curve. This indicates lateral interaction of the chains. Application of Function (2), with the ratio $\Theta_3/\Theta_2 = 0.2$, gives good agreement between the experimental data and the theoretical curve over its entire length, i. e., between 53.24 and 296.64°K.

It is appropriate to stress the increasing importance of concepts of the chain structure of inorganic glasses. The quantum theory of heat capacity of heterodynamic structures leads to weighty arguments in favor of this structure in many glasses. These arguments were detailed in our earlier papers [1a, b, c, d, e, f].

TABLE 1

Heat Capacity of Nb_2O_5, After King [15]

T° K	C	T° K	C	T° K	C
296.64	31.45	196.13	24.88	96.75	12.21
286.50	30.98	186.11	22.02	84.45	10.48
276.76	30.44	176.36	23.06	80.17	9.721
266.49	29.81	166.28	22.04	74.52	8.732
256.19	29.20	155.98	20.89	70.06	7.977
245.82	28.57	146.39	19.76	65.58	7.206
236.41	27.98	136.03	18.42	61.25	6.426
228.17	27.40	124.62	16.85	57.12	5.716
216.60	26.54	114.54	15.39	53.24	5.127
206.15	25.69	104.36	13.76		

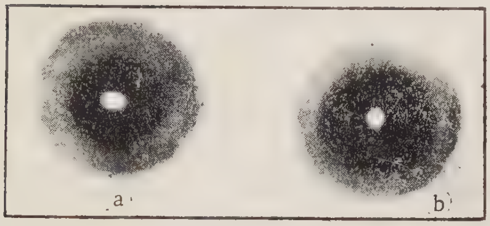

Fig. 10. X-ray diffraction patterns given by fibers of sodium metaphosphate glass. a) Unoriented sample of $NaPO_3$ glass fiber; b) oriented fibers of $NaPO_3$ (fiber axis vertical).

It now seems to be necessary to revise the accepted views on the structure of many glass-formers and multicomponent glasses. The chain structure of glass-forming frameworks satisfactorily reflects many physical and technological properties of glass.

The physicochemical properties of glass seen in a new light on the basis of the concept of a branched-chain framework include the following: the structure of definite and indefinite compounds in glass [17], viscosity (and in particular, structural viscosity), high elasticity in the softening region, structural birefringence [20], the chain structure of metaphosphates [19], the orientation of metaphosphate glass fibers, reported by Goldstein and Davies [20], and others.

In a recent note, Kruch [21] explained the existence of a positive temperature coefficient of surface tension in molten glasses, and likened this effect to the rubberlike elasticity of linear polymers.

Further evidence for the chain structure of inorganic glasses is provided by the strengthening of thin glass fibers, which does not conform to the "defect theory," detected and explained by Bartenev and Bovkunenko [22]. The orientation of metaphosphate chains detected by Goldstein and Davies [20] in $NaPO_3$ glass fibers is seen in Fig. 10, taken from their paper.

Work is continuing in our laboratory on studies of glassy pentoxides of other elements of the fifth group, including phosphorus. The method used is that described above, i. e., measurement and analysis of low-temperature heat capacities.

LITERATURE CITED

[1] a) V. V. Tarasov, "Concerning the theory of heat capacity of high polymers," Doklady Akad. Nauk USSR 58, 577 (1947); "Theory of heat capacity of chain and layer structures," Zhur. Fiz. Khim. 24, 111 (1950).

b) V. V. Tarasov, "Hydrogen bonds in crystals and glasses and the quantum theory of heat capacity," Zhur. Fiz. Khim. 26, 1374 (1952).

c) V. V. Tarasov and Ia. S. Savitskaia, "The heterodynamism of silicate glasses," Zhur. Fiz. Khim. 27, 744 (1953); "Heat capacity and structure of silicate glasses," Doklady Akad. Nauk USSR 88, 1019 (1953).

d) V. V. Tarasov, "The theory of heat capacity and the structure of glasses," Steklo i Keramika 2, 6 (1954).

e) V. V. Tarasov, "Chain and layer structures in crystals and glasses," Trudy Inst. Krist., AN SSSR 10, 310 (1954); "Anisotropy of atomic vibrations and heat capacity of layer and chain structures," Doklady Akad. Nauk USSR 100, 307 (1955).

f) V. V. Tarasov, "The structure of silicate glasses. The formation of glass," Proc. Conference on the Structure of Glass, 1953 [in Russian] (Izd. AN SSSR, 1955), p. 62.

[2] V. Garino-Ganina, "Sur une bande d'absorption du verre de silice dans l'infrarouge," Cahiers Phys. 48, 72 (1954); "Contribution a la connaissance de la silice vitreuse III," Cahiers Phys. 66, 29 (1956); "Bande d'absorption a 2.72 μ de la silice vitreuse," Compt. rend. 239, 12, 705 (1954).

[3] M. Foex, "Remarques sur la transparence dans l'infrarouge de verres de silice prepares au four solaire, en différentes atmospheres," Mem. Pres. Soc. Chimique 159, 767 (1954).

[4] J. M. Stevels, "Glass considered as a polymer, I," Glass Ind. 35, 69 (1954).

[5] J. M. Stevels, "Glass considered as a polymer, II," Glass Ind. 35, 135 (1954).

[6] H. Richter, G. Breitling, and F. Herre, "Structur des glasigen B_2O_3," Z. Naturforsch. 9a, 390 (1954).

[7] H. Richter and G. Breitling, "Struktur des amorphen Sb, Se und des glasigen B_2O_3," Arbeitstagung Festkörperphysik II in Dresden 208 (1955); Leipiz, Verlag: Johann Ambrosius Barth.

[8] K. Fajans and S. W. Barber, "Properties and structures of vitreous and crystalline boron oxide," J. Am. Chem. Soc. 74, 2761 (1952).

[9] K. Grjotheim and J. Krogh-Moe, "A structural explanation of the boron oxide anomaly," Kgl. norske videnskab. selskabs forh. 27, 18, 11 (1954).

[10] V. V. Tarasov and E. F. Stroganov, "A study of microheterogeneous glass and glassy B_2O_3," Trudy MKhTI im D. I. Mendeleev 21, 26 (1956).

[11] E. C. Kerr, H. N. Hersh, and H. L. Johnston, "Low temperature heat capacity of inorganic solids, II. The heat capacity of crystalline boron oxide from 17 to 300°K," J. Am. Chem. Soc. 72, 4738 (1950).

[12] C. E. Weir and L. Shartsis, "Compressibility of binary alkali borate and silicate glasses at high pressures," J. Am. Ceramic Soc. 38, 299 (1955).

[13] F. J. Norton, "Helium diffusion through glass," J. Am. Ceramic Soc. 36, 90 (1953).

[14] E. Kordes, W. Vogel, and R. Feterowsky," Physikalisch-Chemische Untersuchungen über die Eigenschaften und Feinbau von Phosphatgläsern," Z. Elektrochemie 57, 282 (1953).

[15] E. G. King, "Low-temperature heat capacities and entropies at 298, 16°K of manganese sesquioxide and niobium pentoxide," J. Am. Chem. Soc. 76, 3289 (1954).

[16] N. A. Chernoplekov, "Tables of heat-capacity functions of heterodynamic structures," Zhur. Fiz. Khim. 25, 878 (1951).

[17] V. V. Tarasov, "The structure of silicate glasses. The formation of glass," Proc. Conference on the Structure of Glass, 1953 [in Russian] (Izd. AN SSSR, 1955), p. 62.

[18] V. V. Tarasov, "Chain structure of sesquioxides and the theory of heat capacity," Zhur. Fiz. Khim. 29, 198 (1955).

[19] J. R. Van-Wazer, "Structure and properties of the condensed phosphates, II. Theory of the molecular structure of sodium phosphate glasses," J. Am. Chem. Soc. 72, 644 (1950).

[20] M. Goldstein and T. H. Davies, "Glass fibers with oriented chain molecules," J. Am. Ceramic Soc. 38, 229 (1955).

[21] R. Kruch, "On the surface tension and structure of molten glasses," J. Chem. Phys. 25, 1085 (1956).

[22] G. M. Bartenev and A. N. Bovkunenko, "The structure of glass and the strength of glass fibers," Zhur. Fiz. Khim. 29, 508 (1955).

Received February 22, 1957

D. I. Mendeleev Moscow Institute of Chemical Technology

OXIDE FORMATION AND PHOTORESISTANCE OF LEAD SULFIDE FILMS

V. N. Vertsner, N. A. Kel'ner, and A. M. Solov'ev

The changes which take place in the composition of lead sulfide when heated in the open air were investigated by electron diffraction methods. PbS was used as thin films or vacuum sublimated deposits on glass. The relation to the temperature of the rate of oxidation and of the type of oxides formed was established.

Lead sulfide photoresistances have been widely applied in recent years as radiation receivers in spectral and other apparatus. The conductivity and photoresistance of PbS layers depend greatly on their structure, which includes their composition in terms of separate components, as well as their crystalline structure, the sizes of the grains, and their mutual distribution and orientation with respect to the substrate.

Lead sulfide layers become sensitive as a result of activation, which consists in heating them in air, or in an oxygen atmosphere, at 500-600°C. The activation is accompanied by growth of the crystals, which form layers, and by the formation of various compounds of lead and sulfur with oxygen.

Detailed electron diffraction studies of photosensitive layers of lead sulfide were first carried out by Wilman [1]. According to his data chemically stable PbS layers consist of partially oriented crystallites from 150 to 500 A in size. Heating the layers for 10 min in air at 350-370°C induces growth of the crystallites and a partial transition of PbS into the compound $PbO \cdot PbSO_4$, known as lanarkite. In photoelements prepared by Sosnovskii's [2] method, the crystals of lead sulfide were ~ 1000 A in size, but those of lanarkite did not exceed 500 A. The content of lanarkite fluctuated between 10 and 20%. Both types of crystallites were oriented with respect to the substrate.

That lanarkite was formed in photoresistances was confirmed in the studies [3, 4]; in addition it was shown in [3] that it is formed only on the activated surface of the photoresistances.

Sosnovskii [5] showed that in the process of activation at 250° to 400°C, the formation of the sulfate $PbSO_4$ precedes that of lanarkite, and at 550°C lead oxide – PbO – is formed. As a result of these reactions PbS, PbO and $PbSO_4$ and only partially $PbO \cdot PbSO_4$ crystals are formed in the layers. At 600°C a partial reduction of the lead is possible.

Stein and Reuter [6, 7] detected the oxides PbO and PbO_2 in lead sulfide photoresistances. These results agree with those in [8] and [9] which established that deposits of PbO and PbO_2 are formed on the faces of a crystal of galenite when heated (at 500°) at reduced pressure. Under the experimental conditions [9] the formation of $PbSO_4$ and $PbO \cdot PbSO_4$ occurred at a lower temperature and preceded that of PbO and PbO_2.

Results that do not agree with Wilman's conclusions concerning chemically obtained photoresistances are also indicated in [6, 7, 10]. Their data show that the layers of these photoresistances are a mixture of PbS, PbO and $Pb(OH)_2 \cdot PbCO_3$, and not PbS and $PbO \cdot PbSO_4$, as Wilman claimed.

Vertsner, Malakhov and Solov'ev [11], in carrying out a gradual refinement of PbS layers prepared by a physical method, established that the content of lanarkite decreased rapidly with distance inward from the surface of the photoresistance. PbO is the dominant oxide in the surface film; below is an interlayer which consists mainly of PbO with traces of $PbO \cdot PbSO_4$. The lower layer of the photoresistance near the glass substrate is of unreacted lead sulfide. No orientation of the crystallites was observed in the above-mentioned oxides.

The surface film, as was shown in [11] plays a very substantial role in giving rise to photosensitivity; its removal is always accompanied by a practically complete loss of sensitivity. Its restoration takes place only after a repeated temperature treatment, which leads to the re-establishment of the initial composition (PbO_2 and $PbO \cdot PbSO_4$). This latter circumstance makes it possible to assume that the emergence of a definite oxide phase on the surface of the layers is connected with the formation of the supplementary entrapment centers of nonintrinsic conductors. On the other hand, the formation of carriers occurs as a result of light absorption by the PbS layer, located in the lower part of the photoresistance.

Electron microscope studies by different authors [3, 11, 12, 13] made possible a definite conclusion concerning the size and mutual orientation of the crystallites which form the original layers and the photoresistances obtained from them. For those obtained by the physical method, an increase in crystallite size, up to 0.4-1.2 μ during activation, is characteristic.

In the present work the change in the composition of the oxides was studied as a function of the thermal treatment, and the rate of oxidation. The work was done on the EM-3 electron microscope equipped with an electron diffraction attachment [14-17].

The study of the speed of oxidation and the determination of the composition of the oxide films was carried out by the electron diffraction method. Thin, free PbS films 0.1 μ thick which had been subjected to different temperature treatments were studied at the same time. The films were obtained by condensing PbS in a vacuum, on organic substrates fastened to meshes. During the evaporation, the temperature of the substrates was about 100°C. When heated at a higher temperature, the organic substrate burned and a free PbS film remained on the mesh.

The samples were heated in a muffle furnace. A series of temperatures was chosen – 250, 340, 450, 510, 590°C – at which changes in the temperature dependence of conductivity were generally observed in the PbS layers. The films were heated either from room temperature to any of those mentioned above, or else were placed in the furnace preheated to a definite temperature, and were held in it at that temperature. The diagram (see Fig. 1) gives an outline of the formation of the different oxides in PbS layers. If the heating of the films is started at room temperature, then the oxides form only at temperatures higher than 340°C. At 450°C the whole PbS layer turns into lanarkite – the compound $PbO \cdot PbSO_4$ detected by Wilman [1]. Oxidation can occur at lower temperatures, but its speed decreases with temperature decrease. Thus, for example, at 280°C the speed of oxidation is five times smaller than at 340°C.

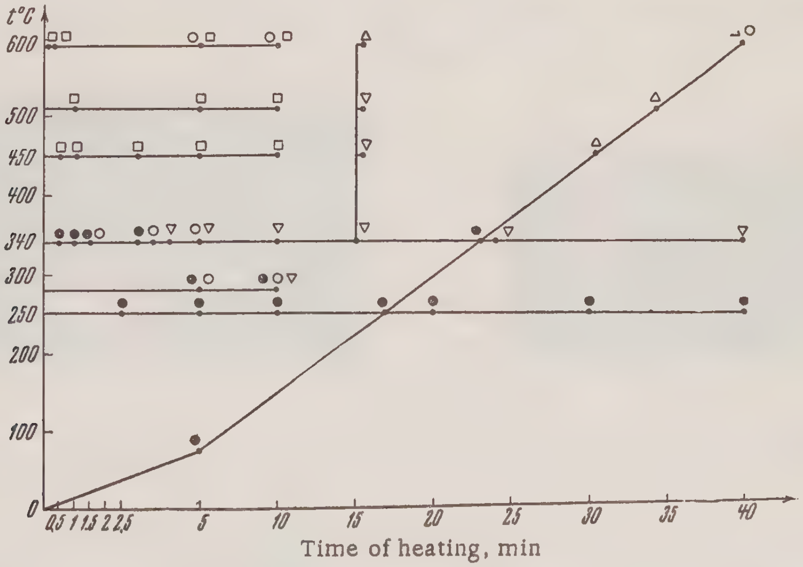

Fig. 1. Diagram of oxide formation during the heating of thin, free PbS films. PbS – ●; lanarkite $PbO \cdot PbSO_4$ – △; low temperature oxide – ▽; $4PbO \cdot PbSO_4$ – □; unknown oxide – ○.

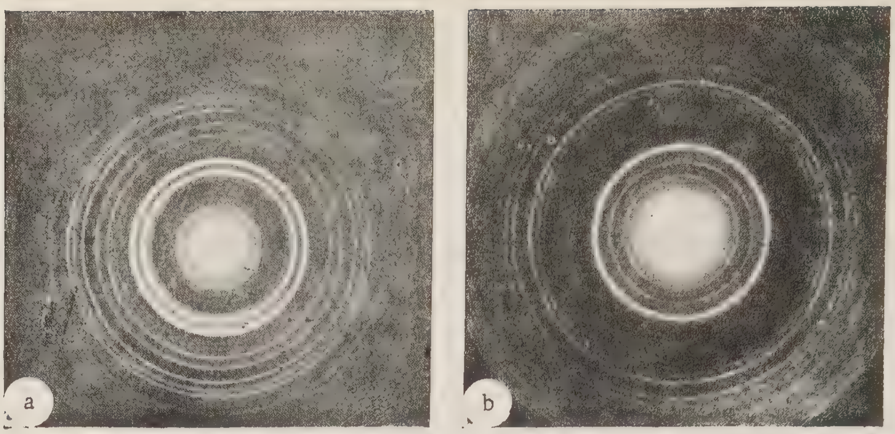

Fig. 2. Electron diffraction patterns from: a) low temperature oxide; b) high temperature oxide (lanarkite).

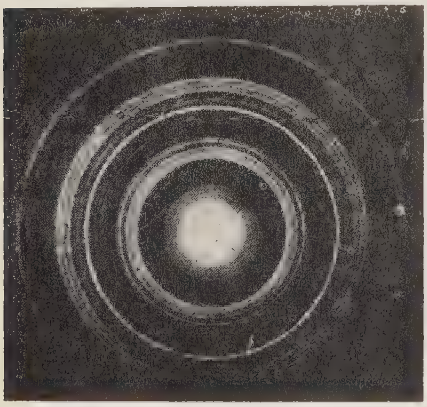

Fig. 3. Electron diffraction patterns from $4PbO \cdot PbSO_4$ films.

The thickness of the films examined coincides with an electron path length at 50 kv which is short enough in these crystals that coherence is not affected [18]. It was found that at 280°C the speed of oxidation is 20 A per min, and at 340°C it is 100 A per min,by calculating the time necessary for the complete transition of PbS into oxides and by the thickness of the layer in which electrons with 50 kv energy scatter coherently.

Fig. 4. Electron diffraction pattern from PbS layer on glass, heated at 590°C for 30 sec.

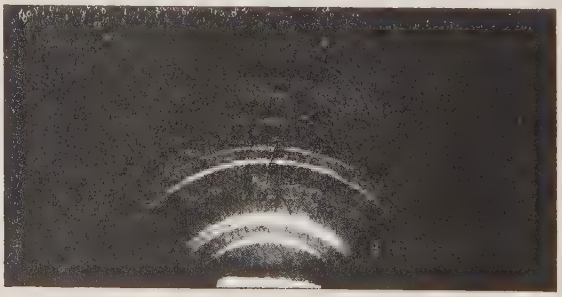

Fig. 5. Electron diffraction pattern from the surface of a lead sulfide photoresistance.

Oxidation at these temperatures leads to the formation of the compound which gives the electron pattern of Fig. 2. The interplanar distances calculated from this pattern (see Table 1) coincide well with those of lanarkite, but with a substantially different relationship between intensities. This circumstance points to the similarity of the lattices of the low and high temperature (lanarkite) oxides, and to the difference in composition and atomic distribution. The low temperature oxide is very stable with respect to further thermal treatment. Thus, for example, it is preserved when the films are heated for several hours at 340°C, as well as for short periods at 450° and 510°C. Its transition into a high temperature oxide (lanarkite) occurs onyl at 590°C. As an exception, the low temperature oxide was observed also on "normal" heating of films, i. e., from room temperature to 450°C.

TABLE 1

Interplanar Distances and Intensities of Reflections of Low Temperature and High Temperature Oxides Formed in PbS Layers

Low temperature oxide (340°C)		High temperature oxide (450°) (lanarkite)		Low temperature oxide (340°C)		High temperature oxide (450°) (lanarkite)	
d, A	I	d, A	I	d, A	I	d, A	I
				1.95	Medium		
6.42	Strong	6.42	Weak	1.82	Medium	1.84	Weak
5.95	Weak	5.95	Weak			1.75	Weak
5.21	Very strong	5.20	Weak	1.72	Medium	1.73	Weak
4.45	Very strong	4.45	Medium	1.67	Medium	1.65	Medium
3.72	Strong	3.69	Weak	1.61	Medium	1.61	Very strong
3.52	Very strong	3.51	Strong	1.57	Weak	1.56	Very strong
3.33	Strong	3.35	Very weak	1.47	Very strong	1.49	Weak
3.12	Weak	3.18	Weak	1.43	Very strong	1.44	Weak
2.90	Very strong	2.96	Very strong	1.38	Weak	1.38	Very strong
2.75	Medium	2.84	Very strong	1.36	Weak	1.36	Very strong
2.59	Very strong	2.57	Medium	1.28	Very strong	1.28	Very strong
2.40	Very strong			1.23	Weak		
2.34	Very strong	2.34	Weak	1.17	Very strong	1.17	Very strong
2.26	Medium	2.25	Weak	1.15	Very strong	1.15	Very strong
		2.17	Very weak			1.13	Very strong
2.10	Medium	2.10	Weak			1.09	Very strong
2.04	Medium	2.05	Medium			1.08	Very strong

TABLE 2

Interplanar Distances According to Data of [19] and Calculated from the Electron Pattern of a PbS Film, Heated at 590°C for One Second

$4\ PbO \cdot PbSO_4$ [19]		Calculated from electron pattern		$4\ PbO \cdot PbSO_4$ [19]		Calculated from electron pattern	
d, A	I	d, A	I	d, A	I	d, A	I
8.23	15	8.22	Strong			2.55	Very weak
7.38	5	7.23	Weak			2.44	Very weak
6.22	5	6.22	Weak			2.40	Very weak
5.78	5	5.76	Very weak	2.35	5	2.33	Very weak
5.45	5	5.40	Very weak			2.28	Very weak
5.17	5	5.20	Weak	2.23	6	2.24	Very weak
		4.53	Very weak	2.15	5	2.19	Very weak
4.28	11	4.22	Very weak	2.06	5	2.02	Very weak
		3.85	Very weak	1.97	20	1.96	Strong
		3.64	Very weak	1.95	23	1.94	Strong
		3.47	Very weak			1.90	Very weak
3.25	100	3.22	Very strong	1.87	5	1.85	Very weak
3.12	37	3.10	Medium	1.84	10	1.82	Medium
3.08	31	3.05	Medium			1.77	Very weak
		2.99	Very weak	1.73	15	1.72	Weak
2.90	37	2.87	Medium	1.70	8		
		2.77	Very weak			1.68	Weak
2.68	37	2.66	Strong	1.66	10	1.64	Medium
2.59	8	2.59	Very weak	1.62	10		
				1.60	10	1.59	Weak
				1.59	5	1.58	Weak

The process of oxidation of PbS layers is entirely different at higher temperatures. When the samples remained in the furnace even for part of a second at 450°C and higher (up to the sensitivity temperature) then the immediate transition of PbS into a compound of the type $4PbO \cdot PbSO_4$ [19] took place (see Fig. 3 and Table 2). This compound is very stable and is preserved for a long time at 450° and 510°C. At 590°C, after 5 min of heating, this oxide partially passes over into an unidentified compound.

The changes in the composition of layers of lead sulfide cited above were among those most frequently observed. However, in several cases, oxides appeared in the layers that were different from the ones described above. This was observed both in analyzing the initial and the final stages of oxidation, i. e., when the samples were heated up to the sensitivity temperature.

The oxidation of PbS layers sputtered onto glass proceeds in the same manner as that of the thin, free films (in the temperature range from 340 to 450°C). Independently of the initial orientation of the lead sulfide crystallites which are formed by the usual slow heating, the oxide crystallites turn out to be unoriented. On the basis of the electron pattern analysis one can conclude that at up to 450°C the orientation and the size of the PbS crystallites remain unchanged.

The initial heating of the lead sulfide layers obtained by sublimation onto glass at 590°C showed that oxidation begins after only 20 sec in the furnace. After 30 sec the surface of the samples becomes covered with a layer of oriented lanarkite crystallites (see Fig. 4). (The latter circumstance corresponds to a speed of oxidation greater than 40 A per min.) With lengthening of the time of initial heating of the orientation of the crystallites is disturbed; an appreciable decrease in the intensities of the reflections from lanarkite is also observed on the electron patterns. Finally, after three minutes of tempering, a surface film [11] is formed, as is usual for lead sulfide photoresistances, which consists of PbO_2 and $PbO \cdot PbSO_4$ (see Fig. 5). As has already been noted above, the appearance of this film is usually accompanied by the emergence of photosensitivity.

On removing the surface layers of the samples, heated for three minutes or longer, the oxides PbO and $PbO \cdot PbSO_4$ appear on the patterns, as is characteristic for the inner layers of photoresistances [11]. At shorter periods of heating there is a layer of unreacted lead sulfide under the lanarkite which was formed on the surface.

SUMMARY

The electron diffraction analysis of lead sulfide sublimates, obtained on glass in the form of thin, free films and layers 1 μ thick, showed that in thin layers at 340°C PbS changes into a stable oxide, with a lanarkite lattice, but differing from it in composition, and that at 450°C and higher, into another stable oxide $4PbO \cdot PbSO_4$. The speed of oxidation depends on the temperature and the type of sublimate. The formation of the surface film of PbO_2 and $PbO \cdot PbSO_4$ on photoresistances is preceded by the development of a lanarkite layer, the crystallites of which lose their orientation on subsequent heating. An interlayer, enriched in PbO, arises after the surface structure, characteristic of sensitive photoresistances, has been formed.

The difference in the course of oxidation between free films and sublimates of lead sulfide on glass is conditioned by the difference in the thickness and structure of the layers, and especially by the substantially different conditions of the reaction of PbS with atmospheric oxygen.

In conclusion, the author wishes to express his gratitude to Academician A. A. Lebedev for his interest in this work and his valuable advice.

LITERATURE CITED

[1] H. Wilman, "The structure of photosensitive lead sulfide and lead selenide deposits and the effect of sensitization by oxygen," Proc. Phys. Soc. 60, 117 (1948).

[2] L. Sosnowski, J. Starkiewicz, and O. Simpson, "Lead sulfide photoresistors," Nature 159, 818 (1947).

[3] J. Doughty, K. Lark-Horovitz, L. M. Roth, and B. Shapiro, "The structure of PbS films,' Phys. Rev. 79, 203 (1950).

[4] R. Ia. Berlaga, S. N. Gural'nik, and M. A. Rumsh, "Electron diffraction analysis of lead sulfide photoresistances," Vestnik LGU 9, 133 (1952).

[5] L. Sosnowski, Badania nad Zjawiskami Fotoelectrycznymi w Polprezewodnikach (Warszawa, 1949).

[6] R. Stein and B. Reuter, "Zur Frage der Photoeffekte in bleisulfid und verwandten substanzen, I," Z. Naturforsch. 10, 655 (1955).

[7] R. Stein and B. Reuter, "Zur Frage der Photoeffekte in Bleisulfid und verwandten Substanzen. II," Z. Naturforsch. 10, 894 (1955).

[8] T. Jamaguti, M. Sakata, and M. Morito, X-Sen 4, 9 (1945).

[9] H. J. Hagihara, "Surface roughening and oxidation of galena cleavage face in vacuum furnace under limited air supply," J. Phys. Soc. Japan 8, 406 (1953).

[10] J. A. James, C. J. Milner, and B. N. Watts, "The structure of lead sulfide films," Phys. Rev. 80, 298 (1950).

[11] V. Vertsner, L. Malakhoff, and A. Solovioff, "Electron microscopic investigation of lead sulfide photoresistors," Report of the First European Regional Conference on Electron Microscopy, Stockholm, 1956.

[12] R. Ia. Berlaga and Iu. N. Shuvalov, "The temperature dependence of the photoconductivity of lead sulfide photoresistances," Vestnik, LGU 9, 121 (1952).*

[13] T. S. Moss, "Lead salt-photoconductors," Proc. IRE 43, 1869 (1955).

[14] V. N. Vertsner, "The Soviet electron microscope," Zavodskaia Lab. 13, 1364 (1947).

[15] V. N. Vertsner, Questions of Microscopy [in Russian] (1956), pp. 117-141.

[16] V. N. Vertsner, "Electron diffraction attachment for an electron microscope,' Zavodskaia Lab. 18, 1481 (1952).

[17] V. N. Vertsner and N. G. Zandin, "Electron diffraction attachment for the electron microscope EM-3," Zavodskaia Lab. 20, 741 (1954).

[18] Z. G. Pinsker, Diffraction of Electrons [in Russian] (1949).

[19] C. L. Clark, J. N. Mrqudich, and N. C. Shieltz, "Die basischen Sulfate des Bleis," Z. anorg. u. allgem. Chem. 229, 401 (1936).

Received March 19, 1957

---

* LGU = Leningrad State University.

X-RAY DIFFRACTION ANALYSIS OF THE CHANGES IN MOSAIC STRUCTURE DURING THE AGEING OF BERYLLIUM COPPER

Ia. Umanskii, V. Eliutina, A. Kagan, and L. Pivovarov

Changes in the size of the sub-grains which occur during isothermal precipitation from supersaturated solid solutions of beryllium in nickel or copper are determined from the intensities of small-angle x-ray diffraction lines.

These intensities increased, i. e., the extinction diminished (the sub-grains fragmented) until the greatest hardness was reached. As the hardness decreased on ageing, the intensities did also, due to the consolidation of the sub-grains. It follows that the fragmentation of sub-grains is important in age-hardening.

Ia. S. Umanskii [1] has assumed that the mosaic structure blocks of a solid solution grow small during ageing. X-ray diffraction [2] showed that this actually takes place during the decomposition of titanwolfram carbide. In the works specified, the decrease in block size was determined by the increase of the integrated intensity of the small-angle x-ray diffraction lines due to the decrease in the initial extinction effect when the blocks grew small (down to dimensions ~ 0.2-0.3 μ).

Averbach [3] and Finkel'[4] likewise observed the strengthening of the small-angle x-ray diffraction lines due to the decrease in block size. Iveronova and Katsnel'son[5] discovered the growth of the blocks during the annealing of plastically deformed solid solutions by noting the significant weakening of the small-angle x-ray diffraction lines. The effect of the initial extinction was utilized in Kochanovska's [6] work for determining the average size of quartz and graphite crystallites.

All these works point to the expediency of further development of the method of determining the block size in materials where the blocks are large by measuring the intensity of the small-angle lines so as to collect comparable data, since, according to modern assumptions, the strengthening of the metal is almost always related to the diminution of block size.

The study of the initial extinction was the method used in this work to determine changes in the size of blocks during the ageing of nickel-beryllium and copper-beryllium alloys.

Procedure and Results of Analysis

A Ni—Be alloy with 2.28% Be and a commercial beryllium copper of the composition: Cu, 97.15%; Be, 2.38%; Ni, 0.37%; Fe, 0.06% were examined. The 0.4 mm thick cold-rolled Ni—Be strip was quenched from 1050°C, and then was quenched once more in water after being exposed to 1100° for 45 sec. Longer exposure of the thin strip led to extreme burning out of the beryllium. The intragranular structure changes of the solid solution caused by chilling were removed at the indicated temperature and exposure. Specimens 30 mm in diameter and 1.5 mm thick were cut out from the Cu—Be alloy and were quenched in water after being tempered for 20 min at 810°. The ageing was done in a muffle furnace. The surface layer was removed by electrolytic etching in HNO_3 solution.

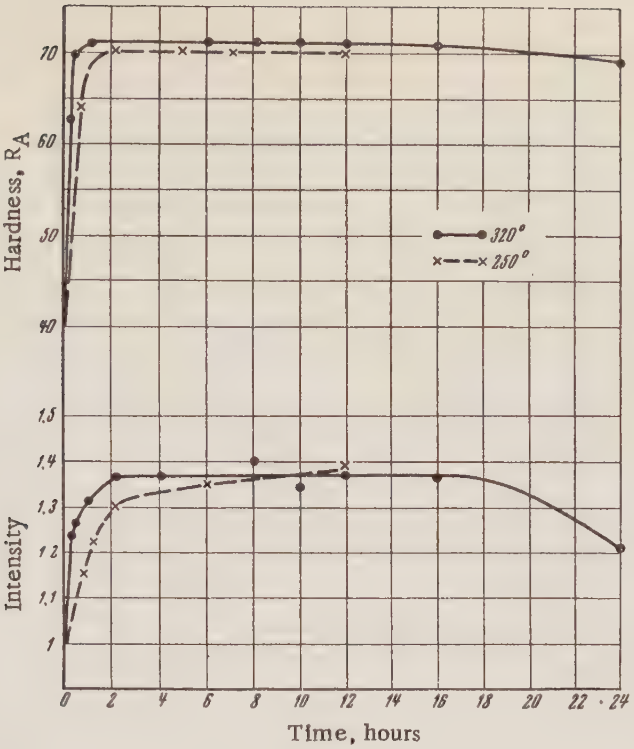

Fig. 1. Variation in hardness and in intensity of the (111) line during ageing of the Cu–Be alloy at 250° and 320°C.

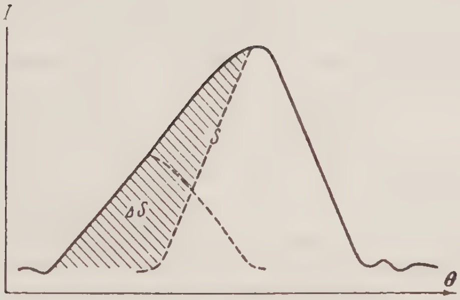

Fig. 2. The (111) line of the Cu–Be solid solution after ageing 4 hrs at 250°C.

The hardness of the Ni–Be alloy was measured on a Vickers apparatus, and of the Cu–Be on a Rockwell scale (R_A).

The x-ray photographs were prepared using Cu-radiation and constant operating conditions; the $(200)_\alpha$ line of the Ni–Be solid solution and the $(111)_\alpha$ line of the Cu–Be alloy were recorded. The specimen was rotated by a special device around an axis perpendicular to the sample plane. The rotation axis was shifted relative to the initial beam to remove the spottiness of the rings. The diffraction pattern of the Ni–Be alloys was recorded photographically, simultaneously with that of a standard; two semi-cylinders – the sample and the standard (molybdenum powder blown onto wood) – were fastened in a cylindrical ring. The rings rotated around an axis which lay in the surface separating the semi-cylinders, so that both semi-cylinders were caught alternately in the cluster of rays. The x-ray patterns which showed both the (200) solid solution lines and (110) molybdenum ones, were photometered on an MF-4 microphotometer.

The (111) line of the Cu–Be alloy was recorded by a URS 50-I self-quenching Geiger-Muller end counter. The results were recorded on the potentiometer chart.

The integrated reflection intensities were determined from the peak areas of the interference curves.

The calculations were carried out on the assumption that the solid solution structure, after the alloys had been treated, is practically ideally mosaic, i. e., the size of the blocks does not exceed 0.2 μ according to the maximum intensity of the lines. For other cases, the size of the blocks was determined from the intensity of the lines according to Darwin's formula

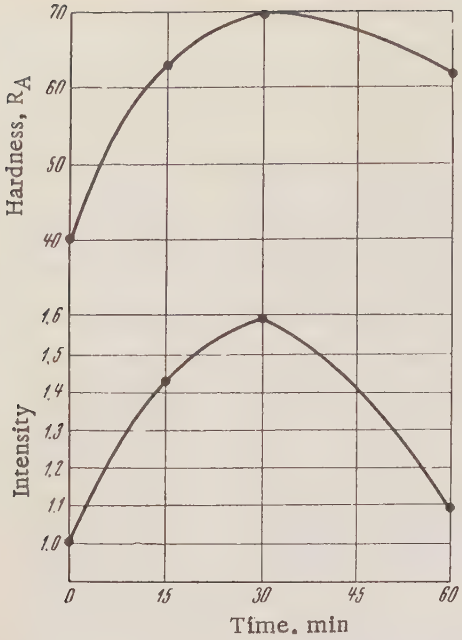

Fig. 3. Variation in hardness and in intensity of the (111) line during ageing of the Cu–Be alloy at 390°C.

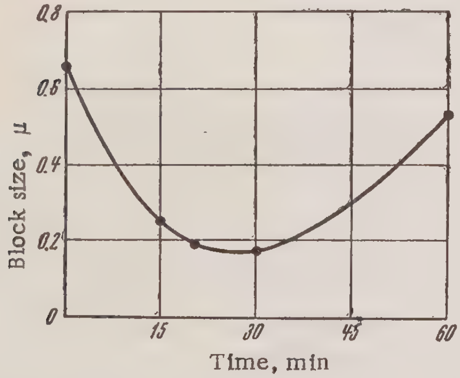

Fig. 4. Variation in the size of blocks during ageing of the Cu–Be alloy at 390°C.

$$\frac{I}{I_{\text{id. mos.}}} = \frac{\tanh(nq)}{nq},$$

where $\underline{q}$ is the reflecting power of the atomic plane, $\underline{n}$ is the number of parallel atomic planes within the limits of the mosaic block.

No account was taken in the calculation of :
a) the variation of the number of solid solution unit cells in 1 cm^3 of alloy, caused by the formation of the second phase, and b) photoelectric absorption.

The quenched specimens of the Ni–Be alloy were annealed at 630°C, which did not result in a maximum hardness; this was done because intensity measurements were impossible after annealing at the optimal temperature of 550° due to the extreme broadness of the line.

The measurements and calculations for the alloys are collected in Table 1.

The ageing of the Cu–Be alloy at 250° and 320°C (Fig. 1) is accompanied by an increase in the intensity of the $(111)_\alpha$ line and in the hardness. After 24 hrs of ageing at 320°C the hardness and the intensity of the $(111)_\alpha$ line decrease simultaneously.

An unsymmetrical broadening of the (111) line is observed occasionally during the ageing process. The line broadens especially in the direction of small angles (Fig. 2). After the line regains its symmetry, it is displaced appreciably towards smaller angles. The sharpness of the line is restored after one hour of ageing at 320°.

The intensity of the (111) line increases simultaneously with the increase of hardness at 390° (Fig. 3) as well as at the other ageing temperatures, and it decreases as hardness decreases. After 15 min of ageing, the line broadens 1.8 times; after 30 min, the sharpness of the line is restored.

Even after 15 min of ageing a considerable displacement of the line towards small angles is observed. Figure 4 depicts the changes in block size during the ageing process of the Cu–Be alloy.

TABLE 1

Treatment	Vickers hardness (kg/cm^2)	$\frac{I}{I_{\max}}$	Mosaic block size (in μ)
Quenching	170	0.6	1.2
Quenching + annealing, 630°, 40 min	310	1	0.3
The same at 30 minutes	260	0.8	1

DISCUSSION OF RESULTS

The following factors can affect the integrated intensity of the x-ray diffraction lines:

1. The mosaic block size on which depends the initial extinction that lowers the intensity.
2. The quantity of the solid solution, which decreases when the second phase is precipitated.
3. Static lattice distortions of the solid solution caused by dissimilarity in atomic radii.
4. Dislocations (static distortions, caused by plastic deformation, related to the decomposition).

The static solid solution lattice distortions cannot affect the intensity of the (111) and (200) lines due to the small value of $\sin^2\theta/\lambda^2$ which is part of the exponent of the temperature factor; the precipitation of the second phase can only decrease the intensity if the quantity of the solid solution decreases; therefore, the intensity increase of the (111) line during ageing is solely the result of the decrease in size of the mosaic blocks.

The intensity decrease after renewed ageing must be explained basically by block enlargement, since about 0.5-0.6% of excess Be remains in the solid solution at its maximum hardness, which can consolidate during the further precipitation of the CuBe and NiBe 4% Cu or Ni compounds, and decrease the line intensity by no more than 8%.

Thus the present study shows that hardening in both alloys is accompanied by the diminution in size of the mosaic structure blocks. This is probably the result of stresses which arise as a new phase of different specific volume is formed, and is an important cause of hardening during ageing.

The broadening of the (111) line of the Cu—Be alloy during ageing can be explained by the development of microstresses and the chemical nonhomogeneity of the solid solution. Since the size of blocks remains rather large in all cases (the extinction effect is observed) the line broadening, caused by the small size of blocks, is not observed.

The presence of elements of a two-phase precipitation accounts for the asymmetry of the (111) line of the Cu—Be alloy; apparently, a superposition of lines of the initial and terminal solid solutions takes place which differ very little in lattice constants (Fig. 2).

These data are in good agreement with the results of the deformation ageing analysis of high-manganese steel.

SUMMARY

1. The size of blocks during ageing of the Cu—Be and Ni—Be alloys was measured using the x-ray diffraction method by determining the changes of the initial extinction.

2. It has been established that during ageing a diminution of block size is observed, accompanied by an increase in hardness, and when the hardness decreases on re-ageing, the blocks become larger again.

LITERATURE CITED

[1] Ia. S. Umanskii, "Application of x-rays to the study of materials," Trudy Vesesoiuz Konfer. pp. 47-53 (1949).

[2] Ia. S. Umanskii and V. P. L'vovskaia, "Some decomposition peculiarities of complex carbide of titan-wolfram," J. Tech. Phys. (USSR) 20, 1167-1174 (1950).

[3] B. L. Averbach, J. Metals 8, 491 (1949).

[4] V. M. Finkel', The Physics of Metals and Metallography [in Russian] (1956), p. 189.

[5] V. I. Iveronova and A. A. Katsnel'son, "Concerning the mosaicity of crystals in polycrystalline metals," J. Tech. Phys. (USSR) 25, 696-699 (1955).

[6] A. Kochanovska, Chekhoslov. Fiz. Zhur. 4, 34 (1954).

[7] O. V. Bogorodskii and Ia. S. Umanskii, "Changes in the fine crystalline structure of austenitic manganese steel during plastic deformation," Izv. AN SSSR, Ser. Fiz. 20, 614-620 (1956).

Received February 28, 1957

I. V. Stalin Moscow Steel Institute

THE X-RAY DIFFRACTION DETERMINATION OF THE THERMAL EXPANSION OF SINGLE CRYSTALS

V. V. Zubenko and M. M. Umanskii

The x-ray investigation of the thermal expansion of substances of low symmetry requires the study of single crystals. The measurements of the parameters of the unit cell (when the temperature is maintained constant with the precision 0.1°) are made with the help of zero-layer line reflections on oscillation patterns.

Two cameras for such measurements (in air) are described. One (with electrical heating) is used for temperatures up to 300-400°C. The other (with liquid thermostat) allows one to obtain temperatures down to −50°C. The stabilization of temperature is obtained with the help of an electronic potentiometer and a battery of thermocouples.

The parameters a and c of Al_2O_3 were determined in the interval 20-272°C by means of rotating crystal photographs. The directions of the axes of rotation: $10\bar{1}0$ and $\sim 10\bar{1}14$. $\alpha_{\perp} = 5.6 \cdot 10^{-6}$ and $\alpha_{\parallel} = 6.6 \cdot 10^{-6}$. The temperature curves of the parameter d_{001} of $Li_2SO_4(H_2O)_6$ are given in Fig. 5. $\alpha = 15.6 \pm 0.5 \cdot 10^{-6}$.

In her addendum Ezhkova gives the temperature variations of the parameter c of $K_2C_4O_6\,{}^1/_2H_2O$ (Fig. 6). $\alpha_{33} = 31.5 \pm 0.5 \cdot 10^{-6}$.

One of the most complicated divisions of x-ray diffraction temperature analyses is the study of the thermal expansion of low-symmetry crystals. Such work requires precise parameter measurements of unit cells and of their changes with temperature. The x-ray diffraction study of thermal expansion can be carried out on polycrystalline samples [1, 2] for crystals of the cubic and, sometimes, the tetragonal and hexagonal systems, but for low symmetries single crystals must be analyzed. In this case the dependence on temperature of several parameters of the unit cell must be determined. Such measurements can be made on reflections of the zero-layer lines of oscillation patterns. A chosen location of the oscillation range must be established and changed in the process of exposure in such a way as to obtain several oscillation patterns on one film [3, 4]. It is easy to thermostat the sample, if no special medium (vacuum) is necessary and the pattern can be obtained in air. A constant high temperature is best created during the x-ray exposure by electric heating, and lower temperatures (down to −50°C) with the help of a fluid thermostat. It is convenient to thermostat only that part of the camera where the sample is. It is also convenient to place the film outside of the thermostat, because it allows one to obtain several exposures without disturbing the thermal treatment of the sample. A short description of two cameras of this type follows.

Camera with an Electric Thermostat

The camera with electric heating and RKVT thermostat was built on the base of a RKV [3] camera and adjusted for work in the interval from room temperature up to 300-400°C (Fig. 1). It can be used to obtain 360° rotation patterns, stationary patterns, or oscillation patterns with a small angular range. The transition from one oscillation range to another can be made without disturbing the thermal procedure. Only a comparatively narrow

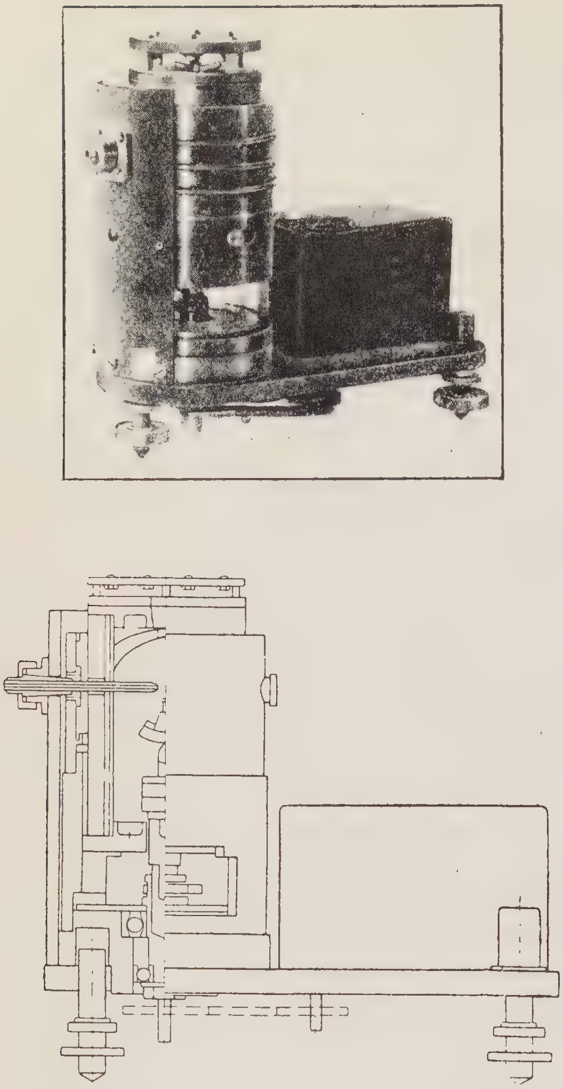

Fig. 1. RKVT camera with electric thermostat (diagram and photograph).

equatorial region of the pattern up to $\vartheta = 84°$ is recorded. The base of the camera, the forward collimator support, the SD-2 motor transmission by gears or by cam and lever, which is fastened to the rotating axis of the goniometer head, are arranged as in the RKV cameras. The axis connecting the goniometer head with the rotating (oscillating) mechanism is made partly from heat-insulating material, i. e., asbestos cement. The thermostat is made from a section of asbestos cement tubing and can easily be lifted off its base which is secured to the camera base. There are two slits in the lateral surface of the camera, which are sealed with a cellulose acetate film on the inner and outer surfaces of the tube. The initial beam and the reflected rays go through these slits. An air space is formed between the films, which is a sufficient heat insulator. Three sections of heater wire are arranged in the thermostat. There is a metal hemispherical screen in the central part of the thermostat for removing thermal gradients in the neighborhood of the sample. The presence of this screen and a correct choice of heating technique makes it possible to obtain a constant temperature along the camera axis for a distance of about 15 mm. The film cassette is located outside the thermostat and can be removed without disturbing the heating rate of the camera. A stream of water passes through a cooling coil in the cassette; it must be regulated so as to keep the cassette several degrees above room temperature to eliminate condensation of water vapor from the air. A metal collimator disturbs the temperature field of the camera; therefore a glass capillary is used in the RKVT as a collimator (internal diameter 0.4 mm and length 65 mm). Such a collimator keeps the temperature stable and shortens the exposure 1.5-2 times in comparison with a metal collimator of the same dimensions.

The measurement and control of the temperature were carried out with the aid of a battery consisting of two chromel-copel thermocouples and an EPD-17 poten-

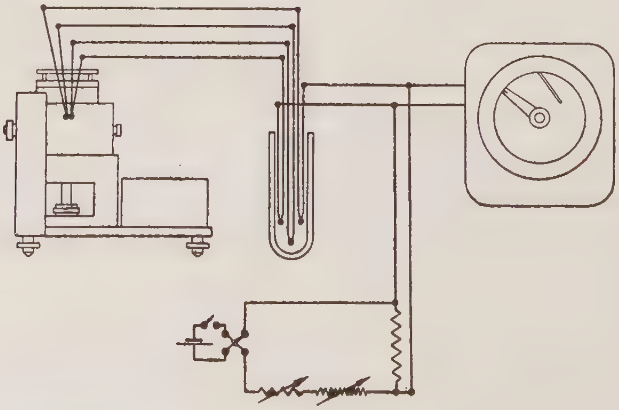

Fig. 2. Diagram of temperature measurement scheme.

tiometer (PP graduation), the full scale of which corresponded to 120° in this case. To expand the range of temperature measurement without loss of sensitivity, an emf counter to the thermal emf was switched into the potentiometer lead. The corresponding diagram is given in Fig. 2. This apparatus allowed the temperature to be controlled to within a few tenths of a degree.

Liquid Thermostat Camera

The cooling or heating of the thermostat, and therefore of the sample, in a liquid thermostat camera, is done by circulating the liquid with a centrifugal pump. It is easy to obtain temperatures down to −50°C by circulating alcohol which first passes through an attachment cooled by dry ice. When water was circulated, heated by a TS-15 thermostat, temperatures up to +85°C could be obtained in the camera.

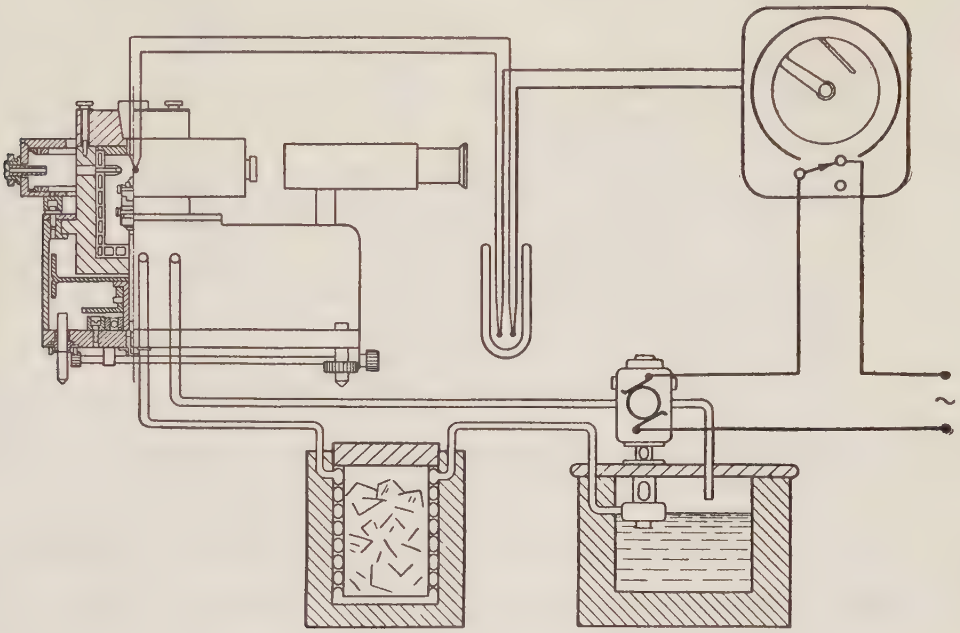

Fig. 3. Apparatus for maintaining constant temperature in the liquid thermostat camera.

Recording of the sample temperature is done in the same manner as in the RKVT camera by a battery composed of two chromel-copel thermocouples in series, connected to the EPD-17 potentiometer. Temperature control in the camera is obtained by switching on and off the stream of cold liquid (see Fig. 3). In this way temperature stabilization to an accuracy of 0.5° is obtained quickly and easily. At higher temperatures, the temperature of the liquid is maintained at a given level by the TS-15 thermoregulator; additional control can be obtained by connecting and disconnecting the pump by means of the EPD-17 potentiometer.

With this type of camera it is possible to obtain rotation and oscillation patterns with the possibility of changing the oscillation range, so as to obtain several exposures on one film.* Reflections can be recorded from $\vartheta = 10°$ to $\vartheta = 82°$. The arrangement of the camera base, and the rotation and oscillation mechanism are similar to the analogous ones in the RKV-86 camera. The goniometer head is placed inside the cylindrical metal thermostat. The head is screwed onto a composite axis, the upper part of which is made of brass, the next of asbestos cement for heat insulation, and the lower again of metal. The metal thermostat cylinder is surrounded by a thick-walled asbestos cement case. There are slits, sealed with a cellulose acetate film, in the body of the thermostat, analogous to those in the RKVT one. The cylindrical cassette (film diameter 114.6 mm) can be removed without disturbing the heating schedule of the camera. The mounting system guarantees the correct position of the cassette. To protect it from heating or cooling, a tube for running water is wound on the cassette.

---

* Drawings of such a camera (RTK-200) were prepared by V. K. Rubtsov, experimental engineer of the Physics Dept. machine shop.

The Thermal Expansion of Corundum Crystals

It is difficult to measure the parameters of the corundum cell from polycrystalline samples, because in the precise regions of the Debye pattern there is a large number of diffraction lines, which makes it difficult to index them uniquely [5, 6]. For this reason, the thermal expansion was studied on a monocrystal. The samples studied were nearly spheres, 0.5-0.7 mm in diameter. Two series of rotation patterns were prepared: one with the axis of rotation close to $10\bar{1}.14$ (for parameter a) and the other close to $10\bar{1}0$ (for parameter c). The patterns were obtained with copper radiation. The parameter determinations were carried out using reflections $3\bar{3}60$, $4\bar{2}\bar{6}1$, $01\bar{1}.16$ and 044.10. Graphic extrapolation of the function $\frac{\cos^2\vartheta}{\sin\vartheta} + \frac{\cos^2\vartheta}{\vartheta}$ was applied to determine the absorption and size of the sample. The values of the parameters at higher temperatures (the accuracy of the temperature stabilization was ± 0.2) were defined more accurately by making corrections for the thickness of the sample, the same for all temperatures. The data for the temperature variation of the parameters are given in Fig. 4. The values $a_{22} = 4.748_{3\pm1}$ kX, $c_{22} = 12.96_{3\pm1}$ kX are obtained for the periods. In the temperature interval (20-270°) the temperature dependence of the cell parameters of α-Al_2O_3 is linear, and correspondingly, the thermal expansion can be characterized by two coefficients $\alpha_\perp = 5.6 \pm 0.1 \cdot 10^{-6}$; $\alpha_\parallel = 6.6 \pm 0.1 \cdot 10^{-6}$ deg^{-1}.

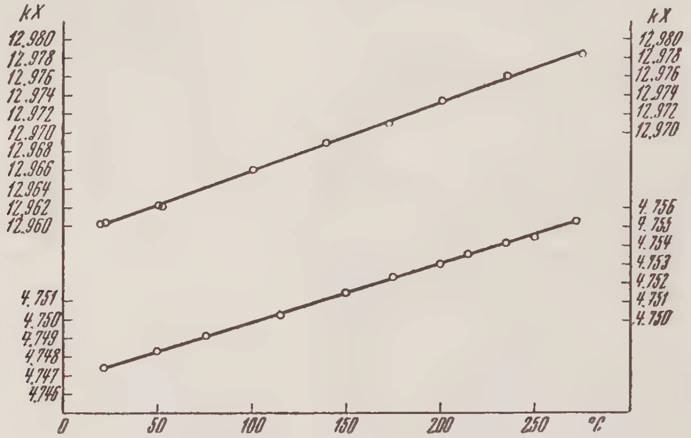

Fig. 4. The temperature dependence of the parameters a and c, α-Al_2O_3.

Thermal Expansion of Crystals of $Li_2SO_4 \cdot H_2O$

The crystals of $Li_2SO_4 \cdot H_2O$ belong to the monoclinic system with the constants a = 5.43, b = 4.83, c = = 8.14 kX, β = 107.58° [8]. A small rod-shaped fragment of a crystal was studied. The b parameter was determined at room temperature by the distances between the layer lines of the rotation pattern and is equal to 4.96 ± ± 0.01 kX. The a and c parameters were determined by reflections of the type h00 and 00l of the oscillation patterns; a = 5.455 ± 0.002 (at 20-22°); c = 8.167_5 ± ± 0.0006 kX (at 20-22°). The temperature dependence of the parameter c = f(t) is represented in Fig. 5. The magnitude of the β-angle was corrected by Laue patterns, photographed on the cylindrical film and, to an accuracy up to 5' (accuracy of measurements), does not depend on the temperature. The temperature dependence of the period is linear. The corresponding coefficient is equal to 15.6 ± 0.5 · 10^{-6} deg^{-1}, which agrees with the data in [8].

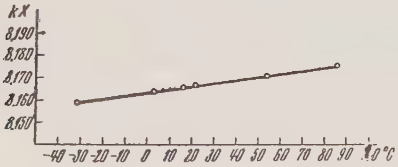

Fig. 5. The temperature dependence of the c parameter, $Li_2SO_4 \cdot H_2O$.

The Thermal Expansion of Di-potassium tartrate*

Di-potassium tartrate $K_2C_4H_4O_6 \cdot {}^1/_2 H_2O$ crystallizes in the monoclinic system [7]. The size of the unit cell and the expansion along the c axis was checked. Samples were sawed out of monocrystals and had the shape of elongated, almost right-angled prisms. Such a shape is convenient for taking precise oscillation pattern measurements, and allows for more accurate measurements of the parameters by graphic extrapolation, or by making corrections for the size of the crystal and magnitude of absorption by Wilson's expression [10].

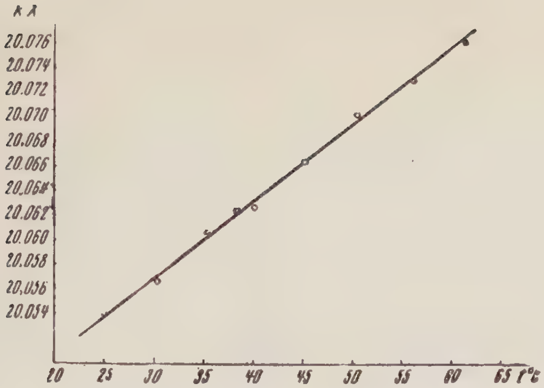

Fig. 6. The temperature dependence of d_{001} of $K_2C_4H_4O_6 \ {}^1/_2 H_2O$.

A series of oscillation patterns using Cu, Ni, Co and Fe radiations was prepared in order to compare the accuracies obtained when corrections were made and graphic extrapolation was applied. It became apparent that when working with reflection angles higher than 65-70° it is possible to use the corrections instead of the graphic extrapolation. Figure 6 gives the data for the thermal expansion along the c axis.

The results of the measurements are: $a = 15.458 \pm 0.004$, $b = 5.038 \pm 0.002$, $c = 20.054 \pm 0.002$ kX. $\beta = 90°50'$, $\alpha_{33} = 31.5 \pm 1.0 \cdot 10^{-6}$ deg^{-1} which agrees with the data in [7, 9].

LITERATURE CITED

[1] H. P. Klug and L. A. Alexander, X-ray Diffraction Procedures (New York, 1954).

[2] V. V. Zubenko and M. M. Umanskii, "X-ray diffraction determination of the coefficients of thermal expansion of polycrystalline substances in the interval −50° +100°C," Kristallografiia 1, 4, 436-441 (1956).

[3] M. M. Umanskii, "Camera for x-ray structural analysis," Application of X-rays in the Study of Materials [in Russian] (Mashgiz, 1949) pp. 401-419.

[4] M. M. Umanskii and S. S. Kvitka, "X-ray analysis of crystals without faces," Izv. AN SSSR, Ser. Fiz. 15, 147-156 (1951).

[5] H. E. Swanson and R. K. Fuyat, "Standard x-ray diffraction powder patterns," Nat. Bureau of Standards Circular 539, II, 20-23 (1953).

[6] N. A. Shal'nikova and I. A. Iakovlev, "X-ray diffraction determination of the crystal lattice constants and coefficients of thermal expansion of leucosaphire and of ruby," Kristallografiia 1, 5, 531-533 (1956).

[7] Landolt-Bornsteen, Bul. Atom-und molekular physik. 4-t. Kristalle (Springer-Verlag, 1955), pp.91, 243.

[8] C. S. Smith and H. H. Landon, "Thermal expansion of $Li_2SO_4 \cdot H_2O$," Bull. Am. Phys. Soc. 24, 3 (1949).

[9] W. Mason, Piezoelectric Crystals and Their Application in Ultrasonics [Russian translation] (IL, 1952).

[10] A. J. C. Wilson, "Geiger-counter x-ray spectrometer-influence of size and absorption coefficient of specimen on position and shape of powder diffraction maxima," J. Sci. Instr. 27, 12, 321, 325 (1950).

Received February 22, 1957

M. V. Lomonosov Moscow State University

---

* This part of the work was done by Z. I. Ezhkova.

X-RAY DIFFRACTION STUDY OF THE STRUCTURAL DISTORTION OF METALS UNDER STATIC AND DYNAMIC COMPRESSION AT ROOM TEMPERATURE AND LOW TEMPERATURE

Iu. S. Terminasov and V. F. Mindukshev

Samples of duralumin and copper were examined by means of radiometallography after a static and dynamic compression at room temperature and at liquid nitrogen temperature.

The effect of "thermal rest" may be stated as responsible for the diminishing of structural distortions, caused by dynamic compression, in comparison with those obtained in the course of static compression.

The deformation of metals at low temperatures essentially extinguishes the effect of "thermal rest," and the structural distortions after a dynamic compression approximate those caused by a static deformation of the same metals at room temperature.

The deformation of metals at low temperature provokes a higher rate of fragmentation and of structural distortions than a similar deformation at room temperature.

By studying the deformation of metals at low temperature and comparing this deformation with that at room temperature, it is possible to make a detailed investigation of the influence of thermal rest and to ascertain the causes leading to the difference between the mechanism of plastic deformation of metals in dynamic and static loading.

The present work was carried out to study the static and dynamic compression of metals at room temperature and at the temperature of liquid nitrogen. Commercial duralumin and electrolytic copper were the materials used for the investigation.

Specimens were prepared in the form of small cylinders 10 mm in diameter and 15 mm high. To ensure uniform reduction of the specimens under compression, drill-holes were made in their end faces and were filled with vaseline; this reduced the friction between the end faces of the specimen and the working surfaces of the deforming apparatus. After a cleaning treatment by grinding, the specimens were polished electrolytically and a network was marked on the lateral surface by means of a dividing engine to enable the total strain and the strain of each layer of the specimen to be determined. To remove work-hardening produced during the preparation of the specimens and to protect their surfaces from oxidation, they were annealed in a vacuum at temperatures of 400 and 350°C, respectively,for duralumin and copper for periods of one-and-a-half hour. The starting condition of the specimens was checked by means of photomicrographs and microhardness determinations.

Deformation of the specimens at the temperature of liquid nitrogen was carried out in a special low-temperature chamber, in which it was also possible to carry out the deformation of the specimens at room temperature. The temperature of the specimen at the moment of its deformation was measured by means of a copper-constantan thermocouple.

The specimens deformed in liquid nitrogen were photographed at a low temperature by means of a special low-temperature apparatus which was fixed to the back of camera Kros-1. The x-ray diffraction patterns were obtained by means of electron tube BSVL (with copper anode) with a nickel filter, the method of back reflection with an independent standard being employed. The specimen, the temperature of which was checked by means of the thermocouple,was sprayed while in the low-temperature chamber with a continuous stream of liquid nitrogen. For the purpose of standardizing the photographic conditions, the diffraction patterns of a complete series were obtained on one film (by the use of a sector type cassette). Fine-grain "Agfa" film was used, treated under identical conditions.

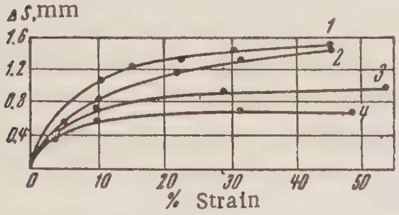

Fig. 1. Width of (511) duralumin line as a function of degree of strain: 1) static strain; 2) dynamic strain at the temperature of liquid nitrogen; 3) static strain; 4) dynamic strain at room temperature.

In addition to the photographic method, the ionization method of obtaining the reflections was also used with automatic recording (apparatus URS-50I) and synchronization of the movement of specimen, counter and paper. In the case of duralumin, in the photographic method, the (511) lines of specimen and standard were used, and in the case of copper, the (331) and (420) lines of specimen and standard. In the ionization method, the (422) and (111) duralumin lines and the (331) and (111) copper lines were recorded, since the lines give a considerable difference in the sum of the squares of the indices. The intensity of the primary x-ray beam was controlled by means of the standard, which was also used as standard for the examination of the broadening of the lines. The width of a line was determined by dividing the area of the K_α curve by the height of the maximum intensity of the line, after separation of the K_α doublet by the geometrical method [1] into the α_1 and α_2 components. The interference lines of the deformed specimens at room temperature and low temperature were compared respectively with the lines of the standards obtained under the same conditions of x-ray photography.

The results of the x-ray studies of the broadening of the (511) line for static and dynamic compression at room temperature and at the temperature of liquid nitrogen are shown in Fig. 1. Since the broadening of the (511) and (422) lines of deformed specimens of duralumin, and of the (331) and (420) lines of copper is governed by a general mechanism and differs insignificantly in numerical values, we shall confine our discussion to the (511) duralumin and (331) copper lines.

From the data reproduced, it is clear that maximum broadening of the (511) duralumin lines was observed for specimens deformed and photographed at temperature of liquid nitrogen, both statically (curve 1) and dynamically (curve 2). Maximum broadening of the lines, as compared with the original width of the standard, was 103.2% for 46% compression for statically strained specimens, and 102% for dynamically deformed specimens. The broadening of the interference line of specimens deformed statically at room temperature (curve 3) terminated at much earlier (up to 18%) stages of strain and had a smaller maximum value (72.4% for 55% compression).

The maximum broadening of the interference line of duralumin strained dynamically at room temperature (curve 4) was only 52.6% for 49.4% compression, the principal broadening of the line being terminated in the initial deformation stage (10-12%).

For copper specimens, strained statically by 57.4% in liquid nitrogen, the broadening of the (331) line at room temperature attained 31%; at the temperature of liquid nitrogen it was 44%, i. e., the difference observed was not so great as in the case of duralumin, although the same regularity appeared.

The considerable broadening of the lines of strained metals observed in a number of papers [2-5] is explained by some authors as due to crystallite deformation, while others consider that the broadening of the lines is due mainly to the fragmentation of the crystalline blocks [6-9]. Most likely of all is that in the plastic deformation of metals, both fragmentation of the blocks and the formation of microstresses occur together [10-11]. One of these factors will, however, predominate, according to the conditions of deformation and the physical state of the metal.

The study of the residual distortions and the fragmentation of the blocks occurring in static and dynamic compression has been the subject of a few papers, and only isolated papers are devoted to the x-ray diffraction study of the plastic deformation of metals at low temperatures [6, 10].

To elucidate the cause of the considerable difference in the broadening of interference lines in the deformation of metals at room temperature and at low temperature, it is necessary to examine the causes leading to the broadening of the lines in either case. We carried out a separation of the effects which produce broadening of interference lines (fragmentation of the blocks and crystallite distortions) by the method of harmonic analysis [11-13]. On the assumption that the broadening of the K_α line is due to lattice distortions and fragmentation of the blocks, it can be shown that the resultant coefficients A_n are products of coefficients corresponding to each of these effects, i. e., $A_n^D \cdot A_n^u$. The dimensions of the regions of coherent scattering (D), the magnitude of the absolute strain $\sqrt{\Delta L^2}$ and the relative strain $\left(\varepsilon = \frac{\sqrt{\overline{\Delta L^2}}}{L}\right)$ were calculated.

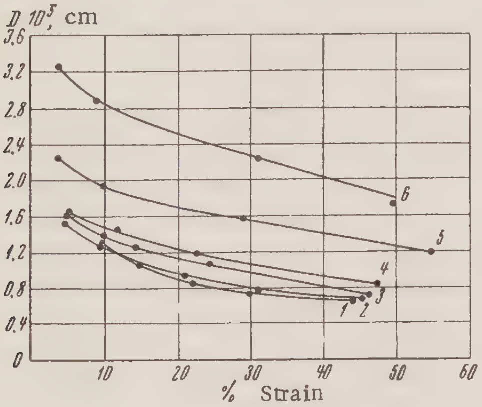

Fig. 2. Size of crystalline blocks as a function of degree of strain of duralumin: 1,2) static and dynamic strain in liquid nitrogen; 3, 4) static and dynamic strain (rested specimens); 5, 6) static and dynamic strain at room temperature.

In deformation at room temperature, the lattice distortions attain considerable magnitude ($1.10 \cdot 10^{-3}$) in static compression, as compared with dynamic compression ($0.90 \cdot 10^{-3}$ in the case of duralumin, and $0.75 \cdot 10^{-3}$ and $0.80 \cdot 10^{-3}$, respectively, for copper). The duralumin specimens deformed at low temperature had practically identical internal distortions, equal to $1.20 \cdot 10^{-3}$ for static strain and $1.16 \cdot 10^{-3}$ for dynamic strain (for copper $0.80 \cdot 10^{-3}$ and $0.90 \cdot 10^{-3}$, respectively). Consequently, dynamic strain at room temperature never produces such large microdistortions of the crystal lattice as are produced by static compression. This phenomenon may be explained by the concept of thermal rest. The process of plastic deformation in dynamic application of the load occurs with extreme rapidity so that, during the short time of the shock, the heat concentrated along the slip planes cannot be dissipated. The rise in temperature at the moment of dynamic deformation at room temperature therefore leads to partial elimination of the crystal lattice distortions.

Such a hypothesis is confirmed in a particularly convincing manner by the variation of the regions of coherent scattering. As will be seen from the form of the curves (Fig. 2), a definite regularity is observed in the diminution of the size of the regions of coherent scattering with increase in strain: in the first stages of strain, fragmentation of the blocks proceeds more intensively. The quantitative relationship, however, shows a fundamental difference. At low degrees of static strain in duralumin (4.3%) at room temperature (curve 5, Fig. 1), the size of the blocks is $2.22 \cdot 10^{-5}$ cm, while at low temperature (curve 1) for 5.3% strain, the size of the blocks is $1.30 \cdot 10^{-5}$ cm, i. e., rather more than half.

With increase in the degree of strain of the specimens in liquid nitrogen, there is considerable fragmentation of the blocks, which attain minimum dimensions at 46% compression (of the order of $0.65 \cdot 10^{-5}$ cm for static strain and $0.70 \cdot 10^{-5}$ cm for dynamic strain). A similar regularity is also observed in the case of the copper specimens. Evidently, this regular relationship is connected with the fact that the stressed blocks withstand only definite stresses for a given metal, after which their fragmentation takes place.

This supposition is confirmed by the character of the curves of the variation of the dimensions of the regions of coherent scattering as a function of the form and temperature of deformation. At the same time, the fact that at room temperature different lattice distortions are produced in static and dynamic compression also becomes clear.

Since in dynamic compression, the distortions are partly removed by the thermal rest, then for 55% compression, the fragmentation of the blocks occurs to a lesser extent (to $1.80 \cdot 10^{-5}$ cm) than in the case of static compression, when the blocks are reduced in size down to $1.20 \cdot 10^{-5}$ cm for 49% compression. After the specimens deformed at the temperature of liquid nitrogen have reached room temperature ("rested specimens") an increase occurs in the regions of coherent scattering, but their dimensions are still much smaller than the regions of coherent scattering of specimens deformed at room temperature. Thus, at low temperature, the influence of the rate of strain is insignificant.

At room temperature, compared with the temperature of liquid nitrogen, the thermal rest is increased, and the effect of the rate is here much greater, while the stresses produced by hardening in compression are partly reduced by the thermal rest, principally in dynamic compression, as is shown by the experimental results. At low temperature, therefore, the microstresses attain a higher magnitude and the dimension of the blocks is almost half the dimension of the blocks in metals strained at room temperature.

SUMMARY

1. The deformation of metals at low temperature produces a considerable reduction in the effect of thermal rest.

2. With deformation in low temperature conditions,there is a more pronounced fragmentation of the crystalline blocks and higher crystallite stresses in comparison with the deformation of metals at room temperature.

3. At low temperature, the influence of the rate of strain becomes insignificant, and therefore, as distinct from room temperature, no essential difference is to be observed at low temperature between static and dynamic compression.

LITERATURE CITED

[1] W. A. Rechinger, "A correction for $\alpha_1\alpha_2$ doublet in the measurement of widths of x-ray diffraction lines," J. Sci. Instr. 25, 7, 254-261 (1948).

[2] N. N. Davidenkov and Iu. S. Terminasov, "X-ray diffraction study of the mechanism of the dynamic and static compression of metals," J. Tech. Phys. (USSR) 14, 12, 644-651 (1944).

[3] Iu. S. Terminasov and E. B. Gasilova, "X-ray diffraction study of residual stresses of second and third order in the static and dynamic compression of metals," Use of X-rays and Investigation of Materials [in Russian] (1949), pp. 95-104.

[4] C. S. Smith and E. E. Stickley, "The width of x-ray diffraction lines from cold-worked tungsten and α-brass," Phys. Rev. 64, 7-8, 191-197 (1943).

[5] G. S. Zhdanov and Ia. S. Umanskii, X-ray Analysis of Metals [in Russian] (1939), Part II, pp. 113-124.

[6] A. Kelly and W. T. Roberts, "Sub-grain formation in Al deformed at −183°C," Acta Met. 3, 1, 96-102 (1955).

[7] S. L. Smith and W. A. Wood, "X-ray structure and elastic strains in copper," Proc. Roy. Soc. 176, 398-441 (1940).

[8] W. A. Wood, "The lower limiting crystalline size and interval strains in some cold-worked metals," Proc. Roy. Soc. 172, 231-236 (1939).

[9] W. A. Wood and W. A. Rechinger, "Crystallite theory of strength of metals," J. Inst. Metals 75, 7, 571-578 (1949).

[10] M. S. Peterson, "X-ray line broadening from metals deformed at low temperatures," Acta Met. 2, 6, 823-831 (1954).

[11] B. E. Warren and B. L. Averbach, J. Appl. Phys. 21, 6, 595 (1950); 23, 4, 497 (1952).

[12] B. Ia. Pines, Sharp Focus X-ray Tubes and Applied X-ray Structural Analysis [in Russian] (1955) pp. 191-206.

[13] G. K. Williamson and R. E. Smallman, "The use of Fourier analysis in the interpretation of x-ray line broadening from cold-worked iron and molybdenum," Acta Cryst. 7, 8-9, 574-583 (1954).

[14] D. E. Wilson and L. Tomassen, "X-ray line broadness of metals and alloys and its relation to high temperature stability," Trans. Am. Soc. Metals 22, 769-777 (1934).

[15] A. H. Lutts and P. A. Black, "Annealing of cold-rolled aluminum single crystal," Trans. Am. Inst. Mining Met. Petrol. Eng. 200, 257-264 (1954).

Received February 22, 1957

V. M. Molotov Leningrad Engineering Economics Institute

CHANGE IN THE CRYSTAL STRUCTURE OF STEEL DURING COLD WORK AND HEAT TREATMENT

E. L. Gal'tserin and Iu. S. Terminasov

Samples of steel 55 C_2 (and some of steel 20) were examined by means of radiometallography, microhardness testing and elastic constants measurement. Their fragmentation, structural distortions, lattice binding forces and mechanical properties were studied before and after heat treatment and cold working.

A small change of binding forces is found in quenched steel in comparison with tempered steel. Heat treatment is found to provoke more fragmentation and distortion changes than cold working of the examined steel.

Static and dynamic distortions after heat treatment were calculated according to diffraction line intensity measurements. Cold-worked steel did not show any regular change of diffraction line intensity.

An attempt was made to state a connection between structural changes in steel and their mechanical properties.

This article describes a study which has been made of the various structural characteristics (block character, elastic and static distortions of the α-phase lattice, characteristic temperature, state of the carbide phase) and their changes during the process of plastic deformation and heat treatment of silicon steel 55 C_2. An attempt has been made at the same time to discover a connection between the structural characteristics and mechanical properties of the above-mentioned steel.

Investigation of Plastically Deformed Specimens

The specimens, after being annealed in a vacuum, were subjected to static compression to different degrees of strain. Microsections and small rods were prepared from the strained specimens and were etched electrolytically in a solution of phosphochromic electrolyte: a surface layer 0.2-0.3 mm thick was removed from the microsections and the rods were etched to a diameter of 0.5 mm.

The powder filed from the annealed specimen was sieved through a silk screen, then part of it was subjected to tempering in a vacuum at a temperature of 700°C. From the strained and tempered powder, flat and cylindrical specimens with a diameter of 1 mm were prepared for x-ray analysis.

The material used for the x-ray diffraction study of the carbide phase was the carbide precipitate separated from specimens deformed by compression and from the specimen tempered at 700°C.

The carbides were separated electrolytically in 1 N aqueous solution of KCl, to which was added 0.5% of citric acid [1]. The separated carbide powder was packed in small celluloid tubes, 0.5 mm in diameter.

Iron radiation (Mn filter) was used for studying the effects associated with the broadening of the interference lines from the carbide and α-phase; corresponding specimens, tempered at 700°C, were used as standards. For studying the intensity of the x-ray lines, molybdenum radiation (Nb filter) was used as well as Fe$-K_\alpha$.

The ionization method ($Fe-K_{\alpha}$) using apparatus URS-50I was employed for the flat specimens, and the photographic method ($K_{\alpha}-Mo$), using an RKD camera, diameter 57.3 mm, for the small rods. The specimens were rotated while the patterns were being obtained.

The magnitude of the coherent regions (blocks) of the α-phase and the microdistortions in the strained specimens were determined from the broadening of the (110) and (220) interference lines, as determined by two methods: analytically [2, 3] and by the method of harmonic analysis [4, 5].

The choice of the most suitable functions for $f(x)$ and $F(x)$ (using the notation of [3]) showed that a function of the form $\frac{1}{(1+k^2x^2)^2}$ satisfied this condition better than others.

Since it did not appear possible by a direct experimental method to select the correct expression for the functions $M(x)$ and $N(x)$ [3], the limit values of the above-mentioned functions were used in the analytical method:

1) all four functions were approximated to a Gaussian function,

2) $f(x)$ and $N(x)$ were approximated by a function of the form $\frac{1}{(1+k^2x^2)^2}$; $F(x)$ and $M(x)$ by the Cauchy function.

By using two orders of reflection from the (110) plane, it was possible, as has been shown [6-8], to apply with adequate strictness the method of harmonic analysis to the separation of the broadening effects. In contradistinction to the method described in [6, 8], the value of the root mean square distortions $\sqrt{\bar{\varepsilon}^2} = \frac{\sqrt{\overline{\Delta L^2}}}{L}$ (corresponding to $\frac{\Delta d}{d}$) was determined not by extrapolation of the curve of $\sqrt{\bar{\varepsilon}^3}$ versus L to L = a, but from the slope of this curve over the section of uniform strain.

TABLE 1

Treatment of specimen	Gauss function		Cauchy function		Harmonic analysis	
	$D_{\text{см}}\cdot$	$\frac{\Delta d}{d}\cdot 10^6$	$D_{\text{см}}\cdot 10^6$	$\frac{\Delta d}{d}\cdot 10^3$	$D_{\text{см}}\cdot 10^6$	$\sqrt{\bar{\varepsilon}^2}\cdot 10^3$
Compression 2.5%	10	1.06	∞	0.78	9.0	0.8
» 6.5%	6.5	1.34	∞	1.15	6.9	1.07
» 12.9%	4.4	1.46	∞	1.36	5.0	1.3
» 25%	3.9	1.84	70—90	1.83	3.25	1.45
» 37%	3.3	1.99	17	1.94	3.2	1.8
» 66.3%	3.3	2.35	20	2.28	2.8	2.1
Filing	2.8	5.0	∞	4.85	2.8	4.6

The x-ray patterns of the strained specimens showed a slight shift of the (220) line towards larger angles ϑ, increasing with increase in the degree of strain and attaining 5-6' (in angle ϑ) at high strains. The expansion of this line (66.3% strain) into a Fourier series, with [9] and without allowance for the shift of the maximum, showed that the expansion coefficients $A_n(l)$ practically did not differ in the two cases. In view of this, we assumed $B_n(l) = 0$ and confined ourselves to a discussion of the coefficients $A_n(l)$.

Table 1 shows the results of the analysis of the broadening of interference lines of the α-phase of specimens of 55 C_2 steel strained by compression and filing.

It will be seen from this table that the values of the microdistortions agree well in all three cases (the maximum discrepancy does not exceed 25% from the determinable value). Much larger discrepancies, depending upon the analytical form of the approximating functions, are observed in the magnitudes of the blocks, which differ among themselves by one order or more.

The use of the Cauchy function implies that practically all the broadening of the lines is due to microdistortion, whereas in the case of the Gaussian function up to 30-40% of the entire broadening of the (220) line for large strain values is due to the fragmentation of the blocks.

On the assumption that all the broadening of the x-ray lines of the carbide precipitates separated from the specimens deformed by compression is due to the fine dispersion of the carbide blocks [10], the dimensions of these blocks were roughly estimated from the broadening of the (112) (021) lines [11]. The curves for the distribution of intensity in the "true" line and the standard line were approximated by a function of the form $\frac{1}{(1+k^2x^2)^2}$.

We also determined the microhardness of the specimens deformed by compression. The results of all these measurements are shown in the form of corresponding plots in Fig. 1.

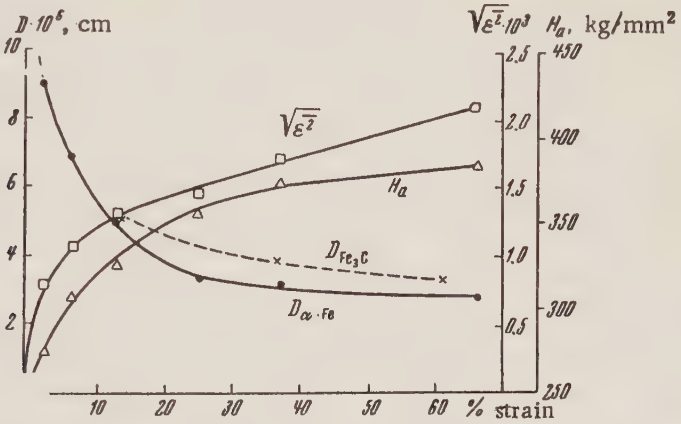

Fig. 1. Microhardness ($H_\square$), magnitudes of the blocks of α-phase ($D_{\alpha\text{-Fe}}$) and carbide phase (D_{Fe_3C}) and microdistortions ($\sqrt{\varepsilon^2}$) as function of degree of strain of steel 55 C_2.

In the general case, the variation in intensity of the intereference lines from strained specimens may be due to four factors.

1. Variation of the thermal factor (characteristic temperature — θ).
2. Extinction effects.
3. Presence of texture.
4. Development of static lattice distortions.

In papers [12, 13] it was shown that θ of steel does not vary as a result of plastic deformation, at least not within the limits of accuracy of the methods employed.

According to our data [14], extinction has no effect on the intensity of interferences from planes with $\Sigma h_i^2 > 4$, but may modify somewhat (up to 10-15%) the intensity of the (110) line. The ratio of the intensities of this line and that of the (220) line for all degrees of strain was found to be equal to 1.06 ± 0.04, i. e., practically constant.

The method employed in this work for preparaing the small rods from the compressed specimens ought to have reduced the influence of texture on intensity to a minimum [15]. This made it possible to utilize the reflections from any planes, and by the use of Mo—K_α radiation, to confirm by observation of a large number of x-ray lines whether strain results in a systematic variation in intensity proportional to the factor

$$e^{-2A\left(\frac{\sin\vartheta}{\lambda}\right)^2}.$$

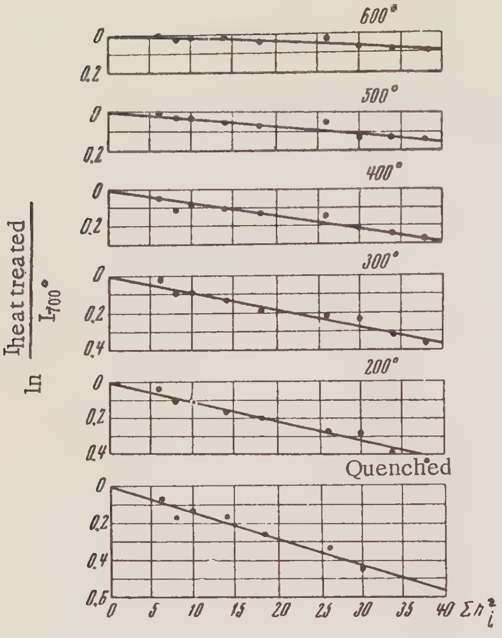

Fig. 2. Plots of ln $\frac{I_{\text{heat treated}}}{I_{700°}}$ as a function of Σh_i^2 for steel 55 C_2 quenched and tempered in the range 200-600°C.

The data we obtained failed to confirm such a relationship, although generally speaking there is a tendency for the intensity to diminish with increase in Σh_i^2. It is possible that the picture of the intensity variation is distorted somewhat, due to texture which, despite the precautions taken, could still exercise some influence on the intensity. However, even an examination of the filed powder failed to reveal any variation in intensity proportional to $e^{-2A\left(\frac{\sin\vartheta}{\lambda}\right)}$. These results agree with the data given in [6, 16, 18].

Specimens of the steel investigated were quenched in oil from 900°C. Tempering of the quenched specimens was carried out in a vacuum at temperatures of 200-700°C for a period of 1 hr; the carbide precipitate was separated from some of the tempered specimens by the method described above.

The preparation of the specimens for x-ray analysis, photography and evaluation of the x-ray diffraction patterns were carried out by the method described above.

It is known [2] that part of the broadening of x-ray lines from specimens of carbon steel tempered at temperatures below 300°C may be due to the presence of a slightly tetragonal character of the martensite lattice. Actually, after tempering at 200°C, the ratio c/a for the steel investigated was found to be 1.005-1.006; after tempering at 300°C and above, practically no tetragonal character was found in the α-phase lattice.

Table 2 gives the values obtained for the magnitude of the blocks and microdistortions in heat-treated specimens, using the various methods of separating the broadening effects.

TABLE 2

Treatment of specimen	Gauss function		Cauchy function		Harmonic analysis	
	$D_{c\text{м}} \cdot 10^6$	$\frac{\Delta d}{d} \cdot 10^3$	$D_{c\text{м}} \cdot 10^6$	$\frac{\Delta d}{d} \cdot 10^3$	$D_{c\text{м}} \cdot 10^6$	$\sqrt{\overline{\varepsilon^2}} \cdot 10^3$
Quenched						
Tempered 300°C	2.1	4.5	5.0	4.0	2.0	4.25
» 400°C	3.9	2.15	17	1.85	4.0	2.3
» 500°C	6.25	0.75	21	0.46	7.0	0.7
» 600°C	10.4	0.27	42	—	20	0.36
» 700°C	—	—	—	—	150*	

---

* Obtained from measurements of intensity reduction due to primary extinction.

It will be seen from the table that just as in the case of cold working, the form of theoretical function selected has a material influence only on the magnitude of the blocks. Quantitatively, however, this influence is much less.

The fact that after annealing at 600°C, when practically all the broadening of the lines is due to the fine dispersity of the blocks, the size of the latter according to the results of harmonic analysis is approximately twice the value obtained with the use of Gaussian and Cauchy functions, evidently indicates that these two functions do not correspond to the true size distribution coefficient of the blocks in the heat-treated specimens of the steel investigated. A function of the form

$$\frac{1}{(1+k^2x^2)^2}.$$

would evidently appear to be more appropriate in this case also.

We determined the characteristic temperature of steel 55 C_2 in the quenched and annealed states by measurement of the resonance frequencies of longitudinal and transverse elastic vibration of the crystal lattice [19]. At the same time, for comparison, θ was determined for carbon steel 20 (0.17% C). The results of these measurements are shown in Table 3.

TABLE 3

Steel	Treatment of specimen	θ, °K
55 C_2	Quenched	480
55 C_2	Tempered at 700°C	496
20	Quenched	485
20	Tempered at 700°C	491

These values of θ are close to those given in [13], but differ substantially from the values obtained for iron and carbon steel from x-ray diffraction data [20] and from specific heat measurements [21]. In our investigations, unlike those of [20], the decrease in θ due to the quenching of steel 55 C_2 did not exceed 3-4%. For steel 20, the variation was still less. The causes of this discrepancy are still obscure.

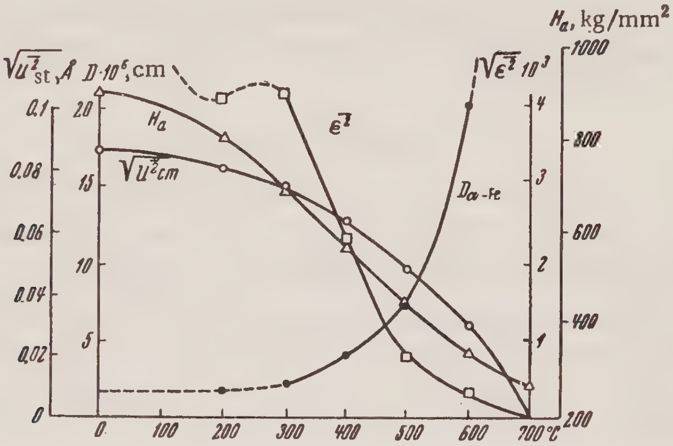

Fig. 3. Microhardness ($H_\square$), magnitude of the α-phase blocks ($D_{\alpha\text{-Fe}}$), microdistortions ($\sqrt{\bar{\varepsilon}^2}$) and third-order static distortions ($\sqrt{\bar{u}^2_{st}}$) as function of the tempering temperature of steel 55 C_2.

The x-ray patterns of heat-treated specimens of steels 55 C_2 and 20 showed a systematic reduction in intensity of the interference lines with increase in Σh_i^2. Figure 2 shows graphs of $\ln \frac{I_{\text{heat treated}}}{I_{700°}}$ as a function of Σh_i^2 for heat-treated specimens of steel 55 C_2. Within the limits of the experimental errors, the points lie on straight lines, the tangent of the slope of which was used for determining the values of $\sqrt{\bar{u}^2_{st}}$, shown in Fig. 3. This figure also gives the results obtained from an analysis of the broadening of the interference lines and the results of measurements of the microhardness of heat-treated specimens of steel 55 C_2.

Investigation of the carbide phase of steel 55 C_2 showed that, as a result of tempering at temperatures of 300-400°C, metastable ϵ-carbide is formed in the steel, having a compact hexagonal lattice with the constants a = 2.72 and c = 4.35 A.

In the range 400-500°C, the ϵ-carbide is transformed into cementite. After 500°C tempering, the x-ray patterns of the carbide precipitate showed only the lines of lamellar cementite; above 500°C, intensive coagulation of the carbide particles occurred.

SUMMARY

1. The use of different methods of separating the effects of line broadening led to satisfactory agreement between the microdistortion values obtained by the different methods. The calculation magnitude of the blocks depends substantially upon the choice of analytical functions, of which in our case the most appropriate appeared to be a function of the form $\frac{1}{(1 + k^2x^2)^2}$.

2. The absence of any regular character in the variation of intensity of the interference lines of x-ray diffraction patterns of deformed specimens is obviously evidence of the fact that in the given case, static lattice distortions cannot be characterized by the magnitude $\sqrt{\overline{u}^2_{st}}$.

3. The data obtained show that the primary factor determining the hardening of strained steel 55 C_2 must be considered to be the formation of a submicroheterogeneous structure, due to the fragmentation of α-phase blocks and the formation of considerably distorted boundary regions.

4. The maximum reduction in the binding forces in steel 55 C_2 during solid solution formation does not exceed 6-8%.

5. An intermediate carbide having a hexagonal lattice with the constants a = 2.72 and c = 4.35 A has been found in steel 55 C_2 quenched and low-temperature tempered (up to 400°C). Above 400°C, there is extensive transformation of this carbide to cementite.

LITERATURE CITED

[1] N. M. Popova, "Determination of iron carbide in steel," Zavodskaia Lab. 11, 10, 887-891 (1945).

[2] G. V. Kurdiumov and L. I. Lysak, "The nature of the broadening of interference lines of x-ray diffraction patterns of tempered martensite," J. Tech. Phys. (USSR) 17, 9, 993-999 (1947).

[3] L. I. Lysak, 'Study of the intragranular mosaic structure of metals from the width of x-ray interference lines," Coll: Inst. Metallofiziki AN SSSR 5 (1954), 45-51.

[4] B. E. Warren and B. L. Averbach, "The effect of cold-work distortion on x-ray patterns," J. Appl. Phys. 21, 6, 595-602 (1950).

[5] B. Ia. Pines, Sharp Focus X-ray Tube and Applied X-ray Structure Analysis [in Russian] (1955), pp. 95-105.

[6] M. McKechan and B. E. Warren, "X-ray study of cold work in thoriated tungsten," J. Appl. Phys. 24, 1, 52-61 (1953).

[7] G. K. Williamson and B. E. Smallman, "The use of Fourier analysis in the interpretation of x-ray line broadening from cold-worked iron and molybdenum," Acta cryst. 7, 8-9, 574-583 (1954).

[8] B. L. Averbach, M. B. Bever, M. F. Comerford, and J. S. Lead, "X-ray and colorimetric investigation of cold work and annealing of a gold-silver alloy," Acta Met. 4, 5, 477-491 (1956).

[9] R. J. Garrod and J. H. Auld, "X-ray line broadening from cold-worked iron," Acta Met. 3, 2, 190-196 (1955).

[10] M. P. Arbuzov, "The crystal structure of the carbide carbon of steel at different tempering stages," Izv. AN SSSR, Ser. Fiz. 15, 1, 16-27 (1951).

[11] E. W. Jones, "The measurement of particle size by the x-ray method," Proc. Roy. Soc. 166 A, 924, 16-24 (1938).

[12] G. V. Kurdiumov, V. A. Il'ina and V. K. Kritskaia, "The problem of the lattice distortions of deformed metals and solid solutions," Coll: NIIChERMET, 2 (1951), pp. 222-231.

[13] V. I. Korotkov and B. N. Finkel'shtein, "Influence of cold work on the characteristic temperature of carbon steel," Doklady Akad. Nauk SSSR 108, 5, 846-955 (1956).

[14] E. L. Gal'tserin and Iu. S. Terminasov, "Influence of extinction on x-ray diffraction intensities in the investigation of steel," J. Tech. Phys. (USSR) 6, 1379 (1957).*

[15] D. M. Vasil'ev, "Method of x-ray study of polycrystalline specimens possessing texture," J. Tech. Phys. (USSR) 26, 3, 695-699 (1956).**

[16] J. H. Hall and G. K. Williamson, "The diffraction pattern of cold-worked metals. II. Changes in integrated intensity," Proc. Phys. Soc. 64 B, 11, 946-953 (1951).

[17] R. J. Weiss and J. R. Clark, "Neutron diffraction studies of cold-worked brass," J. Appl. Phys. 23, 12, 1379-1386 (1952).

[18] G. Wagner and A. Kochendörfer, "Messung der diffusen Streuung von Röntgenstrahlen an Kristallen und ihrer Beeinflussung durch eine plastische Verformung mit dem Interferenzzählrohr," Ann. Physik 6, 129-140 (1949).

[19] B. Ostroumov and L. Poltavskii, "Radiotechnical method of testing metals," Vestnik Metallopromyshlennosti 3, 14-26 (1933).

[20] G. V. Kurdiumov, V. K. Kritskaia and N. M. Nodia, "Influence of carbon on the binding forces and static distortions in martensite crystals," Coll: NIIChERMET 4 (1955), pp. 455-461.

[21] R.James, Optical Principles of X-ray Diffraction [Russian translation] (Il, 1950) pp. 101-132.

Received February 22, 1957

---

* [Soviet Physics — Technical Physics, p. 1276.]

** [Soviet Physics — Technical Physics, p. 671.]

SIGNIFICANCE FOR THE THEORY OF FERROELECTRICITY OF THE OPTICAL STUDY OF DOMAINS IN ROCHELLE SALT

V. L. Indenbom and M. A. Chernysheva

The difference between the extinction positions of opposite domains allows one to observe directly the domain (twin) structure of the crystal and to study the changes in the domain structure occuring under the influence of electrical and mechanical fields. A quantitative measurement of the spontaneous turning angle of the optical indicatrix gives a suitable value for the parameter of the crystal monoclinicity taken into consideration in the thermodynamic theory of ferroelectricity. The paper shows the advantages of the optical method applied to measure the monoclinicity parameter above those methods which make use of measurements of macroscopic parameters of polydomain samples.

INTRODUCTION

It has been shown [1-5] that the optical method enables direct observation of the domain structure of Rochelle salt crystals, the investigation of the changes which take place in these crystals under the influence of external mechanical or electric fields, and also the study of the character of the different defects by the distortion of the domain (twin) structure caused by these defects. In all these applications of the optical method, the optical effects, in a narrow sense of the word, are used only qualitatively. The spontaneous shear deformation upon the formation of domains causes turning of the optical indicatrix about an axis which coincides with the a axis. In this way the optical indicatrices of neighboring anti-parallel domains are found to turn in opposite directions and this leads to the alternate extinction of domains of opposite signs. As a result, under crossed nicols the domains appear as dark and bright stripes.

The quantitative investigation of the mutual turning of the indicatrix of neighboring domains leads to new possibilities for using optical methods. The angle of turning of the indicatrix, which can easily be determined by the angle between the extinction positions of neighboring domains, is a parameter of the monoclinicity of the crystals, just like the monoclinic angle determined by x-ray methods. In the case of Rochelle salt the optical method for determining the monoclinicity parameter becomes particularly important, because the x-ray method [6] does not give results of the desired accuracy, and measurements of the spontaneous polarization [7] or the spontaneous deformation [8] of necessity are carried out on samples which contain a large number of domains and, strictly speaking, it is not possible to give a characteristic degree of monoclinicity of the crystals because in these measurements there may take place a reorganization of interior domains, as well as an uncontrolled motion of the domain boundaries.

Theory

The monoclinicity parameter of Rochelle salt can be considered as a special case of the nonsymmetry parameter η which is involved in the general theory of phase transitions of the second kind [9] on the basis of which a theory of ferroelectric phenomena may be developed as shown by Ginzburg [10]. In the general theory it is shown that in the vicinity of the Curie point $T = \theta$, the expansions of the thermodynamic potential into a series in powers of η has the form

$$\Phi = \Phi_0 + A\eta^2 + C\eta^4 + \dots, \tag{1}$$

where $C > 0$, $A > 0$ in the symmetric phase (for $T > \theta$) and $A < 0$ in the nonsymmetric phase (for $T < \theta$). The stress here, as well as later in this paper, is considered constant.

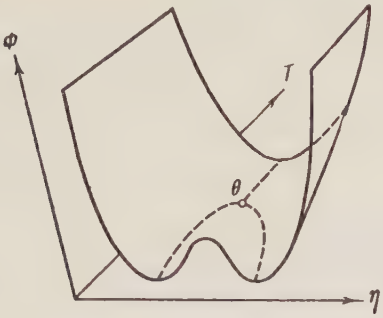

Fig. 1. Surface of the thermodynamic potential Φ near the point of phase transition of the second kind. Branching at T = θ, the dotted line corresponds to equal values of the nonsymmetry parameter.

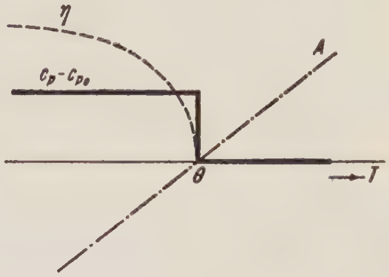

Fig. 2. Temperature dependence of the nonsymmetry parameter η and the heat capacity $c_p - c_{p_0}$ near the Curie point. The calculation is made with the simplest assumption concerning the character of the temperature dependence of the coefficients A and C (C = const and A is linearly dependent upon temperature).

Figure 1 illustrates the relief surface of the thermodynamic potential. The dotted lines indicate the curve of equal values of the nonsymmetry parameter $\eta = \eta_0(T)$, which are found from the condition that Φ is a minimum as a function of η. In the stability region of the symmetric phase this curve lies on the bottom of the hollow, which branches out into a saddle-shaped point corresponding to the Curie point so that in the nonsymmetric phase it is possible to have two values of the nonsymmetry parameter, equal in their absolute value, but opposite in sign.

Generally it is assumed that in Expansion (1) it is sufficient to write down the terms and to assume C = const and

$$A = a(T - \theta). \tag{2}$$

Then for the temperature dependence of the nonsymmetry parameter and the heat capacity one obtains the following expression [9]:

$$\left.\begin{aligned} \eta &= 0 \\ c_p &= c_{p_0} \end{aligned}\right\} T > \theta, \qquad \left.\begin{aligned} \eta^2 &= -\frac{A}{2C} \\ c_p &= c_{p_0} + T\frac{a^2}{2C} \end{aligned}\right\} T < \theta. \tag{3}$$

Here $c_{p_0} = -T\frac{\partial^2\Phi_0}{\partial T^2}$. The heat capacity jump at the Curie point obviously equals

$$\Delta c_p = c_p - c_{p_0} = \theta\frac{a^2}{2C}. \tag{4}$$

The temperature dependence of the values of A, η, and c_p in the vicinity of the Curie point is shown schematically in Fig. 2.

The calculation, however, may be carried out just as well by rejecting the simplifying assumption indicated in [11] for the general form of the function $\Phi = \Phi(T, \eta^2)$. The Curie points correspond to the roots of the equation

$$\left(\frac{\partial\Phi}{\partial\eta^2}\right)_{\eta=0} = 0. \tag{5}$$

The stability region of the nonsymmetric phase (in the given case it is the ferroelectric region) is obtained from the condition

$$\left(\frac{\partial\Phi}{\partial\eta^2}\right)_{\eta=0} < 0. \tag{6}$$

Here, for $\frac{\partial^2\Phi}{\partial(\eta^2)^2} > 0$, there are two equilibrium positions $\eta = \pm\eta_0(T)$, which can be obtained from the equation

$$\left(\frac{\partial\Phi}{\partial\eta^2}\right)_{\eta=\eta_0} = 0. \tag{7}$$

For calculating the entropy and the heat capacity it is necessary to differentiate the thermodynamic potential with respect to temperature along the equilibrium curve $\eta = \eta_0(T)$. Such differentiation will be denoted by the underlined terms:

$$\frac{d}{dT} = \frac{\partial}{\partial T} + \underline{\frac{d\eta_0{}^2}{dT} \cdot \frac{\partial}{\partial\eta^2}}. \tag{8}$$

By means of addition and subtraction of the term $\left(\frac{d\eta_0{}^2}{dT}\right)^2 \frac{\partial^2}{\partial\eta^2}$ the quadratic operator (8) can be transformed to

$$\frac{d^2}{dT^2} = \left(\frac{\partial}{\partial T} + \frac{d\eta_0^2}{\partial T} \cdot \frac{\partial}{\partial\eta^2}\right)^2 = \frac{\partial^2}{\partial T^2} - \left(\frac{d\eta_0^2}{dT}\right)^2 \cdot \frac{\partial^2}{\partial(\eta^2)^2} \underline{+\left(2\,\frac{d\eta_0^2}{dT} \cdot \frac{d}{dT} + \frac{d^2\eta_0}{dT^2}\right)}\frac{\partial}{\partial\eta^2}, \tag{9}$$

because, along the equilibrium curve with $\eta_0 \neq 0$, Φ is identically at a minimum :

$$\frac{\partial\Phi}{\partial\eta^2} = 0. \tag{10}$$

In applying Operators (8) and (9) to the function Φ the underlined terms give zero, and for the entropy and the heat capacity we obtain the expressions

$$S = -\frac{d\Phi}{dT} = -\frac{\partial\Phi}{dT},$$

$$c_p = -T\,\frac{d^2\Phi}{dT^2} = c_{p_0} + T\left(\frac{d\eta_0^2}{dT}\right)^2 \frac{\partial^2\Phi}{\partial(\eta^2)^2}. \tag{11}$$

Hence for the heat capacity jump at the Curie point it follows that

$$\Delta c_p = \theta\left(\frac{d\eta_0^2}{dT}\right)^2 \frac{\partial^2\Phi}{\partial(\eta^2)^2}. \tag{12}$$

The temperature dependence of the monoclinicity parameter and the heat capacity determine the position of the equilibrium curve in Φ, T, η space. The function $\eta = \eta_0(T)$ gives the projection of this curve on the (T, η) surface, and the heat capacity (after integration) is the projection on the (Φ, T) surface. One equilibrium curve is insufficient for constructing the $\Phi = \Phi(T, \eta^2)$ surface; however, this (space) curve permits the determination of the temperature dependence of the coefficients A and C by Expression (1) (if one is limited only to the underlined terms):

$$\left.\begin{aligned} A &= -2C\eta_0^2 \\ C &= \frac{c_p - c_{p_0}}{2T\left(\frac{d\eta_0^2}{dT}\right)^2} \end{aligned}\right\}. \tag{13}$$

This limitation corresponds to the interpolation of the surface of the thermodynamic potential according to the function $\eta_0(T)$ and $c_p(T)$.

As an example, the temperature dependence of the heat capacity and the monoclinicity parameter are shown in Fig. 3 with C = const and a parabolic dependence of the coefficient A upon temperature, when

$$\begin{aligned} A &= a(T-\theta_1)(T-\theta_2), \\ \eta^2 &= -\frac{a}{2C}(T-\theta_1)(T-\theta_2), \\ c_p - c_{p_0} &= \frac{a^2T}{2C}\left[3\left(T-\frac{\theta_1+\theta_2}{2}\right)^2 - \left(\frac{\theta_1-\theta_2}{2}\right)^2\right]. \end{aligned} \tag{13'}$$

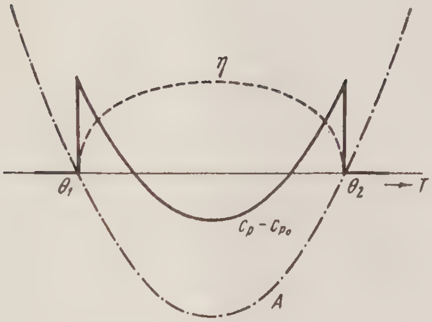

Fig. 3. The temperature dependence of the nonsymmetry parameter η and the heat capacity $c_p - c_{p0}$ in the Curie region. The calculation is carried out for C = const and a parabolic dependence of the coefficient A on temperature.

The surface of the thermodynamic potential (subtracting the term Φ_0) in variable T and η in this case represents a surface of the fourth order with two saddle points θ_1 and θ_2.

The strict construction of the $\Phi = \Phi(T, \eta^2)$ surface (without interpolation) requires the determination of the dependence of the parameter η not only upon the temperature but also upon external influences connected with the parameter η. These external influences may be called the thermodynamic force ξ. (This force, for example, may be the electric field strength if the monoclinicity parameter is the polarization [10] or the tangential stress Y_z if the monoclinicity parameter is the deformation y_z.) Everywhere above it had been supposed that $\xi = 0$. If this is not so, the term $-\eta\xi$ must be added to the thermodynamic potential. As a result, the equilibrium position is displaced and must be found by the equation

$$\xi = 2\eta\frac{\partial\Phi}{\partial\eta^2}, \tag{14}$$

where by Φ is meant the function $\Phi(T, \eta^2)$ as shown above, which now no longer appears as the thermodynamic potential but as the free energy.

From the experimental dependence of $\xi = \xi(\eta)$ with the help of Eq. (14) one can obtain $\frac{\partial\Phi}{\partial\eta^2}$ as a function of η (and temperature) and re-establish the form of the $\Phi(T, \eta^2)$ surface.

Relation Between the Possible Monoclinicity Parameters

As monoclinicity parameter for a Rochelle salt crystal one may choose either the polarization P_x along one of the ferroelectric X axes(a), the tangential deformation y_z or the deflection angle (α) of the optical indicatrix about the X axis. Any two of these quantities can be expressed in terms of the third one and the external field strength. Let us first determine the qualitative relation between the possible monoclinicity parameters.

The sign of the deflection of the indicatrix may be investigated by comparing the extinction positions of two systems of domains. That system of domains (component of the polysynthetic twins) which corresponds to

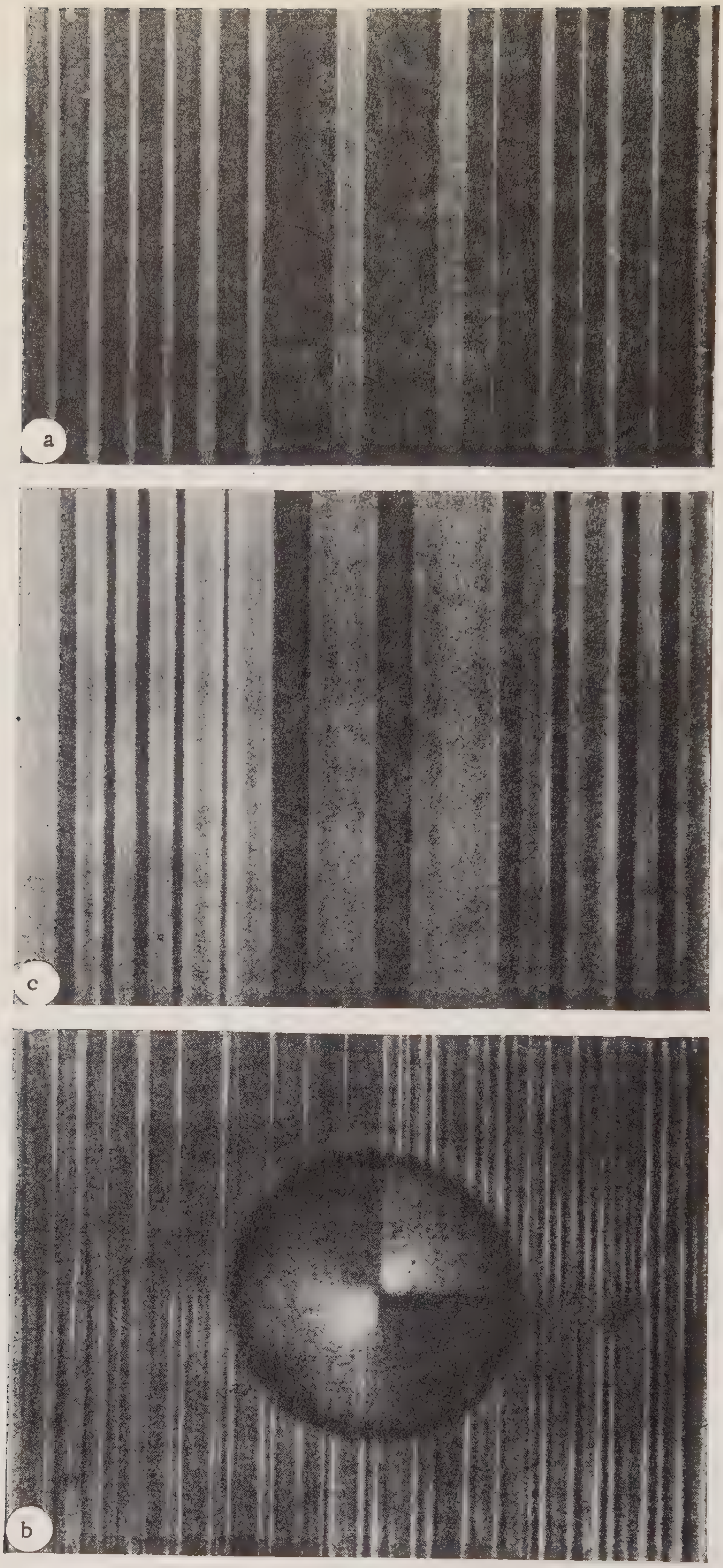

Fig. 4. For finding the sign of the spontaneous polarization, the spontaneous deformation and the angle of spontaneous turning of the optical indicatrix of the domains: a) uncharged plate of an X-cut in the left extinction position; b) the same plate under the influence of an electric field, directed from the top surface of the plate toward the bottom; and c) change in the domain structure on local charging.

the "left" extinction position, i. e., extinction upon turning the microscope stage to the left from the position of equal darkening of the domains, obviously possesses an indicatrix turning to the right.

In order to show the direction of the spontaneous polarization of this system of domains, let us follow the displacement of the domain boundary under the influence of an electric field [3]. Thereby the domains, the polarization of which is directed along the field, are forced to expand. If the positive electrode lies on the top side of the plate of an X-cut, then the width of the darkened domains is diminished in the "left" extinction position as seen from a comparison of Figs. 4 a and b. Consequently, in the system of domains with the right turn of the indicatrix the spontaneous polarization is directed from the bottom side of the plate toward the top. This direction shall be regarded as the positive direction and the domains with $P_x > 0$ are designated as positive.

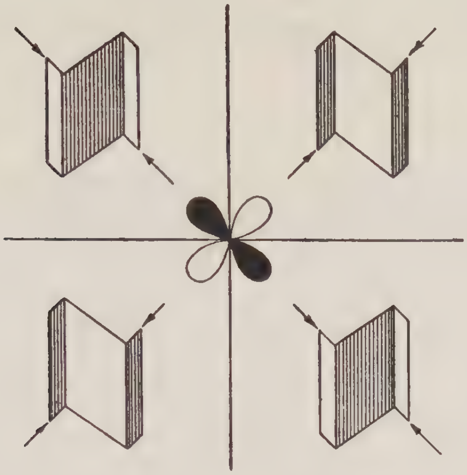

Fig. 5. Scheme of the reorganization of the domain structure in the different quadrants with the position of the load in an X-cut plate. In the center is shown the rosette of equal tangential stress $|Y_z| = C = \text{const.}$ The region of $Y_z > C$ is omitted.

It remains to compare the signs of the spontaneous polarization and the spontaneous deformation. For this, let us submit the X-cut plate to a concentration of load with the aid of a small glass sphere [2]. The appropriate stress distribution is of an extremely complex character; however, it is sufficient to note that in the cylindrical system of coordinates, the axis of which coincides with the axis of loading, the radial stress σ_r will be everywhere a compressive stress ($\sigma_r < 0$) and the tangential stress σ_θ is a tensile stress ($\sigma_\theta > 0$). Hence it follows that the tangential stress

$$Y_z = (\sigma_r - \sigma_\theta) \sin \vartheta \cos \vartheta \qquad (15)$$

(ϑ is read from the Y axis) is positive in the second and fourth quadrants and negative in the first and the third quadrants. Since the external mechanical stress leads to an increase of those domains, the sign of the spontaneous deformation y_z^0 of which coincides with the sign of the stress Y_z in the first and the third quadrants, the domains with $y_z^0 > 0$ are forced to displace domains which possess a negative spontaneous deformation, and in the second and the fourth quadrants the opposite effect is observed. This is schematically illustrated in Fig. 5, where, for simplicity, only the radial stresses are indicated and the complete distribution of the tangential stress Y_z is characterized by the rosette of equal tangential stress, which is calculated by (15) taking equal account (as follows from a more detailed calculation) of the absolute values of the stresses σ_r and σ_θ far from the region of application of the load.

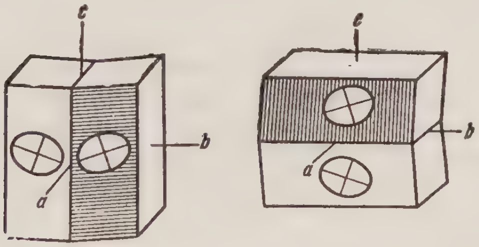

Fig. 6. Schematic representation of the direction of the spontaneous polarization, the spontaneous deformation, and the spontaneous turning of the optical indicatrix in c- and the b-domains of different sign.

As seen in Fig. 4b, upon compression by a small sphere of a sample placed in the "left" extinction position, the darkening of the domain system (i. e., the domain system with $P_x > 0$) contracts in the first and the third quadrants and widens in the second and the fourth quadrants. Hence, it follows that the positive domains possess a positive spontaneous deformation.

The results obtained are summarized in Fig. 6 where the relation among the spontaneous polarization P_x^0, the spontaneous deformation y_z^0 and the spontaneous angle of turning of the indicatrix α for the b- and the c-domains of opposite sign are shown schematically. If one were to consider as positive the turning of the indicatrix in the clockwise direction about the positive direction of the X axis then for the positive domains $P_x^0 > 0$, $y_z^0 > 0$, and $\alpha < 0$. Figure 6 enables one to distinguish easily the domains of different sign by the optical method without resorting to the application of external electrical and mechanical effects.

The quantitative relation between the possible monoclinicity parameters of Rochelle salt is still insufficiently investigated at present. It is known that in the absence of mechanical stress the polarization P_x and the deformation y_z are proportional to each other [10, 12]:

$$y_z = b_{14} P_x, \tag{16}$$

where the coefficient $b_{14} > 0$ (which agrees with Fig. 6) and depends slightly upon the temperature. The relation (16) is also probably correct for the electric field equal to zero when the role of the polarization and the deformation is played by the spontaneous polarization and the spontaneous deformation of the domains:

$$y_z^0 = b_{14} P_x^0 . \tag{16'}$$

Analogous relations can also be set up between the deformation y_z and the turning of the optical indicatrix. From the general equations of the piezooptic effect [13] it follows that the coefficient a_{ik} in the equation of the optical indicatrix

$$a_{ik}\, x_i x_k = 1 \tag{17}$$

is a linear function of the deformation ϵ_{mn}

$$a_{ik} = a_{ik}^0 + p_{ikmn}\, \varepsilon_{mn}. \tag{18}$$

The tensor component p_{ikmn} is called the optical constant of deformation. Relation (18) is equivalent to the equation

$$a_{ik} = a_{ik}^0 - \pi_{ikmn} \sigma_{mn}, \tag{18'}$$

connecting the value of a_{ik} with the stress σ_{mn} through the tensor π_{ikmn}, which is the tensor of the optical stress constants. According to Neumann [14] the physical reason for the distortion of the indicatrix is the deformation and not the stress. Maxwell [15] expressed exactly the opposite point of view.

The difference in the points of view of Neumann and Maxwell can be checked experimentally neither with elastic bodies in which the stress and the deformation are connected by Hooke's law nor with plastics where the optical effect is complicated by the orientation effect. It is therefore curious to note that spontaneous deformation of crystals is not possible according to Maxwell and that the spontaneous distortion of the indicatrix is possible according to Neumann. Actually the substitution of the conditions $\epsilon_{mn} = \epsilon_{mn}^0$ and $\sigma_{mn} = 0$ in Eqs. (18) and (18') gives

$$a_{ik} = a_{ik}^0 + p_{ikmn}\, \varepsilon_{mn}^0 \tag{19}$$

according to Neumann and

$$a_{ik} = a_{ik}^0, \tag{19'}$$

i. e., the absence of the optical effect, according to Maxwell.

Using the point of view of Neumann and the consideration brought forward by Cady [12] the importance of the optical constant of deformation for Rochelle salt* is obtained from (19):

$$a_{23} = p_{44} y_z^0 = -0.009\, y_z^0. \tag{20}$$

(Here and in the remaining the abbreviation of the designation of the index of the optical constant is assumed.) The changes of a_{22} and a_{33} cannot be taken into consideration, as will be shown below.

---

* The author especially regrets the insufficient reliability of these data.

Let us express the turning of the axis of the indicatrix about the X axis through the coefficients of the indicatrix

$$\tan 2\alpha = \frac{2a_{23}}{a_{22}-a_{33}}. \tag{21}$$

Using (20) and taking into account the smallness of α and assuming $a_{22} = a_{22}^0 = \frac{1}{n_y^2}$ and $a_{33} = a_{33}^0 = \frac{1}{n_z^2}$, it is possible, due to the large anisotropy of the crystal ($n_y = 1.492$, $n_z = 1.490$), to obtain

$$\alpha = \frac{p_{44} y_z^0}{n_y^{-2} - n_z^{-2}} \cong -30 y_z^0. \tag{21'}$$

Strictly speaking, the numerical evaluation of the coefficients in Relation (21') is useful only for that (not exactly known) temperature at which the value of p_{44} was measured. However, one can hope that this coefficient, analogous to b_{14}, is slightly dependent upon temperature within the limits of the comparatively narrow ferroelectric interval (−18° to +24°). By noting that the sign of the coefficient of proportionality in (21') is the same as the sign of the coefficient in (16), this corresponds to the scheme of Fig. 6.

Temperature Dependence of the Monoclinicity Parameter

The selection of the angle of spontaneous turning of the optical indicatrix as the monoclinicity parameter makes it possible to determine easily its temperature dependence. The appropriate results have already been given briefly [16].

The measurement of the angle between the extinction positions of domains of the two systems was conducted on an X-cut plate with the help of a polarizing microscope provided with two quartz wedges. In connection with the detection of the dispersion of the extinction position, a filter at 540 mμ with a narrow (10 mμ) band passage is used. Each measurement was repeated from 5 to 10 times and was made with an accuracy of 0.1°. The scatter of the readings amounts to 0.1° on the average.

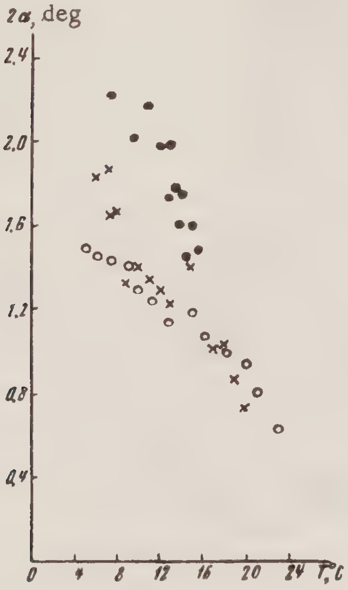

Fig. 7. Change of the angle 2α between the extinction positions of domains of opposite sign in an X-cut plate. ●) First, ×) second, ○) ninth series of measurements.

For the measurement the plate was placed in a special thermostatic stage, the temperature of which was maintained with the help of liquids circulating through the ultra thermostat and the cold accumulator. Before each measurement the temperature was maintained constant for 15-20 min. This period of time, established from preliminary experiments, is completely adequate in work with samples of small dimensions (8 × 8 × 0.3 mm).

The angle between the extinction positions of the domains continuously changes in the Curie interval and reaches its maximum value in the middle of this interval (about 3°C). The comparison of the following series of measurements enables one to determine also that a repitition of the "heating and cooling" cycle leads to a decreased initial value of the monoclinicity parameter.

In Fig. 7 are shown the results of the 1st, 2nd and 9th series of measurements, carried out one after another on the same sample at positive temperatures. At 7°C, if 2α = 2.2° was obtained in the first series, then in the second series a value of 1.85° and in the ninth series a value of about 1.5° was obtained.

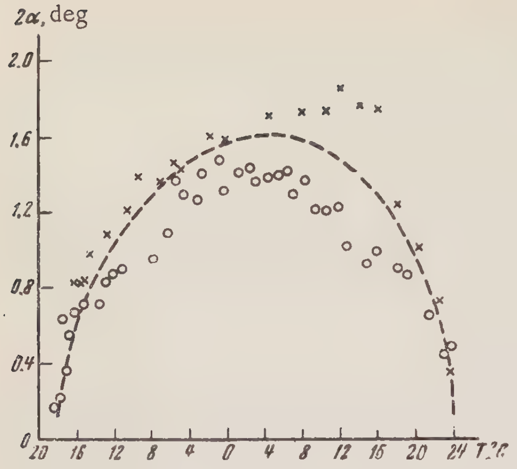

Fig. 8. Same as in Fig. 7 for another sample with measurements over the whole ferroelectric region. ×) First, ○) seventh series of measurements. The dots show the average value of the 8 series of measurements used for calculating the thermodynamic potential.

Figure 8 illustrates the same phenomenon for another sample, measurements on which were conducted in the whole ferroelectric region. Only after 7 or 8 series of measurements did the readings become relatively stable, whereupon the maximum value of 2α decreased from 1.8° to 1.6°. On the same figure the dotted curve shows the average of all the eight series of measurements.

According to this curve, with the assumption that C = constant, we calculated the temperature dependence of the coefficient A and constructed a model of the surface of the thermodynamic potential for Rochelle salt as shown in Fig. 9. Outside the ferroelectric region the surface $\Phi = \Phi(T, \eta)$ becomes valleys, the bottoms of which are located in the plane $\eta = 0$. The Curie points correspond to the saddle points between which is located the hollow with double cavities of depth 2 cal/mole. The presence of the crest, which connects the Curie points, lead to the instability of the rhombohedral modification of the crystal in the ferroelectric region and forces the sample to break up into monoclinic domains corresponding to the potential depressions distributed on both sides of the $\eta = 0$ surface.

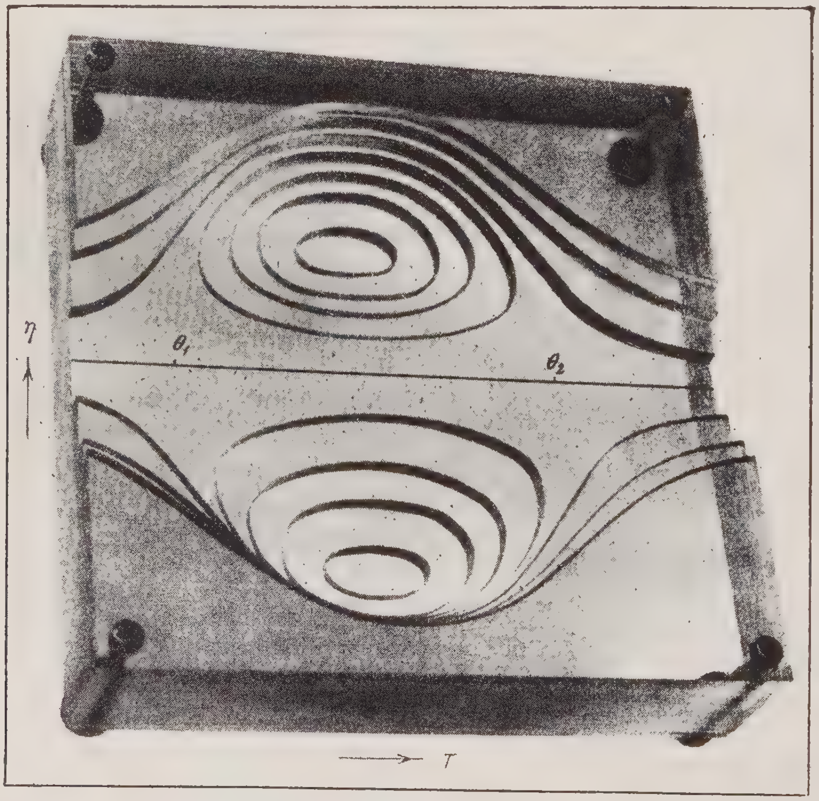

Fig. 9. Model of the thermodynamic potential of Rochelle salt in the vicinity of the Curie region. Height of steps is 5.5 cal/mol.

According to Eqs. (16') and (21') , the same model, after a simple change of scale, can be considered as a model for the surface of the thermodynamic potential as a function of temperature as well as polarization P_x

and deformation y_z. The slope of the curve which is obtained from the cross section of the model's surface at T = const gives the value which corresponds to the generalized force (i. e., the electric field strength E_x in the first case or the value of the tangential stress Y_z in the second) and the curvatures of these curves correspond to the moduli (dielectric permeability or shear modulus).

As was already mentioned above, Fig. 3 shows the model of the thermodynamic potential constructed according to the average for several series of measured values of the monoclinicity parameter while a consistent decrease in the value of this parameter took place from series to series. The data available at present are not sufficient for the explanation of the phenomenon mentioned above. In particular, it is not clear whether this is connected with the successive cycles of heating and cooling of the sample in the ferroelectric region or directly with the successive changes of the monoclinicity parameter, caused by these temperature fluctuations. In this connection it is particularly interesting to compare the monoclinicity parameters obtained by different methods.

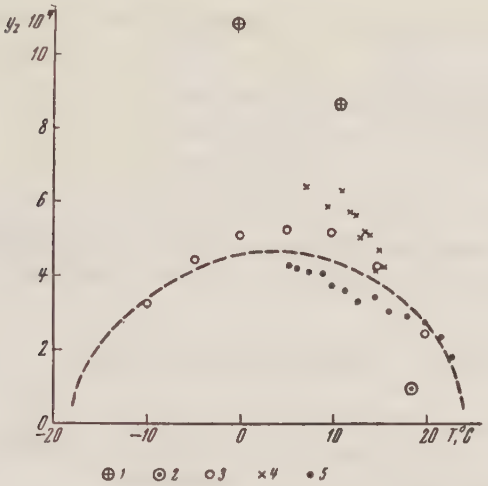

Fig. 10. The temperature dependence of the monoclinicity parameter of Rochelle salt according to the data of different authors. All the results are reduced to the value of the spontaneous deformation with the help of Formulas (16') and (21'). 1) Direct measurement of the angle between the Y and the Z faces (Mueller [8]); 2) calculated according to the residual deformation (Hinz [12]); 3) calculated according to the spontaneous polarization (Mueller [8]); 4) calculated according to the results of the optical measurements, shown in Fig. 7 (the first series of measurements); 5) same for the ninth series of measurements. The dotted curve corresponds to the average values given in Fig. 8.

In Fig. 10 are given Cady's [12] results of the measurements of the temperature dependence of the spontaneous polarization and the spontaneous deformation of Rochelle salt compared with the data obtained in this study on the temperature dependence of the spontaneous turning of the optical indicatrix. All the results are reduced to the value of the spontaneous deformation y_z^0 with the help of Eqs. (16') and (21'). The temperature dependence of the constant b_{14} was calculated from the data of Mueller as given by Cady. The constants p_{44}, n_y and n_z are assumed to be constant in the whole ferroelectric region. As seen in Fig. 10, according to the optical method the spontaneous deformation in the central portion of the ferroelectric region initially attains a value of the order of $8 \cdot 10^{-4}$. In the following series of measurements the maximum value of y_z^0 decreases to 4 or $5 \cdot 10^{-4}$. Therefore, the optical method casts some light on the source of the gross diversity of the experimental data on the spontaneous deformation and the spontaneous polarization. If the values of the deformation are determined by a single measurement then generally the determination of the spontaneous polarization from the hysteresis loops is inevitably connected with the repeated repolarization of the sample. Therefore, it is not surprising that the value of y_z^0 calculated from the spontaneous polarization fits the results of optical measurements of steady state and the direct measurements of y_z^0 are much closer to the results of the first series of optical measurements.

These interesting results are, of course, subject to more refinement in view of the absence of sufficiently reliable data concerning the value of the coefficient p_{44} used in this study and its possible temperature dependence. The remaining open question concerns the source of the nonstationary value of the monoclinicity parameter, which, in the authors' view, is impossible to explain, for instance, by a shift of surface charges.

It is impossible, however, to doubt at all the fact that the quantitative use of the optical method to obtain the monoclinicity parameter, instead of essentially unreliable methods of determining the parameter by the macroscopic characteristics of the multidomain sample, reveals new possibilities for making more precise the theory of the ferroelectric properties of Rochelle salt.

LITERATURE CITED

[1] M. V. Klassen-Nekliudova, M. A. Chernysheva, and A. A. Shternberg, "Concerning the real structure of Rochelle salt," Doklady Akad. Nauk SSSR 63, 527-530 (1948).

[2] M. A. Chernysheva, "Mechanical twinning in crystals of Rochelle salt," Doklady Akad. Nauk SSSR 74, 247-249 (1950).

[3] M. A. Chernysheva, "The effect of electric field on the twin structure in crystals of Rochelle salt," Doklady Akad. Nauk SSSR 81, 1065-1068 (1951).

[4] M. A. Chernysheva, "The effect of zonal and sectorial structure on the distribution of twins (domains) in crystals of Rochelle salt," Doklady Akad. Nauk SSSR 91, 87-88 (1953).

[5] V. L. Indenbom and M. A. Chernysheva, "Rings of edge dislocation in crystals of Rochelle salt," Doklady Akad. Nauk SSSR 111, 596-598 (1956).

[6] A. R. Ubbelohde and I. Woodward, "Structure and thermal properties of crystals. VI. The role of hydrogen bonds in Rochelle salt," Proc. Roy. Soc. 185, 448-465 (1946).

[7] J. Hablützel, "Schweres Seignettesalz. Dielectrische Untersuchungen an $KNaC_4H_2D_2O_6 \cdot 4D_2O$ — Kristallen," Helv. Phys. Acta 12, 489 (1939).

[8] H. Mueller, "Properties of Rochelle salt," Phys. Rev. 57, 829-839; 58, 565-573 (1940).

[9] L. D. Landau and I. M. Lifshits, Statistical Physics [in Russian] (1951) p. 428.

[10] V. L. Ginzburg, "The theory of ferroelectric phenomena," Uspekhi Fiz. Nauk 38, 490 (1949).

[11] V. L. Indenbom and M A. Chernysheva, "The construction of the thermodynamic potential of Rochelle salt according to the results of the optical investigation of the domains," J. Exptl.-Theoret. Phys. (USSR) (in press).*

[12] U. Cady, Piezoelectricity and Its Practical Applications [Russian translation] (Moscow, 1948).

[13] F. Pockels, Lehrbuch der Kristalloptik (1906).

[14] F. E. Neumann, "Die Gesetze des Doppelbrechung des Lichtes in komprimierten oder ungleichförmig erwärmten unkristallinischen Körpen," Abhandl. d. Kön. Akad. Wissenschaft Berlin, II, 1-254 (1841).

[15] J. C. Maxwell, "On the equilibrium of elastic solids," Trans. Roy. Soc., Edinburgh 20, 87-120 (1853).

[16] M. A. Chernysheva, "Some details of the domain structure in crystals of Rochelle salt (according to optical observations)," Izv. AN SSSR, Ser. Fiz. 2, 289-292 (1957).

Received February 23, 1957

Institute of Crystallography, Academy of Sciences, USSR

---

* [See Soviet Physics — JETP]

STUDY OF PHASE TRANSFORMATIONS AT VERY HIGH PRESSURES

V. P. Butuzov

An intensifier has been designed for pressures of up to 34,000 kg/cm^2. By means of this apparatus, it is possible to compress liquids at temperatures of up to 600°C and gases to 1500°C. A method has been developed for the study of phase transformations and the determination of polymorphic transition temperatures.

The method and apparatus have been used for the determination of the melting points of a number of metals as a function of pressure.

The polymorphic transitions of phosphorus have been studied.

A phase diagram has been constructed for bismuth for pressures of up to 30,000 kg/cm^2.

The method has also been employed to calculate the magnitude of the thermal effects and specific volume changes in $\alpha \rightleftharpoons \beta$ and $\beta \rightleftharpoons \gamma$ transitions.

In the course of recent years, research work has been conducted in collaboration with colleagues of the Institute of Crystallography of the Academy of Sciences, USSR, G. P. Shakhovskii, S. S. Boksha and E. G. Poniatovskii, on the development of very high pressure apparatus and on the study of phase transformations at very high pressures. It is the purpose of this paper to summarize the results obtained.

Considerable progress has recently been made in the production and application of very high pressures in various branches of chemistry and physics [1-4]. After many years, work by American scientists on the production of artificial diamonds has been brought to a successful conclusion [5, 6 *]. Soviet scientists have made considerable contributions to the development of very high pressure techniques [7-9].

P. W. Bridgman carried out a systematic research at very high pressures; in his experiments, however, at pressures of up to 30,000 kg/cm^2, the maximum temperature did not exceed 200°C. The literature contains no descriptions of intensifiers operating for any considerable length of time at high temperatures in conjunction with very high pressures.

Intensifier for the Production of Very High Pressures

In the production of very high pressures of above 15,000 kg/cm^2, the principle known as "external support" is used. As a rule, the intensifier constructed with external support comprises two independent presses, one of which creates a pressure in the pressure chamber of the stopper or cone, while the other moves the cone in a supporting member.

With ordinary mechanical support, the maximum pressure in the intensifer does not exceed 24,000 kg/cm^2. For producing higher pressures, we have designed and constructed an intensifier with double mechanical support

---

* The published articles do not give any description of the high pressure chambers.

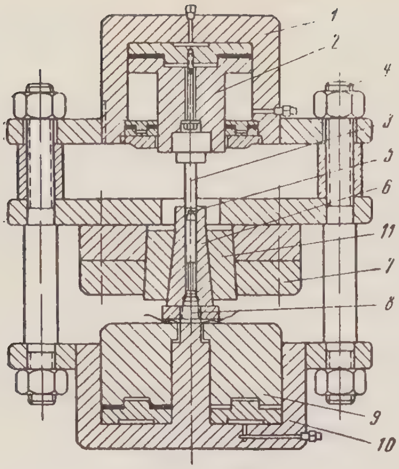

Fig. 1. Diagram of intensifier for producing pressures of up to 40,000 kg/cm^2.

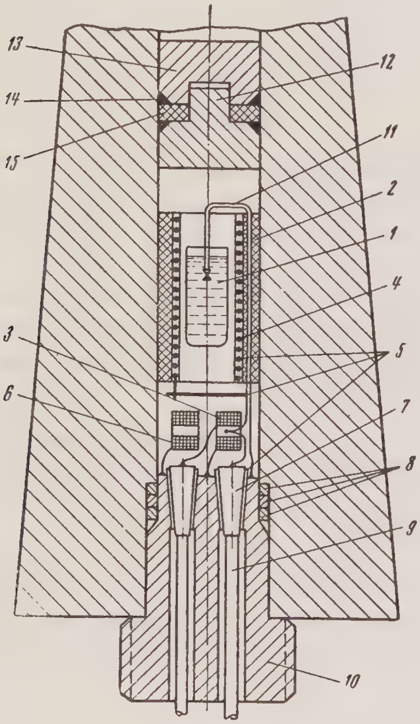

Fig. 2. Diagram of apparatus for melting-point determinations under pressure.

[10], designed to produce pressures of up to 40,000 kg/cm^2 in the pressure chamber, 10 to 20 cc of liquid or gas being subjected to the maximum pressure. This intensifier is shown diagrammatically in Fig. 1.

A very important part of the apparatus is the electrical bushing, the construction of which is shown diagrammatically in Fig. 2. Inserted in the body of the electrical bushing 10 are four small cones 7, insulated from the body of the bushing by thin mica sheets. As the pressure in the pressure chamber increases, these small cones are forced into their seats, thus producing a reliable seal. Sealing of the electrical bushing itself in the pressure chamber is effected by means of three sealing rings 8, the principle of the "uncompensated area" being used. The free unoccupied space below the bottom ring forms an uncompensated area, which is gradually filled up by the substance of the sealing rings as the pressure in the pressure chamber increases. Preliminary sealing of the rings of the electrical bushing is produced by the lower press when it provides the supporting pressure for the conical pressure chamber. Mounted in the pressure chamber of the intensifier cone (see Fig. 2) are: electric furnace 4, differential thermocouple 11, copper thermometer 3 and manganin pressure gauge 6, situated in the cold zone of the chamber, plugs 12, 13 and crucible 1 containing the substance under investigation. The cone construction described was used for studying the influence of pressure on the melting point of substances.

In the intensifier described, we have produced pressures of up to 34,000 kg/cm^2 by the compression of isopentane, permitting the application of temperatures of up to 600°C. Further increase in temperature within the pressure chamber was difficult, since the isopentane began to decompose, causing the heating elements to get out of order. It was therefore necessary to design very high pressure apparatus for use with gases. As is known, very high temperatures can be obtained in an inert gas atmosphere, but the construction of such an apparatus gives rise to considerable experimental difficulties. An apparatus is described in the literature [11], in which a gas pressure of up to 10,000 kg/cm^2 was obtained at temperatures of up to 1400°C. This apparatus was used for determining the variation of the melting point of diopside with the applied pressure.

The intensifier described in the foregoing, after considerable modification in the cone design, was used for the production of very high pressures at high temperatures. In view of the high compressibility of gases in the first stage of compression, a preliminary pressure of several thousands of atmospheres had to be created in the pressure chamber.

In the first attempts to produce very high gas pressures, the preliminary pressure was applied to the upper part of the pressure chamber through a special union, such as that used in the Vereshchagin intensifier [12]. The small orifice in the inner surface of the cone through which the gas entered the chamber resulted in the forma-

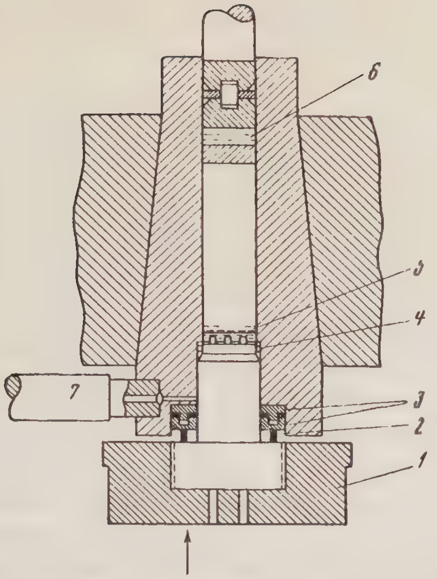

Fig. 3. Diagram of apparatus for production of very high gas pressures.

tion of microscopic cracks in the closure plug, and gas leaked through these cracks when the plug was moved. With a cone of this design, we were unable to produce gas pressures higher than 10,000 kg/cm^2. It was therefore found necessary to apply the preliminary pressure to the pressure chamber in a part of the cone where there were no moving sealing parts. Figure 3 shows such a device, consisting of two profiled rings 3 with gaskets of vinyl chloride plastic and a steel pressure ring 2. Before the admission of gas to the pressure chamber, the plastic gaskets in the cutoff are sealed by the bottom press of the intensifier. This pressure is transmitted via the base 1, electrical lead-in bushing and pressure ring 2. Gas is then admitted to the pressure chamber through the union 7 and passes freely through the sealing rings 4, which are still in the uncompressed state. When the required preliminary pressure has been reached in the pressure chamber, the lower press of the intensifier is switched on, causing the pressure ring 2 to be compressed and the electrical lead-in bushing to move upward, the sealing rings 4 of the latter becoming gas-tight and the gas in the pressure chamber being cut off. The pressure ring is of such a thickness that it does not collapse under a stress 1.5-2 times the stress required for sealing the plastic gaskets. The dimensions of the cutoff device are designed so that at the moment the gas in the pressure chamber is cut off, the supporting base 1 has come into contact with the lower face of the cone, this being necessary for producing the supporting stress on the cone during the further movement of the lower press. The cone construction described was found to be fully satisfactory since it permitted the production of gas pressures of up to 20,000 kg/cm^2.

Further attempts, however, to produce a gas pressure higher than 20,000 kg/cm^2 were unsuccessful, since there was gas leakage either through the movable plug or through the seal of the electrical lead-in bushing. It was natural to use liquid seals in front of all the gaskets in the apparatus. By using such liquid seals (see Fig. 3), it was possible to produce a gas pressure of up to 30,000 kg/cm^2.

If the equipment necessary for producing the preliminary pressure is not available, the gas pressure may be produced by the use of solid carbon dioxide for the compression [13].

The apparatus for the compression of gas was used in the determination of the influence of pressure on the melting points of aluminum and copper and in a study of the polymorphism of phosphorus.

Method of Measuring Temperature and Phase Transformations

Pressure was measured directly in the pressure chamber from the variation in electrical resistance of a manganin wire. The accuracy of the pressure measurement was approximately ± 100 kg/cm^2.

The temperature in the intensifier chamber was measured by means of differential thermocouples. Differential thermocouples were used because of the difficulty of leading the two different ends of a thermocouple out of the high pressure vessel without additional junctions. By the use of this method, it is possible to position both junctions of the thermocouple in the pressure chamber, and to carry to the outside the two identical ends of the thermocouple, which are welded to an electrically insulated small cone pressed into the seating of the electrical lead-in bushing, and to the lead-in bushing. Figure 2 shows diagrammatically the measurement of the melting points of metals at very high pressures. It will be seen from the diagram that the "hot" junction of the thermocouple 11 is situated in the crucible 1 containing the metal investigated, while the "cold" junction is in the lower part of the pressure vessel, inside the coil of the copper resistance thermometer 3, which was used for measuring the temperature of the "cold" junction. The emf of the differential thermocouple was measured by means of a needle millivoltmeter. The accuracy of measurement of the temperature difference of the junctions was ± 0.5°C. We ignored any correction for the influence of pressure on the emf of the thermocouple. According to data given by Birch [15], this correction is quite small.

The resistance thermometer was made of thin copper wire having a total resistance of 14-15 ohms. The temperature of the cold junction was measured with an accuracy of 0.1°C. Since an increase in temperature from 30° to 75°C has no effect on the variation in resistance of copper, for an increase in pressure up to 30,000 kg/cm^2 [16], it is unnecessary to make any corresponding corrections.

The melting points of metals as a function of the applied pressure were determined in the intensifier described in the foregoing. The required pressure was produced in the pressure chamber by movement of the plug, the electrical heating was then switched on and the rise in temperature was followed from the readings of the millivoltmeter. At first the temperature was raised to a point higher by about 50°C than the melting point, the latter being observed from the arrestment of the instrument needle. The melt was then allowed to cool gradually and the freezing temperature was noted from the constancy of the millivoltmeter readings over a considerable interval of time. The temperature of the cold junction of the thermocouple and the pressure on freezing were measured at the same time. With the pressure kept constant, eight to ten determinations were made, giving a deviation of not more than 0.5°C from the mean value of the freezing point. By means of this method, it is possible to plot the curve of melting point as a function of pressure in the course of one experiment.

Subsequently, the method of measuring the temperature was improved [17]. We no longer used the copper resistance thermometer, essential for measuring the temperature of the cold junction of the thermocouple, since we employed combined differential thermocouples, which eliminated the need for determining the temperature of the cold junction of the thermocouple, and furthermore we adopted automatic recording of the temperature, thereby considerably facilitating the observation of polymorphic transition processes.

Up to the present time, polymorphic transitions of substances at very high pressures have been determined either by a method based on the change in electrical resistance of the substance investigated, or by the change in volume, ascertained by the "piston displacement" method. Both methods have decided drawbacks. The first method does not permit the character of the polymorphic transition to be determined with sufficient reliability, since a change in the electrical resistance of the specimen may occur in the process of varying the temperature and pressure. The piston displacement method also is unable to ensure exact determination of the commence-

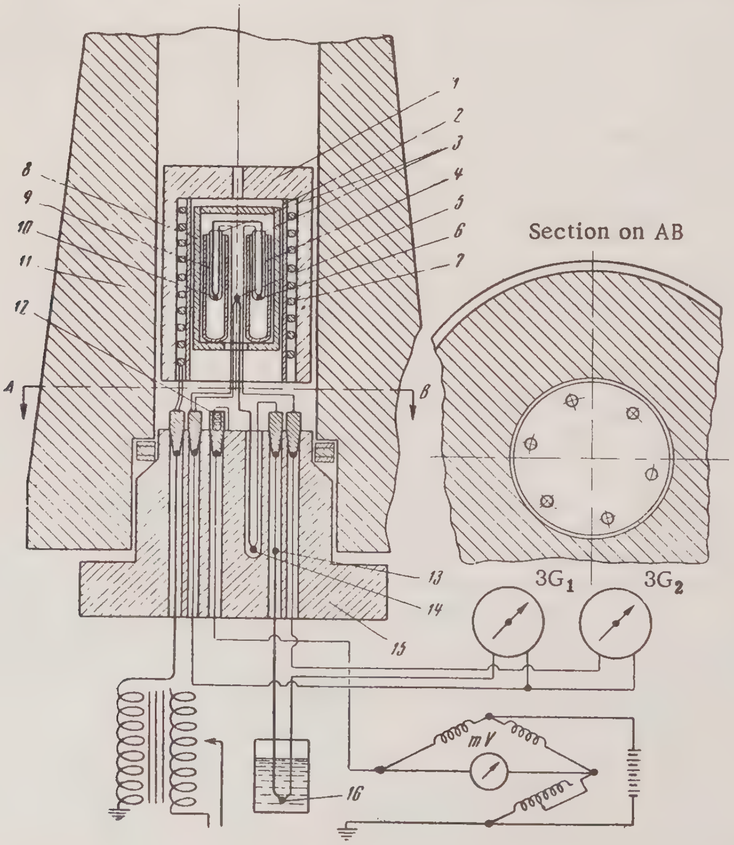

Fig. 4. Diagram of apparatus for studying polymorphic transitions in intensifiers.

ment of transition, due to high friction of the plug against the wall of the pressure chamber, especially in those cases where the polymorphic transition is accompanied by only a slight change in volume or the amount of investigated substance taken is small.

Figure 4 shows an apparatus for the study of polymorphic transitions at very high pressures. In the pressure chamber 11 is an electrical heating element 7, which is insulated from the walls by the thermally insulating cup 1. The crucible 8, with a hole in the bottom, is insulated from the electrical heating element by a mica layer 2. Inside the crucible are two porcelain ampoules 4 and 9, one of which contains the substance investigated, while the other contains any substance which does not suffer polymorphic transition at the pressures and temperatures produced. Two mutually independent thermocouples were used. The first thermocouple, the junctions 6 and 10 of which were situated in the investigated substance and in the control substance, made it possible to determine fairly accurately polymorphic transitions accompanied by an evolution or absorption of heat. The second thermocouple, termed by us the combined thermocouple, was for measuring the absolute value of the temperature; it consisted of four junctions 5, 14, 13, 16. In the body of the electrical lead-in bushing 15 are two junctions of the combined thermocouple, the emf's of these junctions compensating each other. We ignored the influence of pressure on the emf's of the thermocouples. Pressure was measured by means of a manganin gauge 12 and the emf's of the thermocouples by two mirror galvanometers, or the variation in emf of the two thermocouples was recorded photographically by means of a Kurnakov pyrometer.

Measurement of the Melting Points of Metals Under Pressure

Until recently, information on the influence of very high pressure on the melting points of metals was limited to the results obtained by Bridgman [18, 19], who investigated the melting of some fusible metals (potassium, sodium, lithium, rubidium and cesium) at pressures of up to 12,000 kg/cm² and bismuth at pressures of up to 17,000 kg/cm².

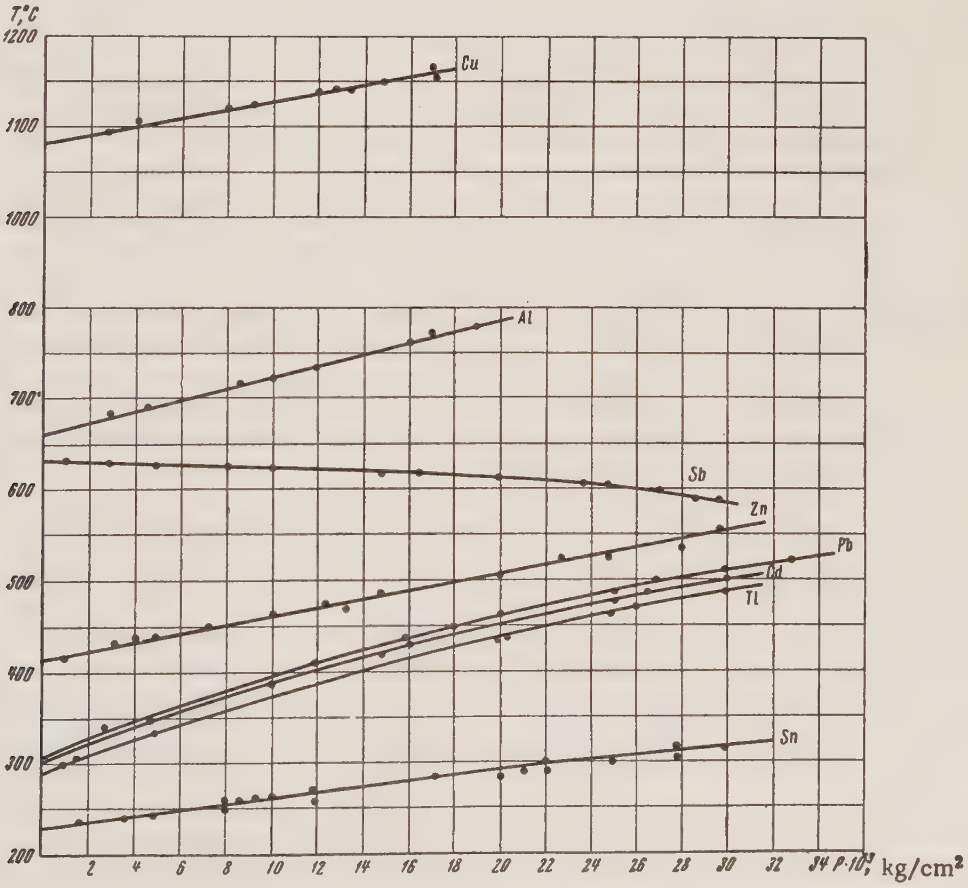

Fig. 5. Melting points of metals as a function of pressure.

In 1955, measurements were published of the melting point of germanium [20] at pressures up to 180,000 kg/cm^2. The germanium specimen was contained in a graphite crucible, which at the same time formed the heating element. The pressure was determined from the polymorphic transition points of bismuth, thallium, cesium and barium. Temperature was measured by means of a platinum-platinum-rhodium thermocouple. It was found that the melting point of germanium fell smoothly throughout the entire pressure range from 936°C at a pressure of 1 atmos to 347 ± 18°C at 180,000 kg/cm^2. No polymorphic transitions were found in the pressure range investigated.

The study of the phase transformations of metals under conditions of very high pressure by the method we have developed [13, 14, 17] dates back to 1953. The melting points of tin and lead were measured at pressures of up to 34,000 kg/cm^2 [21], and of antimony, cadmium, zinc and thallium [22] as well as indium [23] at pressures of up to 30,000 kg/cm^2. The melting points of aluminum and copper [24] were determined at pressures of up to 18,000 kg/cm^2. Since the melting points of the metals in these determinations were fairly high, the necessary thermal insulation of the furnace from the pressure chamber walls was effected by filling the entire unoccupied space of the pressure chamber with powdered alumina, with the exception of the upper part where the plug was situated. Figure 5 shows graphically the results of the measurements on the basis of the experimental data.

A study of the curves shown in Fig. 5 leads to the conclusion that the metals investigated may be classed in the following groups: Zn, Cu, Al, for which $\frac{dT_{m.p.}}{dP}$ is positive and constant; K, Na, Rb, Cs, Sn, Pb, Te, for which $\frac{dT_{m.p.}}{dP}$ is positive and diminishes with increase in pressure; Sb, Ge, for which $\frac{dT_{m.p.}}{dP}$ is negative throughout the entire pressure range investigated; and bismuth, for which $\frac{dT_{m.p.}}{dP}$ is negative to the ternary point $Bi_{\alpha}-Bi_{\beta}$ −melt.

Study of the Polymorphic Transitions of Phosphorus and Bismuth at Very High Pressures

Studies of the polymorphic transition of phosphorus [1, 25, 26] have all been made at moderate temperatures and in the solid phase. It was not possible to follow the kinetics of the transition, since the polymorphic transitions were determined by the "piston displacement" method. We have investigated the polymorphic transitions over a wider range of temperature and pressure [13, 17].

A series of experiments made on commercial yellow phosphorus at pressures of up to 23,000 kg/cm^2 and temperatures of up to 250°C, however, failed to result in the formation of black crystalline phosphorus, although in the case of Bridgman and Jacobs, polymorphic transition occurred at lower pressures. The supposition was made that the transition point had been considerably displaced towards higher temperatures and pressures, due to the presence of impurities soluble in the phosphorus. (It may be remarked that examples of the influence of small quantities of impurities on polymorphic transitions are given in [27].) After purification of the yellow phosphorus, the latter did indeed show the formation of black crystalline phosphorus over a wide pressure range.

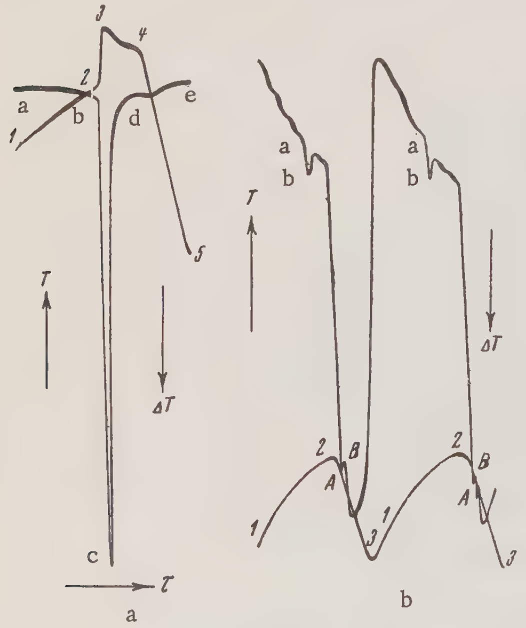

Fig. 6. a) Thermogram of the polymorphic transition of yellow phosphorus to black crystalline phosphorus; b) thermogram of the polymorphic reversible transition of red phosphorus.

Figure 6a shows a portion of a thermogram with simultaneous recording of both thermocouples. Curve T, denoted by numbers, corresponds to the indications of the combined thermocouple, which determines the transition temperature (points 2–3). Curve ΔT, denoted by letters, corresponds to the indications of the differential thermocouple, which determines the rise in temperature due to the transition alone (points b–c). In this case, the temperature discontinuity due to the polymorphic transition is shown much more distinctly, so that it is possible to observe weak polymorphic transitions, which cannot be detected by other methods. This method was employed to investigate the behavior of black crystalline phosphorus at very high pressures and high temperatures ($P = 20{,}000$ kg/cm^2, $T = 1200$°C), but no new modifications of phosphorus were discovered. With increase in pressure there is merely a gradual increase in the melting point of the black crystalline phosphorus. At 18,000 kg/cm^2, the melting point of phosphorus is ≈ 1000°C.

In studying the behavior of red phosphorus, at 40,000 kg/cm^2 and 600°C we found that a new modification of phosphorus was formed, the process being reversible with a slight thermal effect. Figure 6b shows a portion of the thermogram, with the temperature discontinuity recorded by the differential thermocouple (points a-b), indicating the occurrence of a polymorphic transition, with simultaneous recording of the reverse process (points A-B). The curve given by the combined thermocouple, determining the transition temperature, showed practically no temperature discontinuity (points 1-2-3).

It is of some interest to make a detailed study by the thermometric method of the phase diagram of bismuth over a wide temperature and pressure range, and to ascertain the magnitude of the thermal effects and changes in specific volume in polymorphic transitions. As is known, when bismuth is subjected to hydrostatic pressure, it undergoes a number of polymorphic transitions, first discovered by Bridgman, who used the piston displacement method [19]. Thus, at a temperature of 20°C up to a pressure of 25,900 kg/cm^2, a first modification of bismuth, having a rhombohedral lattice, is stable; a second modification is stable in the pressure range 25,900-27,760 kg/cm^2; at pressures above 27,760 kg/cm^2 there is a third modification. The crystal lattice of the last two modifications is unknown. Following the system of notation adopted in the physics of metals, we shall call these three modifications the α-, β- and γ-modifications, respectively. Bridgman determined the dependence of the melting point of α-Bi on pressure, the equilibrium curves of the α-β and β-γ modifications in the temperature range from -50 to $+170$°C, the specific volume changes due to the $\alpha \rightleftharpoons \beta$ and $\beta \rightleftharpoons \gamma$ transitions, and calculated the thermal effects of the transitions and the coordinates of the three points $\alpha-\beta-$liq, $\beta-\gamma-$liq, $\alpha-\beta-\gamma$.

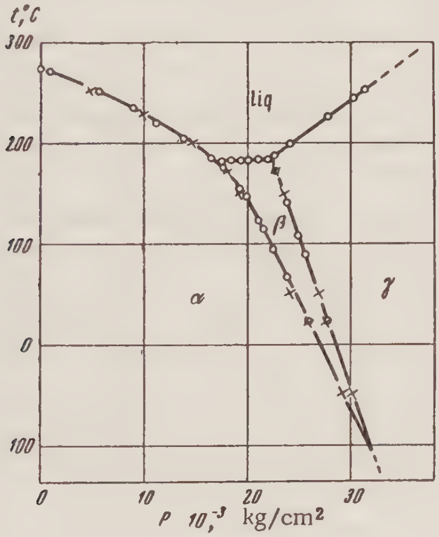

Fig. 7. Phase diagram of bismuth (o — our data, X — Bridgman's data).

The pressures at which the bismuth transitions occur at room temperature are at the present time employed as fundamental reference points for the calibration of manganin resistance pressure gauges. It is natural that Bridgman repeatedly determined the parameters of the polymorphic transitions of bismuth [28-31].

We carried out an investigation on bismuth of 99.995% purity. The principal impurities were: Pb $\simeq$ 0.003%, Fe $\simeq$ 0.001%, Hg $\simeq$ 0.0003%. The bismuth specimen was heated and cooled at the rate of ~ 1 deg/sec. The polymorphic transitions of bismuth investigated [32] were clearly recorded not only by the differential thermocouple, but also by the combined thermocouple, due to the high magnitude of the thermal effects and the high speed of these transitions. Both transitions occur with appreciable temperature hesteresis. Table 1 gives some data regarding the temperature of the $\alpha-\beta$ and $\beta-\gamma$ transitions at different pressures. As will be seen from the table, the hysteresis of the $\alpha \rightleftharpoons \beta$ transitions increases with increase in the transition temperature from 3° at $T_m = 163$°C to 15° at $T_m = 65.5$°C, where T_m is the mean value of the temperatures of the $\alpha-\beta$ and $\beta-\alpha$ transitions at the given pressure.

From the data of the thermographic analysis, we constructed the phase diagram of bismuth in P-T coordinates, shown in Fig. 7. The points plotted on the diagram correspond to the T_m temperatures. Each point represents the mean of not less than six separate measurements. As will be seen from Fig. 7, the α-Bi melting curve and the equilibrium curves of the $\alpha-\beta$ and $\beta-\gamma$ modifications are in good agreement with earlier data.

TABLE 1

P, kg/cm²	T, °C (heating)	T, °C (cooling)	T_m °C	ΔT
19 300	165	162	163.5	3
21 500	128	122	125.0	6
23 800	73	58	65.5	15

Within the limits of the experimental errors, the melting point of β-Bi is independent of pressure; consequently β-Bi melts without change in volume. The melting point of γ-Bi increases with increase in pressure from 184°C at 22,400 kg/cm² to 239°C at 30,000 kg/cm². The mean slope of the melting point curve with respect to the pressure axis is 0.0072 deg/kg · cm^{-2}.

The thermal effects of the α ⇌ β and β ⇌ γ transitions were determined by the following method. The bismuth specimen weighing 6 g was placed in a container, which in its turn was situated in the pressure chamber. The pressure was increased from 25,000-28,000 kg/cm² in a time of from 0.5-10 min. The mean rate of increase or decrease in pressure was varied in the limits from 5 to 100 kg/cm²/sec. The temperature of the apparatus remained equal to 20°C during the experiment. The ratio of the areas on the thermograms, corresponding to the thermal effects of the α ⇌ β and β ⇌ γ transitions, were used for determining the ratio of the thermal effects of these transitions. The magnitudes of the thermal effects and specific volume changes were determined from the system of four equations with four unknowns

$$\frac{1}{T}\left(\frac{dT}{dP}\right)_1 = -\frac{\Delta v_1}{Q_1},$$

$$\frac{1}{T}\left(\frac{dT}{dP}\right)_2 = -\frac{\Delta v_2}{Q_2},$$

$$\Delta v_1 + \Delta v_2 = -0.0085 \text{ cm}^3/\text{g} \ [36, 37]$$

$$Q_1 : Q_2 = n.$$

Here Δv_1 is the specific volume change for the α ⇌ β transition, Δv_2 is the specific volume change for the β ⇌ γ transition, $\left(\frac{dT}{dP}\right)_1$ and $\left(\frac{dT}{dP}\right)_2$ are the tangents of the angles of slope of the equilibrium curves of the α − β and β − γ modifications to the pressure axis at 20°C. $Q_1 : Q_2 = n$ is the ratio of the transformation heats as determined from the thermograms.

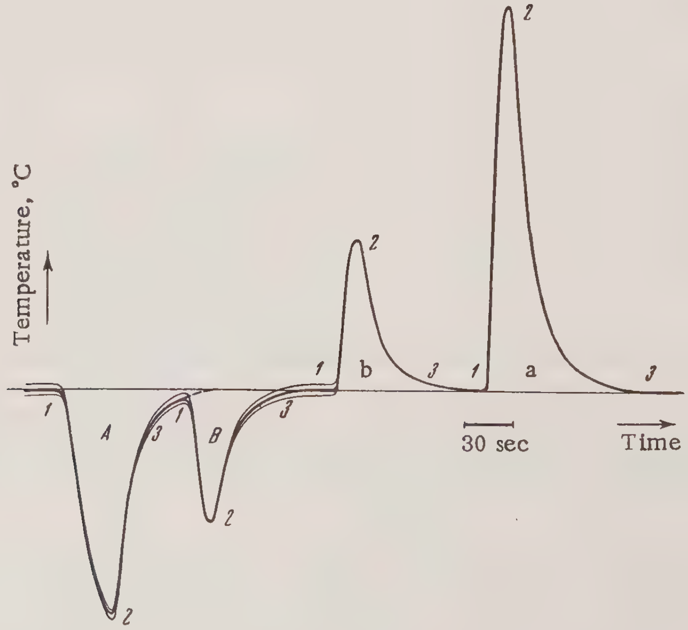

Fig. 8. Thermograms of the thermal effects of the α ⇌ β and β ⇌ γ transitions of bismuth.

Altogether, six experiments were made on the determination of the thermal effects. In four of them, the specimen was in a plexiglas container and in the other two, it was in a copper container. Figure 8 shows a typical thermogram from one of the experiments. The letters A and B denote curves corresponding to the $\alpha-\beta$ and $\beta-\gamma$ transitions with increasing pressure, while the letters a and b relate to curves of the $\gamma-\beta$ and $\beta-\alpha$ transitions with decreasing pressure. The portions 1-2 of the curves correspond to the absorption (evolution) of heat in the transition process, and the portions 2-3 correspond to the equalization of temperature after termination of the transitions. We shall examine more closely the character of the α-Bi and β-Bi transition with increase in pressure. Due to the fact that the density of the β-modification is greater than the density of the α-modification, the transition is accompanied by a decrease in volume. If the applied pressure does not greatly exceed the transition pressure, the decrease in volume of the bismuth during transition causes the pressure to drop to the equilibrium pressure and the transition ceases. In these conditions, the α- and β-modifications will exist simultaneously. For continuing the transition, it is again necessary to raise the pressure, and so forth until all the α-Bi has been transformed into β-modification. For low rates of pressure increase, the 1-2 portion, corresponding to the $\alpha-\beta$ transition, has a small slope to the zero line and all the transition takes place at one pressure. For high rates of pressure rise, the 1-2 portion is practically perpendicular to the zero line of the thermogram. This indicates that the transition occurs in a very short interval of time of less than 1 sec. The transition time is estimated from the recording speeds used and the inertia of the system. The slope of the 2-3 portion of the curves depends little upon the rate of change of pressure. All this is also true for the $\beta-\gamma$, $\gamma-\beta$ and $\beta-\alpha$ transitions.

TABLE 2

	Q_1, cal/g	Q_2, cal/g	Δv_1, cc/g	Δv_2, cc/g	$\alpha-\beta-$liq.		$\beta-\gamma-$liq.		$\alpha-\beta-\gamma$	
					P, kg/cm^2	T, °C	P, kg/cm^2	T, °C	P. kg/cm^2	T, °C
Our data	—1.78	—1.71	—0.0055	—0.0030	17 300	184	22 400	184	32 200	—108
Bridgman's data	—1.62	—0.68	—0.0047	—0.0035	17 300	183	22 400	185	32 300	—110

The mean ratio $Q_1 : Q_2$ was found to be 2.51. Despite the considerable variations in the experimental conditions (use of containers of different materials, variation in the rate of pressure change), the values of the ratios $Q_1 : Q_2$ as determined from different experiments did not differ from the mean by more than 2%. Table 2 shows the basic parameters of the polymorphic transitions of bismuth as obtained by us and, for comparison, the data published by Bridgman.

It should be pointed out that both the transitions investigated proceed at 20°C with considerable pressure hysteresis. The hysteresis of the $\alpha \rightleftharpoons \beta$ transition is ≈ 1000 kg/cm^2, and the hysteresis of the $\beta \rightleftharpoons \gamma$ transition is ≈ 900 kg/cm^2. The magnitude of the hysteresis is independent of the rate of change of pressure. The mean of the pressure of the forward and reverse transitions was taken as the equilibrium point of the corresponding phases. The literature contains no information on the hysteresis of bismuth transitions. The question as to whether the hysteresis we have observed is due to impurities or is inherent in the transition of pure bismuth is still undecided and requires further investigation.

The values found for the thermal effects of the $\alpha \rightleftharpoons \beta$ and $\beta \rightleftharpoons \gamma$ transitions of bismuth may be used for the determination by the thermometric method of the thermal effects of phase transformations of various substances at very high pressures.

SUMMARY

1. An intensifier design with double mechanical support and internal electrical heating has been developed. In constructed intensifiers, pressures of up to 30,000-34,000 kg/cm^2 were obtained with simultaneous production of high temperatures: in a compressed liquid of up to 600°C, in compressed gas of up to 1500°C.

2. A method has been developed for measuring in high pressure vessels: temperatures, heats of phase transformations and first-order polymorphic transitions.

3. Experimental work has been done on the determination of the pressure dependence of the melting points of a number of metals at very high pressures, a phase diagram of bismuth has been constructed and polymorphic transitions in phosphorus have been studied.

LITERATURE CITED

[1] P. W. Bridgman, Recent Work in the Field of High Pressures [Russian translation] (Moscow, 1948).

[2] D. S. Tsiklis, Technique of Physicochemical Investigations at High Pressures [in Russian] (Moscow-Leningrad, 1951).

[3] B. A. Korndorf, High Pressure Technique in Chemistry [in Russian] (Moscow-Leningrad, 1952).

[4] M. G. Gonikberg, Chemical Equilibrium and Reaction Velocity at High Pressures [in Russian] (Moscow, 1953).

[5] F. P. Bundy, H. T. Hall, H. M. Strong, and R. H. Wentorf, "Man-made diamonds," Nature 176, 4471, 51-55 (1955).

[6] P. W. Bridgman, "Synthetic diamonds," Scient. Amer. 193, 5, 42-46 (1955).

[7] L. F. Vereshchagin, "Hydraulic compressor for very high pressures," J. Tech. Phys. (USSR) 16, 669-680 (1946).

[8] S. S. Boksha, "A new method of producing a very high gas pressure," Kristallografiia 2, 1, 199-200 (1957).

[9] Iu. N. Riabinin, "Production of very high pressures and high temperatures by adiabatic compression," J. Exptl.-Theoret. Phys. (USSR) 23, 461-467 (1952).

[10] V. P. Butuzov, G. P. Shakhovskoi, and M. G. Gonikberg, "Intensifiers for investigations at very high pressures and high temperatures," Trudy Inst. Krist. 11, 233-238 (1955).

[11] H. S. Yoder, "High-low quartz inversion up to 10,000 bars," Trans. Am. Geophys. Union 31, 6, 827-835 (1950).

[12] L. F. Vereshchagin, L. Kh. Fredlin, A. M. Rubinshtein, and I. U. Naumov, "Influence of very high pressures on the catalytic properties of alumina," Izv. AN SSSR, OTN 6, 809 (1951).

[13] V. P. Butuzov and S. S. Boksha, "A new method of investigating phase transformations at high pressures and temperatures and its application to the study of the polymorphism of phosphorus," Collection: Growth of Crystals [in Russian] (1957).

[14] V. P. Butuzov, M. G. Gonikberg, and S. P. Smirnov, "Study of the melting points of metals at very high pressures," Doklady Akad. Nauk SSSR 89, 4, 651-653 (1953).

[15] F. Birch, "Thermoelectric measurement of high temperatures in pressure apparatus," Rev. Sci. Instr. 10, 137-140 (1939).

[16] P. W. Bridgman, Proc. Am. Acad. Arts Sci. 72, 157 (1938).

[17] V. P. Butuzov, S. S. Boksha, and M. G. Gonikberg, "Polymorphic transitions of phosphorus at very high pressures," Doklady Akad. Nauk SSSR 108, 5, 837-840 (1956).

[18] P. W. Bridgman, The Physics of High Pressures (London, 1949).

[19] P. W. Bridgman, "Polymorphism principally of the elements up to 50,000 kg/cm^2," Phys. Rev. 48, 11, 893-906 (1935).

[20] T. Hall, "The melting point of Ge as a function of pressure to 180,000 kg/cm^2," J. Phys. Chem. 59, 11, 1144-1146 (1955).

[21] V. P. Butuzov and M. G. Gonikberg, "Melting points of tin and lead at pressures up to 34,000 kg/cm^2," Doklady Akad. Nauk SSSR 91, 5, 1083-1084 (1953).

[22] V. P. Butuzov, E. G. Poniatovskii, and G. P. Shakhovskoi, "Melting points of zinc, cadmium, thallium and antimony at pressures up to 30,000 kg/cm^2," Doklady Akad. Nauk SSSR 109, 3, 519-520 (1956).

[23] V. P. Butuzov and E. G. Poniatovskii, "Melting point of indium at pressures up to 30,000 kg/cm^2," Kristallografiia 1, 6, 736-737 (1956).

[24] M. G. Gonikberg, G. P. Shakhovskoi, and V. P. Butuzov, "Measurement of the melting points of aluminum and copper at pressures up to 18,000 kg/cm^2," Zhur. Fiz. Khim. (1957).

[25] R. Jacobs, "Phosphorus at high temperatures and pressures," J. Chem. Phys. 5, 945-953 (1937).

[26] V. Ipat'ev and V. Nikolaeva, "Allotropic modifications of phosphorus produced at high temperatures and pressures," Zhur. Russ. Fiz.-Khim, Obshchestva, ch. khim. 60, 6, 885-892 (1928).

[27] V. K. Semenchenko, N. L. Pokrovskii, and V. B. Lazarev, "Influence of small quantities of impurities on the polymorphic transition in tin," Doklady Akad. Nauk SSSR 89, 6, 1021-1024 (1953).

[28] P. W. Bridgman, "Compressions to 50,000 kg/cm^2," Phys. Rev. 57, 3, 237 (1940).

[29] P. W. Bridgman, "Compressions and polymorphic transitions," Phys. Rev. 60, 4, 351 (1941).

[30] P. W. Bridgman, "The effect of pressure on several properties of the alloys of Bi−Sn and Bi−Cd," Proc. Amer. Acad. Arts Sci. 82, 2, 101-156 (1953).

[31] P. W. Bridgman, "The use of electrical resistance in high pressure calibration," Rev. Scient. Instr. 24, 5, 400-401

[32] V. P. Butozov and E. G. Poniatovskii, "Study of polymorphic transitions at very high pressures," Kristallografiia 1, 5, 572-576 (1956).

Received February 28, 1957

Institute of Crystallography, Academy of Sciences, USSR

ETCH PITS ON SLIP LINES AND ON THE BOUNDARIES OF POLYGONAL BLOCKS IN SILVER CHLORIDE CRYSTALS

M. P. Shaskol'skaia and Iu. Kh. Vekilov

Prolonged high-temperature annealing causes polygonization in plastically deformed silver chloride crystals. When etched, such crystals show etch pits arranged in rectangular networks. In the case of crystals deformed after annealing, etch pits appear only along the wavy slip lines. Etching reveals a gradual displacement of grain boundaries.

A number of experimental studies in recent years has shown that the etch patterns on the surface of a crystal are formed at the exit sites of dislocations. At the same time, the cause of the greater vulnerability of a crystal surface is still unknown, whether it is the stress field at the core of the dislocation, or some secondary factors, indirectly connected with the dislocation, for instance a concentration of impurities, rupture of the surface film and so forth. Regardless of this, the regular patterns observed when metals [1], sodium chloride [2], lithium fluoride [3] and other substances are etched leave no doubt as to the unique connection between etch pits and dislocation exits on the crystal surface.

We have used etching to study the processes of plastic deformation and annealing of polycrystalline silver chloride, which has an ionic lattice of the rock salt type and a remarkable combination of transparency and mechanical properties, similar to the properties of metals [4].

It has previously been shown [5] that when silver chloride is subjected to uniform tension, the slip lines produced are of two types: straight and wavy. The difference in the type of slip lines evidently depends upon the geometry of shear and the direction of observation. Nye [6], who made a most detailed study of the plastic deformation of silver chloride,came to the conclusion that the slip occurring in this case was similar to that in a bundle of pencils: only the [110] slip direction appears to be definitely determined, and the plane of slip can be any plane containing this direction, not necessarily a crystallographic plane.

Preparation of the Specimens

Polycrystalline specimens of silver chloride, single-crystal in thickness, were studied. The preparation of the specimens is described in detail in Zhitnikov's papers [7] and our paper [5]. A single crystal of silver chloride, grown by the method of lowering a crucible containing the molten substance down a furnace having a given temperature gradient, was forced through a die having a rectangular cross section in a 30-ton press and then rolled into a ribbon. The high plasticity of silver chloride permits very considerable deformation without previous annealing. After rolling, the ribbon had a thickness of 0.3 mm, corresponding to a deformation of 98%. Specimens 30 × 6 × 0.3 mm were cut from the ribbon with the aid of a template. Annealing of the specimens at 150-200°C for 6-8 hrs was adequate for complete stress relief and recrystallization. The specimens obtained were fine-grained, free from internal stresses and often single-crystal in thickness. The absence of internal stresses was indicated by the fact that the specimen transmitted no light under crossed Nicols. After this preliminary annealing, the specimens was etched with a saturated solution of hyposulfite (for cleaning the surface) and was then pressed in a hand vise between two plates of plastic. This was sufficient to impart mirror smoothness to the surface of the specimen. A second annealing, this time at a temperature of 400 ± 10°C for 6 hrs or more (see below), resulted in a coarsely granular structure with a grain size of 1 cm^2 or more. In thickness, such specimens were always single-crystal. The internal stresses in them were completely relieved.

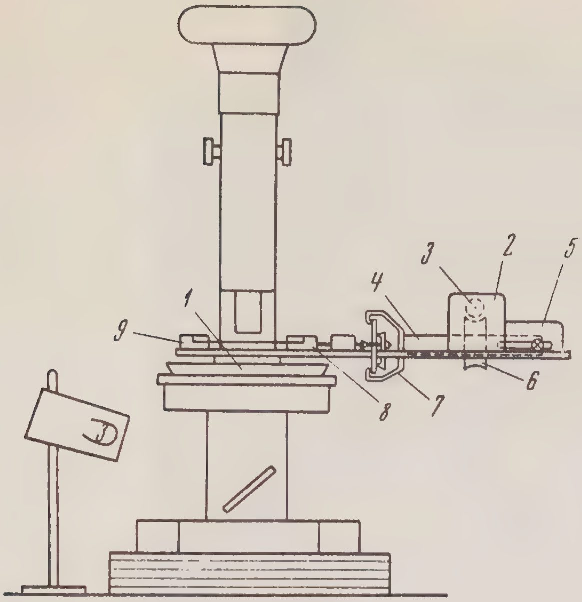

Fig. 1. Diagram of tension apparatus with constant rate of strain and simultaneous microscopic observation.

The specimens were subjected to tensile stress in a specially designed apparatus giving constant rate of strain with simultaneous microscopic observation of any part of the specimen. Figure 1 shows the apparatus diagrammatically. The tension device is mounted directly on a preparation support 1 fixed on the stage of a polarizing microscope. The drive from a SD-2 electric motor 2 is transmitted through a worm reducing gear 3 to the screw 4 which is moved progressively by means of a speed regulator 5. The wormwheel 6 is also a nut producing the tensile stress. By means of the stress indicator 7, the screw moves the movable grip 8 in which the specimen is clamped. The second grip 9 is stationary.

The rate of strain in our experiments was 0.07 mm/min. The specimen was observed by transmitted light, using a polarizing microscope MIN-5, or by reflected light, using a metallurgical microscope.

Polygonization in Silver Chloride

As described in the foregoing, the polycrystalline specimens were subjected to preliminary annealing, repeated deformation for producing a mirror surface and then to lengthy high-temperature annealing at a temperature of 400 ± 10°C for 24 hrs or more (up to 7 days). In these specimens, slight etching immediately after annealing reveals the patterns shown in Figs. 2 and 3, i. e., etch pits arranged in straight parallel rows or in parallel, almost rectangular networks.

These structures are revealed only in some of the grains, evidently depending on the crystallographic orientation of the grains, which has not yet been defined exactly. In the grains in which the rows or networks of etch pits are visible, a perfectly analogous pattern is revealed on the reverse side of the specimen. It may be assumed that these networks are not only characteristic of the surface structure, but of that passing through the entire crystal.

An essential condition for the appearance of the etch pit networks was the annealing period. After 6-8 hrs annealing at the same temperature, the networks were not revealed.

If a specimen showing rows of etch pits after annealing and etching is then subjected to slow tensile strain, only rectilinear slip lines appear in this specimen. At the same time, the slip lines pass through the rows of etch pits always perpendicularly or almost perpendicularly to the rows (Fig. 4). If tension is continued until a second system of slip traces appears, these traces are also rectilinear and pass perpendicularly or almost perpendicularly to the first system of slip traces, i. e., they are perpendicular to the second side of the etch pit networks (Fig. 5). The geometry of the rectilinear slip lines is thus directly connected with the geometry of the etch pit networks.

Nye [6],on the basis of x-ray data, convincingly showed that strain in silver chloride is accompanied by curvature of the slip planes. It is evident that strain produces excess edge dislocations, the accumulation of which results in curvature of the slip planes. During annealing, the dislocations of opposite sign cancel each other, while the residual edge dislocations of one sign are displaced, forming transition surfaces. The crystal is broken up into blocks separated by walls of edge dislocations.

On the basis of the pencil glide mechanism, inherent in silver chloride, it may be assumed that straight slip lines are observed only in the case where the shear vector lies in the plane of observation. Consequently, the etch pits arranged in rows of networks correspond to the exits of the edge dislocations. These etch pit networks are similar to those which usually reveal the existence of polygonization blocks in metals. In silver bromide crystals, which is very similar to silver chloride in the mechanism of its plastic deformation, the existence of dislocation networks was confirmed by Hedges and Mitchell by the separation of photolytic silver [8].

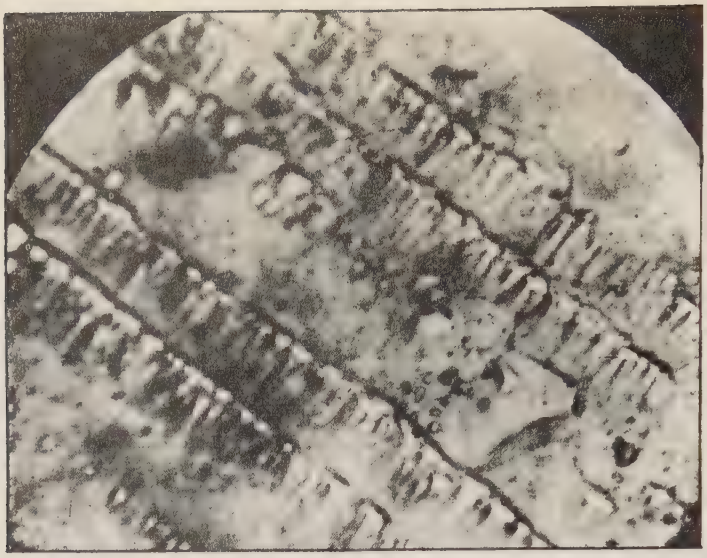

Fig. 2. Rows of etch pits on an AgCl crystal. Crystal annealed for 48 hrs at 400°C; x 300; reflected light.

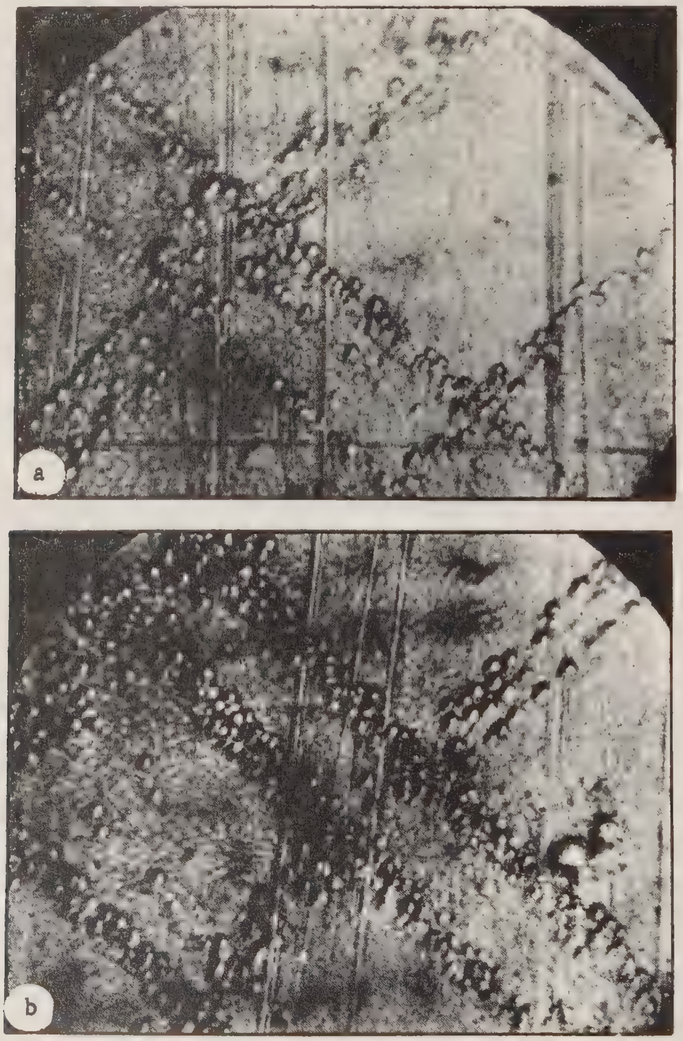

Fig. 3. Networks of etch pits on an AgCl crystal. Crystal annealed for 48 hrs at 400°C; x 300; reflected light.

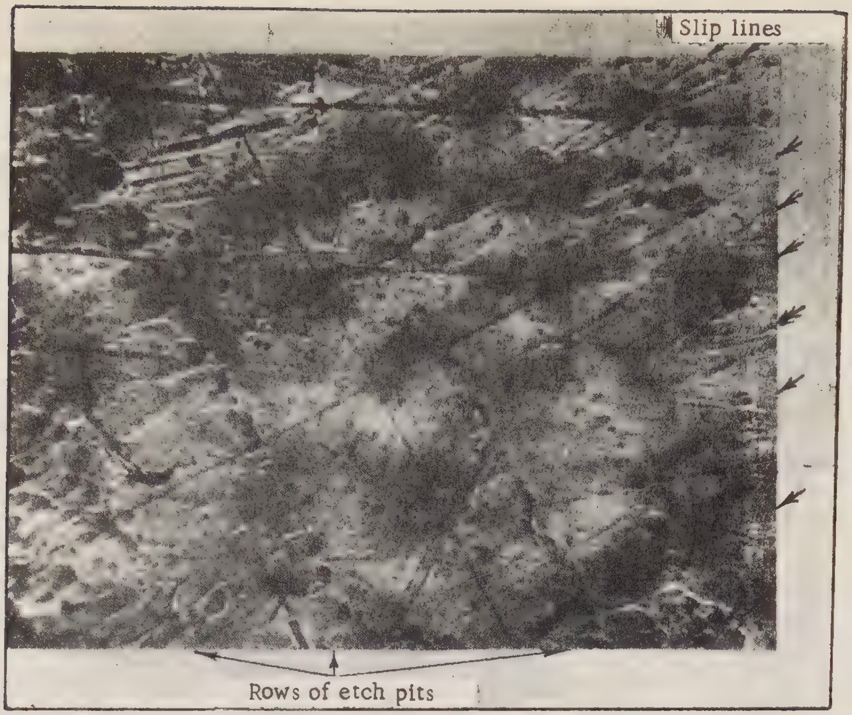

Fig. 4. Slip lines on an AgCl crystal, perpendicular to the rows of etch pits; × 240; transmitted light.

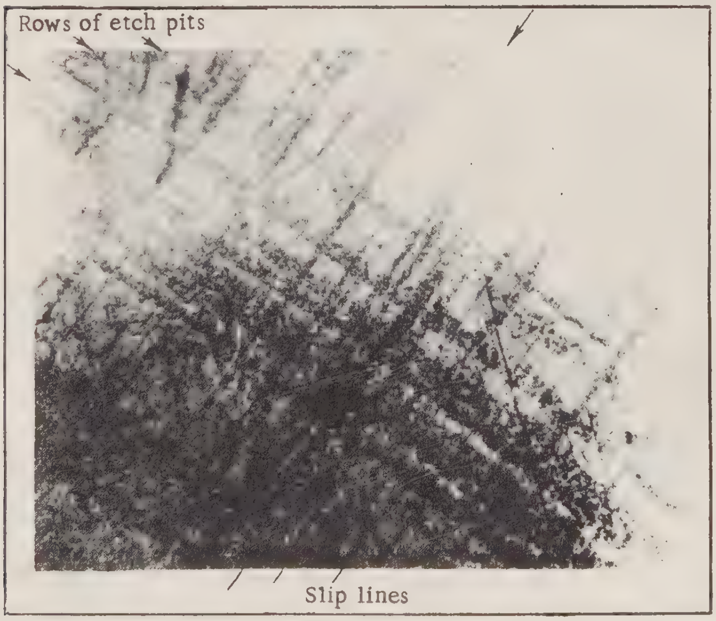

Fig. 5. Two systems of slip lines on an AgCl crystal, perpendicular to the rows of etch pits. × 300; reflected light.

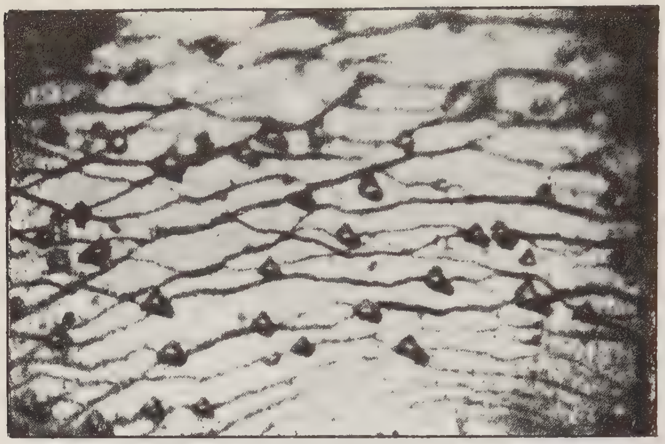

Fig. 6. Etch pits on wavy slip lines. × 300; reflected light.

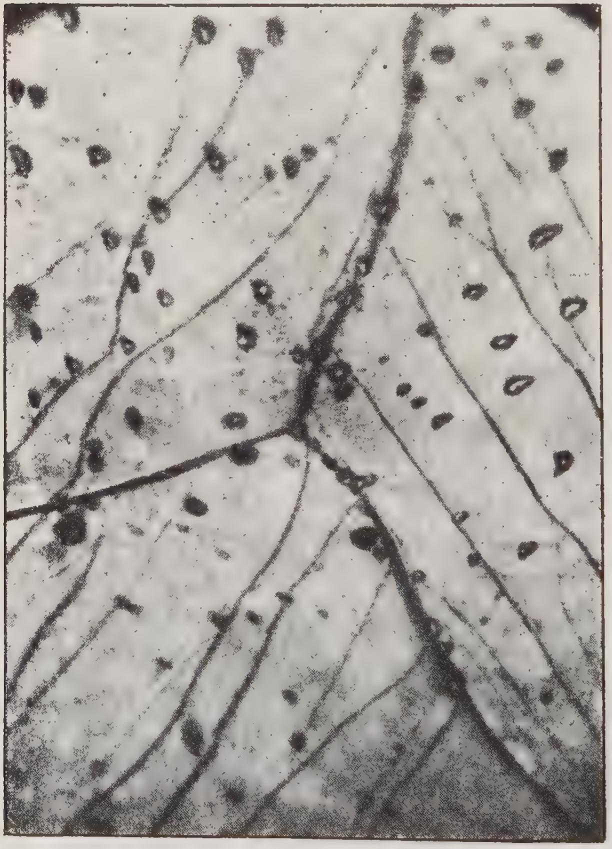

Fig. 7. Junction of three grains and etch pits on wavy slip lines. × 300; reflected light.

According to Hedges and Mitchell, the size of the cells of the polygonal network in silver bromide is ~ 10 μ. As will be seen in Fig. 3, the size of the polygonal blocks in silver chloride (i. e., the distance between the rows of the rectangular network of etch pits) is 10-100 μ.

Van der Vorst and Dekeyser [9] in a short note have described the etch figures on the {111} faces of microscopically small single crystals of AgCl, and also expressed the view that these figures corresponded to the networks of Hedges and Mitchell. They did not, however, observe true etch pit networks and the photographs of the etch figures of AgCl reproduced by them are not clear enough, while the article contains no photographs of AgBr.

Etch Figures on Slip Lines

The coarse-grain specimens, annealed for 6-8 hrs at 400°C, were then subjected to uniform tension at a constant rate of strain, followed by etching.

Before the appearance of slip lines, the surface of the specimen etches more or less uniformly. The appearance of slip lines is accompanied by the appearance of etch pits. The etch pits are formed only directly on the wavy slip lines (Fig. 6). Exit of the slip lines on the grain boundary is likewise terminated by an etch pit (Fig. 7). Figure 7 shows the junction of three grains; it will be seen that the orientation and form of the etch pits is different in different grains and that all the pits are situated only on the wavy slip lines. We have not yet carried out an x-ray determination of the relative orientation of the grains. In this case, the direction of the shear vector is also not known. The wavy slip lines can be observed if the shear vector is perpendicular or almost perpendicular to the surface of observation. Consequently, in this case, the etch pits can correspond only to the exits of screw dislocations.

Observations on the Displacement of Grain Boundaries During Annealing

The specimen annealed at 250°C for 4 hrs was etched and then subjected to a second annealing at 400°C and again etched. The trace of the etched boundary was left and the second etching revealed a new grain boundary. The specimen (Fig. 8) thus showed at the same time the trace of the old boundary (a) and the new boundary (b). The photograph of the reverse side of the specimen was absolutely identical.

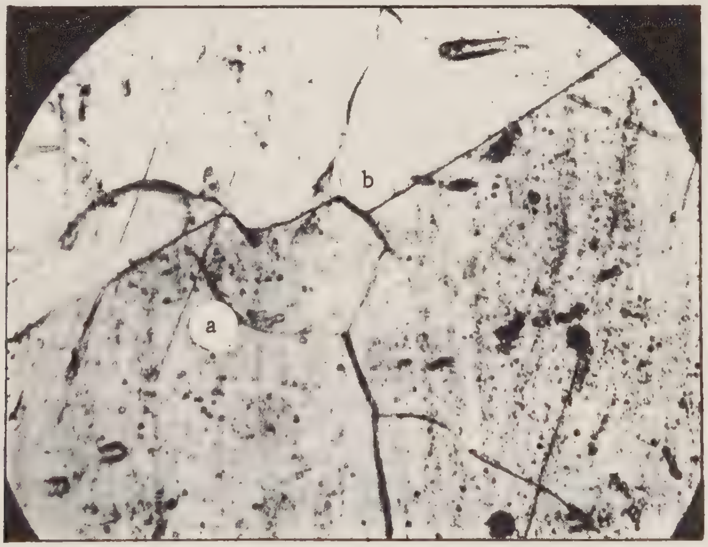

Fig. 8. Displacement of grain boundary during annealing of an AgCl crystal. a) Row of etch pits, remaining on the site of the old boundary; b) new boundary. × 140; reflected light.

Similar observations on the displacement of grain boundaries in aluminum are described by Wyon and Lacombe [10].

We expect that the application of the etch pit method will enable the mobility of grain boundaries to be studied as a function of the angle of disorientation and curvature. The method is also a convenient one for studying the kinetics of recrystallization.

LITERATURE CITED

[1] F. L. Vogel, W. J. Pfann, and E. E. Thomas, "Observations of dislocations in lineage boundaries in germanium," Phys. Rev. 90, 3, 489 (1953);

[2] S. Amelinckx, "Etch pits and dislocations along grain boundaries, slip lines and polygonization walls," Acta Met. 2, 6, 848 (1954).

[3] J. J. Jilman and W. G. Johnston, "Observations of dislocation glide and climb in LiF crystals," J. Appl. Phys. 27, 9, 1018 (1956).

[4] A. W. Stepanow, "Plastic properties of single crystals of silver and thalium halides," Sow. Phys. 6, 312 (1934).

[5] V. E. Kochnov and M. P. Shaskol'skaia, "Study of slip lines in silver chloride crystals," Kristallografiia 2, 1, 274-277 (1957).

[6] J. F. Nye, "Plastic deformation of silver chloride. I. Internal stresses and the glide mechanism," Proc. Roy. Soc. 198, 1053, 190 (1949).

[7] P. A. Zhitnikov and A. V. Stepanov, "Optical method of studying the mean stress conditions in fine-grain polycrystalline specimens. I. Silver chloride," J. Tech. Phys. (USSR) 26, 4, 772 (1956).*

[8] J. M. Hedges and J. W. Mitchell, "The observation of polyhedral substructures in crystals of silver bromide," Phil. Mag. 44, 349, 223 (1953).

[9] W. van der Vorst and W. Dekeyser, "Sur la corrosion des faces (111) de cristaux de chlorure d'argent," Naturwiss 40, 11, 316 (1953).

[10] G. Wyon and P. Lacombe, "The influence of dislocations and impurities on the distribution and size of etch figures on pure aluminum," Report of the Conference on Defects in Crystalline Solids, Bristol, p. 487 (1955).

Received March 5, 1957

I. V. Stalin Moscow Steel Institute

---

* [Soviet Physics — Technical Physics, p. 754.]

A SURVEY OF ELECTRON DIFFRACTION STRUCTURAL ANALYSIS

Z. G. Pinsker and B. K. Vainshtein

This paper presents a historical outline, some problems of the theory of electron scattering, the process of structure determination, the Fourier synthesis of potential, and experimental investigations of organic and inorganic compounds, metals and alloys.

I. Introduction

The year 1957 marked thirty years since the appearance of Davisson and Germer's work [1] dealing with the selective angular electron reflection from a nickel single crystal. Widespread development of electron diffraction research has taken place in these 30 years.

Those studies in which fast electrons (30-60 kv) were used proved to be the most fruitful. Thomson's [2] experiments in England in 1928, and Tartakovskii's [3] in the USSR provided their foundation.

Let us analyze and compare some peculiarities and basic results of this development.

It can be said that the most important experimental data were obtained and that the theoretical principles of the scattering of electrons by atoms, molecules and crystals were worked out in the first ten years. This includes the apparatus, the conditions for obtaining and interpreting the various types of electron patterns, kinematic dispersion, refraction by the average inner lattice potential, the principles of dynamic scattering theory, molecular scattering and, finally, some special applications: the study of oriented crystallization, polished surfaces, etc. The work [4] on the determination of the locations of hydrogen atoms in ammonium chloride should be particularly noted.

Toward the end of this first decade, the goal in the USSR was to develop electron diffraction structure analysis as a method for complete and independent crystal structure determination. At this time some prominent researchers thought of it as of a method applicable only to the study of surface phenomena and structures — a point of view refuted by the subsequent development of electron diffraction.

It must be pointed out that x-ray diffraction analysis began to develop almost immediately following Laue's discovery. This was the basic condition of its development, and it might account for a comparative delay in evaluating the electron diffraction possibilities for studying atomic structures.

The first group of studies [5-8] (1941-1942) in which there was a conscious goal of determining atomic structure, was devoted to lamellar lattices of cadmium halides. The characteristics of the phenomenon, later called polytypism, first appears in these studies, and it is shown that the structural diversity of the compounds studied is based on the insignificant value of the interaction energy between the lamellar lattice blocks in comparison with that of the binding inside the block. These researches laid the bases for the principles of atomic structure determination by electron diffraction, and the possibility of preparing accurate electron patterns and photographs of skew textures was demonstrated.

After the war much was done toward the development of the structural trend at the electron diffraction laboratory of the Institute of Crystallography [9]. The studies there soon led to important results of general interest. It was shown that the kinematic theory can be applied to typical electron diffraction objects, and that the Fourier synthesis of the crystal lattice potential [10] could be used successfully on experimental structure amplitudes obtained from electron patterns [11].

About 1950, there appeared a series of electron diffraction structure researches by Australian workers.

In the last ten years much work related to electron scattering in crystals, to the geometric theory [12] and to the theory of the reflection intensities of electron patterns of any type [13, 14] and especially to the solution of various structural problems was done at the electron diffraction laboratory of the Institute of Crystallography and at laboratories connected with it. The survey of this work is given in part IV.

At present structural electron diffraction has at its disposal apparatus in no way inferior to that of modern x-ray diffraction analysis [15].

Progress in determining the structure of molecules in the vapor phase also deserves some attention. This trend is developing especially in the US and in Norway; recently, substantial results have been obtained in the USSR. The application of the segment method and the recording of the diffraction pattern over a large angular range increased greatly the possibilities of the method.

A number of researchers, especially in Japan and Germany, are working toward further experimental and theoretical electron diffraction studies on ideal crystals.

The development of the independent problems of the dynamic theory is of great interest. This comprises the examination of the problem with respect to its approximation by two strong beams [16, 17], and of the theory of the fine structure of the reflections on electron patterns of MgO or CdO [18, 19]. A result of this theory is the possibility of calculating the potentials V_{000} and V_{hkl} from the fine structure parameters, similar to what had been suggested earlier in the method of the convergent beam. Studies [20, 21] which show the inapplicability of Friedel's law in the case of dynamic reflection must also be noted.

No incontrovertible rules or generalizations have as yet been established concerning oriented crystallization in spite of many studies devoted to it. Apparently, certain conditions of relationship in the atomic distribution in the contact faces are not fulfilled in the lamellae and in the films examined by electron diffraction.

Important results [22-24] were obtained from studies devoted to oxidation processes; however, much remains to be done before any certain rules can be established concerning these complex phenomena.

II. Some Problems of Electron Scattering Theory

The problem of the limits of the applicability of the kinematic and dynamic scattering theories has great significance in the development of electron diffraction structure analysis.

It was pointed out in Z. G. Pinsker's book [9] that the kinematic theory is applicable to crystallites of linear size $\sim 10^{-6}$ cm, i. e., in the case of scattering by the films used in structure studies. This assertion was criticized by many scientists in the reviews of the book, although the applicability of the kinematic theory was proved experimentally in several works of the Institute of Crystallography and in those done in Australia.

The limit of the applicability of the kinematic theory was found in the following manner (B. K. Vainshtein, [13]).

Proceeding from the dynamic problem with the approximation by two strong beams, in the region of selective reflection, the ratio between the intensities scattered by an ideal crystallite A_3 thick and the impinging intensity is given by

$$\frac{I_{hkl}}{J_0 S} = \sin^2\left\{A_3\lambda\left|\frac{\Phi}{\Omega}\right|\right\}. \qquad (1)$$

Here Φ_{hkl} is the structure amplitude

$$\Phi_{hkl} = \sum f_{el}\, e^{-2\pi i(\bar{r}\bar{H})} \qquad (2)$$

Ω is the volume of the unit cell, λ is the wavelength, S is the exposed area of the crystal.

At small thicknesses:

$$\frac{I_{hkl}}{J_0S}\approx\left\{A_3\lambda\left|\frac{\Phi}{\Omega}\right|\right\}^2. \tag{3}$$

The terms (1) and (3) (in other symbols) were used in Blackman's work [25]. The term (1) can also be derived independently by the kinematic analysis of the scattering of fast electrons from an isolated crystallite [13].

Kinematic analysis, the condition for which is the weakness of the secondary beams ($I_{hkl} < J_0S$), becomes inapplicable if

$$\lambda\left|\frac{\Phi}{\Omega}\right|A'_3\approx 1. \tag{4}$$

The dependence of this term on Φ means that the atomic numbers of the scattering atoms (i. e., magnitude of f_{el} in (2)) must be taken into account, and also the degree of complexity of the structure (i. e., factor $e^{-2\pi i(rH)}$ in (2)). Obviously, the magnitude A'_3 will decrease as Z increases. For simple structures with high symmetry

$$\Phi\approx\sum_i f_i, \tag{5}$$

while for structures with a large number of atoms in the unit cell (low symmetry) $\Phi<\sum\limits_i f_i$. Using the formula for the mean value of the structure amplitude in a structure containing n atoms

$$\overline{\Phi}=\overline{f}_{el}\sqrt{n}, \tag{6}$$

an estimate can be made of the limiting thickness (in A) of a crystallite which scatters kinematically:

$$A'_3\approx 200\frac{\sqrt{n}}{f_{el}}, \tag{7}$$

where f_{el} is expressed in absolute units (in A) [27].

The expression (7) for structures with 20-25 light atoms in the unit cell (for example, organic) reduces to $A'_3\approx 1200$ A when $\lambda = 0.05$, and for structures with average or heavy atoms, respectively, to $A'_3\approx 500$-600 A and 250-400 A. For the majority of cubic metals $A'_3 < 100$ A; for Al, $A'_3\approx 200$ A.

Thus the great variety of factors which influence the value of the critical thickness A'_3 can be taken into account. It is interesting to point out that the simplest structures are usually chosen for the experimental study of the laws of electron scattering in crystals, but it is exactly in that type of structure that dynamic effects most often arise. On the other hand, more complex structures are used as objects for electron diffraction structure analysis, and for them the kinematic approximation is more often justified.

An experimental check of the applicability of the kinematic or dynamic theories makes it possible to elucidate the accuracy of the estimates given, if a parallel measurement is also made of the size of the scattering crystallites. At present the following experimental methods can be cited: a) obtaining experimental scattering curves, b) measuring the parameters of the striped structures on electron patterns in a convergent beam; c) measuring the parameters of the fine structure caused by dynamic double refraction.

a) We shall first refer to the results of Iamzin and Pinsker's [26] and Lennander's [28] works, which deal with electron scattering by metal lattices. Basically, these data agree with the results of the estimates given above. A number of authors had already observed a deviation from kinematic scattering in gold at small values of $\sin\vartheta/\lambda$.

The average values of the structure amplitudes or their squares [15, 29] can be used for establishing the character of scattering in complex structures:

$$|\overline{\Phi}|^2=\sum_i f_i^2\sim f_{av}^2 \text{ and } \overline{\Phi}\sim f_{av} \tag{8}$$

The curves of $|\overline{\Phi}|^2$ and $\overline{\Phi}$ can be compared with the magnitudes of I_{exp}/pL (p is the frequency factor). These magnitudes must correspond to the experimental structure amplitudes for dynamic scattering, and to the structure factors for kinematic scattering.

Cases of intermediate scattering (between the laws f and f^2) are possible (see for example, Pinsker and Kaverin [30]). The treatment of general scattering is given in Vainshtein's article appearing in the previous issue of this journal [31].

b) It is known that the equations of the dynamic theory give a periodic solution for the function of the angular argument, when the value of the crystallite thickness A_3 is fixed. This phenomenon was observed experimentally during exposure in a convergent beam and was first calculated by MacGillavry [32], who noticed the possibility of calculating, from the striped structure corresponding to the periodic solution, the values of the inner average potential and structure amplitudes Φ_{hkl}. An important result of this calculation is the possibility of determining the thickness of the scattering lamina from the parameters of the striped structure. In treating such electron patterns one should have in mind that the kinematic approximation also gives a stiped structure composed of the main and the secondary maxima, in agreement with Laue's function

$$\frac{\sin^2 \pi A_i h_i}{(\pi h_i a_i)^2}. \tag{9}$$

It is possible to check the applicability of the dynamic theory by comparing the values of Φ_{hkl} calculated from the experiment with the theoretical ones. A similar banded structure was observed for mica at $\sim 8 \cdot 10^{-6}$ cm thickness and greater, and also for PbI_2.

Ueda, with his co-workers [33], obtained fine structure, apparently of dynamic nature, by x-raying with a beam of very small cross section molybdenum foils 210 A thick.

These authors assume that with the improvement in experimental technique, and especially with the decrease of the cross section of the initial beam at the specimen, there will be a decrease in the limiting thickness of crystallites which give the dynamic effect.

They also observed the banded structure of the Kikuchi lines on the electron patterns obtained from molyddenum in a convergent beam. Such a structure can be calculated with the aid of the expression derived in Kainuma's [34] work devoted to the Kikuchi line theory:

$$J = M\left(1 - \frac{\sin 2\pi M \sqrt{e'^2 - (2dq)^2}}{2\pi M (\sqrt{e'^2 - (2pq)^2}}\right). \tag{10}$$

The calculated thickness of the molybdenum foil came to 520 A.

c) During recent years a number of authors [16-19] studied thoroughly theoretically and experimentally the phenomena connected with the formation of fine structure in the reflections on electron patterns made from MgO.

In Moliere's works and in those of his co-workers and also in those of the Japanese authors convenient expressions were derived which made it possible to calculate structure amplitudes and the mean inner lattice potential [19] from the fine structure parameters.

In many cases important structural problems are solved on the basis of qualitative or semiquantitative evaluation of the experimental intensities; with this method the checking of the applicability of the kinematic theory is not essential. However, studies which include precise determination of the atomic coordinates, especially of light elements, require the checking of the law of scattering.

In connection with this, the question arises of the possibility of using various electron patterns with dynamic effects.

It was indicated in Pinsker and Vainshtein's work [35] that it is possible to use secondary reflections to determine absolute intensities (Fig. 1). In Vainshtein's works [14, 31], questions concerning the calculation of the intensities of the dynamic scattering for real compounds are examined. The possibility of using other types of dynamic scattering and especially of Kikuchi lines and streaks is also of interest. Substantial success was

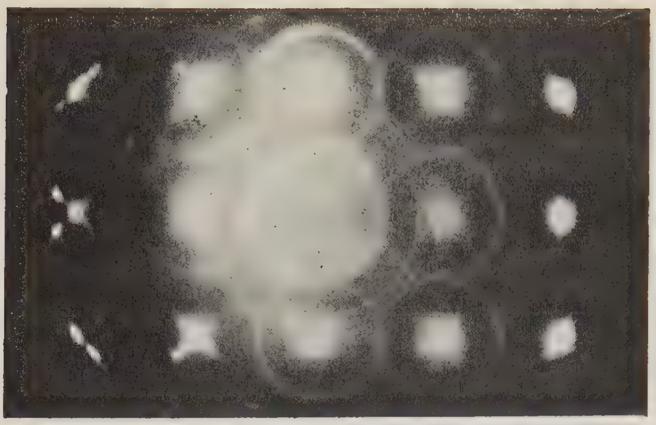

Fig. 1. Secondary scattering of the beams diffracted by a paraffin film in a silver preparation.

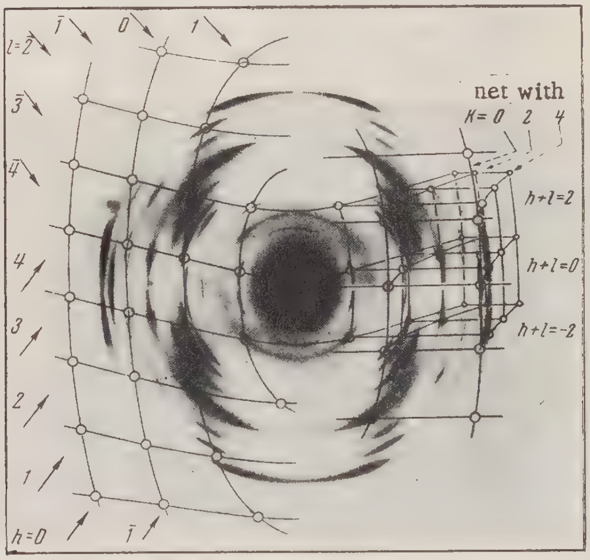

Fig. 2. Electron pattern of the texture of $NiCl_2 \cdot 2H_2O$ with a net of intereference lines superimposed.

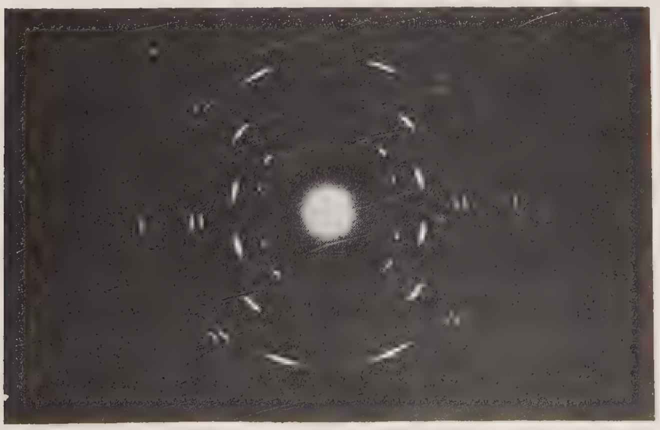

Fig. 3. Electron pattern from the texture of cryptohalite $(NH_4)_2SiF_6$.

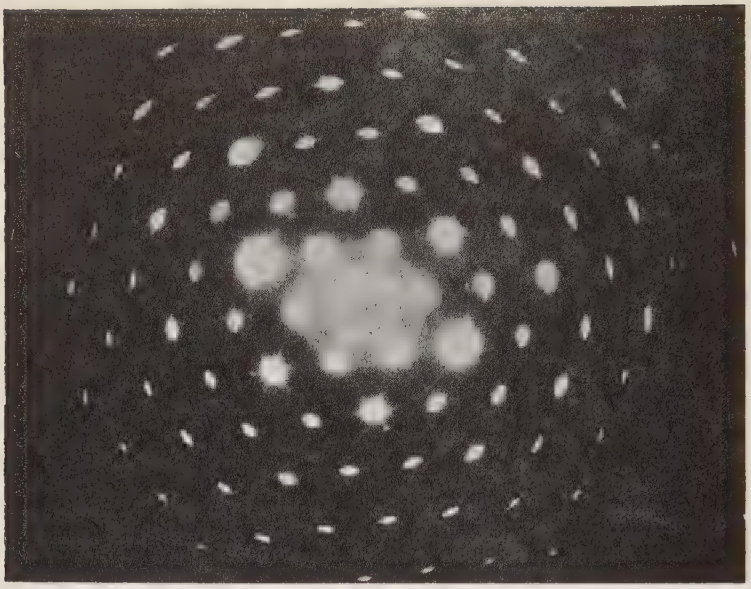

Fig. 4. Electron spot pattern of the semiconducting alloy CdFe.

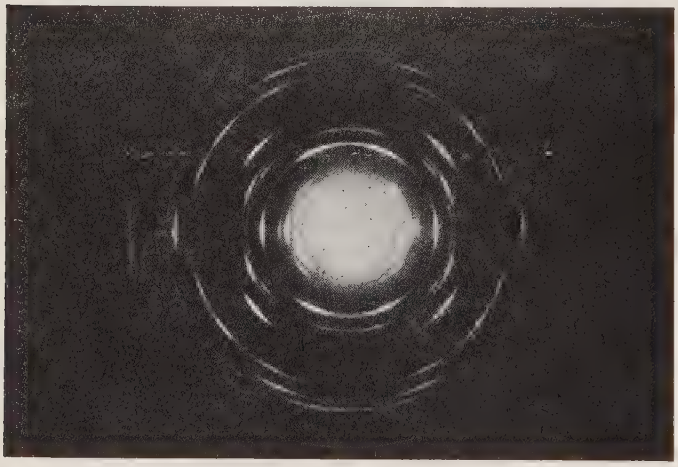

Fig. 5. Electron pattern from a texture of $Tl_2Sb_2Se_4$.

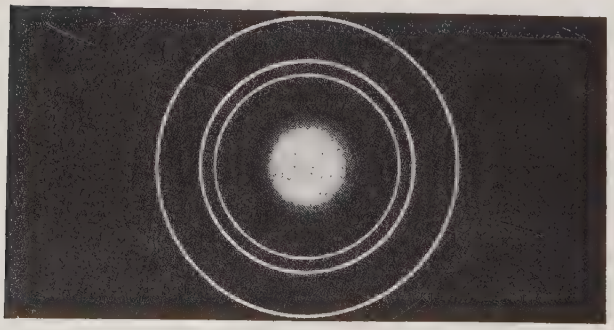

Fig. 6. Electron pattern from cubic chromium nitride CrN.

achieved by Kainuma [34] in developing the theory of Kikuchi electron patterns. He obtained the following expression for the intensity of the Kikuchi electron pattern:

$$J = N_1N_2N_3\left[\frac{S(k_0+\bar{k}_0,\ k_0+\bar{k}_0)}{(k_0+\bar{k}_0)^4}\frac{\bar{\Gamma}_0}{\bar{\gamma}_0}+\left\{\frac{S(k_0+\bar{k}_{\bar{H}},\ k_0+\bar{k}_{\bar{H}})}{(k_0+\bar{k}_{\bar{H}})^4}\frac{\bar{\Gamma}_0}{\bar{\gamma}_H}-\right.\right. \tag{11}$$

$$\left.\left.-\frac{S(k_0+\bar{k}_0,\ k_0+\bar{k}_0)}{(k_0+\bar{k}_0)^4}\frac{\bar{\Gamma}_0}{\bar{\gamma}_0}\right\}\frac{1}{2(1+\bar{W}^2)}-\frac{S(k_0+\bar{k}_H,\ k_0+\bar{k}_0)}{(k_0+\bar{k}_0)^2(k_0+\bar{k}_{\bar{H}})^2}\frac{\bar{\Gamma}_0}{\sqrt{\bar{\gamma}_0\gamma_H}}\frac{\bar{W}}{(1+\bar{W}^2)}\right],$$

which consists of three parts. The first part concerns the scattered rays with a monotonic decrease, i. e., the background of the electron pattern. The second part (in braces) concerns the Kikuchi lines, the intensity of which is calculated from the background intensity and the character of which (extinction or reinforcement line) is determined by the sign of the indicated difference. Finally, the third part gives the Kikuchi streak intensity. In this term the functions S (structure amplitudes of the Kikuchi patterns) are of interest to us. They are formed according to the law

$$S(k_g+\bar{k}_g,\ k_h+\bar{k}_h)=\sum_l s_l(k_g+\bar{k}_g, k_g+\bar{k}_h)\exp\{2\pi i(k_g+\bar{k}_h-k_h-\bar{k}_h), r_e\}. \tag{12}$$

Here the functions S_l are the atomic aplitudes for Kikuchi patterns.

Thus, in principle, a way is opened to the possibility of using Kikuchi electron patterns for structure analyses.

The following should be noted in this connection. Equation (11) is related to the intensity perpendicular to the Kikuchi lines and the direction of the streaks, i. e., it gives their "profiles." Kainuma assumes that the intensity distribution along the Kikuchi streaks can also be derived from (11). Thus this distribution must be determined by the structure of the scattering object. On the other hand, Blackman and Khan [36] contrasted the experimental scattering curves along the Kikuchi streak for fused and natural quartz and did not find any difference.

These authors assume that scattering at large angles does not depend on the structure of the object scattered. Probably this theory needs further development and refinement.

III. The Course of Electron Diffraction Structure Determination and Its Peculiarities

In the majority of researches on structure a more or less definite order of operations is maintained, which constitutes the course of the structure determination. First of all it is necessary to determine the unit cell. Different types of electron patterns (Figs. 1-6) are used for this. The most important of these are: electron spot patterns from mosaic single crystal films, patterns from textures and polycrystalline samples. The exact meaning of these expressions, as well as the conditions for obtaining such photographs has been repeatedly explained in our works, and particularly, in monographs [9, 15]. The types of electron patterns mentioned above make it possible to solve the problem at hand in full, even when any preliminary x-ray or goniometric data are absent.

Using one type of combination of photographs of different types from a given compound, the Laue symmetry, the unit cell and the space group of the structure under study can be determined systematically. Then the reflections are indexed, which is done very simply for the electron spot patterns, but is most complex for patterns of textures of skew-angled crystals. In addition, in the case of orthogonal lattices, the electron patterns of textures show layer lines. Ellipses (independently of the symmetry of the crystals under study) and in general other second order curves are always present along which the reflections are located, corresponding to one or another straight line of the reciprocal lattice (see Fig. 2).

The value of examining electron patterns of textures must be stressed since, from them, by two measurements, the whole reciprocal crystal lattice is reflected almost in full.

The most accurate determinations of lattice constants, with an error of ~ 0.001 A, is obtained by using photographs of polycrystals.

Sometimes when studying many-phase systems by electron diffraction, the composition of the phase under study is unknown. In such cases, the diffraction data themselves in combination with crystallochemical and geometric considerations allow the identification of the given phase.

The next step is the transition from the measured intensities to the $|\Phi|^2$ or $|\Phi|$ values. The formulas for such a transition contain the L factor, which takes into account the structure of the sample, and is analogous in function, but not identical in meaning,to the Lorentz factor in x-ray diffraction. The systematic derivation of the L factors for different types of electron patterns is given in Vainshtein's work [14, 15], and a summary of it appears in [31].

The experimental $|\Phi|$ or $|\Phi|^2$ values obtained can be used directly for structure analysis. The number of reflections used in various electron diffraction structure studies varies from a few dozen to 500.

Basically, it is of no importance to the researcher whether the values of the structure amplitudes are obtained from x-ray, electron or neutron diffraction data, as these magnitudes are useful in all cases for the establishment of the coordinates of the centers of gravity of atoms — the basic problem of structure analysis. The feature common to all the three methods is that the distribution of scattering material in the object has a single basic feature: its maxima correspond to the atoms, whether of electron density $\rho(\bar{\mathbf{r}})$ in x-ray diffraction, of the potential $\varphi(\bar{\mathbf{r}})$ in electron diffraction or of the "nuclear density" $\delta(\bar{\mathbf{r}})$ in neutron diffraction. The special nature of each method appears when account is taken of the peculiarities in the distribution of the scattering material in the atoms themselves, i. e., in the final analysis, by accounting for the peculiarities of the f-curve of atomic scattering, which determines the laws of the whole aggregate of the structure amplitudes Φ_{hkl} of the crystal.

The "sharper" the distribution of the scattering power in the atom, the slower is the decrease in the f-curve and vice versa. It follows from Thomas-Fermi's statistical theory of the atom that the $\varphi(r)$ of the atomic potential is a more diffuse function than its electron density, so that

$$\varphi(r) \sim \rho(r)^{2/3}. \tag{13}$$

Because of the greater diffuseness of $\varphi(\mathbf{r})$, the f_{el} curves decrease faster than the $f_{x\text{-ray}}$ curves.

The rapid decrease of the f_{el} curves produces a decline of the reflection intensities with increasing $\sin\vartheta/\lambda$ more severe than in the x-ray case. Therefore the number of terms in the Fourier series of the potential is usually 2-4 times smaller than in analogous series for electron density. In other words, the convergence of the Fourier series for potential is better and the termination error is smaller, but the function obtained is less sharp. Nevertheless, its basic property is a smaller sensitivity to differences in atomic number [15, 37, 38] in comparison with the electron density function.

Actually, all the information that can be obtained about a given atom by a diffraction experiment is contained in the sum (i. e., in the integral) of its scattering power, which has to be taken over the whole of reciprocal space:

$$\int f(s)\, dv_{\bar{\mathbf{H}}}. \tag{14}$$

Converting to spherical coordinates and to the vector $\mathbf{s} = 2\pi\bar{\mathbf{H}}$, the sum can be written as follows:

$$\frac{1}{2\pi^2}\int_0^\infty f(s)\, s^2 ds = \varphi(0). \tag{15}$$

This formula determines the density of scattering material at the center of the atom ($r = 0$), expressed through its f-curve, and gives the peak height on the Fourier synthesis, viz. the peak height of the electron density $\rho(0)$ in x-ray analysis, of the potential $\varphi(0)$ in electron diffraction, and of the nuclear scattering density $\delta(0)$ in neutron diffraction. These peak heights are the means for locating the atoms by one or the other method. Computation and experimental data show that if the peak heights are expressed as dependent on the atomic number, then the following relationship is maintained in x-ray diffraction:

$$\rho(0) \sim Z^{1.2}. \qquad (16)$$

But the dependence is much weaker in electron diffraction:

$$\varphi(0) \sim Z^{0.75}. \qquad (17)$$

Thus one of the most important characteristics of electron diffraction is that, compared to the x-ray diffraction method, it simplifies the locating of light atoms in the presence of heavy ones; for example, it is possible to locate hydrogen atoms [39, 40] by the Fourier series method.

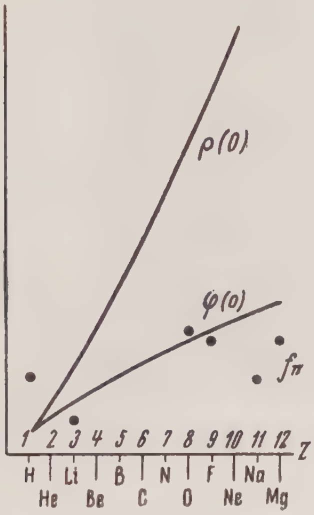

Fig. 7. The curves of the relative appearance of atoms in x-ray diffraction [$\rho(0)$] and in electron diffraction [$\varphi(0)$];dots are for the appearance of atoms in neutron diffraction (when B = 2).

In neutron diffraction the peak heights $\delta(0)$ do not depend on the atomic number, but are proportional to the atomic amplitudes f_n. Figure 7 compares the ease of detecting atoms by electron, x-ray and neutron diffraction methods for the first few elements of the periodic system.

Standardization methods recently worked out [15] make it possible to express directly in volts the results of Fourier syntheses

$$\varphi(xyz) = \frac{1}{\Omega} \sum_{hkl} \Phi_{hkl} e^{-2\pi i(\mathbf{rH})} \qquad (18)$$

These methods are often used in the first steps of structure interpretation with different variants of Φ^2. The trial and error method is used in the simplest cases. The accuracy of determining atomic positions with the aid of three-dimensional Fourier series for the potential [41] amounts to ~ 0.01 A, and in the case of projections to 0.02-0.03 A. Thus, the conditions for determining light atoms when heavy ones are present are more favorable in electron diffraction than in x-ray diffraction.

Various methods for approximating experimental amplitudes by calculated ones, in particular, the minimizing of the reliability factor

$$R = \Sigma \| \Phi_{\text{calc.}}| \sim |\Phi_{\text{exp.}} \| / \Sigma |\Phi_{\text{calc.}}| \qquad (19)$$

have been used successfully in electron diffraction for the analysis of a number of structures. In the final step the magnitude of this factor reflects the accuracy of intensity measurement and amounts in different analyses to 15-25%.

In conclusion, we should like to stress the importance of further perfecting all the methods of intensity recording on electron patterns. Together with the photographic methods, which when carefully done can be correct to 10% or lower, it is necessary to use counters and scintillators. This will allow an increase in the accuracy of Fourier series, widen the limits for determining the light atom positions (up to a ratio 30 : 1 for the atomic numbers Z of the heavy and light atoms), and to determine the valence state of the atoms.

IV. Some Results of Structure Determination by the Electron Diffraction Method

As had been mentioned above, in the last 15 years structures of various objects have been studied by the electron diffraction method. It is desirable to show the general results of these studies and, if possible, to make graphic the growing role of this method in structural crystallography. In conformity with the characteristics of the electron diffraction method, the most valuable results were obtained in areas not easily accessible to x-ray diffraction. Among these can be included: a) the study of substances that occur only in a highly dispersed condition, b) structures, stable in a vacuum, but unstable in ordinary atmospheric conditions, c) organic and inorganic compounds which contain light atoms together with heavy ones, d) multiple-component metallic systems in samples of variable or constant composition obtained by vacuum evaporation; all these are extremely convenient for electron diffraction analysis (see surveys [42-45]).

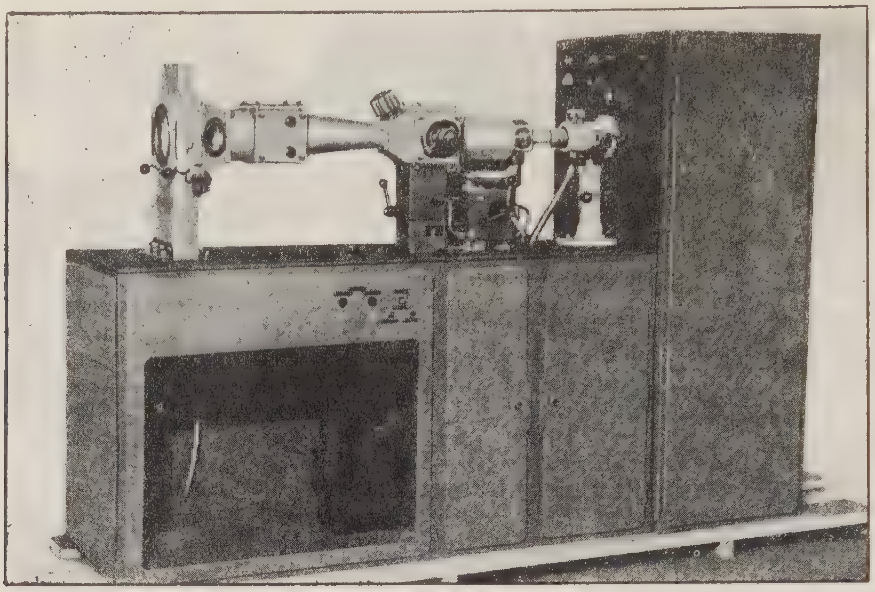

Fig. 8. Overall view of the new electron diffraction apparatus of the Institute of Crystallography.

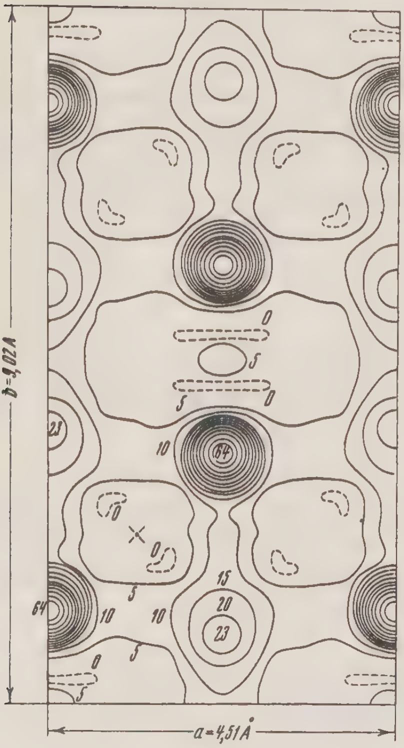

Fig. 9. The projection of the potential of the $BaCl_2 \cdot H_2O$ structure. The first Fourier synthesis constructed from electron diffraction data.

At present, the apparatus for electron diffraction studies makes it possible to solve a great variety of problems. Together with appliances which the researchers themselves construct, the periodic industrial output of electron diffraction units is of constantly increasing importance.

Figure 8 shows the apparatus constructed at the Institute of Crystallography intended basically for structure studies. It has a great resolving power. Electron patterns (see Figs. 1-6) are obtained on films 13 × 18 cm, the high voltage can be varied up to 75 kv, the distance from the samples to the screen is ~ 700 mm.

With this apparatus it is possible to photograph (at close range) Kikuchi electron patterns, and also to put into effect Trillat's [46] scheme of diffraction onto a moving film.

In the first series in which Fourier potential syntheses were used the structures of the crystal hydrates $BaCl_2 \cdot H_2O$ and $BaBr_2 \cdot H_2O$ were determined, and later those of $MeCl_2 \cdot 2H_2O$ where Me = Co, Mn, Ni [47, 49].

The study of these structures was carried out on electron patterns from mosaic single crystals, skew textures and on polycrystalline patterns.

In this study different versions of the Fourier method and occasionally the trial and error method were used.

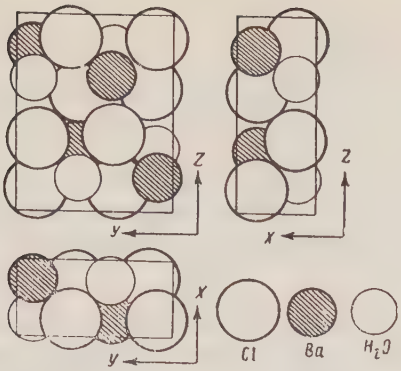

Fig. 10. $BaCl_2 \cdot H_2O$ structure.

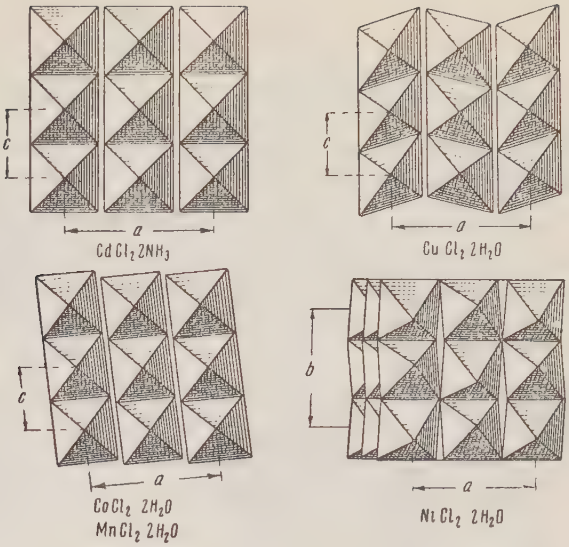

Fig. 11. A group of related structures $CdCl_2 \cdot 2NH_3$, $CuCl_2 \cdot 2H_2O$, $CoCl_2 \cdot 2H_2O$, $NiCl_2 \cdot 2H_2O$. The central vertical octahedral chain, drawn in finer lines, centers the base plane of the cells. The front octahedral vertices are occupied by H_2O molecules (except for the $CdCl_2 \cdot 2H_2O$ structure, in which the front vertex is NH_3).

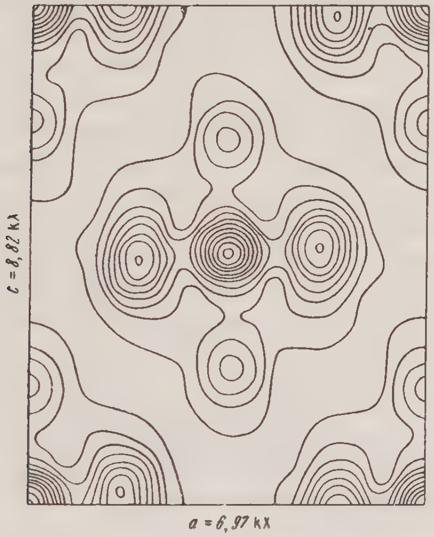

Fig. 12. The projection of the potential of the $NiCl_2 \cdot 2H_2O$ structure on the ac plane.

As a result of these studies, various crystallochemical laws were established related to the octahedral coordination of complex forming metals, and to the function of molecular water in crystal lattices.

Figure 9 shows the Fourier projection for $BaCl_2 \cdot H_2O$ and Fig. 10 gives a sketch of this structure.

Next, the phase $BaBr_2 \cdot H_2O$ was studied and proved to be completely isomorphous with the corresponding chloride.

The preparations of $CoCl_2 \cdot 2H_2O$ were obtained by crystallization from water solution at temperatures of 52-85°. It was possible to obtain from these samples spot patterns which corresponded to reflections of zone rows. In addition, patterns of skew textures were obtained with the reflections located along layer lines, i. e., with the texture axis parallel to the b (or b*) axis. As a result, a monoclinic unit cell was established: a = 7.31, b = 8.54, c = 3.58 A and β = 97°30'. The space group is C_{2h}^3.

The structure (see Fig. 11) can be described as an aggregate of parallel chains, formed by the $CoCl_4 \cdot 2H_2O$ octahedra.

Hydrogen bonds connect the chains; these are formed by the interaction of the water molecules with the chloride ions. Inside the octahedra the binding is ionic. $MnCl_2 \cdot 2H_2O$ has an analogous structure.

The $NiCl_2 \cdot 2H_2O$ [49] structure proved to be more complex. It was determined only on the basis of a pattern from a skew texture.

The monoclinic unit cell of this salt is nearly orthorhombic: a = 6.97, b = 6.90 and c = 8.81kX, β = 91°30 . The space group is C_{2h}^3. Figure 12 gives one of the syntheses for this structure and Fig. 11 a sketch of it.

The accuracy of the determination of the positions of chlorine atoms and water molecules (Ni atoms are in positions without parameters) is:

$$\Delta x_{\mathrm{Cl}} = 0.012\,\text{Å} \text{ and } \Delta x = \Delta y = \Delta z_{\mathrm{H_2O}} = 0.023\,\text{Å}.$$

The general appearance of the $NiCl_2 \cdot 2H_2O$ structure is given in Fig. 14.

Comparing the structures of the series of crystal hydrates $CdCl_2 \cdot 2NH_3$, $MnCl_2 \cdot 2H_2O$, $FeCl_2 \cdot 2H_2O$, $CoCl_2 \cdot 2H_2O$, $NiCl_2 \cdot 2H_2O$ and $CuCl_2 \cdot 2H_2O$ made it possible to ascertain some interesting crystallochemical laws.

Electron diffraction analysis was also successfully applied to the study of complex compounds. Thus in studying $KPtCl_3NH_3$ [50] the interatomic distances in the square complex $PtCl_3NH_3$ were established, and also the effect of the transinfluence of the NH_3 group, and as a result of the determination of the Cs_2CoCl_4 [51] structure, the tetrahedral nature of the $CoCl_4$ complex was elucidated.

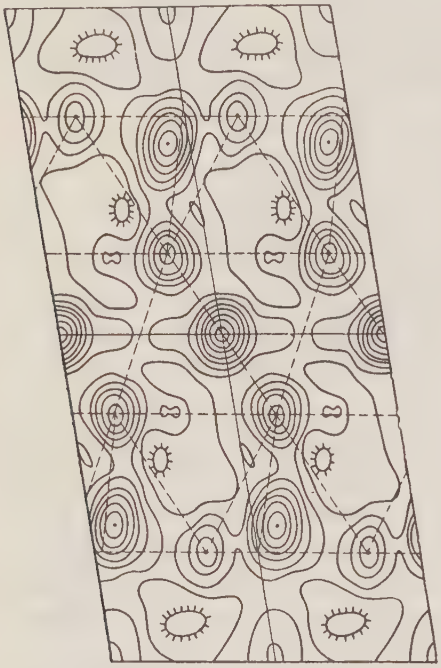

Fig. 13. Lateral projection of the potential in the clay mineral celadonite. The octahedral and tetrahedral lattices, set off by dashed lines, are shown clearly.

An important area of electron diffraction application is the study of clay minerals, to which x-ray analysis is quite inapplicable owing to their high state of dispersion. Although at present there is no doubt of the soundness of Pauling and Gruner's general idea of the structure of these minerals as octahedral lattices (Al, Mg, Fe) with tetrahedral Si-lattices adjoining them, the application of these ideas to the great variety of real structures is just in its practical beginning. This application must follow the line of establishing the laws of lattice coupling, of the distances in coordinate polyhedra, of isomorphous replacement, of the study of the degree of structure perfection, etc. Electron diffraction of clay minerals was developed in Pinsker's work and in that of his co-workers [52, 53] and then further in Zviagin's works [54-56]. Interesting data were also obtained by the Japanese authors (see for example, [57]).

In the first studies, the interest was mainly in the geometry of these lattices, but at present there is an example of a complete structure determination of one of the clay minerals — celadonite [56].

Figure 13, which is the lateral projection of the celadonite potential, shows clearly the three-storeyed structure of the silicate layer, and also the presence of K atoms in the interlayer spaces. (This drawing is taken from Zviagin's article [56].)

One of the most interesting uses of electron diffraction is the location of hydrogen atoms [39, 40]. The accuracy achieved in determining the hydrogen atoms is ~ 0.03 A; x-ray diffraction gives an accuracy of about 0.1 A, and neutron diffraction ~ 0.02 A. The first example of a study of H atoms was Lashkarev and Usyskin's establishment by the trial and error method [4] of the N—H distance in ammonium chloride. Following Vainshtein and Pinsker's work on paraffin [58] the application of Fourier synthesis of the potential became the basic method for such studies. Next, in the Soviet Union, urotropin [59], diketopiperazine [60], NH_4Cl [61], cryptohalite [62], and in Australia, dicetyl [63] and boric acid [64] were studied. Figure 15 shows the three-dimensional Fourier synthesis of diketopiperazine.

Here, the hydrogen atoms are seen clearly, together with the carbon, nitrogen and oxygen atoms. The accuracy of determination of the "heavy" C, N, O atom coordinates is $\Delta x \approx 0.008$ kX and for the hydrogen atoms $\Delta x = 0.03$ kX. Analyses of the peak height of the H_{III} atom, which forms the hydrogen bond with the neighboring molecules, shows that this atom is ionized.

Figure 16 gives the projection of the boric acid potential according to Cowley [64]. An interesting example is the study of the cryptohalite $(NH_4)_2SiF_6$ [62] structure, in which, as it turned out, the NH_4 tetrahedron occupies statistically six orientations (in close pairs), as is shown in Fig. 17. By using different syntheses it was possible to

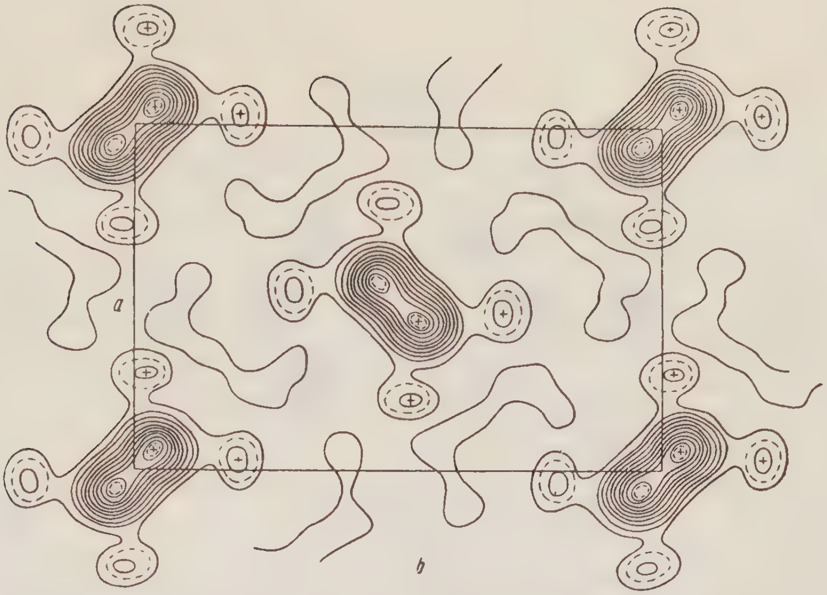

Fig. 14. Projection of paraffin potential. Hydrogen atoms appear along with carbon atoms.

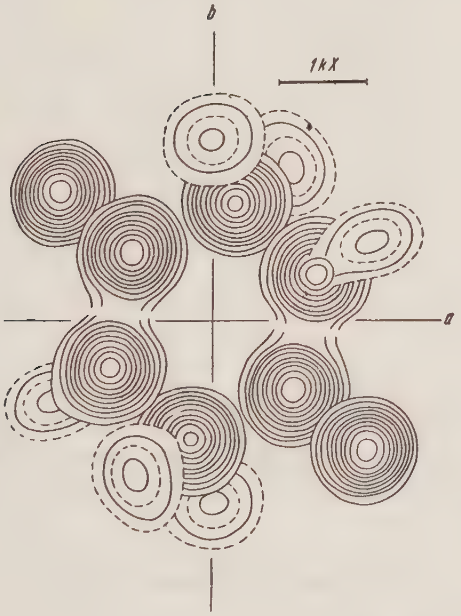

Fig. 15. Three-dimensional Fourier synthesis of the diketopiperazine molecular potential. The solid lines correspond to the 15 v contours, and the dashed lines to the 7.5 v.

determine the H coordinate for each orientation, whereby the $^1/_3$ H peak was detected experimentally, with Si (Z = 14), N (Z = 7), F (Z = 9) present. This agrees approximately with the determination of the "usual" hydrogen atom in a structure with an average Z for the other atoms of about 30. Figure 18 gives the projection of the $(NH_4)_2SiF_6$ structure potential.

From this precise determination it was possible to detect the effect of atomic ionization directly from the three-dimensional synthesis. It is easy to establish the influence of ionization on a model of the atom in the shape of a spherical condenser (Fig. 19): for an anion it reduces qualitatively to a decrease in height and a narrowing of the peak as compared to the neutral atom; for a cation, to its expansion and broadening. Figure 20 gives the experimental curves of the Si and F atomic potential conditionally reduced to the same height. The F peak is narrower, and the Si wider, which (just as does the analysis of their heights) indicates a positive Si ionization and a negative F one.

The strong influence on electron scattering of not only the ionization, but also in general of the valence state of the electron shell, follows from the well-known formula

$$f_{\mathrm{el}} \sim \frac{Z - f_{\text{x-ray}}}{(\sin\theta/\lambda)^2}, \tag{20}$$

which indicates that the magnitude of the atomic amplitude f_{el}, especially at small scattering angles, is very sensitive to changes in the atomic amplitude for x-ray scattering, $f_{\text{x-ray}}$, which is determined by the structure of the electron shell. It is important to stress that small changes in $f_{\text{x-ray}}$, which are almost impossible to detect

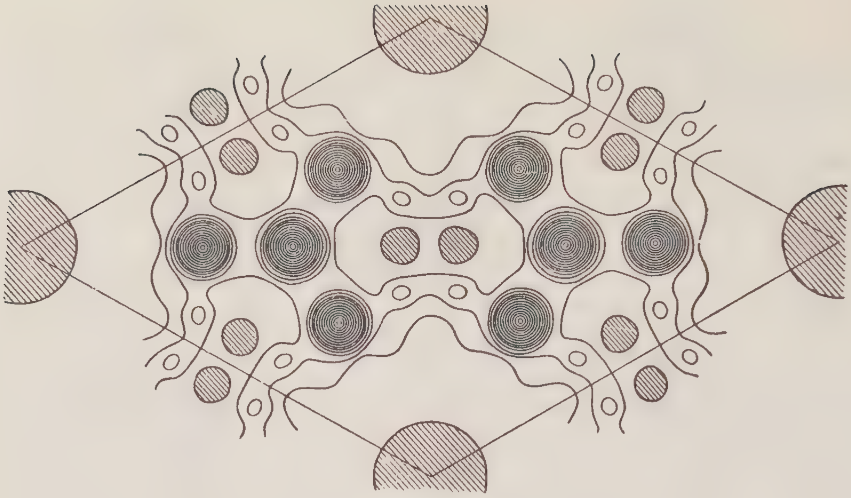

Fig. 16. Fourier projection of boric acid.

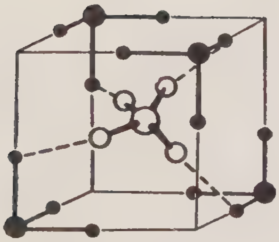

Fig. 17. One of the six equivalent orientations of the NH_4 tetrahedra in an octant of the $(NH_4)_2SiF_6$ structure.

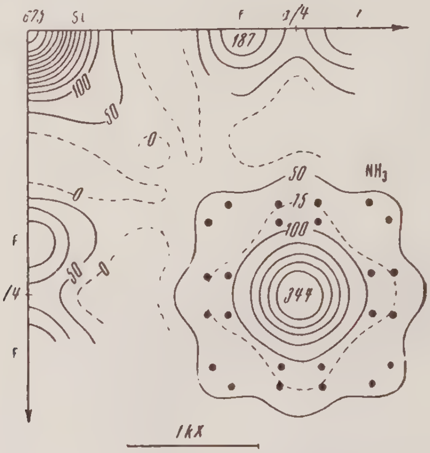

Fig. 18. Projection of the $(NH_4)_2SiF_6$ structure. Black circles are the locations of hydrogen atoms when the orientations of the NH_4 tetrahedra are statistically equivalent. The figures show the projected values of the potential in volts.

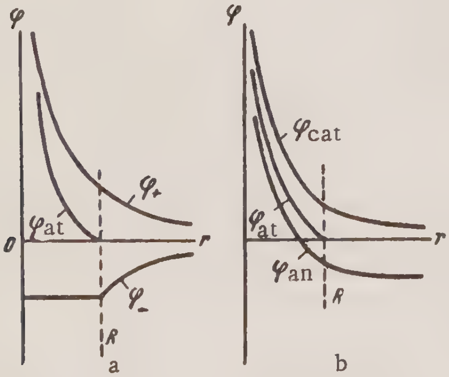

Fig. 19. a) The superposition of the nuclear φ_+ potential and of the φ_- potential of the electron shell in the spherical condenser model of the atom; b) shows the difference in the trends of the potentials of the cation, of the neutral atom and of the anion.

in x-ray analysis, give a strong change in f_{el}. This was used in the work [65] in which the atomic amplitude f_{el} of the scattering oxygen was determined in the compound Li_2O. It is evident from Fig. 21 that the experimental curve of f_{el} for O agrees best of all with the theoretical curve based on $f_{x\text{-ray}}$ according to McWeeny [66], who took into account the atomic binding in the lattice, and which deviates from the curve for the free O atom (according to Hartree [67]). A stronger decrease of the experimental curve for f_{el} of oxygen indicates the need for taking the temperature factor into account. The best agreement with experiment gives the value $B = 1.0\ A^2$.

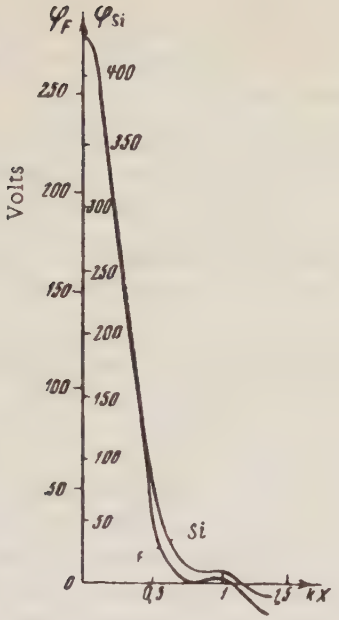

Fig. 20. The potential distribution in the Si and F peaks (in volts) in the $(NH_4)_2SiF_6$ structure.

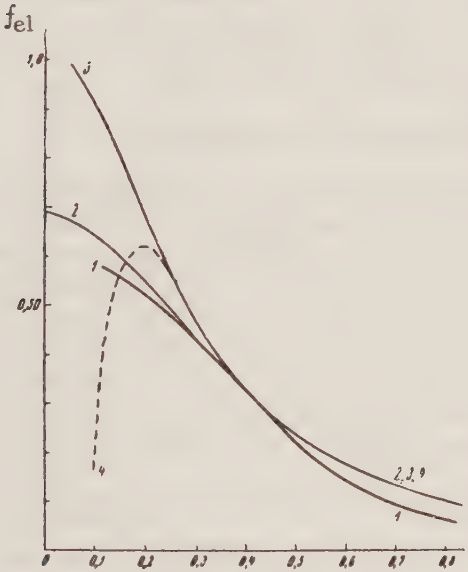

Fig. 21. Theoretical and structural experimental f_{el} curves for oxygen. (The coefficient converting to absolute values of f_{el}:$2.393 \cdot 10^{-8}$ cm .) 1) The experimental curve for oxygen; 2) the theoretical curve [8, 9] for a bound oxygen atom; 3) the theoretical curve [10] for a free oxygen atom; 4) the theoretical curve [10] for the anion O^{--}.

Another interesting property of Formula (20) should be noted. It is not essential, as is generally assumed, that the nucleus (term in Z) and the electron shell (term in $f_{x\text{-ray}}$) or even its isolated layers (exterior and interior) have the same thermal motion. Therefore, the temperature factors B can be different in these terms, and the data concerning this magnitude can be different in x-ray, electron and neutron diffraction.

This brings to notice the necessity for precise studies of some simple structures by all three methods.

Interesting studies, based on the analysis of spot patterns only, are being carried out by the Australian authors Cowley, Rees and Spink [63, 64, 68-70]. In most cases, layer lattices were studied, in which the effects of superposition disorder are possible, due to the weak bond between the layers. The characteristic superposition function of the layers as well as the structure of the layer itself can be established from electron patterns. Together with the above-mentioned study of boric acid [64], a similar determination was carried out for the structures of basic lead carbonate [68]. After finding the Pb coordinates with the use of difference syntheses, the author also determined the locations of the C and O atoms.

Electron diffraction metallography is a broad and important division of structural electron diffraction research. There is no point in discussing works, important as they are, that do not contain new structural data on electron diffraction identification of one or another phase in different types of samples, and the reader is therefore referred to the literature [22, 24].

Much of the work of the electron diffraction laboratory of the Institute of Crystallography is devoted to the study of semiconducting alloys [71-78]. Electron diffraction can be successfully used for the solution of the following problems:

a) In preparing semiconductor devices from monocrystal stock, the monocrystal blocks are given different treatments, in the course of which one or another transformation takes place in the surface layer. Electron diffraction makes possible more successfully than other methods structure control and the study of the processes just described.

b) More profound structural studies are concerned with multicomponent semiconducting alloys. The various phases in two, three and even four-component systems, which include Bi, Sb, Se, Te, Tl, As and other elements, have been studied only partially by the x-ray method, because of certain difficulties.

In developing the method, the main attention was given to the study of the structures of thin layers, prepared by vacuum evaporation onto neutral or oriented substrates at different temperatures.

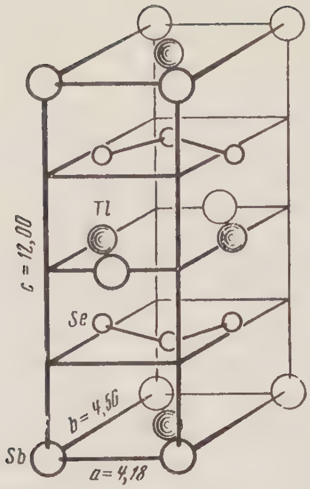

Fig. 22. $Tl_2Sb_2Se_4$ structure.

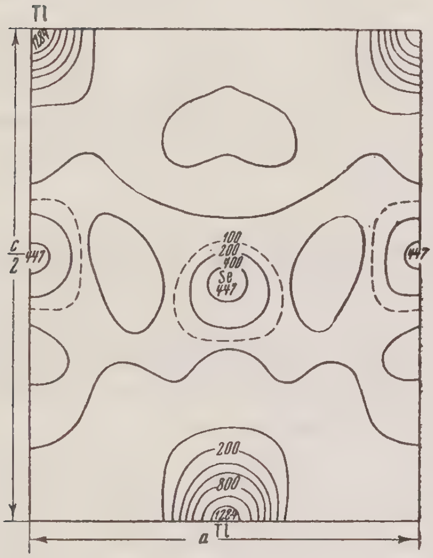

Fig. 23. Cross section of the three-dimensional series for the potential in the plane y = $^1/_2$ of the $Tl_2[Sb, As]_2Se_4$ lattice.

Layers of CdS, CdSe and CdTe were crystallized on different substrates, and it was shown that all these compounds have two lattices: cubic ZnS-type and a hexagonal Wurtzite type.

The systematic studies of the Bi–Se and Bi–Te systems carried out in 1953-1954 are of great interest as to method.

The structures of all the phases observed in the systems indicated were studied in detail in the course of this work.

The method of densest packing was used successfully in studying the structure of these phases.

Interesting examples of structural determinations of the chemical composition of the phases also appear in these works.

In studying the various samples it was established that the lattice constants of isolated compounds change within certain limits. This was explained by the solubilities of the separate components in the corresponding phases.

Thus, in studying Bi_2Se_3 the following limits of variation of the lattice constants were observed:

$$a: 4.12—4.17\ (\pm 0{,}01kX);$$

$$c = 28.6—29.2\ (\pm 0{,}2kX).$$

The addition of Bi to the film of the compound Bi_2Se_3 led either to an increase in the lattice constants, or to the formation of the phase Bi_3Se_4 and even of BiSe, depending on the quantity of Bi. On the contrary, the addition of Se led to a decrease in lattice constants. Analogous observations were made on other phases. All this can be explained naturally, since Bi forms interstitial solid solutions by addition with the compounds indicated, and Se forms subtraction solutions.

On further study of semiconducting alloys more complex systems had to be dealt with. The three component system Tl–Sb–Se was studied and also films obtained by the sublimation of the alloys Tl_2Se, Sb_2Se_3 and $Tl_2Sb_2Se_4$.

The structure of the compound $Tl_2Sb_2Se_4$ (Fig. 22) was determined from electron patterns of skew textures with the aid of geometric analysis, of detailed study of Φ^2 series, and finally by calculation of sections through three-dimensional series of the potential (Fig. 23). The structure is described as an aggregate of flat, centered nets of Tl and Sb atoms, which together form a thoroughly face-centered orthorhombic lattice. Between the nets mentioned zigzag-shaped chains of Se atoms are oriented parallel to the X axis.

The four component system Tl–Se–Sb–As was examined next.

As antimony was replaced by arsenic in the three-component system a decrease in the perfection of the structure and a predominantly amorphous state were observed.

The results of this study established that arsenic enters the $Tl_2Sb_2Se_4$ lattice, replacing Sb (Fig. 23) statistically. Thus the basic structural trend in the corresponding phases proved to be of the $Tl_2Sb_2Se_4$ type.

Another essential problem is the study of the amorphous component [76, 78] which enters into the constitution of many alloys, closely associated with the corresponding crystalline structures, and also with ordering processes and crystallization [79, 80].

Systematic studies of nitriding and of gas carburization of transition metals and of the structures of the corresponding nitrides and carbides [81, 84] are an important trend in electron diffraction metallography.

Interesting and as yet unsolved problems of the nature of the chemical bond in similar interstitial phases can be treated experimentally by electron diffraction structural study. This question is elucidated in [30].

Our survey is of necessity brief and does not include the study of amorphous bodies and high polymers, glasses, coals, nor studies at high and low temperatures, processes of corrosion, etc.

Neither did we discuss that independent division of electron diffraction, the study of molecular structure in vapor and gas.

Our task was only to show by isolated examples the great possibilities of electron diffraction analysis of solid bodies. Further success depends on systematic experimental studies as well as on more serious treatment of the experimental material, based on the whole aggregate of data on electron scattering by atoms, molecules and crystals.

LITERATURE CITED

[1] C. J. Davisson and L. H. Germer, "Electron scattering by a single crystal of nickel," Nature 119, 538 (1927).

[2] G. P. Thomson and W. Cochran, Theory and Practice of Electron Diffraction (London, 1939).

[3] P. S. Tartakovskii, Experimental Bases of the Wave Theory of Matter [in Russian] (GTTI, 1932).

[4] V. E. Lashkarev, Electron Diffraction (GTTI, 1933).

[5] Z. G. Pinsker, "Electron diffraction study of the structure of cadmium iodide," Zhur. Fiz. Khim. 25, 559 (1941).

[6] Z. G. Pinsker and L. I. Tatarinova, "Electron diffraction study of cadmium chloride," Zhur. Fiz. Khim. 25, 1006 (1941).

[7] Z. G.Pinsker, "Electron diffraction study of the structure of cadmium bromide," Zhur. Fiz. Khim. 26, 1-10 (1942).

[8] Z. G. Pinsker, L. I. Tatarinova, and V. A. Novikova, "Electron diffraction study of the structure of lead iodide," Zhur. Fiz. Khim. 28, 420-428 (1944).

[9] Z. G. Pinsker, Electron Diffraction [in Russian] (1949).

[10] B. K. Vainshtein and Z. G. Pinsker, "Application of harmonic analysis of electron diffraction," Doklady Akad. Nauk SSSR 1, 49-52 (1949).

[11] B. K. Vainshtein, "Concerning the study of the potential in the crystalline lattice by the electron diffraction method," Trudy Inst. Krist. AN SSSR 9, 259-276 (1954).

[12] B. K. Vainshtein, "Electron patterns from textures," Trudy Inst. Krist. AN SSSR 6, 173-192 (1951).

[13] B. K. Vainshtein, "Kinematic electron scattering by an ideal single crystal," Doklady Akad. Nauk SSSR 104, 537-539 (1955).

[14] B. K. Vainshtein, "The kinematic theory of the reflection intensity of electron patterns. I. Electron spot patterns. II. Electron patterns from textures and polycrystals," Kristallografiia 1, 17-26, 150-158 (1956).

[15] B. K. Vainshtein, Structural Electron Diffraction [in Russian] (1956).

[16] N. Kato and R. Ueda, "Dynamical theory of electron diffraction for a finite polyhedral crystal I, II; Comparison with the results of kinematical theory," Acta Cryst. 4, 227-229; 229-231 (1951).

[17] N. Kato, "Dynamical theory of electron diffraction for a finite polyhedral crystal I, Extension of Bethe's; II. Fraunhofer formulas," J. Phys. Soc. Japan 7, 397-406, 406-414 (1952).

[18] J. M. Cowley and A. L. G. Rees, "Refraction effects in electron diffraction," Proc. Phys. Soc. 59, 287-301 (1947).

[19] K. Moliere and H. Niehr, "Interferenzbrechung v. Elektronenstrählen. I. Zur Theorie d. Elektroneninterferenzen an parallelipipedischen Kristallen," Z. Physik 445-462 (1954); H. J. Altenhein and K. Moliere, "II. Die Feinstructur d. Interferenzen v. Magnesiumoxyd—Kristallen," 139, 103-114 (1954); K. Moliere and H. Niehrs, "III. Bestimmung d. Kristallorientierung,d. Strukturfaktoren u. der Brechungspotenzials v. Magnesiumoxyd—Kristallen," 140, 581-607 (1955); G. Honjo and K. Mihama, II, 9, 184-198 (1954); G. Honjo, "Fine structure due to refraction effect in electron diffraction, I," J. Phys. Soc. (Japan) 8, 776-781 (1953).

[20] K. Kohra, "Simultaneous reflection in electron diffraction as a cause of the failure of Friedel's law," J. Phys. Soc. Japan 9, 690-701 (1954).

[21] H. Niehrs, "Die Friedelsche Regel in Lichte der dynamischen Interferenztheorie," Z. Physik 140, 106-118 (1955).

[22] P. D. Dankov, D. V. Ignatov, and N. A. Shishakov, Electron Diffraction Studies of Oxide and Hydroxide Films on Metals [in Russian] (1953).

[23] J. F. Radavich, "Oxidation at elevated temperatures," special technical publication No. 171 (Am. Soc. Testing Materials, 1955).

[24] J. E. O. Mayne, J. W. Meuter, and M. J. Pryor, "The mechanism of inhibition of the corrosion of iron by sodium hydroxide solution," J. Chem. Soc. (November, 1950), pp. 3229-3236.

[25] M. Blackman, "On the intensities of electron diffraction rings," Proc. Roy. Soc. 173, 68-82 (1939).

[26] I. I. Iamzin, "Atomic scattering of electrons," Trudy Inst. Krist. AN SSSR 5, 69-112 (1949).

[27] B. K. Vainshtein, "Atomic factors for electronic scattering," J. Exptl.-Theoret. Phys. (USSR) 25, 157-168 (1953).

[28] S. Lennander, "Measurements of electron diffraction intensities by means of Geiger counters," Arkiv for Fysik 8, 54, 551-513 (1954).

[29] B. K. Vainshtein and A. N. Lobachev, "Concerning the establishment of the character of electron scattering (dynamic or kinematic) in electron diffraction structural studies," Kristallografiia 1, 4, 472-473 (1956).

[30] Z. G.Pinsker and S. B. Kaverin, "Electron diffraction study of carbides and nitrides," Kristallografiia 2, 3 (1957) [Soviet Physics — Crystallography, p. 380].

[31] B. K. Vainshtein, "Intensities of reflections of electron patterns (general case)," Kristallografiia 2, 3 (1957) [Soviet Physics — Crystallography, p.334].

[32] C. H. MacGillavry, "Verification of the dynamical theory of electron interference by a crystal lattice," Physica 7, 329-343 (1940).

[33] R. Ueda,Y. Fukano, and T. Ichinokawa, "Subsidiary maxima electron diffraction net patterns from molybdenite," Acta Cryst. 7, 216-217 (1954).

[34] Y. Kainuma, "The theory of Kikuchi patterns," Acta Cryst. 8, 247-257 (1955).

[35] Z. G. Pinsker and B. K. Vainshtein, "Dynamic electron scattering," Izv. AN SSSR, Ser. Fiz. 14, 2, 212-222 (1950).

[36] M. Blackman and J. A. Khan, "The intensity of high angle Kikuchi bands," Proc. Phys. Soc. London 67, 553-555 (1954).

[37] B. K. Vainshtein, "Concerning the heights of maxima on syntheses of electron density and potential," Trudy Inst. Krist. AN SSSR 11, 78-84 (1955).

[38] B. K. Vainshtein, "Quantitative relationships in Fourier series of electron density of crystals," J. Exptl.-Theoret. Phys. (USSR) 27, 1, 44-61 (1954).

[39] B. K. Vainshtein and Z. G. Pinsker, "Electron diffraction determination of the hydrogen atom in crystalline lattices," Trudy Inst. Krist. AN SSSR 10, 62-70 (1954).

[40] B. K. Bainshtein, "Electron diffraction studies of crystals with hydrogen bonds," Trudy Inst. Krist. AN SSSR 10, 49-61 (1954).

[41] B. K. Vainshtein, "The accuracy of Fourier series of the potential in electron diffraction," Kristallografiia 1, 5, 495-501 (1956).

[42] Z. G. Pinsker, "Application of electron diffraction in chemistry," Uspekhi Khimii 20, 104-131 (1951).

[43] Z. G. Pinsker, "Electron diffraction analysis of solid bodies," Trudy Inst. Krist. AN SSSR 10, 91-101 (1954).

[44] Z. G. Pinsker, "Electron diffraction and electron microscopic study of clay minerals," Trudy Inst. Geokhimii 116-141 (1955).

[45] B. K. Vainshtein, "Structure analysis by electron diffraction," Nuovo Cimento (supplement) vol. 3, ser. X, 773-797 (1956).

[46] J. J. Trillat and N. Takahashi, "Energistrement continu par diffraction electronique de transformations chimiques ou physiques et applications," Acta Cryst. 7, 15 (1954).

[47] B. K. Vainshtein and Z. G. Pinsker, "Electron diffraction determination of the structure of barium chloride monohydrate $BaCl_2 \cdot H_2O$," Zhur. Fiz. Khim. 23, 9, 1058-1069 (1949).

[48] B. K. Vainshtein, "Electron diffraction determination of the structure of $CoCl_2 \cdot 2H_2O$," Doklady Akad. Nauk SSSR 68, 2, 301-304 (1949); B. K. Vainshtein, "Crystalline structure of $MnCl_2 \cdot 2H_2O$," Doklady Akad. Nauk SSSR 83, 2, 227-230 (1952).

[49] B. K. Vainshtein, "Electron diffraction determination of the structure of $NiCl_2 \cdot 2H_2O$ and the crystal chemistry of compounds of this type," Zhur. Fiz. Khim. 26, 12, 1774-1784 (1952).

[50] G. B. Bokii, B. K. Vainshtein, and A. A. Babareko, "Electron diffraction study and crystal chemistry of $KPtCl_3NH_3$ and $KPtBr_3NH_3$," Bull. Acad. Sci., Div. Chem. Sci. 6, 667-673 (1951).

[51] G. N. Tishchenko and Z. G. Pinsker, "Electron diffraction determination of the structure of Cs_2CoCl_4," Doklady Akad. Nauk SSSR 100, 5, 913-916 (1955).

[52] Z. G. Pinsker, E. L. Lapious, and L. I. Tatarinova, "Electron diffraction study of the structure of kaolinite," Zhur. Fiz. Khim. 1017-1027 (1948); Z. G. Pinsker, "The determination of the unit cell and the space group of kaolinite," Doklady Akad. Nauk SSSR 73, 107-110 (1950).

[53] B. B. Zviagin and Z. G. Pinsker, "Electron diffraction study of montmorillonite," Doklady Akad. Nauk SSSR 68, 65-67 (1949); Z. G. Pinsker and B. B. Zviagin, "Electron diffraction determination of the unit cells of pyrophillite and talc and the structural connection of these minerals with montmorillonite," Doklady Akad. Nauk SSSR 68, 505-508 (1949).

[54] B. B. Zviagin, "Electron diffraction study of hydrated micas," Kristallografiia 1, 2, 214-217 (1956); B. B. Zviagin, "Concerning certain pecularities of diffraction patterns of layer silicates," Doklady Akad. Nauk SSSR 97, 251-253 (1954).

[55] B. B. Zviagin, "Electron diffraction study of minerals of the kaolinite group," Doklady Akad. Nauk SSSR 96, 809-812 (1954).

[56] B. B. Zviagin, "Electron diffraction study of celadonite," Kristallografiia 2, 3 (1957) [Soviet Physics — Crystallography, p. 388].

[57] G. Hanjo and K. Mihama, "A study of clay minerals by electron diffraction diagrams due to individual crystallites," Acta Cryst. 7, 511-513 (1954).

[58] B. K. Vainshtein and Z. G. Pinsker, "Determination of the location of hydrogen in the crystalline lattice of paraffin," Doklady Akad. Nauk SSSR 72, 1, 53-56 (1950).

[59] A. N. Lobachev, "Electron diffraction determination of the location of hydrogen atoms in urotropine crystals," Trudy Inst. Krist. AN SSSR 10, 71-75 (1954).

[60] B. K. Vainshtein, "Electron diffraction study of diketopiperazine," Zhur. Fiz. Khim. 29, 2, 327-344 (1955).

[61] M. M. Stasova and B. K. Vainshtein, "Refinement of the structure groups in the structure of ammonium chloride," Trudy Inst. Krist. AN SSSR 12, 18-24 (1956).

[62] B. K. Vainshtein and M. M. Stasova, "Electron diffraction study of cryptohalite," Kristallografiia 1, 3, 312-320 (1956).

[63] J. M. Cowley, A. L. Rees, and J. A. Spink, "Secondary elastic scattering in electron diffraction," Proc. Phys. Soc. London 64, 609-619 (1951).

[64] J. M. Cowley, "Structure analysis of single crystals by electron diffraction," Acta Cryst. 6, 516-529 (1953).

[65] B. K. Vainshtein and V. F. Dvoriankin, "The influence of the chemical bond on atomic electron scattering," Kristallografiia 1, 6, 626-630 (1956).

[66] R. McWeeny, "X-ray scattering by aggregates of bonded atoms," Acta Cryst. 4, 513-519 (1951).

[67] Internationale Tabellen zur Bestimmung von Krystallstrukturen (Berlin, 1935), Band. II.

[68] J. M. Cowley, "Electron diffraction study of the structure of basic lead carbonate," Acta Cryst. 9, 391-396 (1956).

[69] J. M. Cowley, "Stacking faults in γ-alumina," Acta Cryst. 6, 53 (1953).

[70] J. M. Cowley and J. A. Ibers, "The structures of some ferric chloride—graphite compounds," Acta Cryst. 9, 421-431 (1956).

[71] S. A. Semiletov, "Electron diffraction study of the structure of sublimed layers of the compound Bi—Se and Bi—Te," Trudy Inst. Krist. AN SSSR 10, 76-83 (1954).

[72] S. A. Semiletov, "Electron diffraction study of the alloy system of cadmium-tellurium," Trudy Inst. Krist. AN SSSR 11, 121-123 (1955).

[73] Z. G. Pinsker, S. A. Semiletov, and E. N. Belova, "Electron diffraction determination of the structure $Tl_2Sb_2Se_4$," Doklady Akad. Nauk SSSR 106, 1003-1006 (1956).

[74] S. A. Semiletov, "Electron diffraction determination of the structure of antimony-telluride," Kristallografiia 1, 403-406 (1956).

[75] S. A. Semiletov and Z. G. Pinsker, "Oxidation of samples of Bi_2Se_3 and Bi_2Te_3 on annealing in air," J. Tech. Phys. (USSR) 25, 2336-2338 (1955).

[76] L. I. Tatarinova, "Electron diffraction study of amorphous antimony," Trudy Inst. Krist. AN SSSR 11, 104-114 (1955).

[77] L. I. Tartarinova, "Electron diffraction study of amorphous GaSe," Kristallografiia 1, 5, 534-536 (1956).

[78] L. I. Tatarinova, "Electron diffraction study of amorphous antimony sulfide," Kristallografiia 2, 2 (1957) [Soviet Physics — Crystallography, p.251].

[79] S. A. Semiletov and Z. G. Pinsker, "Electron diffraction study of the degree of perfection of single crystals of germanium," Kristallografiia 1, 210-213 (1956).

[80] Z. G. Pinsker and G. A. Kurov, "Electron diffraction study of thin films of alloys," Doklady Akad. Nauk SSSR 94, 439-441 (1954).

[81] Z. G. Pinsker and S. V. Kaverin, "Electron diffraction study of the structure of hexagonal iron nitride," Doklady Akad. Nauk SSSR 96, 519-522 (1954); Z. G. Pinsker and S. V. Kaverin, "Electron diffraction study of the structure of cubic iron nitrides," Doklady Akad. Nauk SSSR 95, 797-799 (1954).

[82] Z. G. Pinsker and S. V. Kaverin, "Electron diffraction study of the structure of iron carbide, Fe_4C_3," Kristallografiia 1, 66-72 (1956).

[83] Z. G. Pinsker and S. V. Kaverin, "The mechanism of phase transitions in nondiffusion transformation iron nitrides," Trudy Inst. Krist. AN SSSR 12, 3-17 (1956).

[84] Z. G. Pinsker, S. V. Kaverin, and N. N. Troitskaia, "Electronographic investigations of nitrides of molybdenite," Kristallografiia 2, 1 (1957) [Soviet Physics — Crystallography, p. 169].

Received March 11, 1957

Institute of Crystallography, Academy of Sciences, USSR

SOVIET PHYSICS – CRYSTALLOGRAPHY

(Translation of the journal "Crystallography" of the USSR, Vol. 2, No. 4
published by the American Institute of Physics, January 1959)

VOLUME 2, NUMBER 4 JULY-AUGUST, 1957

CONTENTS

	PAGE	RUSS. PAGE
On the Representation of Crystal Atoms as Symmetrical Bodies. S. T. Konobeevskii	445	447
Concepts of Organic Crystallography. A. I. Kitaigorodskii	454	456
X-ray Diffraction Determinative Table of Minerals. V. I. Mikheev	463	466
Concerning the Peculiarities of the Collagen Structure. N. S. Andreeva, N. G. Esipova, and M. I. Millionova	467	470
Electron Diffraction Analysis of the Molecular Structures of Halides of Group II Elements. P. A. Akishin and V. P. Spiridonov	472	475
Electron Diffraction Investigation of Phase Transitions in Thin Films of Metals and Oxides. D. V. Ignatov	480	484
Atomic Chains and the Fine Structure of Glass. V. V. Tarasov	487	489
Oxide Formation and Photoresistance of Lead Sulfide Films. V. N. Vertsner, N. A. Kel'ner, and A. M. Solov'ev	494	497
X-ray Diffraction Analysis of the Changes in Mosaic Structure During the Ageing of Beryllium Copper. Ia. Umanskii, V. Eliutina, A. Kagan, and L. Pivovarov	500	503
The X-ray Diffraction Determination of the Thermal Expansion of Single Crystals. V. V. Zubenko and M. M. Umanskii	505	508
X-ray Diffraction Study of the Structural Distortion of Metals Under Static and Dynamic Compression at Room Temperature and Low Temperature. Iu. S. Terminasov and V. F. Mindukshev	510	514
Change in the Crystal Structure of Steel During Cold Work and Heat Treatment. E. L. Gal'tserin and Iu. S. Terminasov	515	519
Significance for the Theory of Ferroelectricity of the Optical Study of Domains in Rochelle Salt. V. L. Indenbom and M. A. Chernysheva	522	526
Study of Phase Transformations at Very High Pressures. V. P. Butuzov	533	536
Etch Pits on Slip Lines and on the Boundaries of Polygonal Blocks in Silver Chloride Crystals. M. P. Shaskol'skaia and Iu. Kh. Vekilov	544	548
A Survey of Electron Diffraction Structural Analysis. Z. G. Pinsker and B. K. Vainshtein	551	552

SIGNIFICANCE OF ABBREVIATIONS MOST FREQUENTLY ENCOUNTERED IN SOVIET CRYSTALLOGRAPHY LITERATURE

AN SSSR	*Academy of Sciences, USSR*
FIAN	*Physics Institute, Academy of Sciences USSR*
GITI	*State Scientific and Technical Press*
GITTL	*State Press for Technical and Theoretical Literature*
GOI	*State Optical Institute*
GONTI	*State United Scientific and Technical Press*
Gosfizkhimizdat	*State Physical Chemistry Press*
Gozkhimizdat	*State Chemistry Press*
GOST	*All-Union State Standard*
Goztekhizdat	*State Technical Press*
GTTI	*State Technical and Theoretical Press*
GUPIAE	*State Office for Utilization of Atomic Energy*
IF KhI	*Institute of Physical Chemistry Research*
IFP	*Institute of Physical Problems*
IK	*Institute of Crystallography*
IL	*Foreign Literature Press*
IPF	*Institute of Applied Physics*
IPM	*Institute of Applied Mathematics*
IREA	*Institute of Chemical Reagents*
ISN (Izd. Sov. Nauk)	*Soviet Science Press*
IIaP	*Institute of Nuclear Studies*
Izd	*Press (publishing house)*
KISO	*Solar Research Commission*
LETI	*Leningrad Electrotechnical Institute*
LFTI	*Leningrad Institute of Physics and Technology*
LIM	*Leningrad Institute of Metals*
LITMiO	*Leningrad Institute of Precision Instruments and Optics*
MATI	*Moscow Aviation Technology Institute*
MGU	*Moscow State University*
Metallurgizdat	*Metallurgy Press*
MOPI	*Moscow Regional Pedagogical Institute*
NIAFIZ	*Scientific Research Association for Physics*
NIFI	*Scientific Research Institute of Physics*
NIIMM	*Scientific Research Institute of Mathematics and Mechanics*
NII ZVUKSZAPIOI	*Scientific Research Institute of Sound Recording*
NIKFI	*Scientific Institute of Motion Picture Photography*
OIIaI	*Joint Institute of Nuclear Studies*
ONTI	*United Scientific and Technical Press*
OTI	*Division of Technical Information*
OTN	*Division of Technical Science*
RIAN	*Radium Institute, Academy of Sciences of the USSR*
SPB	*All-Union Special Planning Office*
Stroiizdat	*Construction Press*
TsNIIChERMET	*Central Scientific Research Institute for Ferrous Metallurgy*
URALFTI	*Ural Institute of Physics and Technology*

NOTE: Abbreviations not on this list and not explained in the translation have been transliterated, no further information about their significance being available to us.—*Publisher.*

The expanded program of the American Institute of Physics comprises translation of six leading Soviet physics journals, as listed below. These translations, by competent, qualified scientists, provide all research laboratories and libraries with accurate and up-to-date information of the results of research in the U.S.S.R.

Soviet Physics—Technical Physics

A translation of the "Journal of Technical Physics" of the Academy of Sciences of the U.S.S.R. The translation began with the 1956 issues. Twelve issues per year, approximately 3,000 Russian pages. Annually $75.00 domestic, $79.00 foreign. Libraries* $35.00 domestic, $39.00 foreign. Back numbers, all issues $8.00.

Soviet Physics—Acoustics

A translation of the "Journal of Acoustics" of the Academy of Sciences of the U.S.S.R. The translation began with the 1955 issues. Four issues per year, approximately 400 Russian pages. Annually $12.00 domestic, $14.00 foreign. (No library discounts.) Back numbers, all issues $4.00.

Soviet Physics—Doklady

A translation of all of the "Physics Sections" of the Proceedings of the Academy of Sciences of the U.S.S.R. The translation began with the 1956 issues. Six issues per year, approximately 1,500 Russian pages. Annually $35.00 domestic, $38.00 foreign. Libraries* $15.00 domestic, $18.00 foreign. Back numbers for Volumes 1 and 2, $5.00 per issue; Volume 3 and subsequent, $7.00 per issue.

Soviet Physics—JETP

A translation of the "Journal of Experimental and Theoretical Physics" of the Academy of Sciences of the U.S.S.R. The translation began with the 1955 issues. Twelve issues per year, approximately 4,000 Russian pages. Annually $75.00 domestic, $79.00 foreign. Libraries* $35.00 domestic, $39.00 foreign. Back numbers, all issues $8.00.

Soviet Physics—Crystallography

A translation of the journal "Crystallography" of the Academy of Sciences of the U.S.S.R. The translation began with the 1957 issues. Six issues per year, approximately 1,000 Russian pages. Annually $25.00 domestic, $27.00 foreign. Libraries* $10.00 domestic, $12.00 foreign. Back numbers, all issues $5.00.

Soviet Astronomy—AJ

A translation of the "Astronomical Journal" of the Academy of Sciences of the U.S.S.R. The translation began with the 1957 issues. Six issues per year, approximately 1,100 Russian pages. Annually $25.00 domestic, $27.00 foreign. Libraries* $10.00 domestic, $12.00 foreign. Back numbers, all issues $5.00.

Subscriptions should be addressed to the American Institute of Physics, 335 East 45th Street, New York 17, N. Y.

---

* For libraries of non-profit academic institutions.